



**US Army Corps
of Engineers**
Waterways Experiment
Station

Miscellaneous Paper CERC-96-7
November 1996

Southern Guam Typhoon Stage-Frequency Analysis

by David J. Mark

Approved For Public Release; Distribution Is Unlimited

Prepared for U.S. Army Engineer Division, Pacific Ocean

The contents of this report are not to be used for advertising, publication, or promotional purposes. Citation of trade names does not constitute an official endorsement or approval of the use of such commercial products.



PRINTED ON RECYCLED PAPER

Miscellaneous Paper CERC-96-7
November 1996

Southern Guam Typhoon Stage-Frequency Analysis

by David J. Mark

U.S. Army Corps of Engineers
Waterways Experiment Station
3909 Halls Ferry Road
Vicksburg, MS 39180-6199

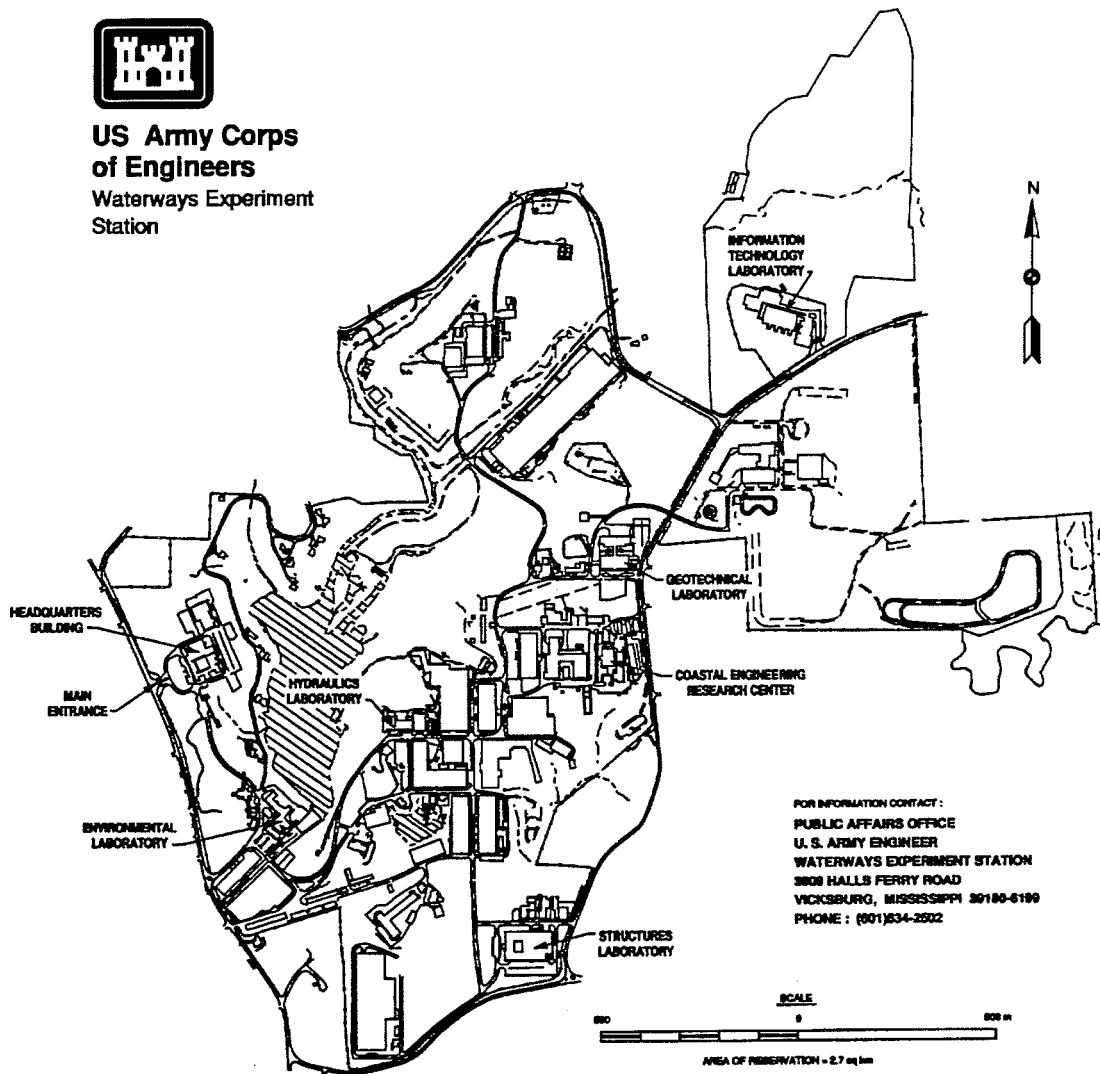
Final report

Approved for public release; distribution is unlimited

Prepared for U.S. Army Engineer Division, Pacific Ocean
Ft. Shafter, HI 96858-5440



**US Army Corps
of Engineers**
Waterways Experiment
Station



FOR INFORMATION CONTACT:
PUBLIC AFFAIRS OFFICE
U. S. ARMY ENGINEER
WATERWAYS EXPERIMENT STATION
3808 HALLS FERRY ROAD
VICKSBURG, MISSISSIPPI 39180-6199
PHONE: (601)634-2502

Waterways Experiment Station Cataloging-in-Publication Data

Mark, David J.

Southern Guam typhoon stage-frequency analysis / by David J. Mark ; prepared for U.S. Army Engineer Division, Pacific Ocean.

169 p. : ill. ; 28 cm. — (Miscellaneous paper ; CERC-96-7)

Includes bibliographic references.

1. Typhoons — Guam — Mathematical models. 2. Storm surges — Guam — Mathematical models. 3. Wind waves — Guam — Mathematical models. 4. Finite differences. I. United States. Army. Corps of Engineers. Pacific Ocean Division. II. U.S. Army Engineer Waterways Experiment Station. III. Coastal Engineering Research Center (U.S. Army Engineer Waterways Experiment Station) IV. Title. V. Series: Miscellaneous paper (U.S. Army Engineer Waterways Experiment Station) ; CERC-96-7.

TA7 W34m no.CERC-96-7

Contents

Preface	v
Conversion Factors, Non-SI to SI Units of Measurement	vi
1—Introduction	1
2—Storm Selection and Assignment of Probability	4
Overview of Technique	4
Review of Typhoon Analysis Study for Agana Bay, Guam	5
3—Description of Numerical Models	12
Description of Storm Surge Model	12
Description of Wave Model	13
Description of Meteorological Model	14
4—Implementation of the Storm Surge Model	15
Calibration of Storm Surge Model	15
Validation of Storm Surge Model	21
5—Development of Stage-Frequency Relationships	24
Storm Surge/Tidal Elevation Relationship	24
Wave Impoundment Correction Procedure	26
Convolution of Surge, Tide, and Ponding Level	27
Wave Setup and Runup	28
6—Summary and Conclusions	38
References	40
Appendix A: Stage-Frequency Relationship Figures	A1
Appendix B: Wave Setup and Runup Profile Figures	B1
SF 298	

List of Figures

Figure 1.	Study area	3
Figure 2.	Probability distribution of central pressure deficit	7
Figure 3.	Probability distribution of forward speed	8
Figure 4.	Probability distribution of radius to maximum winds	9
Figure 5.	Probability distribution of landfall point	10
Figure 6.	Calibration sites	17
Figure 7.	Comparison of time-series of water surface elevations for Merizo	18
Figure 8.	Comparison of time-series of water surface elevations for Ajayan Bay	19
Figure 9.	Comparison of time-series of water surface elevations for Inarajan Bay	20
Figure 10.	Maximum water surface elevations in study area	23
Figure 11.	Gauge locations for stage-frequency relationships	25
Figure 12.	Stage-frequency relationship for Bile Bay	29

List of Tables

Table 1.	Parameter Statistics for Joint Probability Method	11
Table 2.	Statistical Comparison of Model- and Constituent- Generated Tidal Time-Series	22
Table 3.	Typhoon Russ Storm Parameter Data	22
Table 4.	Ponding Water Level Coefficients	28
Table 5.	Apra Harbor Tidal Constituents	30
Table 6.	100- and 500-year Ponding and Wave Setup Elevations	33
Table 7.	Wave Setup and Runup Elevations	34

Preface

This report describes the procedures and results of a typhoon stage-frequency analysis for the southern coast of Guam. This study was performed by the U.S. Army Engineer Waterways Experiment Station (WES) Coastal Engineering Research Center (CERC) for the U.S. Army Engineer Division, Pacific Ocean (CEPOD). This analysis represents one component of a flood insurance study being conducted to define flood hazard locations in the study area.

The investigation reported herein was conducted by Mr. David J. Mark, Coastal Oceanography Branch (COB), Research Division (RD), CERC. The final report was prepared by Mr. Mark, and Ms. Mary T. Guzzo, Computer Science Corporation, assisted in report formatting and physical production. Appreciation is extended to Mr. Steven H. Yamamoto, Planning Division, CEPOD, for his assistance during this study.

This study was performed under the general supervision of Dr. James R. Houston and Mr. Charles C. Calhoun, Jr., Director and Assistant Director, respectively, CERC. Direct supervision of this project was provided by Mr. H. Lee Butler, Chief, RD; and Dr. Martin Miller, Chief, COB.

During this study, Director of WES was Dr. Robert W. Whalin. Commander was COL Bruce K. Howard, EN.

The contents of this report are not to be used for advertising, publication, or promotional purposes. Citation of trade names does not constitute an official endorsement or approval of the use of such commercial products.

Conversion Factors, Non-SI to SI Units of Measurement

Non-SI units of measurement used in this report can be converted to SI units as follows:

Multiply	By	To Obtain
feet	0.3048	meters
knots (international)	0.5144444	meters per second
miles (U.S. nautical)	1.852	kilometers
miles (U.S. statute)	1.609347	kilometers

1 Introduction

With the recent flooding induced by Typhoon Russ in December 1990 and Typhoon Yuri in November 1991, the U.S. Army Engineer Division, Pacific Ocean (POD) undertook a Flood Insurance Study for the Territory of Guam to delineate flood hazard areas. The purpose of this study was to develop frequency-of-occurrence relationships of typhoon-induced flood elevations along the southern shore of the Island of Guam. Shown in Figure 1, the area of interest for this study extends from Bile Bay, residing on the southwest side of the island, to Guaifan Point, which is located on the southeast side.

The Island of Guam is the largest and most populous island in the Mariana group, a chain of islands which delineates the boundary between the Western Pacific Ocean and the Philippine Sea. The island is located at approximately latitude $13^{\circ} 27' N$ and longitude $144^{\circ} 45' E$, or approximately 3,300 n.m.¹ west of Hawaii and 1,350 n.m. south of Tokyo. The island, being volcanic in origin, is mountainous with a peak elevation of 1,292 ft. A relatively narrow shelf surrounds the island, and coral barrier reefs encompass Guam in shallower water. Also, on average, approximately three typhoons influence water surface elevations at Guam each year.

Coastal inundation induced by typhoons can be attributed, in part, to high water levels caused by the combination of storm surge, astronomical tide, and wave impoundment. Impoundment refers to waves breaking on the coral reef, resulting in increased water levels within a lagoon. To incorporate each of the above processes into the stage-frequency relationships, a multi-faceted modeling approach was used in this study. A joint probability method was employed for synthesizing hypothetical typhoons representative of those which occurred in the vicinity of the Mariana Islands. With these synthetic storms, meteorological, wave, and storm surge models were then used to simulate each typhoon. The contribution of each process to the total water surface elevation was then determined for each simulated typhoon. Using the total water surface elevations, together with the frequency-of-occurrence of each synthetic typhoon, stage-frequency relationships within the study area were generated.

¹ A table of factors for converting non-SI units of measurement to SI units is presented on page vi.

This report is divided into six chapters, with Chapter 1 being the introduction. Chapter 2 describes the joint probability method (JPM) and selection of storm parameters for synthesizing typhoons subsequently simulated by the numerical models. Chapter 3 describes the hydrodynamic, meteorological, and wave models applied in this study. Model calibration and validation to the study area are presented in Chapter 4 and development of the stage-frequency relationships is discussed in Chapter 5. Chapter 6 summarizes the procedures and results of this study.

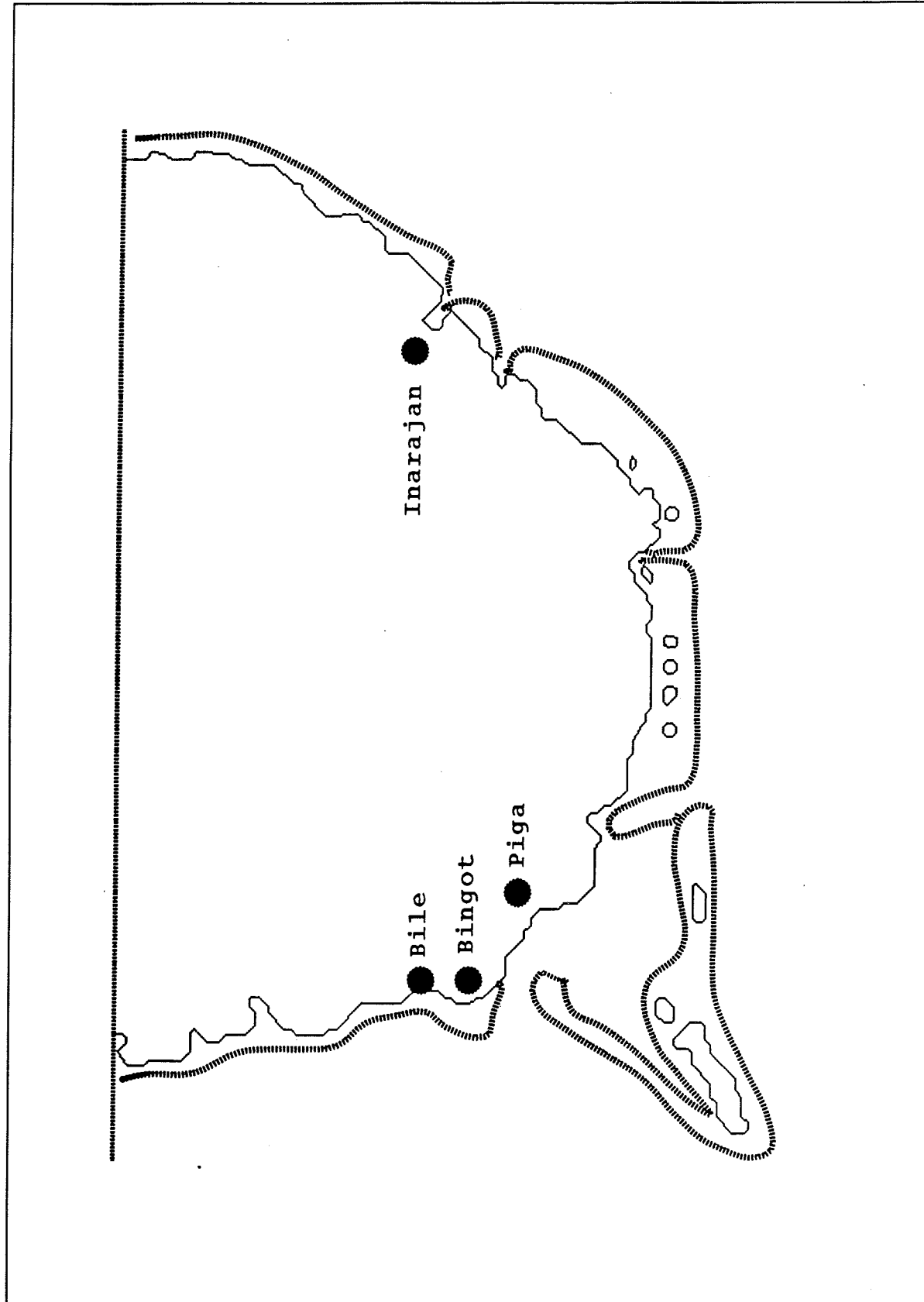


Figure 1. Study area

2 Storm Selection and Assignment of Probability

Delineating flood hazard areas typically requires a storm surge analysis to obtain the peak water surface elevation for design water levels. Standard statistical ranking methods cannot generally be used in a stage-frequency analysis because of the lack of peak storm surge stages at a particular site. Thus, numerical models are often applied for simulating a population of storm surge events for areas lacking historical storm surge elevations. The approach taken in this study is to synthesize a population of typhoons, whose characteristics are representative of those storms which have occurred in the study area, and compute via numerical models the peak water surface elevations these storms would produce. Knowing the probability of each storm, stage-frequency relationships can then be generated.

Overview of Technique

The joint probability method (JPM) was used to synthesize a population of storms. With this method, storms are characterized using a set of parameters, such as central pressure deficit, and an ensemble of synthetic typhoons is created by combining, in every possible combination, the values selected for each of the parameters that describe the storm. This ensemble of synthetic events, representing those events which can occur in the study area, are then simulated using the numerical models. The probability of each individual event is determined from the probability of each parameter value used in that event. If the parameters are independent, which was assumed in this study, then the probability of that event is the product of the individual parameter probabilities composing that event.

The five parameters used in describing a typhoon are defined below:

- a. *Central pressure deficit* is the difference between the minimum pressure of the storm and the surrounding ambient pressure and is an indicator of the intensity of the storm.

- b. *Radius to maximum winds* is the average distance from the center or eye of the typhoon to the region of greatest wind speed.
- c. *Forward speed* is the translational speed of the storm, measured at the eye, and induces asymmetric wind fields.
- d. *Track angle* is the direction in which the storm is moving.
- e. *Landfall point* is a reference point through which the typhoon will pass.

The first three parameters describe the intensity of a typhoon, whereas the latter two parameters are used to position the storm in space.

An infinite number of storms can be described by these five parameters. Consequently, the adopted JPM approach involves choosing discrete values, representative of the range in values which have historically occurred, and assigning a probability to these chosen values. A synthetic event can then be constructed by combining one value from each parameter. The number of synthetic events created equals the number of combinations of the chosen parameter values. The number of events to be simulated is a compromise between the number needed to accurately model the range of possible water levels and the level of funding to perform the study.

Review of Typhoon Analysis Study for Agana Bay, Guam

A typhoon analysis study has been performed for Agana Bay, located on the northwest coast of Guam and approximately 15 miles from the study area. A JPM analysis was performed as a part of that previous study. Because Agana Bay and the present study area are in close vicinity to one another, the JPM analysis performed for Agana Bay is applicable for use in the present study.

The JPM is employed using the following steps:

- a. Historical data are gathered for each of the five typhoon parameters.
- b. A probability distribution function (PDF) is established for each parameter which relates the value of the parameter to its frequency of occurrence as determined from historical records. Probability is determined using the standard ranking method:

$$P = \frac{m}{n+1} \quad (1)$$

where P is the probability, m is the rank of the historical occurrence, and n is the total number of historical values used in developing the probability distribution function.

- c. Discrete values of each parameter are selected from the PDF to reflect the range of parameter values which can occur in the study area.
- d. Probabilities are assigned to the chosen parameter values based on the portion of the PDF which the discrete value represents.
- e. Parameters are assumed independent from one another; thus, the probability of occurrence of a given synthetic storm is the product of the probabilities of each individual parameter.
- f. The number of storms per year λ is determined from historical records. The probability of a particular synthetic storm is determined by multiplying times the probability determined in Equation 1.

Data used in creating the parameter probability distribution functions were obtained from the Joint Typhoon Warning Center annual report (JTWC 1959-79), and Weir (1983) which summarizes these data for storms passing within 180 n.m. of the Island of Guam. These two sources provided all parameter data except for the radius to maximum winds, which was obtained from the National Oceanic and Atmospheric Administration (NOAA) Technical Report NWS 23 (1979). Parameter probability distributions are illustrated in Figures 2 through 5.

Based on the information presented in Weir (1983) and the JTWC annual reports, six values of central pressure deficit (i.e., 20, 40, 60, 80, 100, and 120 mb) and two values of forward speed (i.e., 8 and 16 knots) were chosen. Two values of radius to maximum winds (i.e., 8 and 15 n.m.) were selected based on the information given in NOAA Technical Report NWS 23.

Typhoons passing within the vicinity of Guam have a dominant track angle of 150 deg, measured clockwise from north, or from the south-southeast to the north-northwest. The 150-deg track angle was selected for this study. Seven landfall points were chosen for this study. The central landfall point was specified at 13° 26' N latitude and longitude 144° 45' E. The remaining landfall points were specified to fall on a line perpendicular to the predominant track angle of the typhoon. These points are located 120, 60, 25, -25, -60, and -120 n.m. from the central landfall point, where positive distances denote locations to the northeast and negative distances define locations to the southwest of Guam. Table 1 presents the discrete parameter values used in this study.

Using the discrete parameter values described above, a total of 168 typhoons are synthesized using the JPM. From Weir (1983), 94 storms passed within 180 n.m. of Guam during the period 1948 through 1980. Thus, the typhoon frequency of occurrence is 2.85 storms per year.

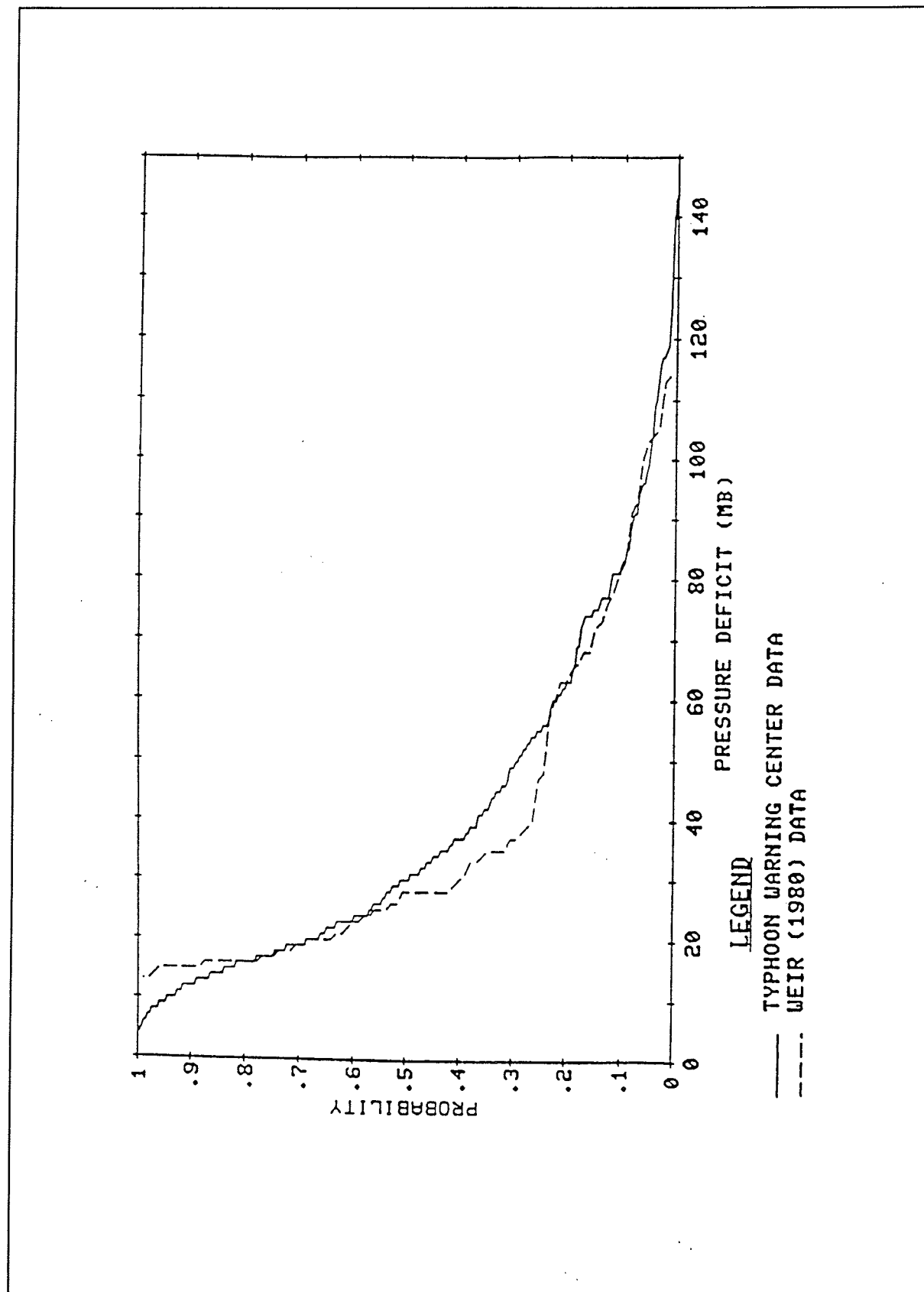


Figure 2. Probability distribution of central pressure deficit

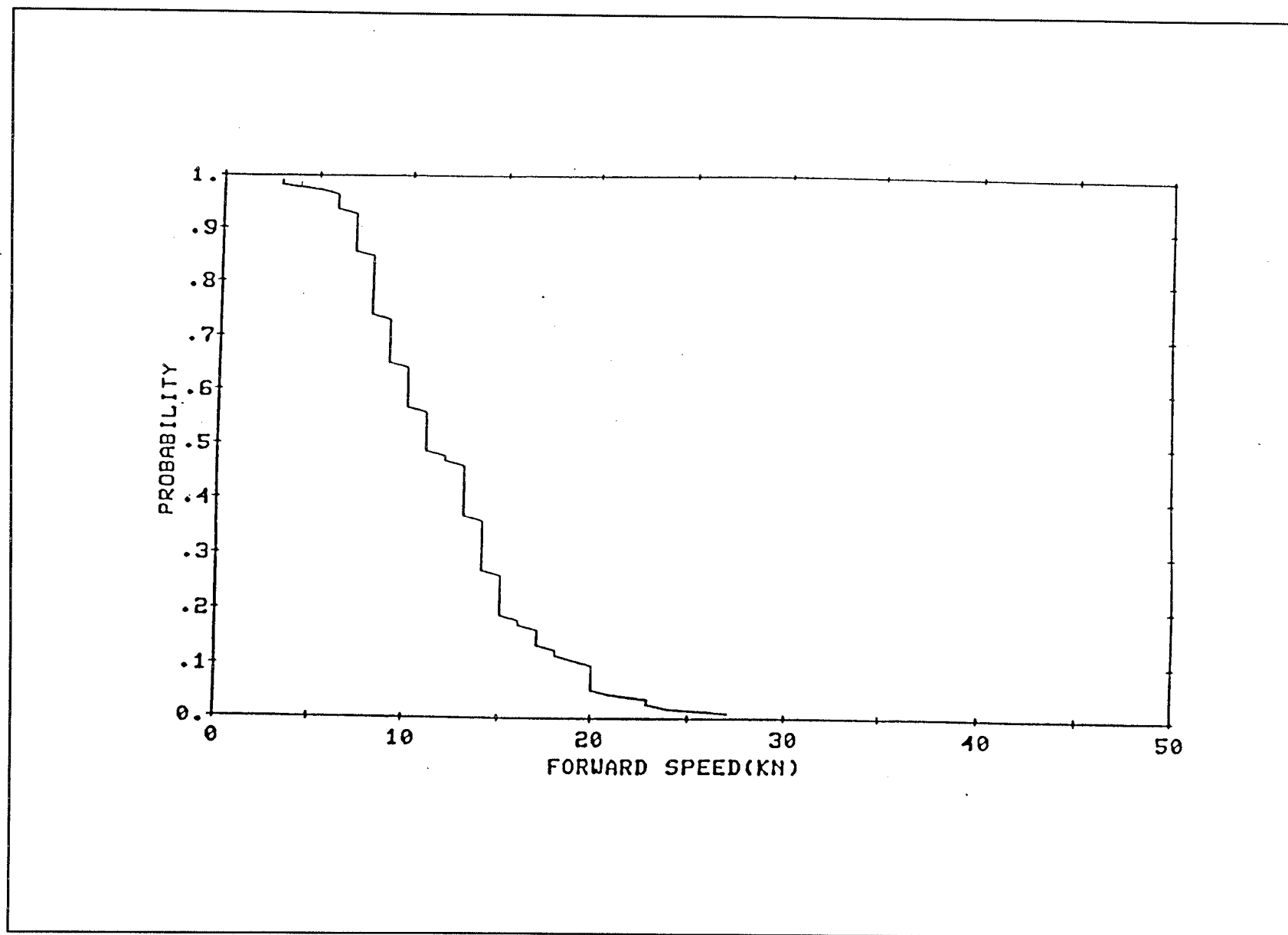


Figure 3. Probability distribution of forward speed

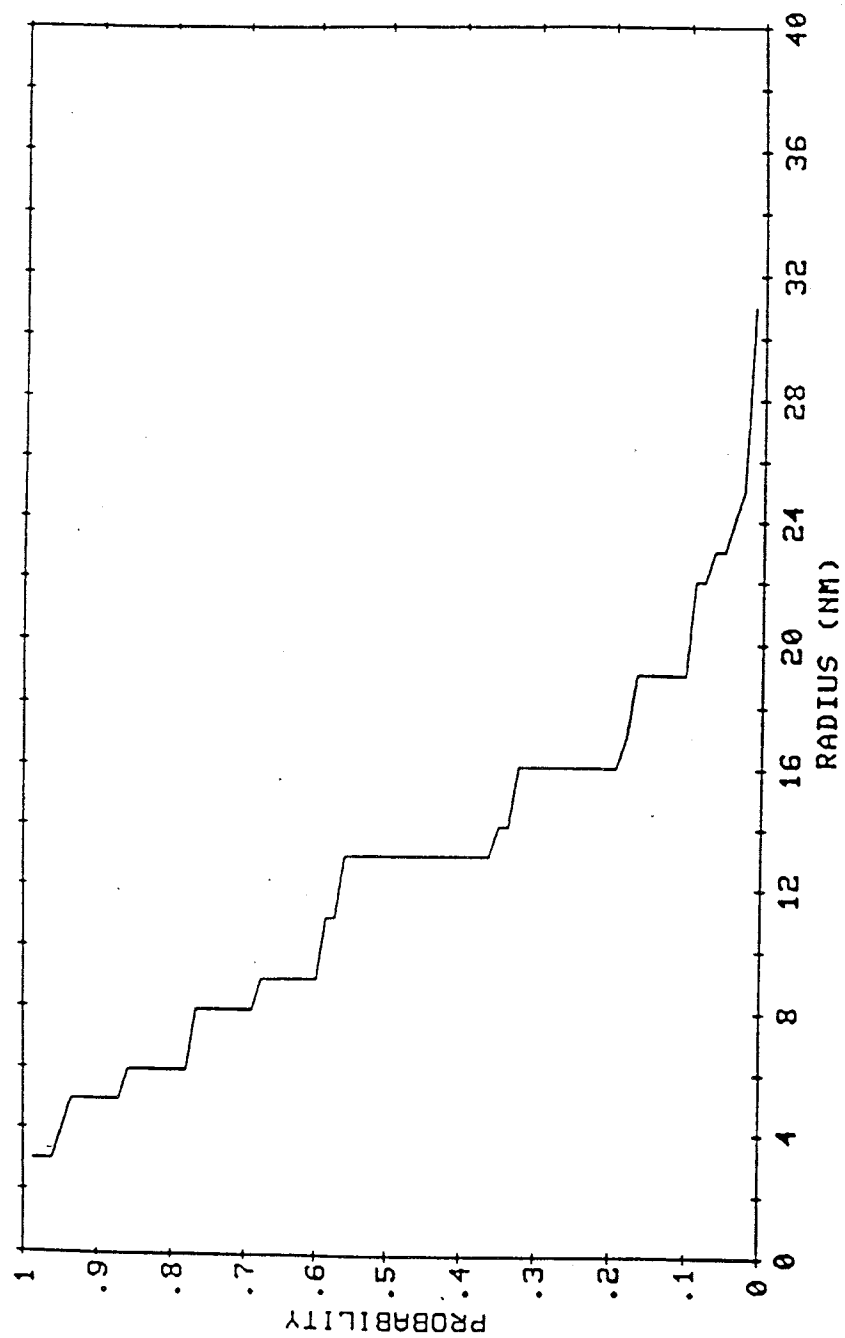


Figure 4. Probability distribution of radius to maximum winds

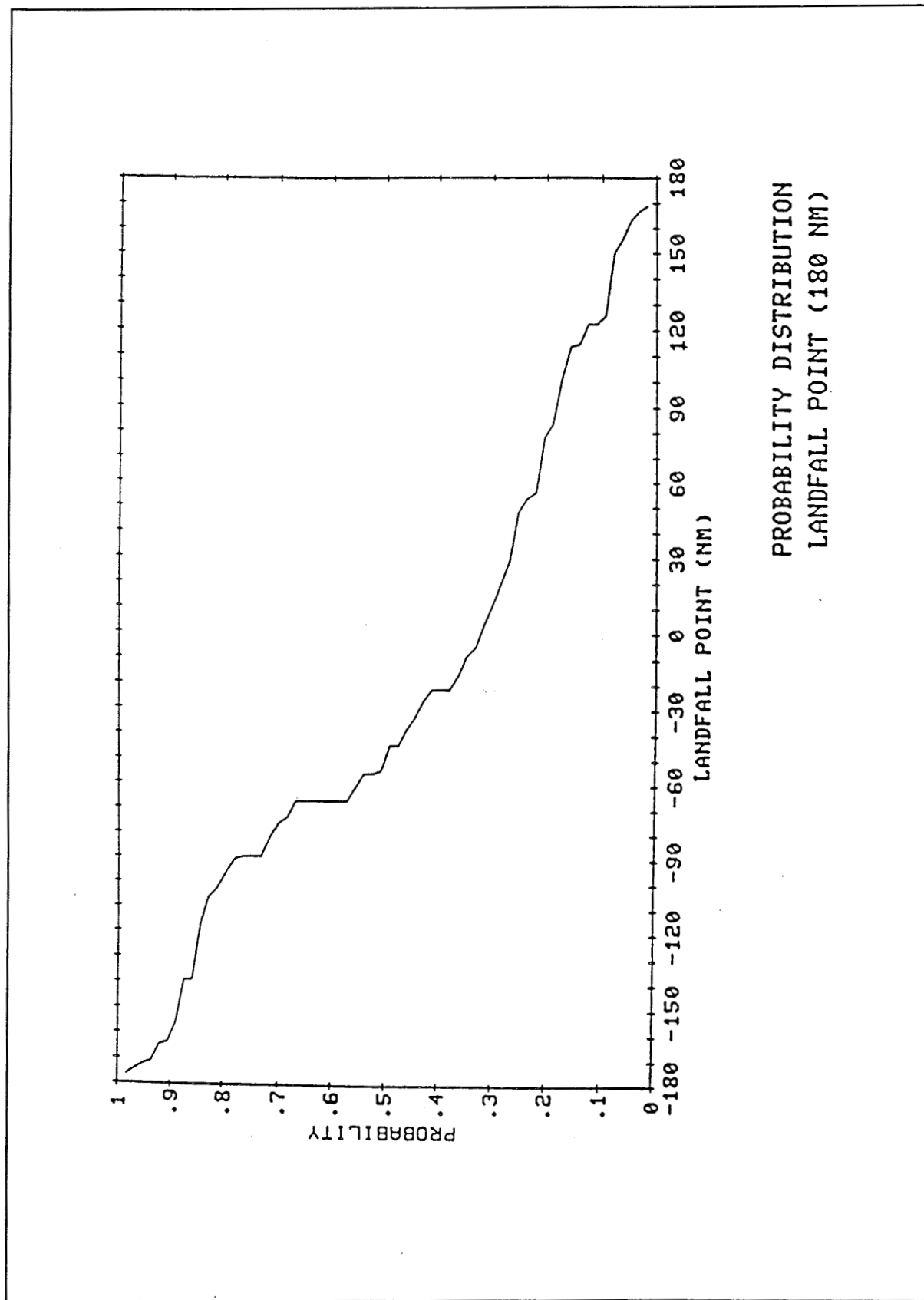


Figure 5. Probability distribution of landfall point

Table 1
Parameter Statistics for Joint Probability Method

Central Pressure Deficit	
Pressure Deficit, mb	Probability
20	0.510
40	0.220
60	0.100
80	0.085
100	0.050
120	0.035
Forward Speed	
Velocity, knots	Probability
8	0.52
16	0.48
Radius to Maximum Winds	
Radius, n.m.	Probability
8	0.48
15	0.52
Landfall Point	
Distance, n.m	Probability
-120	0.285
-60	0.235
-25	0.115
0	0.070
25	0.050
60	0.090
120	0.155

3 Description of Numerical Models

The models selected for this study are the WES Implicit Flooding Model (WIFM) (Cialone et al. 1991) for simulating long-wave hydrodynamics, the Wave Information Studies Wave (WISWAVE) model for synthesizing deep-water wave fields, and the Standard Project Hurricane (SPH) wind-field model (Cialone et al. 1991) for generating typhoon-induced wind and atmospheric pressure fields. Each model is described below.

Description of Storm Surge Model

Model WIFM is a two-dimensional, time-dependent, long-wave model for solving the vertically integrated continuity and Navier-Stokes equations in a stretched Cartesian coordinate system. The model simulates shallow-water, long-wave hydrodynamics such as tidal circulation and storm surge. It also contains features for simulating flooding and drying of low-lying areas and subgrid flow boundaries such as reefs, breakwaters, or small barrier islands. Model output includes vertically integrated water velocities and water surface elevations. The governing equations are approximated with a three-time-level (i.e., leap frog), implicit finite-difference scheme. These equations are solved via an alternating-direction implicit algorithm. For this study, advective and dispersive terms have been neglected.

Bottom shear stress is represented in the model with a nonlinear formulation. Manning's n friction factor serves as the bottom friction coefficient and is specified either as a function of local water depth or is specified manually. This permits flood-prone areas, such as marshes, to have higher coefficients than deepwater areas. Surface shear stress is computed using a nonlinear formulation and Garratt's (1977) linear drag coefficient.

The WIFM employs a deterministic approach for simulating flooding and drying of low-lying terrain. Initially, water is transferred from a "wet" cell to an adjacent "dry" cell based on discharges computed by a broad-crested weir formula. To ensure that water is conserved in the system, the volume of water added to the receiving cell is subtracted from the donating cell. Once the

water level in a receiving cell exceeds a user-defined value, that cell is incorporated into the Navier-Stokes computational scheme and becomes a "wet" cell.

Initially, the model's drying algorithm is essentially the opposite of the flooding algorithm. As the water level in a cell falls below a user-defined value, that cell is removed from the Navier-Stokes computational scheme, and water is transferred to an adjacent cell based on discharges computed with a broad-crested weir formula. Once the water level falls below a second user-defined value, however, a second draining technique is used. With this technique, draining is accomplished by transferring a fixed percentage of remaining water volume contained in a drying cell to an adjacent cell at each subsequent time-step.

The origin of the hydrodynamic grid is located at latitude $13^{\circ} 5' N$, longitude $144^{\circ} 30' E$. The grid contains a total of 17,640 cells, with 168 cells in the east-west direction and 105 cells in the north-south direction. In order to better represent complex coastal features, such as narrow lagoon widths and curving shoreline, higher cell resolution in the east-west direction was specified along the reach from Bile Bay to the village of Merizo, and in the vicinity of Agfayan Bay. In the north-south direction, greater resolution was placed in the reach extending from Bile Bay to the village of Merizo.

Minimum cell dimensions measured 160 ft by 160 ft, in contrast to the outer grid boundaries, where cell widths reached 6,080 ft by 5,000 ft at the grid corners. In deeper water, cell depths were digitized from National Oceanic and Atmospheric Administration (NOAA) navigation chart 81048. For areas on the shelf, water depths and topographic elevations were obtained from Defense Mapping Agency maps (sheets 3126 II NE and 3126 III NW, series W844).

Discharges of all rivers entering the grid were omitted in the model setup. However, cell depths were adjusted for the larger streams in order to approximate their water storage capacity and conveyance. Also, rainfall was ignored.

Description of Wave Model

WISWAVE is a second-generation discrete directional spectral wave model where the spectral wave height computations are based on integration of energy over the discrete frequency spectrum. Model output includes time-series of significant wave height, peak (dominant) or mean wave period, and mean wave direction. Peak or dominant wave periods are not integral quantities in that they are not derived by summation over the spectrum. Peak period is defined as the period associated with the mid-band frequency of that frequency band containing the largest spectral energy density. Mean wave period, calculated by the model, is an energy-weighted quantity integrated over all user-specified frequencies of interest. Model input includes a computational grid, with corresponding water depths at each node in the grid, wind

speeds and directions over the entire modeling domain, and wave conditions along the outer boundary of the grid.

The grid origin specified in the WISWAVE model is located at latitude 12° 42' 30" N, longitude 143° 57' 30" E. This grid has a mesh resolution of 2.5' in both latitude and longitude. Furthermore, the mesh contains a total of 1,369 nodes; 37 nodes in the north-south and east-west directions. This modeling area was selected to correspond to the region used in validating the Quick Typhoon Surge and Waves (QTSW) system (Tracy 1993). The grid resolution was increased from 11 nodes to 37 nodes in each axis direction to ensure that sheltering effects imposed by the island were accurately represented in the wave model.

Description of Meteorological Model

Model SPH is a two-dimensional, parametric model developed in a stretched Cartesian coordinate system for estimating wind and atmospheric pressure fields generated by hurricanes. Based on the Standard Project Hurricane criteria developed by NOAA (1979), the SPH represents a steady-state, hypothetical hurricane defined by the following set of interrelated parameters; central pressure, peripheral pressure, track angle, translational speed, radius to maximum winds, maximum wind speed, ingress angle, landfall location, azimuth angle to the point of maximum wind speed measured in a clockwise direction from the forward velocity vector, and an effective-radius-to-maximum-winds parameter, which controls the shape of the far-field radial wind distribution.

Model SPH was developed in a modular structure, permitting model WIFM to execute the windfield model without the user needing to make separate SPH model simulations. Wind and atmospheric pressure fields computed within model WIFM were generated at each time-step during storm surge simulations. Furthermore, wind and pressure fields were computed at each cell in the numerical grid. Model WISWAVE, lacking linkages with the wind field model, requires that the wind fields be generated and stored on computer disk prior to simulating typhoon-induced wave fields.

Wind fields required by model WISWAVE were computed at hourly intervals for each hour of the simulation period. A nonlinear interpolation scheme is used for updating nodal wind velocities at those time-steps falling between the full hour. Furthermore, wind fields were computed using the identical grid used by model WISWAVE.

4 Implementation of the Storm Surge Model

During construction of a numerical model, the model must undergo calibration and validation exercises to ensure that it accurately predicts hydrodynamic conditions within a given study area. The accuracy of model results is greatly influenced by the accuracy of boundary and forcing conditions, representation of the geometry of the study area (i.e., bathymetry and land/water interface), and to a lesser degree, the choice of certain “calibration” parameters. Calibration is the procedure where certain model parameters, such as the bottom friction coefficient, are adjusted to maximize agreement between model results and measured data.

Once the calibration procedure is completed, the model undergoes a validation procedure to ensure that it can replicate conditions during a time period different than that used in the calibration procedure. In the validation procedure, the model is applied without adjusting those parameters optimized in the calibration procedure. Obtaining a good comparison between model and measured data in the validation procedure provides confidence that the model can accurately predict hydrodynamic processes in the study area.

The strategy for calibrating and validating the storm surge model consists of two criteria. First, it must be demonstrated that the model can accurately predict tidal propagation in the study area. Second, in order to show that the model can replicate storm surge effects in the study area, a storm surge simulation of a medium-to-large-intensity typhoon, which affected water levels on the Island of Guam, must be simulated. The procedures used in conducting model testing and the results obtained in these tests are summarized in the following sections.

Calibration of Storm Surge Model

The hydrodynamic model was calibrated by adjusting model parameters (i.e., bottom friction coefficient and depths) so that model-generated water surface level time-series compared favorably to those reconstructed from tidal constituents. Tidal constituents developed from gauge records collected at

Apra Harbor were used to make this comparison. Locations at which comparisons were made include Merizo, Ajayan Bay, and Inarajan Bay. These locations are shown in Figure 6. Calibration simulations were conducted over a 14-day period beginning at 0:00 Greenwich Mean Time on 1 August 1992. A 60-sec time-step was used in these simulations. Comparisons of computed and constituent-generated water surface levels are presented in Figures 7 through 9.

Parametric and nonparametric statistical tests were performed to quantitatively assess the model's ability to replicate the hydrodynamic processes occurring in the study area. One test is the root-mean-square (rms) difference calculations of the model- and constituent-generated water surface level time-series. One limitation of the rms difference test is that no information is provided as to the source of error being measured. For example, one source of error can be a shift in phase between measured and computed water oscillation periods, whereas a second source could be discrepancies in predicted water surface elevations. To overcome this limitation, a series of nonparametric or "skill" tests were used to differentiate between phase and magnitude errors (Hess and Bosley 1991).

Skill tests selected for analyzing the hydrodynamic model include statistical comparisons of the timing and amplitude of local water level extrema (minimum and maximum) computed with tidal constituents at the three gauging stations. These tests are average gain or ratio of predicted-to-measured extrema, the rms difference in amplitudes, average lag or phase shift between predicted and measured extrema, and the rms difference in lag.

The average gain can be expressed as:

$$G = \frac{1}{v} \sum \left(\frac{Y_c}{Y_m} \right) \quad (2)$$

where G represents the gain, v is equal to the number of extrema pairs contained in the time-series data, and Y_c and Y_m signify the computed and measured (i.e., model- and constituent-generated) extrema values, respectively.

The *rms* difference in amplitude has the following formulation:

$$A_{rms} = \frac{1}{v} \left[\sum (Y_c - Y_m)^2 \right]^{1/2} \quad (3)$$

where A_{rms} represents the *rms* difference in amplitude and the remaining variables have been previously defined.

The average lag between computed and measured extrema can be written as:

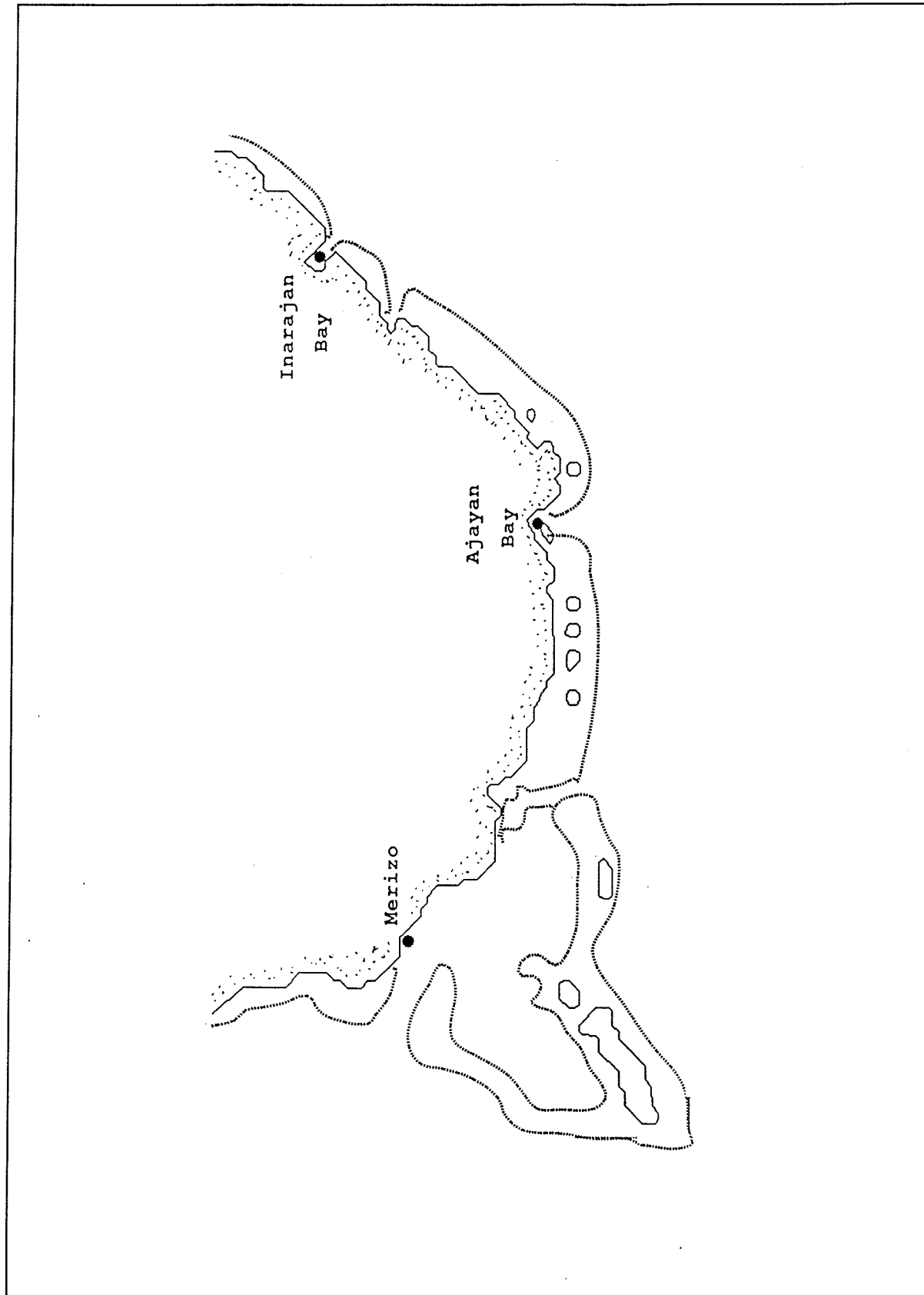


Figure 6. Calibration sites

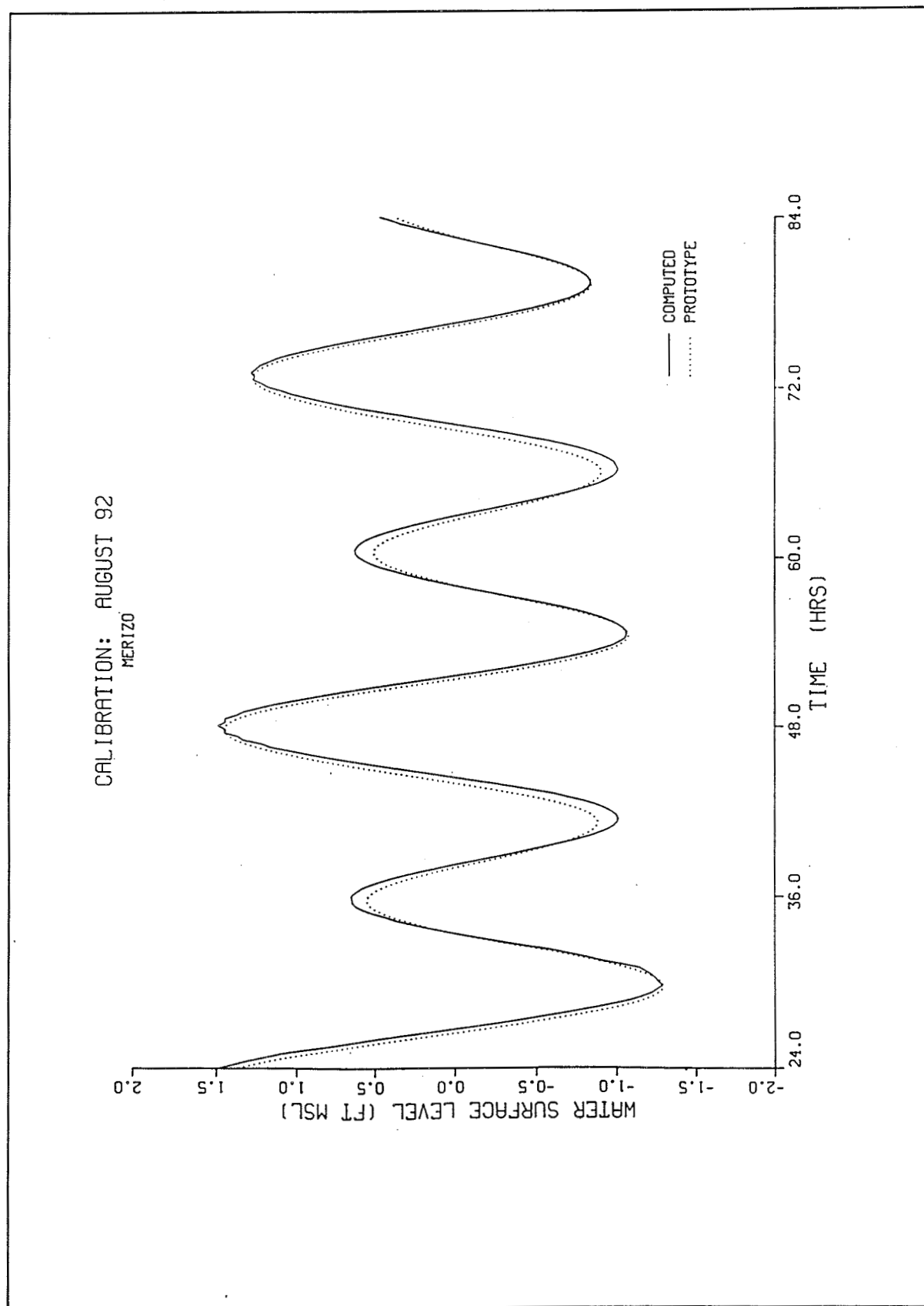


Figure 7. Comparison of time-series of water surface elevations for Merizo

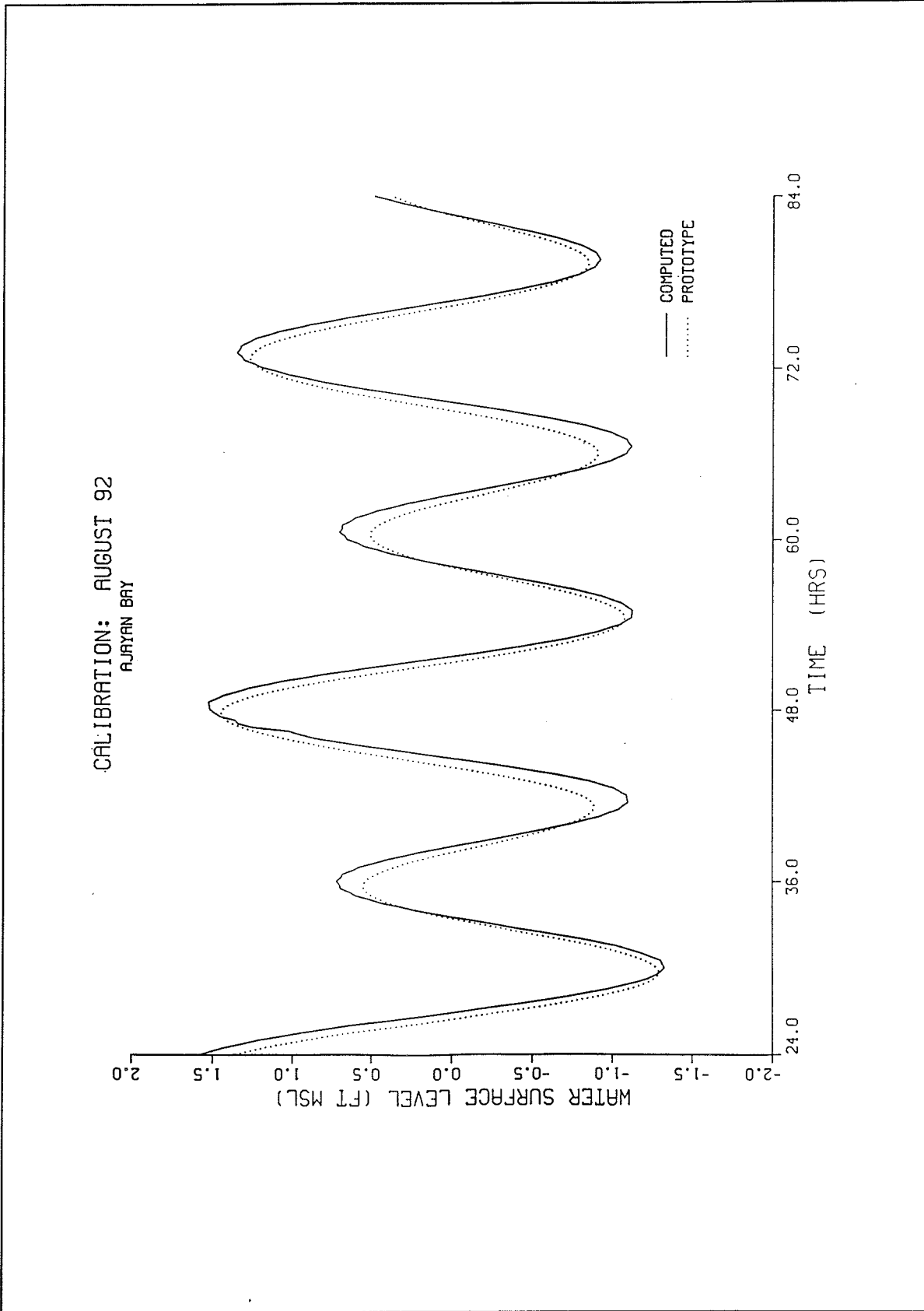


Figure 8. Comparison of time-series of water surface elevations for Ajayan Bay

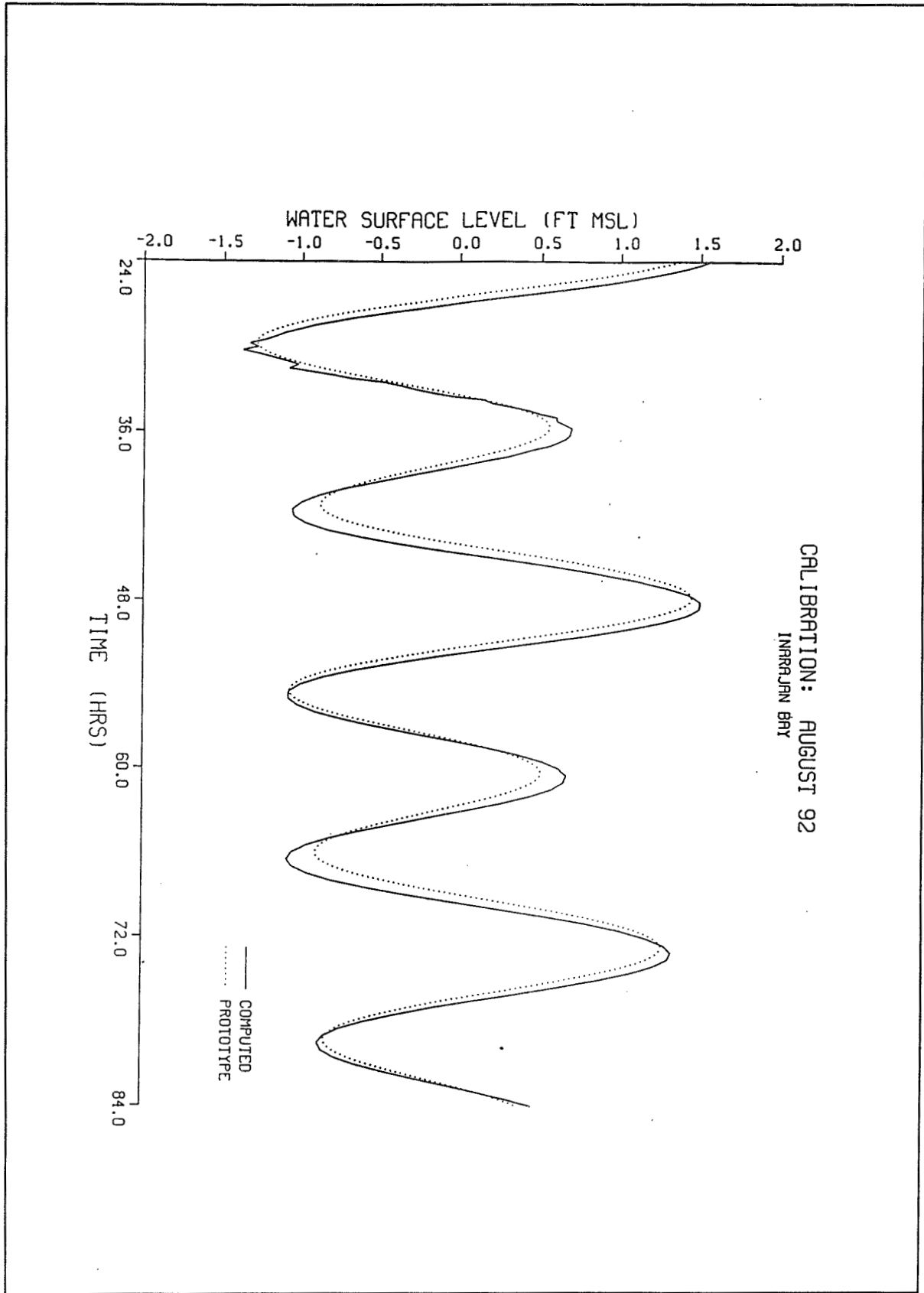


Figure 9. Comparison of time-series of water surface elevations for Inarajan Bay

$$L_m = \frac{1}{V} \sum (T_c - T_m) \quad (4)$$

where L_m represents the average lag and T_c and T_m signify the time of extrema occurrence in the computed and measured time-series, respectively.

The *rms* difference in lag can be expressed as:

$$L_{rms} = \frac{1}{V} \left[\sum (T_c - T_m)^2 \right]^{1/2} \quad (5)$$

where L_{rms} represents the rms lag.

Model-generated water surface level time-series at the three numerical gauge locations were analyzed with the preceding skills tests. As a consequence of starting a model from static conditions, artificial oscillation modes are generated by the model. Sufficient simulation time must be provided in order for the model to dampen these artificial oscillation modes. Thus, skill tests were performed using time-series data "recorded" over the latter 13 days of the calibration period. Furthermore, tests were performed using a 15-min sampling interval. Table 2 presents a summary of this analysis.

The average gain in extrema water surface levels for the three gauges varied from 1.04 to 1.13, representing a difference of 4 and 13 percent between the computed and constituent-generated extrema. (Average gains greater than 1.0 denote that the model-generated extrema were greater than the constituent-generated extrema.) Furthermore, the greatest extrema rms was found at the Ajayan Bay station and had a value of 0.21 (ft). The average tidal range at this station is approximately 1.13 ft. As shown in Figure 7, the model tends to match the higher high tidal peaks, whereas the model overestimates the lower high peak tidal elevations. Phase differences between the computed and constituent-generated tidal oscillations ranged from 0.12 to 0.39 hr. Computed tidal oscillations at all stations lagged the constituent-generated oscillations.

Validation of Storm Surge Model

Model validation was achieved by performing a storm surge simulation of Typhoon Russ which impacted the study area in December 1990. The hindcast began on 18 December 1990 at 0600 GMT and ended on 20 December at 0000 GMT. A 30-sec time-step was used in the simulation and tidal forcing was specified at the open water boundary. Table 3 presents the typhoon parameter values.

From the beginning of the hindcast simulation to 18 December at 1800 GMT, no wind or atmospheric pressure gradients were included in the

Table 2
Statistical Comparison of Model- and Constituent-Generated Tidal Time-Series

Station	Gain	Extrema rms, ft	Average Lag, hr	Lag rms, hr
Merizo	1.04	0.12	0.12	0.25
Ajayan Bay	1.13	0.21	0.27	0.38
Inarajan Bay	1.10	0.17	0.39	0.44

Table 3
Typhoon Russ Storm Parameter Data

Date	Time	Lat deg N	Long deg E	Central Pressure, mb	Track Angle, deg	Max Vel, kts	Forward Speed, kts
19	1800	11.7	148.0	914.0	156.8	125.0	7.6
20	0000	12.0	147.3	914.0	156.8	125.0	7.6
20	0600	12.2	146.4	914.0	167.5	125.0	9.2
20	1200	12.4	145.4	914.0	168.7	125.0	10.2
20	1800	12.7	144.2	914.0	166.0	120.0	12.4
21	0000	13.2	142.9	914.0	159.0	120.0	13.9

model. This 12-hr period provides sufficient simulation time to develop an accurate tidal current field and to dampen any start-up errors. Thereafter, from 18 December at 1800 through the end of the hindcast at 0000 GMT on 20 December, wind and atmospheric pressure fields were computed by the storm surge model at each time-step. Furthermore, wind and pressure values were computed for each cell.

Figure 10 compares maximum water surface elevations computed with the storm surge and wave models to the estimated elevations presented in JTWC (1991). Maximum water surface elevations ranged from approximately 10.5 ft msl in the vicinity of Inarajan Bay to 4.5 ft msl around Julog.

Figure 10 shows that model-generated maximum water surface elevations compare favorably with the JTWC-estimated elevations. The model reproduced the trend shown by the JTWC-estimated elevations where peak water levels were highest along the southeast reach of the island, with decreasing peak water levels towards the west. The model produced a peak water surface elevation of 10.3 ft msl, about 0.2 ft lower than the JTWC-estimated elevation. The greatest differences in peak water levels were in the vicinity of Julog, where the JTWC-estimated and model-generated peak water levels were 4.5 and 5.0 ft msl, respectively. These differences are attributed to discrepancies between the wind and pressure fields predicted by the SPH model and the fields which actually occurred.

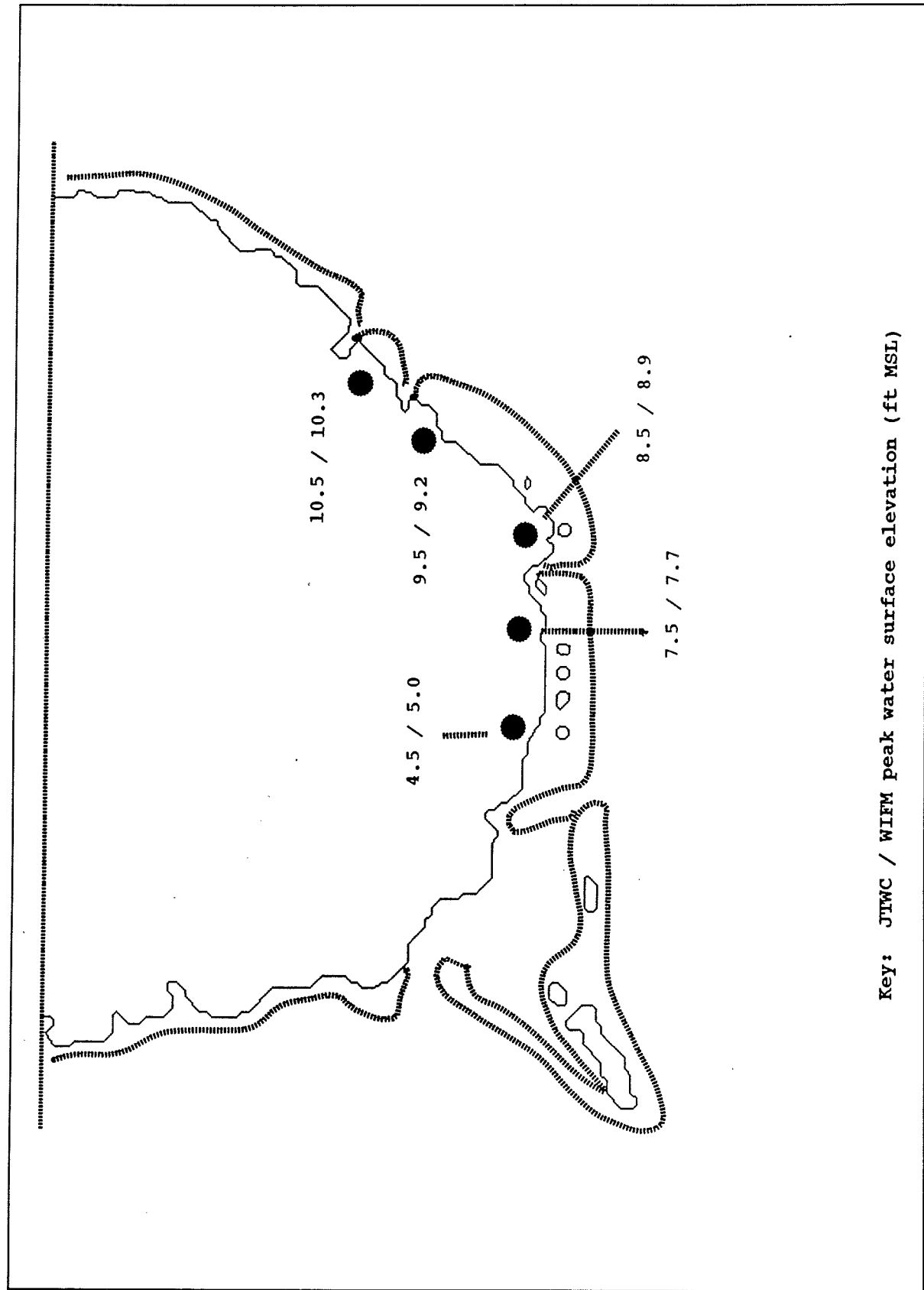


Figure 10. Maximum water surface elevations in study area

5 Development of Stage-Frequency Relationships

Coastal inundation induced by typhoons can be attributed, in part, to high water levels caused by the combination of storm surge, astronomical tide, and wave impoundment. (Impoundment refers to waves breaking on the coral reef, resulting in increased water levels within a lagoon.) A multi-faceted modeling approach was used in this study to incorporate each of the above processes in developing the stage-frequency relationships. With the models, a population of hypothetical typhoons, representative of those which occurred in the vicinity of the Mariana Islands, are simulated to obtain the peak water surface elevations. These storms were synthesized via a joint probability method, which also provides the probability of a given storm's frequency of occurrence.

With these synthetic storms, the meteorological, wave, and storm surge models were used to simulate each typhoon. The contribution of each process to the total water surface elevation was then determined for each simulated typhoon. Using the total water surface elevation, together with the frequency of occurrence of each synthetic typhoon, stage-frequency relationships within the study area were generated.

A total of 168 synthetic typhoons were developed via the JPM. Each synthetic storm was simulated by the storm surge model, WIFM, and each simulation was conducted independently of tide. Each simulation had a duration of 24 hr, prototype time, with a time-step of 30 sec. Wind and atmospheric pressure fields were computed using the SPH modules in model WIFM at each time-step in the simulation. Time-series of water surface elevations were saved, at 10-min interval, at 17 numerical gauge locations within the study area. These locations are presented in Figure 11.

Storm Surge/Tidal Elevation Relationship

Storm surge elevations were computed independently of tide. However, surge elevations are not only dependent on the intensity of the storm, but also on the water depths. Incorporating tide into the surge calculations would be the most precise method to obtain accurate surge elevations. However, this

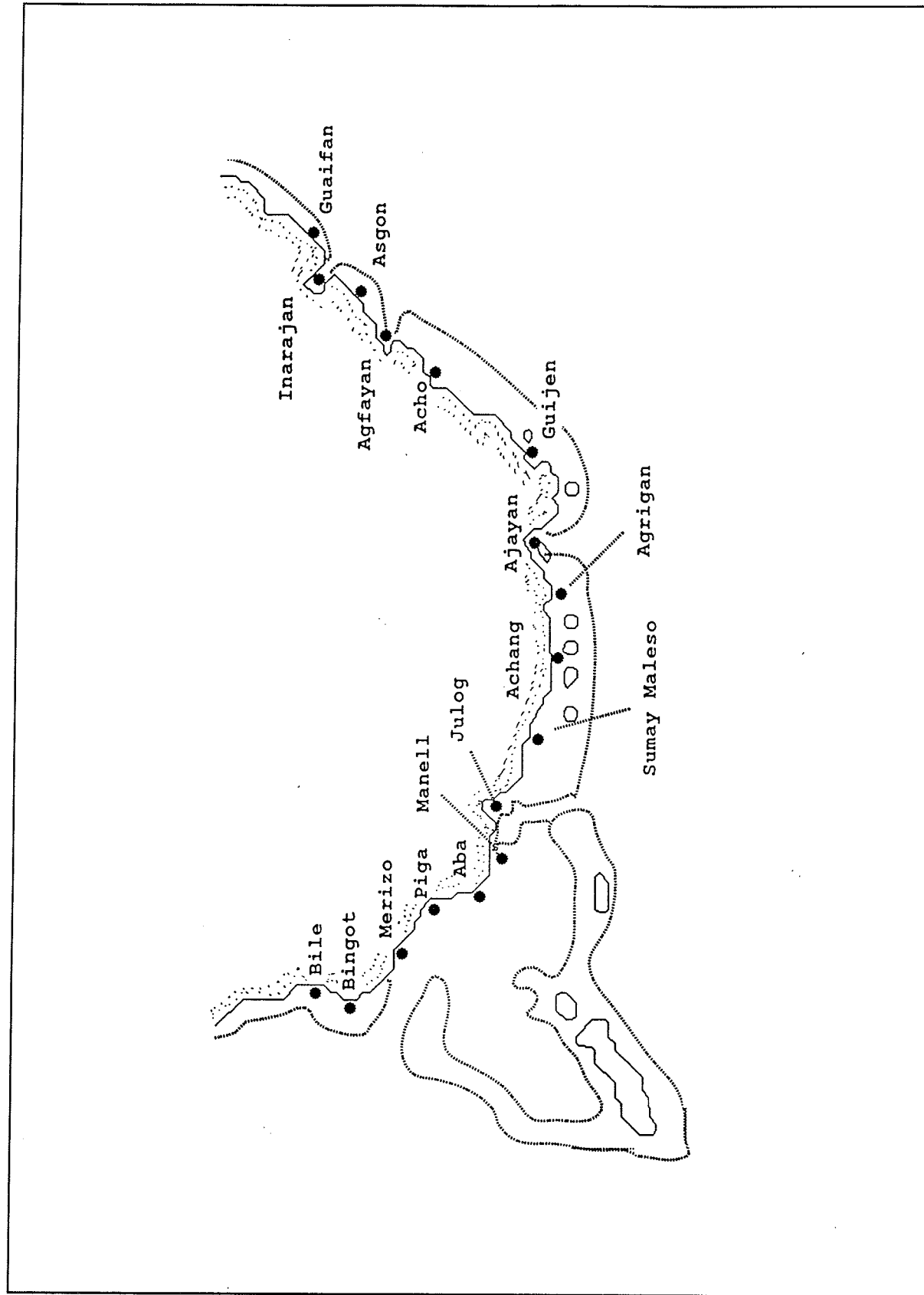


Figure 11. Gauge locations for stage-frequency relationships

method was not feasible because of the vast number of tide scenarios that must be modeled in conjunction with each storm in the ensemble to yield a representative sample of possible combined surge-tide events.

An alternative method, which permits storm surge to be modeled independently of tide, is to develop a numerical nomograph or relationship that corrects surge elevations given a tidal elevation. Each storm in the ensemble may then be simulated at a common starting depth, in this case mean lower low water, to produce a time-series of storm surge elevations. Adjustments to the surge level can then be performed in the convolution process of combining surge, tide, and wave impoundment elevations to form a total water surface elevation.

Surge-tide relationships were developed by simulating a high-intensity typhoon, with five initial water surface elevations to obtain the maximum surge elevations. Initial water surface elevations ranged from -2.0 ft mllw to 2.0 ft mllw, with a 1.0 ft increment. With the maximum storm surge elevation, the slope of each depth interval is computed by dividing the change in surge level by the change in water depth. The average slope for each depth interval is computed and, using these slopes, an equation is formulated that represents the surge-tide relationships. A separate relationship was computed for each numerical gauge.

Wave Impoundment Correction Procedure

Deepwater wave heights and periods were simulated with model WISWAVE for the 168 synthetic typhoons mentioned above. The duration of each simulation was 24 hr, prototype time, with a time-step of 60 sec. Wind and atmospheric pressure fields were first computed using the SPH model at hourly intervals and subsequently stored for input to the WISWAVE model. Time-series of computed wave heights and periods were saved, at 10-min interval, at 11 numerical gauge locations surrounding the study area.

Deepwater waves generated by WISWAVE cannot be directly used in the convolution procedure because of the uncertain hydraulic conditions within a lagoon due to waves breaking on its barrier reef. Seelig (1983) studied the hydraulic effects of an idealized lagoon-reef system with respect to wind-generated, irregular waves using a physical model having a reef cross section typical for the coast of Guam.

Laboratory tests were performed with a physical model constructed of roughened concrete at a 1/64 undistorted scale. Unlike a natural reef, the model reef was impermeable, did not contain channels, and had a uniform height. Although these features are idealized, Seelig noted that the ponding levels generated in the experiments produce conservative results.

Experiments were performed over a range of values: The still-water depth at the reef crest elevation varied from 0.0 to 2.0 m; wave periods ranged from 8.0 to 16.0 sec; and the irregular deepwater significant wave height varied from 2.5 to 10.7 m. Seelig found that wave energy is either dissipated or transmitted into the lagoon; only a fraction of the wave energy is reflected towards open water.

Seelig found that the total water level within a lagoon is a function of the still-water level, resulting from the combined effects of astronomical tide and storm surge, deepwater significant wave height, and wave period. Ponding level is defined as the mean water level in the lagoon above the still-water level, and includes the wave setup due to waves breaking on the reef. It does not, however, include the contribution in setup caused by the breaking of secondary waves (produced by the re-forming and breaking of those waves originally breaking on the coral reef). Seelig proposed the following equation for predicting ponding levels in a lagoon:

$$\eta = a_1 + a_2 \log (H_0^2 T) \quad (6)$$

where η is the ponding level, H_0 is the deepwater significant wave height, and T is the wave period. Coefficients a_1 and a_2 are dependent on the still-water level. Coefficient values are presented in Table 4 and are representative of irregular waves.

Using the empirical relationship developed by Seelig, the time-series of wave heights and periods were combined with the time-series of still-water levels (composed of tide and storm surge) to form a single time-series of total water surface elevations or ponding levels. The peak water surface level was extracted from each ponding level time-series. With the probability assigned to each storm and its corresponding peak ponding level, probability density functions were generated for the 17 gauging locations within the study area. Cumulative density functions, representing the stage-frequency relationships, were computed using these probability density functions.

Convolution of Surge, Tide, and Ponding Level

The algorithm for combining the surge, deepwater wave, and tide components to form the total water surface elevation or ponding level is as follows:

- a. A starting time for a time-series of tidal elevations is chosen using a random number generator. The time-series of tidal elevations, computed using tidal constituents for the Apra Harbor gauge (Table 5), consists of a 19-year period with elevations provided at 10-min increments.

Table 4 Ponding Water Level Coefficients		
depth, m	a₁	a₂
0.0	-0.92	0.77
2.0	-1.25	0.73
Note: Depth measured relative to reef crest.		

- b. The time-series of tidal elevations is combined with the time-series of storm surge for the 17 gauging stations using the relationship described in the previous section to produce a time-series of still-water levels.
- c. Ponding levels are computed, using the method presented by Seelig, using the time-series of deepwater wave heights and periods together with the still-water levels computed in Step b.
- d. The peak total water surface elevation contained in each of the 17 ponding level time-series is found and stored with its corresponding probability (i.e., the probability of that storm used in generating the storm surge and deepwater wave time-series).

Steps a through d were performed 100 times for each of the 168 storms contained in the ensemble. This procedure results in 16,800 events from which the stage-frequency relationships are developed.

The probability density function for each gauge was created by first selecting a number whose value is greater than the maximum ponding level computed for all 16,800 storms. This value is divided into a range of discrete intervals or bins. An interval of 0.1 ft was selected for this study. Second, the probability density for each bin is found by summing the probabilities of all 16,800 storms whose peak ponding level is within the range of levels for that particular bin. The cumulative density for a particular bin equals the probability associated with that bin in addition to the summation of probabilities of all bins associated with higher ponding levels. Figure 12 presents the stage-frequency relationships for Bile Bay. Figures for all stations are contained in Appendix A.

Wave Setup and Runup

Ponding levels presented in the stage-frequency relationships include the effects of wave setup at the reef, the superelevation of the still-water level caused by wave action due to waves breaking on the barrier reef. Another potential increase in water level is caused by wave setup on the beach of those waves which form within the lagoon system. This contribution to peak water

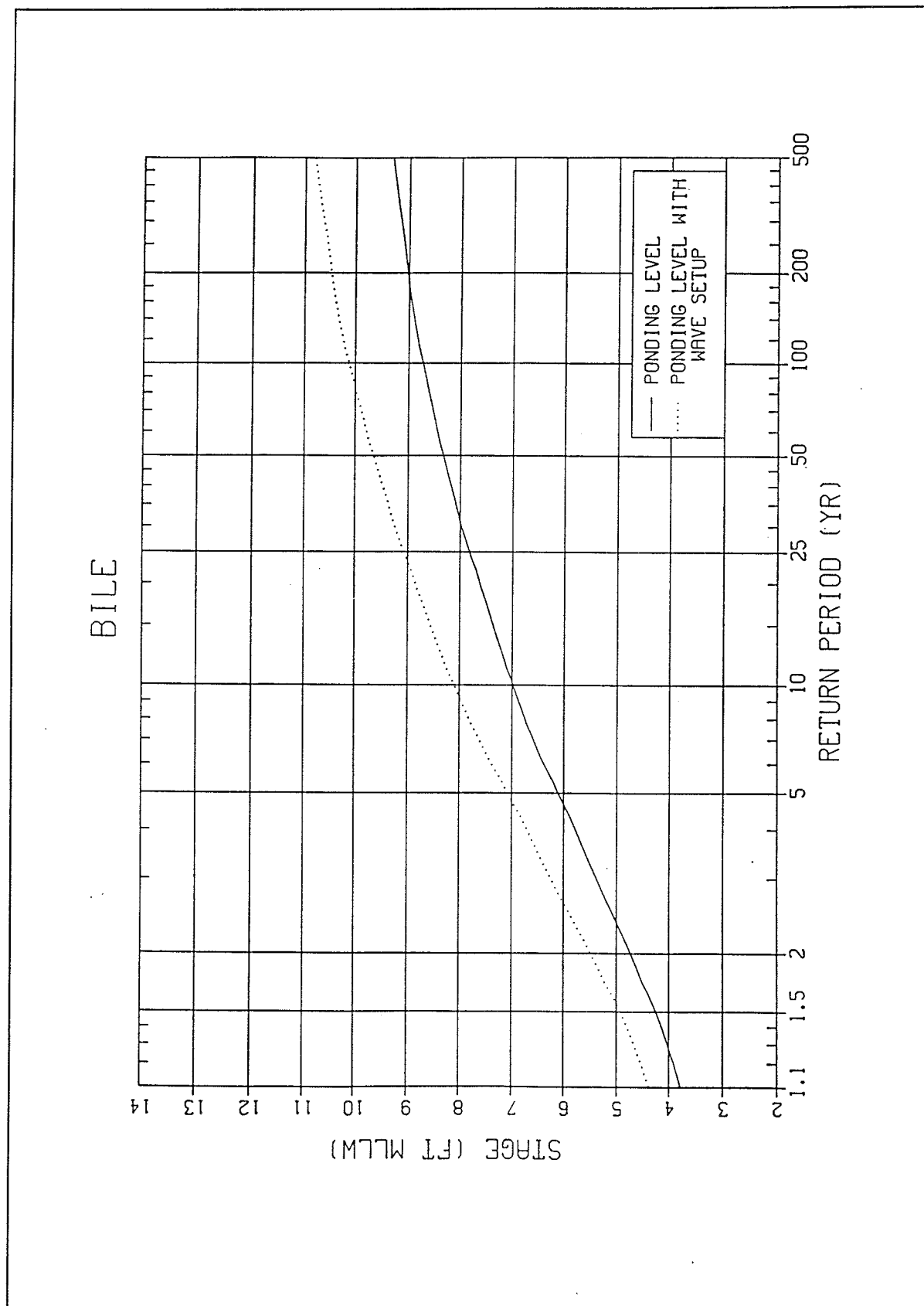


Figure 12. Stage-frequency relationship for Bile Bay

Table 5 Apra Harbor Tidal Constituents		
Constituent	Amplitude, ft	Epoch, deg
M ₂	0.722	220.5
S ₂	0.193	238.6
N ₂	0.157	203.0
K ₁	0.566	209.4
O ₁	0.380	186.8
Nu ₂	0.042	184.0
2N ₂	0.020	185.5
OO ₁	0.016	232.0
S ₁	0.037	317.6
M ₁	0.027	198.1
J ₁	0.030	220.7
P ₁	0.014	177.1
Q ₁	0.079	180.7
T ₂	0.011	238.6
P ₁	0.168	202.8
L ₂	0.040	242.7
K ₂	0.052	231.4

elevations, which are not included in the ponding levels, is caused by the re-forming and subsequent breaking of those waves which initially break on the reef.

Wave setup results when the pressure gradient of the sloping water surface (i.e., mean still-water level) is in equilibrium with the cross-shore directed radiation stress, which represents the gradient of momentum of incoming waves in the shoreward direction:

$$\frac{d\bar{\eta}}{dx} = -\frac{1}{\rho g d} \frac{dS_{xx}}{dx} \quad (7)$$

where η is the mean still-water level, ρ is water density, g is gravitational acceleration, S_{xx} is the cross-shore component of the cross-shore-directed radiation stress, d is depth, and x is the cross-shore distance.

Assuming linear wave theory, wave setup in the surf zone reduces to:

$$\frac{d\bar{\eta}}{dx} = -\frac{3}{16} \frac{1}{d+\bar{\eta}} \frac{d(H^2)}{dx} \quad (8)$$

where H is the wave height.

Wave setup was computed, using Equation 8, along 109 transects within the study area. Transects were distributed so as to provide an accurate representation of runup in the study area. Hence, a greater number of transects were placed in areas having abrupt changes in planform geometry. Furthermore, more transects were placed in developed areas, such as the village of Piga, as opposed to relatively underdeveloped areas, such as Liguana Point.

Transect information was taken from topographic maps supplied by POD. Transect lines were placed such that each line was approximately perpendicular to the 10- and 20-ft MSL contours, as opposed to the 0-ft MSL contour. With the still water level exceeding 7 ft msl, transects perpendicular to the 10- and 20-ft contours provide a more accurate representation of the sloping topography on which wave setup will take place. This is especially true in areas where the 10- and 20-ft contours are not parallel with the 0-ft contour, such as in the vicinity of hills.

In addition to the "secondary" wave setup, wave runup, the maximum water surface elevation caused by the uprush of water from a breaking wave, also contributes to the typhoon-induced peak water surface elevations; thus, this phenomenon was computed for the 100- and 500-year return periods.

Wave runup was computed using the computational procedures presented in the *Shore Protection Manual* (1984). The composite slope method, developed by Saville (1958), was used to account for changes in grade along a given profile. Parameters required by this procedure include water depth (still-water elevation), together with the wave height and period of the re-formed wave.

Many of the figures contained in the *Shore Protection Manual* for computing runup were developed using physical models with smooth slopes. Therefore, a roughness and porosity correction factor has been used in the runup calculations to account for differing land characteristics, such as foliage, in the study area. Roughness coefficients for each transect were estimated using photographs provided by POD, and were based on the percentage of slope length having certain characteristics (e.g., a roughness coefficient of 0.8 was assigned to developed areas, whereas a coefficient of 0.7 was used for areas with dense foliage).

The wave height used in this procedure was assumed equal to the breaking wave height, which is controlled to a great extent by the water depth in a lagoon. Wave height was estimated by:

$$H_b = \gamma_b h_b \quad (9)$$

where H_b is the breaking wave height, γ_b is the breaking depth index, and h_b is the breaking water depth. A breaking depth index of 0.78, typical for relatively flat lagoons, was used in this procedure.

In contrast to other regions in the study area, bathymetry in the vicinity of Inarajan Bay is relatively deep, with water depths exceeding 60 ft, and the bay does not have a barrier reef at its entrance serving as a breakwater. Because the average deepwater wave heights associated with the 100-year and 500-year peak water elevations are 46.9 ft and 52.9 ft, respectively, deepwater waves are capable of propagating into and breaking within the bay. Thus, the Numerical Model of the LONGshore current (NMLONG) was used for estimating the 100-year and 500-year peak water surface elevations in the vicinity of Inarajan Bay.

Input required by model NMLONG includes elevations and distances along the transect running along the bay's longitudinal axis, wave height, period, and combined surge and tide water level. Wave data and combined surge and tide data were extracted from the wave and storm surge model output used in generating the stage-frequency relationships, and are representative of those used in computing the 100-year and 500-year ponding levels. In computing the 100-year peak water elevations, the deepwater wave height and period were 46.9 ft and 12.5 sec, respectively, whereas the combined surge and tide water level was 4.1 ft. Deepwater wave height and period were 52.9 ft and 14.3 sec, respectively, and the combined surge and tide water level was 4.6 ft for the 500-year peak water elevations.

In using model NMLONG, it was assumed that deepwater waves entering the bay would propagate along the bay's longitudinal axis. Furthermore, for transects perpendicular to this axis, peak water levels were assumed equal to the wave crest elevation computed with the model. These transects are 15-6, 16-1, 16-6, and 16-7. For transects 16-2 through 16-5, peak water surface elevations were computed using the wave runup algorithm described above.

For transects 15-1 through 15-3 and 16-10 through 17-1, peak water surface elevations were found by using model NMLONG to compute the wave height and setup within the reef flat. These elevations were then adjusted to account for the effects of wave runup.

For transects 15-4, 15-5, 16-8, and 16-9, peak water surface elevations were assumed equal to the wave crest elevation computed on the seaward edge of the barrier reef. Because of the large wave heights and sharp bottom gradients, model NMLONG failed to produce reliable results within the reef flat; thus, wave runup could not be computed for these transects.

Table 6
100- and 500-year Ponding and Wave Setup Elevations

Station	100-yr Return Period		500-yr Return Period	
	Ponding level (ft msl)	Wave Setup (ft msl)	Ponding level (ft msl)	Wave setup (ft msl)
Bile	8.7	10.2	9.4	10.9
Bingot	9.4	10.9	10.3	11.9
Merizo	10.3	12.0	11.7	13.5
Piga	10.4	12.1	11.2	13.0
Aba	9.8	11.4	10.6	12.3
Manell	10.2	11.8	10.8	12.5
Julog	10.2	11.8	10.9	12.7
Sumay	9.7	11.3	10.5	12.2
Achang	9.3	10.7	9.9	11.5
Argrigan	9.3	10.7	9.9	11.5
Ajayan	8.9	10.3	9.6	11.1
Guijen	8.9	10.3	9.5	11.0
Acho	9.2	10.7	9.8	11.4
Agfayan	8.9	10.3	9.8	11.3
Asgon	8.8	10.2	9.6	11.1
Inarajan	9.1	10.5	9.8	11.4
Guaifan	9.1	10.5	10.4	12.0

Table 7
Wave Setup and Runup Elevations

Profile	100-yr Return Period		500-yr Return Period	
	Wave Setup (ft msl)	Wave Runup (ft msl)	Wave Setup (ft msl)	Wave Runup (ft msl)
1-1	9.24	10.42	9.49	11.03
1-2	9.48	10.34	9.66	11.08
1-3	9.30	10.33	9.83	11.12
1-4	9.52	10.48	10.00	11.23
1-5	9.68	10.69	10.17	11.49
1-6	9.71	11.05	10.34	11.85
2-1	9.49	11.69	10.49	12.53
2-2	9.63	11.11	10.69	11.85
2-3	9.77	11.16	10.89	11.71
2-4	9.91	11.42	11.09	12.10
2-5	10.05	12.11	11.29	12.82
2-6	10.19	11.98	11.49	12.83
2-7	10.33	11.38	11.69	12.85
2-8	11.13	11.70	11.89	13.04
3-1	10.46	11.91	11.89	13.04
3-2	10.48	12.48	11.87	13.57
3-3	10.50	12.59	11.85	13.59
3-4	10.52	11.71	11.83	12.75
3-5	10.54	11.73	11.81	12.73
3-6	10.56	11.72	11.79	12.71
4-1	10.58	11.74	11.77	12.69
4-2	10.59	11.75	11.75	12.67
4-3	10.60	11.79	11.73	12.65
4-4	10.62	11.78	11.71	12.63
4-5	10.63	11.82	11.69	12.61
4-6	10.65	11.81	11.67	12.59
4-7	10.66	11.82	11.65	12.57
4-8	10.68	11.84	11.62	12.56
4-9	10.69	11.85	11.59	12.51
(Sheet 1 of 4)				

Table 7 (Continued)

Profile	100-yr Return Period		500-yr Return Period	
	Wave Setup (ft msl)	Wave Runup (ft msl)	Wave Setup (ft msl)	Wave Runup (ft msl)
5-1	10.15	11.61	10.89	12.35
5-2	10.14	11.40	10.92	12.01
5-3	10.26	11.44	10.95	12.07
5-4	10.31	11.31	10.98	11.95
5-5	10.47	11.35	11.01	12.00
5-6	10.61	11.39	11.04	12.03
5-7	10.64	11.44	11.07	12.06
6-1	10.60	11.76	11.09	12.25
6-2	10.78	11.76	11.12	12.26
6-3	10.51	11.76	11.15	12.27
6-4	10.69	11.76	11.18	12.27
6-5	10.69	11.76	11.21	12.28
6-6	11.06	11.76	11.24	12.26
7-1	10.91	11.76	11.29	12.21
7-2	10.58	11.52	11.23	12.08
7-3	10.65	11.38	11.17	12.04
7-4	10.45	11.34	11.11	12.01
7-5	10.33	11.23	11.05	11.91
7-6	10.31	11.19	10.99	11.87
7-7	11.03	11.15	10.93	11.83
7-8	10.96	11.12	10.86	11.81
8-1	10.14	11.09	10.79	11.78
8-2	10.52	11.05	10.71	11.77
8-3	10.10	11.01	10.63	11.75
8-4	10.26	10.98	10.55	11.73
8-5	9.67	10.94	10.47	11.70
8-6	9.66	10.90	10.39	11.67
8-7	9.58	10.86	10.31	11.64
8-8	10.20	10.81	10.25	11.51

(Sheet 2 of 4)

Table 7 (Continued)				
Profile	100-yr Return Period		500-yr Return Period	
	Wave Setup (ft msl)	Wave Runup (ft msl)	Wave Setup (ft msl)	Wave Runup (ft msl)
8-9	10.23	10.94	10.17	11.58
9-1	10.04	11.93	10.09	12.52
9-2	9.82	11.30	10.09	11.92
9-3	10.29	10.78	10.09	11.29
9-4	9.66	10.78	10.09	11.29
9-5	10.19	10.78	10.09	11.29
9-6	9.71	11.34	10.09	11.95
10-1	9.29	11.33	10.09	11.72
10-2	9.41	11.78	9.99	12.36
10-3	9.77	10.76	9.89	11.26
10-4	9.27	10.48	9.79	11.07
11-1	10.04	10.38	9.69	11.05
11-2	10.16	10.38	9.67	11.03
11-3	8.94	10.38	9.65	11.01
11-4	8.89	11.68	9.63	12.30
11-5	8.90	10.38	9.61	10.97
12-1	9.18	10.38	9.59	10.95
12-2	10.24	10.42	9.65	10.99
12-3	9.13	10.47	9.71	11.40
12-4	9.90	10.52	9.77	11.08
12-5	9.99	11.03	9.87	11.66
12-6	10.27	10.62	9.89	11.17
12-7	9.86	10.85	9.94	11.40
13-1	9.71	10.83	9.99	11.36
13-2	10.34	10.60	9.97	11.20
13-3	9.68	10.56	9.95	11.21
13-4	9.10	10.34	9.93	11.01
13-5	9.11	10.11	9.91	10.88
13-6	9.26	11.19	9.90	12.01
(Sheet 3 of 4)				

Table 7 (Concluded)				
Profile	100-yr Return Period		500-yr Return Period	
	Wave Setup (ft msl)	Wave Runup (ft msl)	Wave Setup (ft msl)	Wave Runup (ft msl)
14-1	8.90	10.95	9.89	11.82
14-2	9.32	11.87	9.84	15.03
14-3	9.51	11.39	9.79	12.12
14-4	9.46	10.31	9.47	11.10
15-1	12.10	14.60	15.40	18.30
15-2	15.10	17.30	18.30	20.80
15-3	14.50	18.30	17.50	21.30
15-4		20.30		24.40
15-5		20.30		24.40
15-6		26.05		26.30
16-1		18.15		18.55
16-2		12.10		14.10
16-3		12.10		14.10
16-4		12.10		14.10
16-5		12.10		14.10
16-6		19.65		19.90
16-7		26.10		26.35
16-8		20.70		23.90
16-9		19.10		22.90
16-10	13.40	14.90	16.10	17.90
16-11	9.30	10.60	11.40	12.90
17-1	9.30	13.00	11.40	15.40
(Sheet 4 of 4)				

6 Summary and Conclusions

A typhoon stage-frequency analysis was conducted for the southern coast of Guam. The area of interest for this analysis extends from Bile Bay, residing on the southwest side of the island, to Guaifan Point, which is located on the southeast side. Three models were employed in this analysis, including a wind and atmospheric pressure field model, a long-wave hydrodynamic model, and a deepwater wave model. The Standard Project Hurricane (SPH) model was used for generating typhoon-induced wind and atmospheric pressure fields supplied to the hydrodynamic and wave models.

The WES Implicit Flooding model (WIFM) was used for simulating the long-wave hydrodynamic processes in the study area. This program employs a two-dimensional, depth-integrated finite difference solution of the continuity and Navier-Stokes equations. This model contains features for simulating flooding and drying of low-lying areas and subgrid flow boundaries, such as reefs or small barrier islands.

The WIFM model was calibrated by adjusting local bottom friction coefficients in order that model-generated water surface level time-series favorably matched those reconstructed from NOAA-published tidal constituents for Apra Harbor. Comparisons were made at five locations along the southern shore of the island. Parametric and nonparametric statistical tests were used to quantitatively assess the model's accuracy. Furthermore, model validation was achieved by performing a storm surge simulation of Typhoon Russ, which impacted the study area in December 1990.

Model SPH is a two-dimensional, parametric model developed in a stretched Cartesian coordinate system for estimating wind and atmospheric pressure fields generated by hurricanes. Based on the SPH criteria developed by NOAA (1979), the SPH represents a steady-state, hypothetical hurricane defined by a set of 10 interrelated parameters, such as maximum wind speed.

These parameters were obtained by analyzing historical typhoon data using a joint probability method. Synthetic storms based on these parameters, which are representative of those storms which have occurred in the region, are subsequently used for generating the wind and atmospheric pressure fields by the SPH model.

A total of 168 typhoons were simulated using the hydrodynamic and wave models. Each time-series of storm surge was combined with 100 randomly chosen time-series of tidal elevations to form 100 time-series of still-water levels, effectively increasing the total number of simulated events from 168 to 16,800.

Using an empirical relationship, each time-series of wave heights and periods was combined with the 100 time-series of still-water levels. Peak water surface elevations were extracted from each combined time-series and, with the probability assigned to that particular storm, stage-frequency relationships were generated. Stage-frequency relationships were determined at 17 locations within the study area. Wave setup and runup were also investigated. These phenomena were computed along 109 transects in the study area.

References

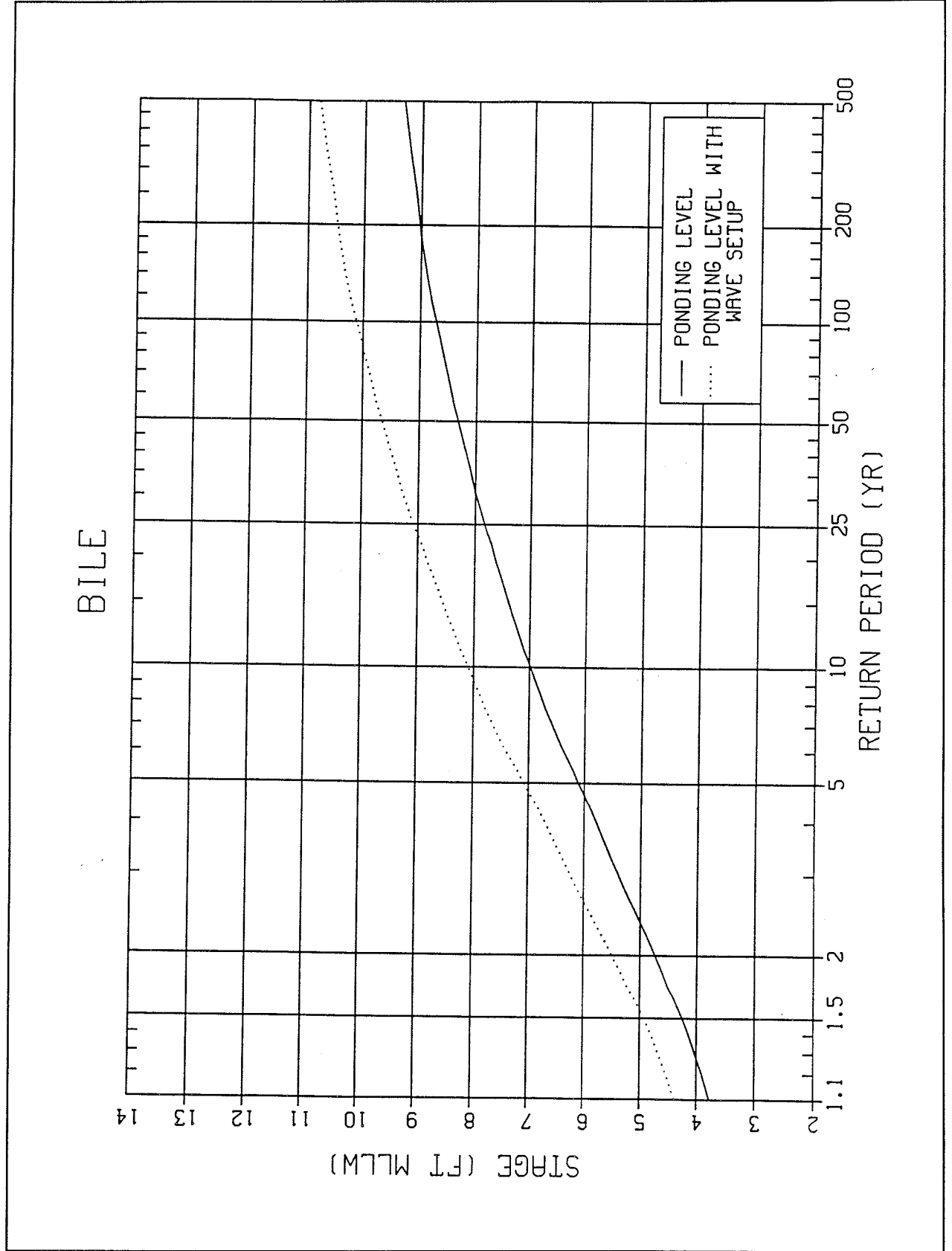
- Cialone, M. A., Mark, D. J., Chou, L. W., Leenknecht, D. A., Davis J. E., Lillycrop, L. S., Jensen, R. E., Thompson, E. F., Gravens, M. B., Rosati, J. D., Wise, R. A., Kraus, N. C., and Larson, P. M. (1991). "Coastal Modeling System (CMS) User's Manual," Instruction Report CERC-91-1, U.S. Army Engineer Waterways Experiment Station, Vicksburg, MS.
- Garratt, J. R. (1977). "Review of drag coefficients over oceans and continents," *Monthly Weather Review* 105, 915-929.
- Hess, K., and Bosley, K. (1991). "Validation of a Tampa Bay circulation model," *2nd International Conference on Estuarine and Coastal Modeling*, Tampa, FL, 13-15 November 1991.
- National Oceanic and Atmospheric Administration. (1979). "Meteorological criteria for standard project hurricane and probable maximum hurricane wind fields, Gulf and east coasts of the United States," Technical Report NWS 23, National Weather Service, Washington, DC.
- Saville, T., Jr. (1958). "Wave Runup on Composite Slopes," *Proceedings of Sixth Conference on Coastal Engineering*, American Society of Civil Engineers, Council on Waves.
- Schwiderski, E. W., Szeto, L. T. (1981). "The NSWC global ocean tide data tape, its features and application, random-point tide program," Technical Report NSWC 81-254, Naval Surface Weapons Center, Dahlgren, VA.
- Seelig, W. N. (1983). "Laboratory study of reef-lagoon system hydraulics," *Journal of Waterway, Port, Harbors, ASCE*, 109(4), 380-391.
- Shore protection manual*. (1984). 4th ed., 2 Vol, U.S. Army Engineer Waterways Experiment Station, U.S. Government Printing Office, Washington, DC.
- Tracy, B. A. (1993). "QTS AW (Quick Typhoon Surge and Waves)," WIS Report 31, U.S. Army Engineer Waterways Experiment Station, Vicksburg, MS.

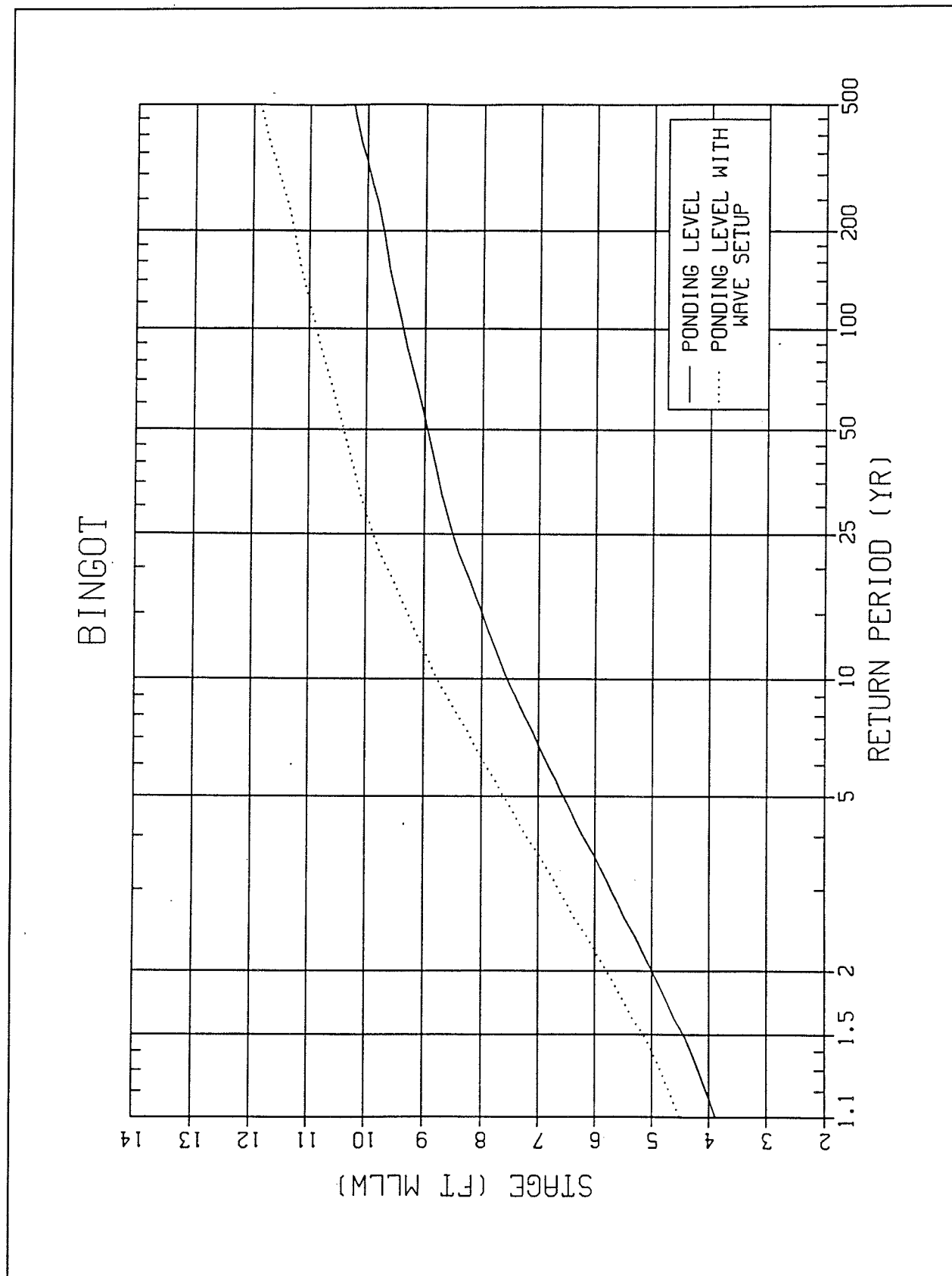
Weir, R. C. (1983). "Tropical storms affecting Guam (1671 - 1980)," Technical Note, U.S. Naval Oceanography Command Center/Joint Typhoon Warning Center, San Francisco, CA.

Appendix A

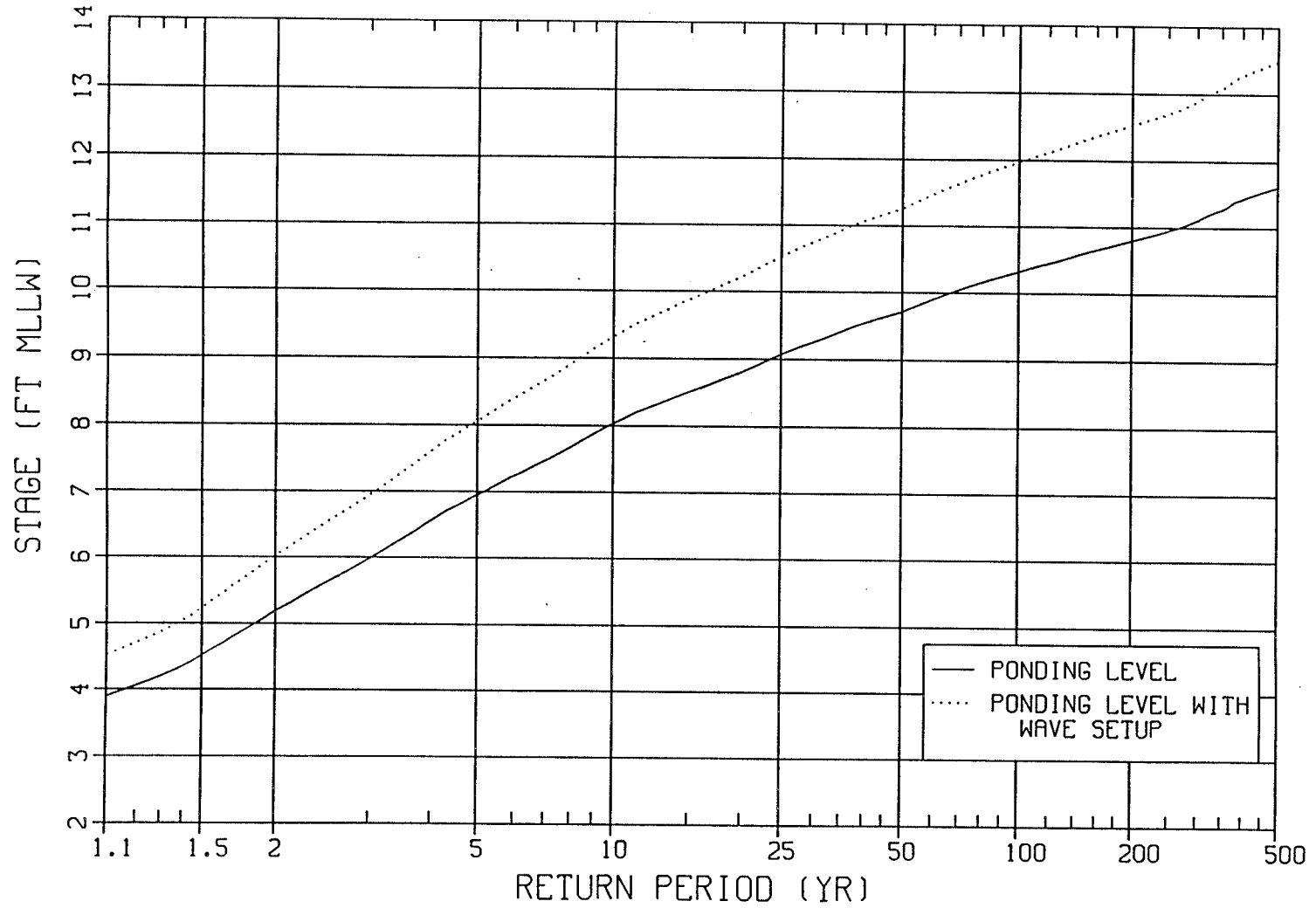
Stage-Frequency Relationship

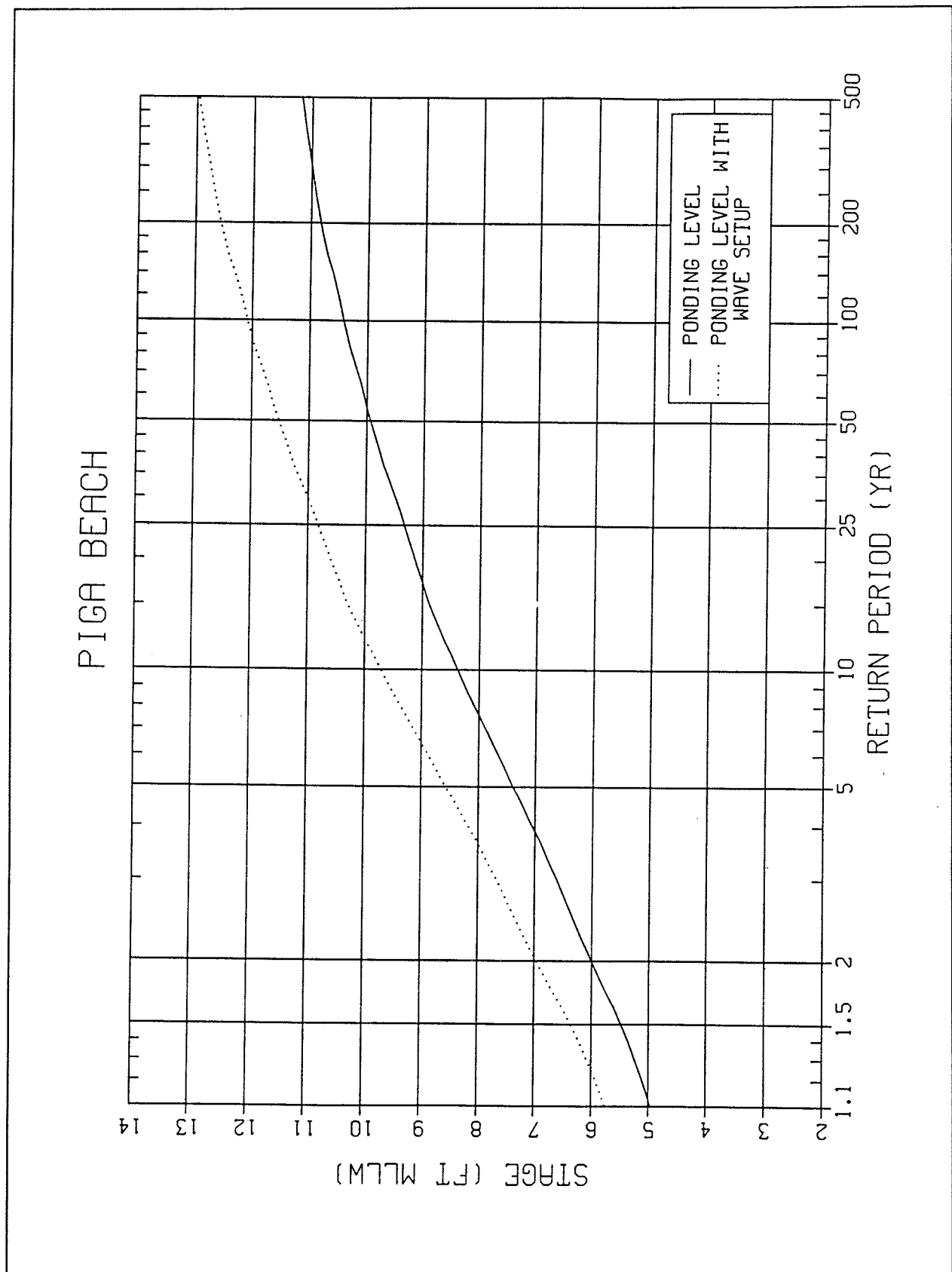
Figures



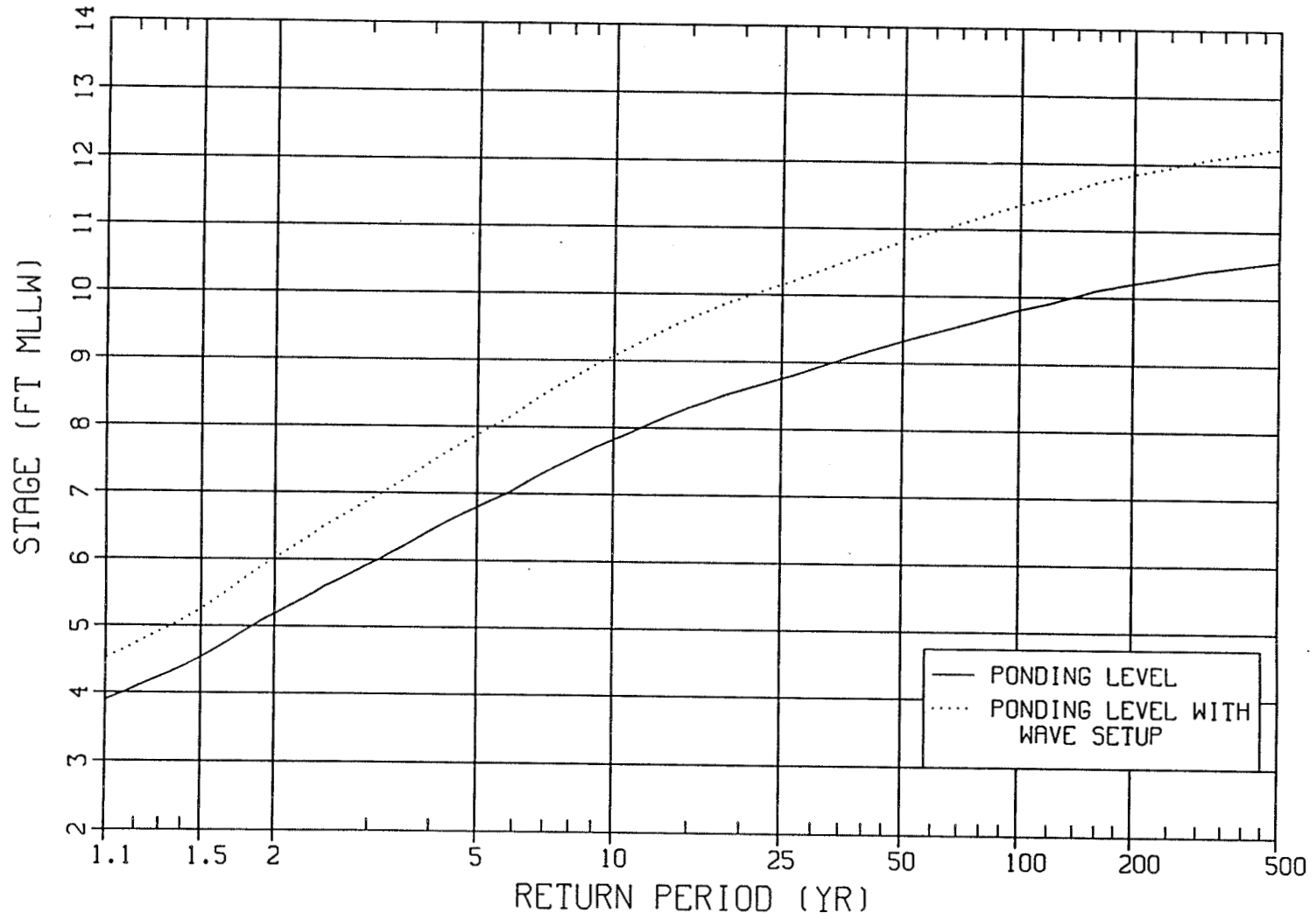


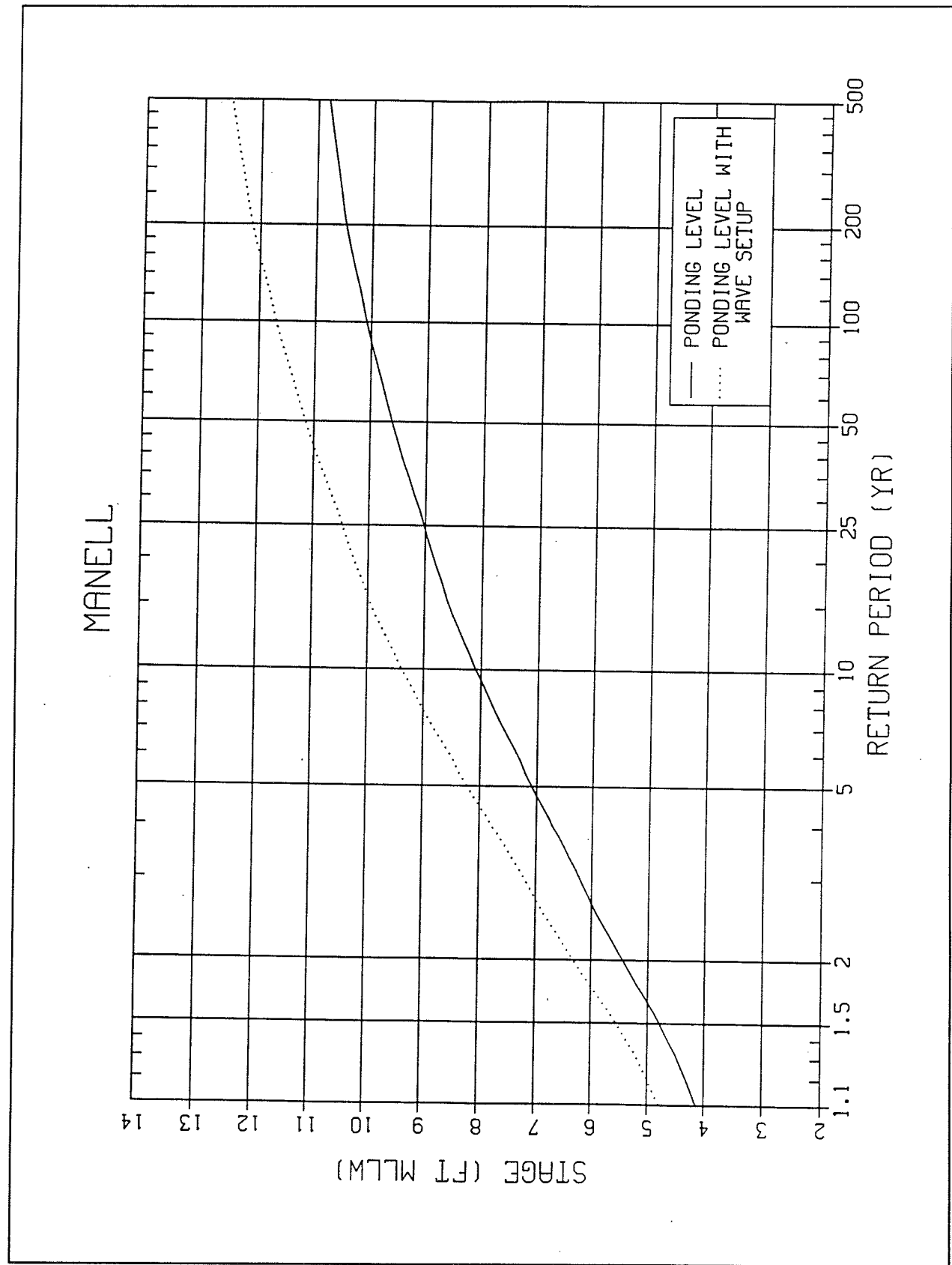
MERIZO



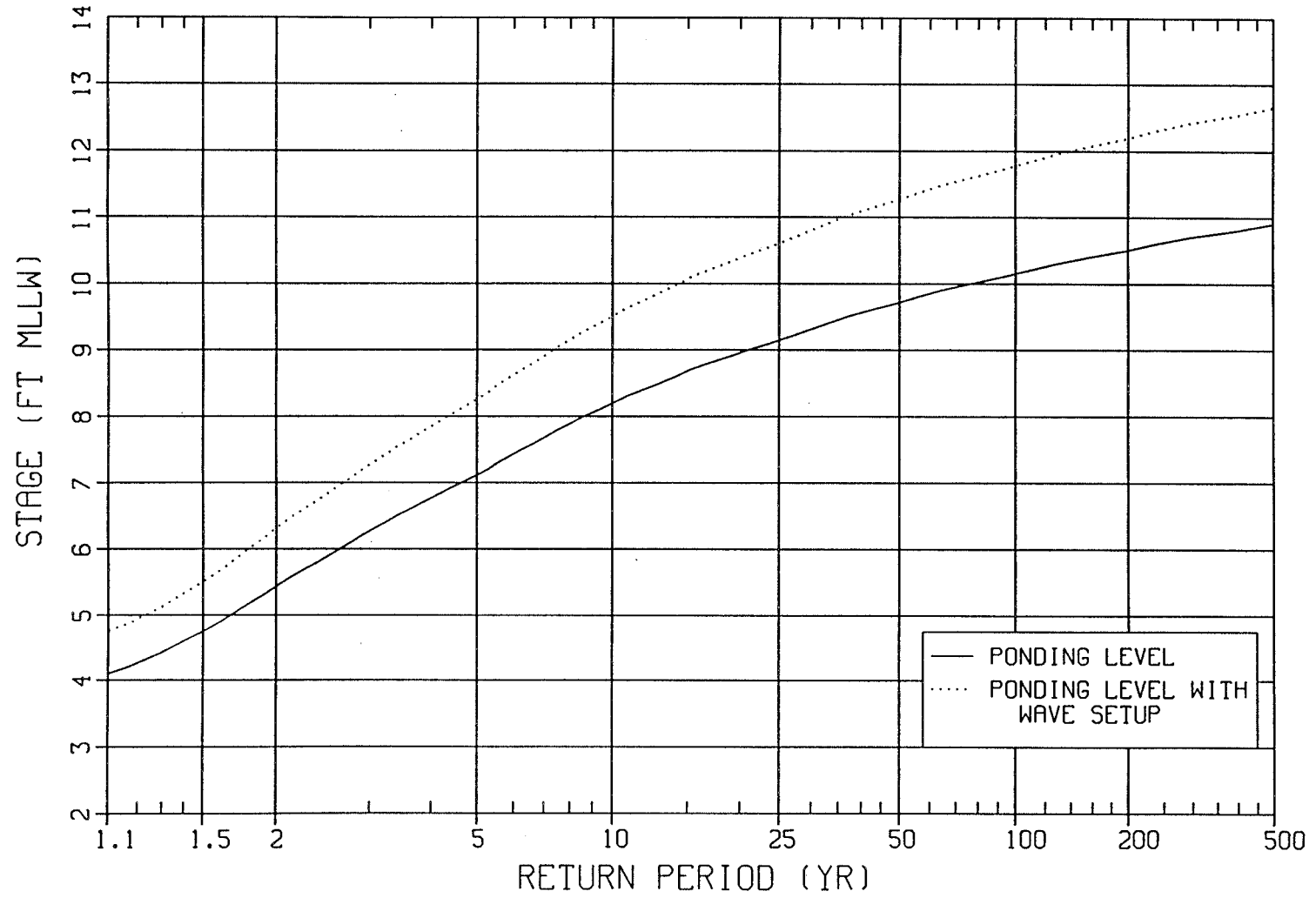


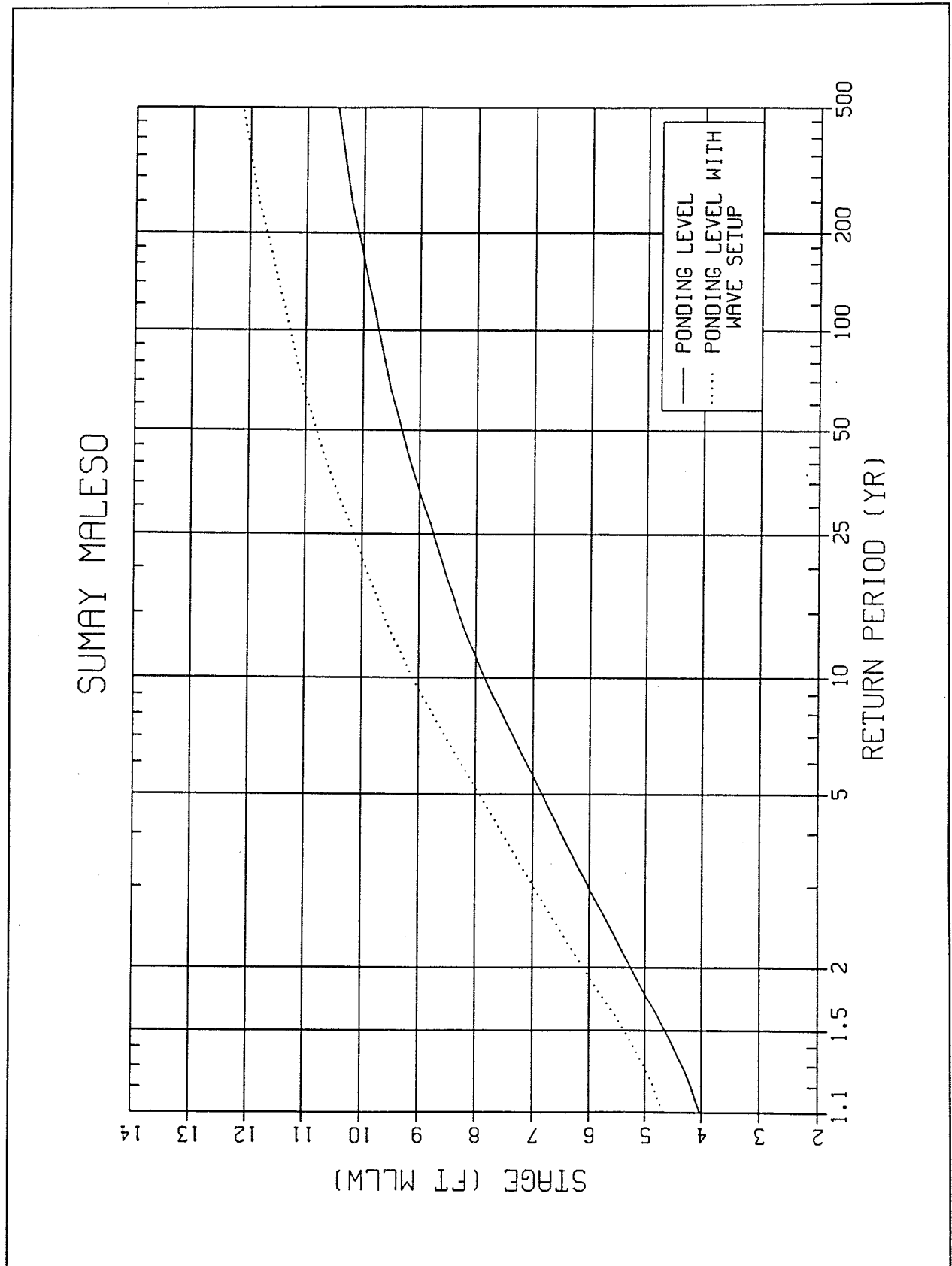
ABA BEACH

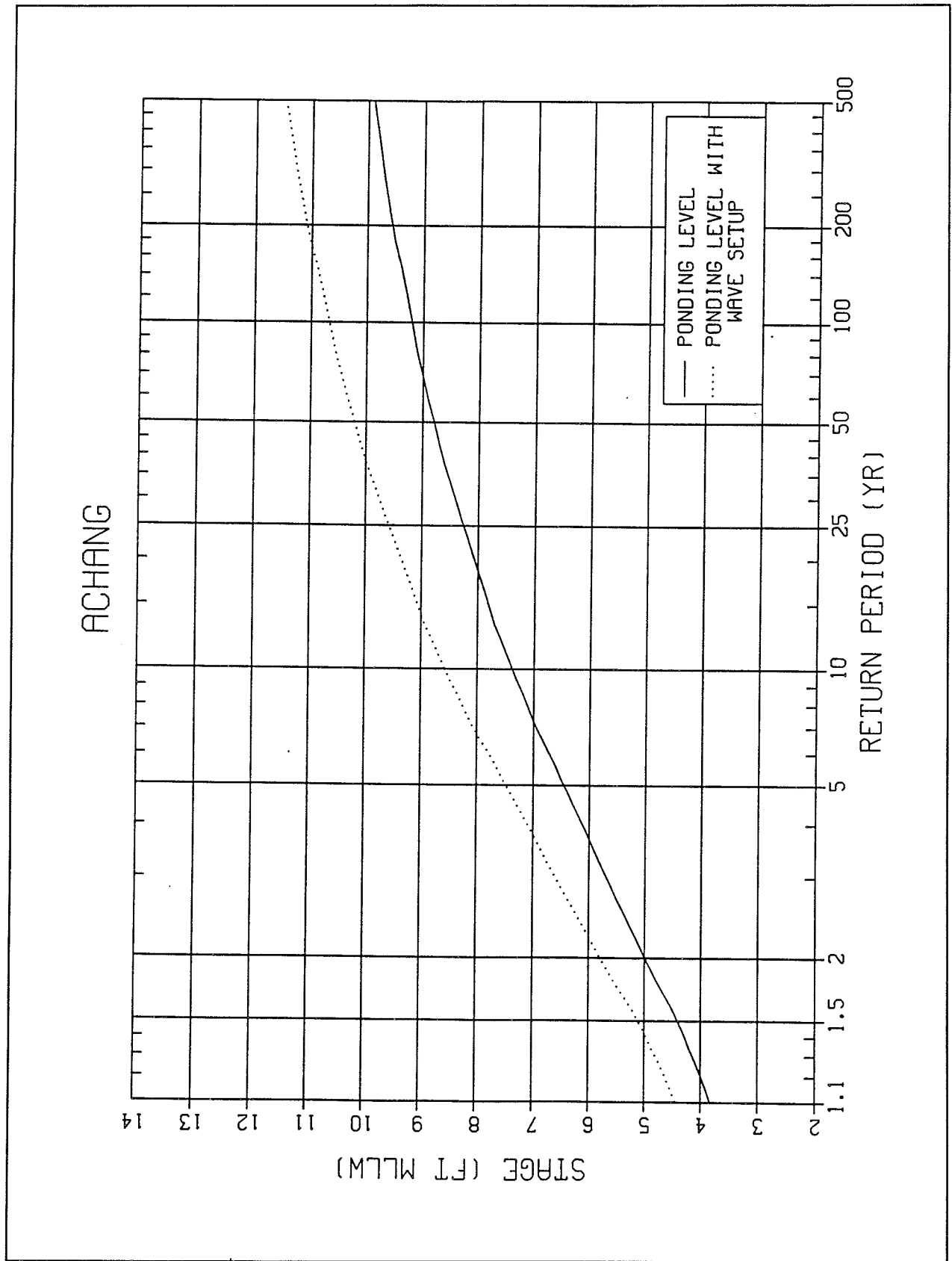


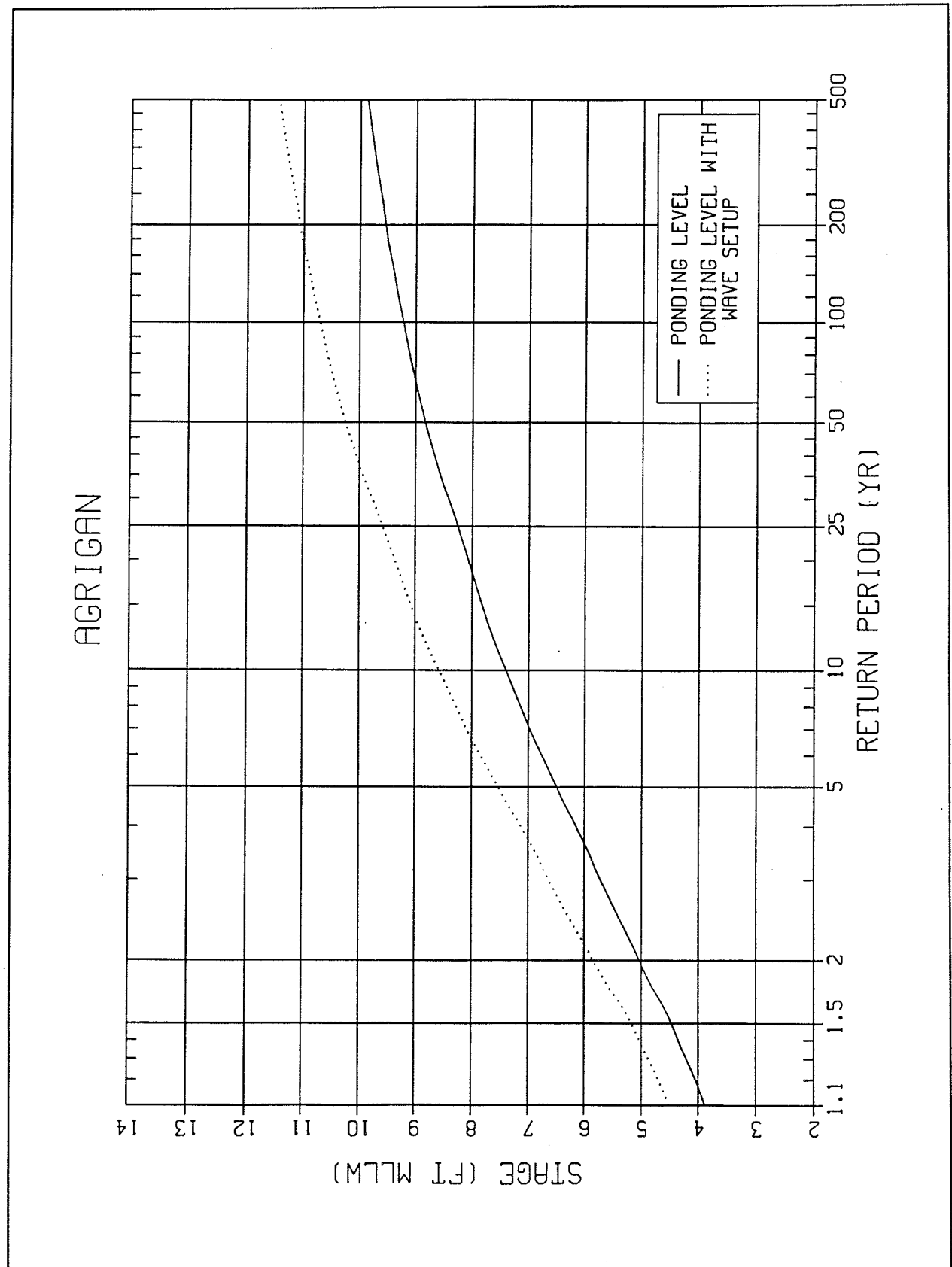


JULOG

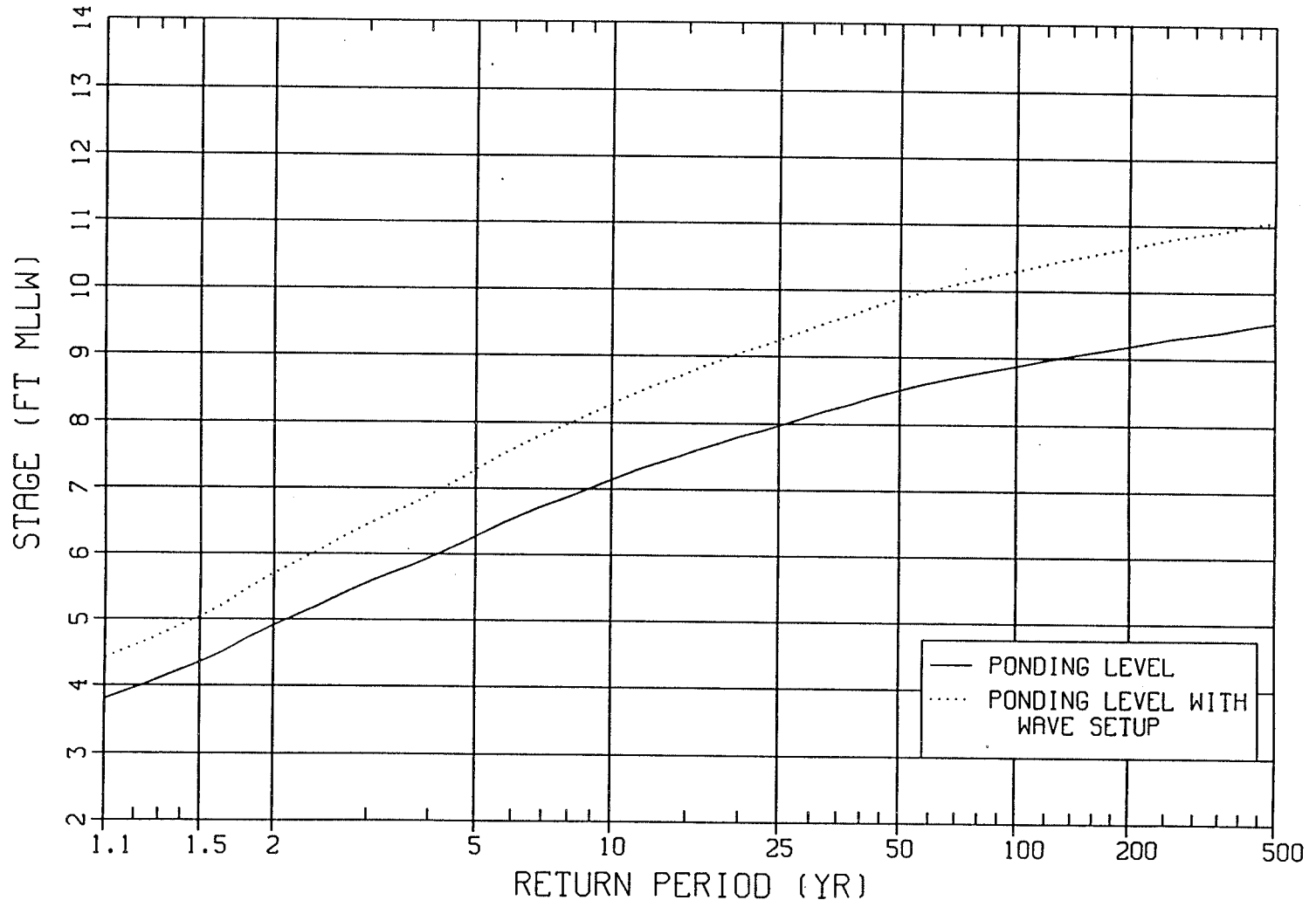


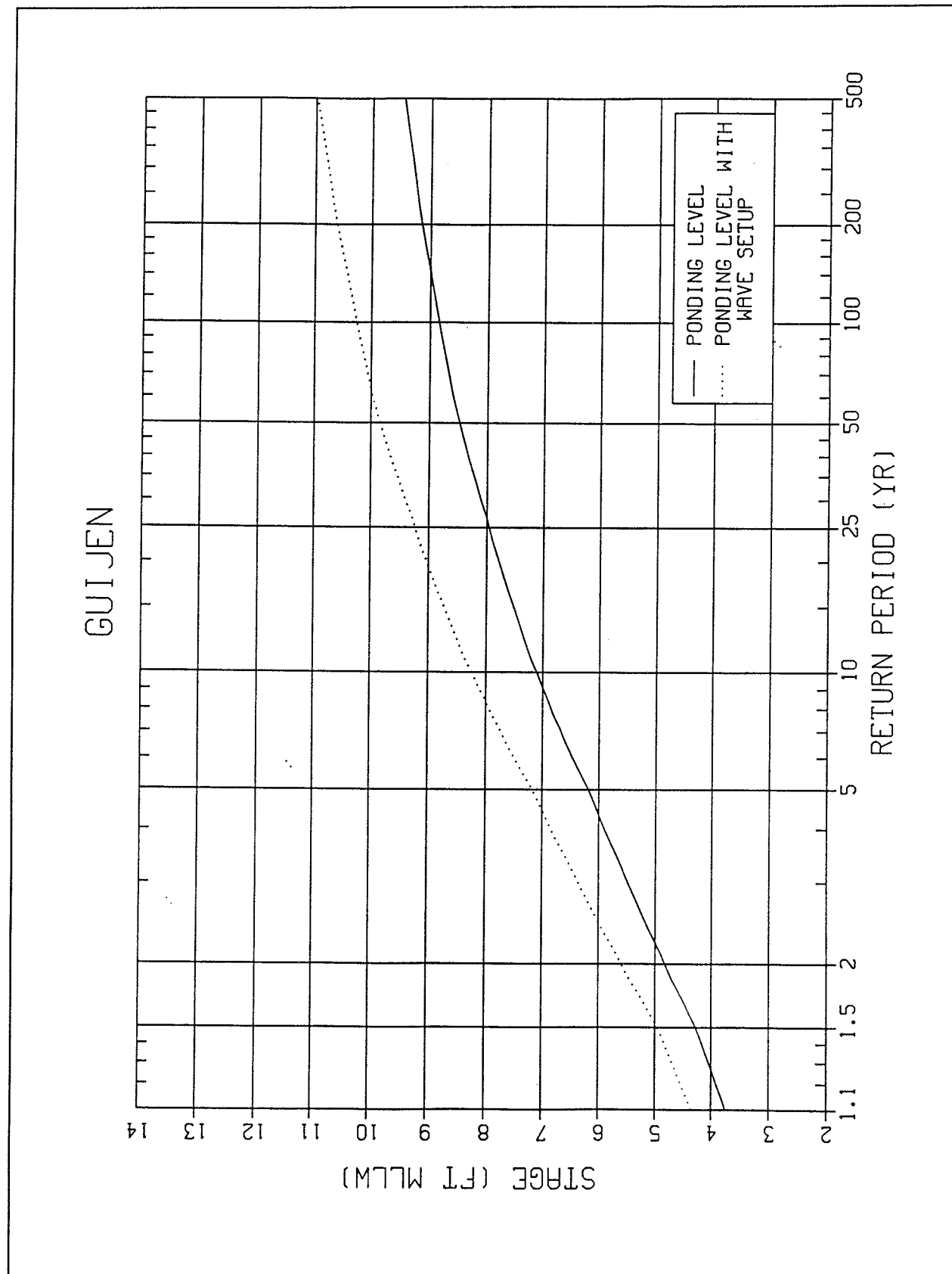




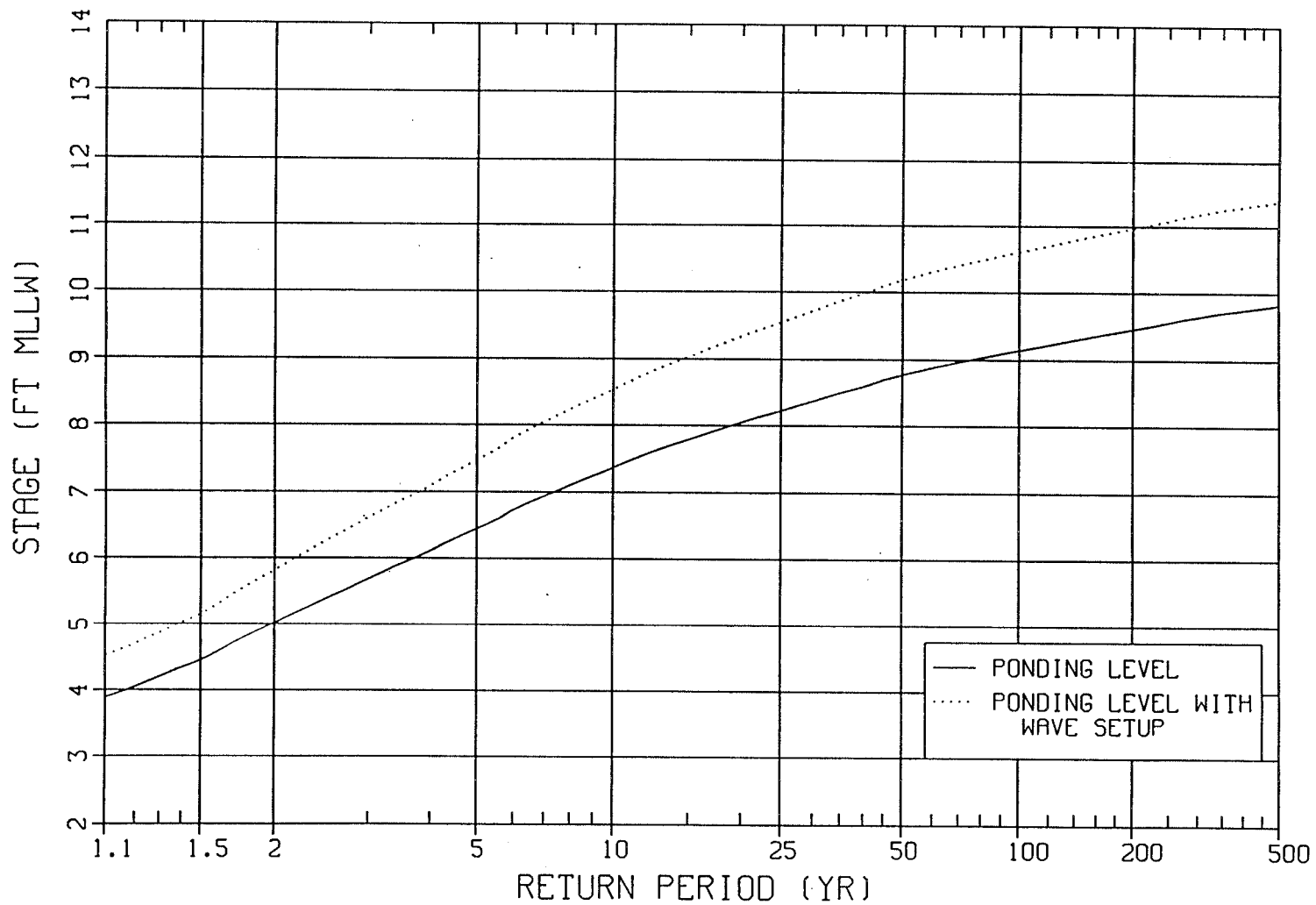


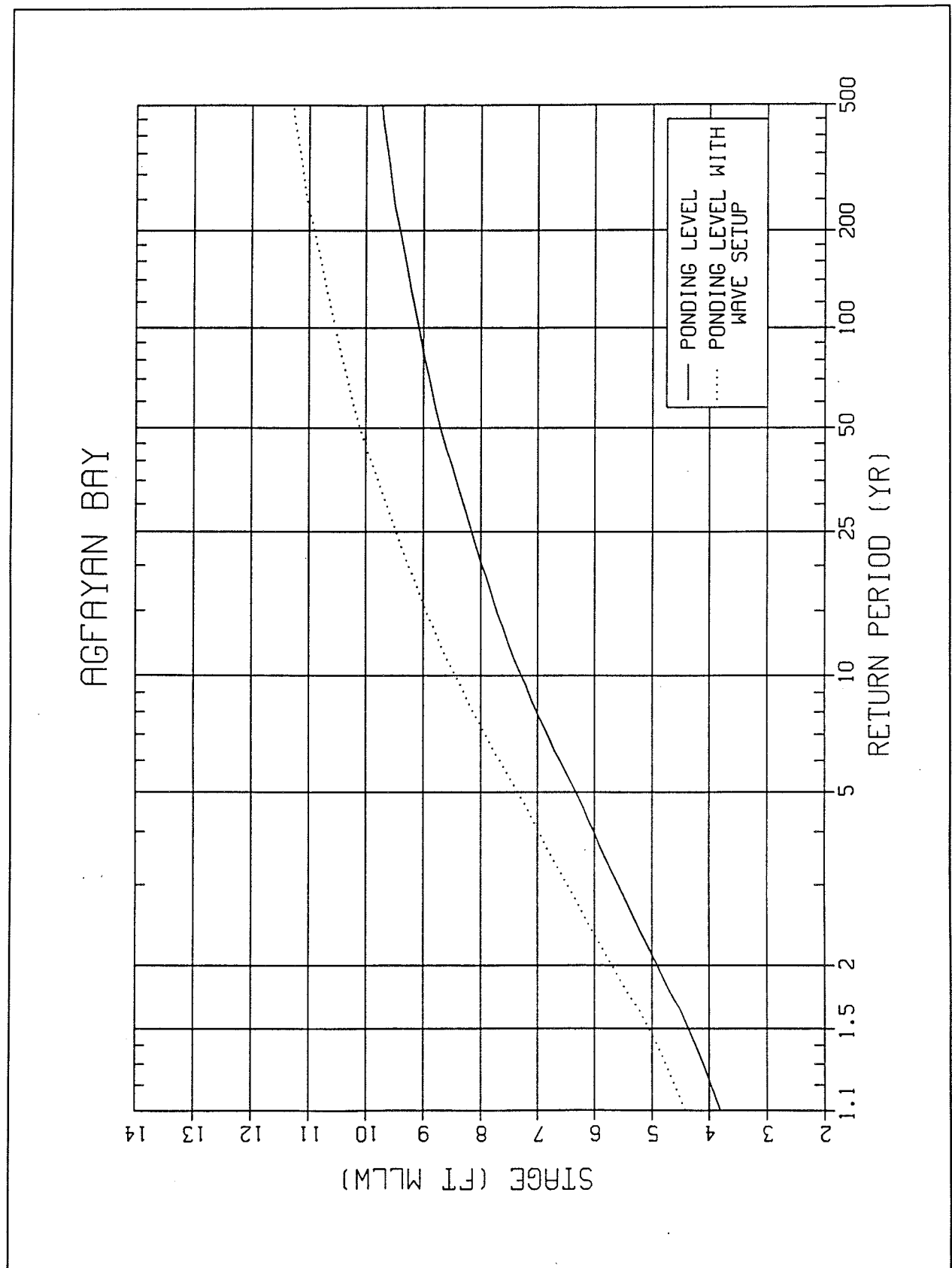
AJAYAN BAY

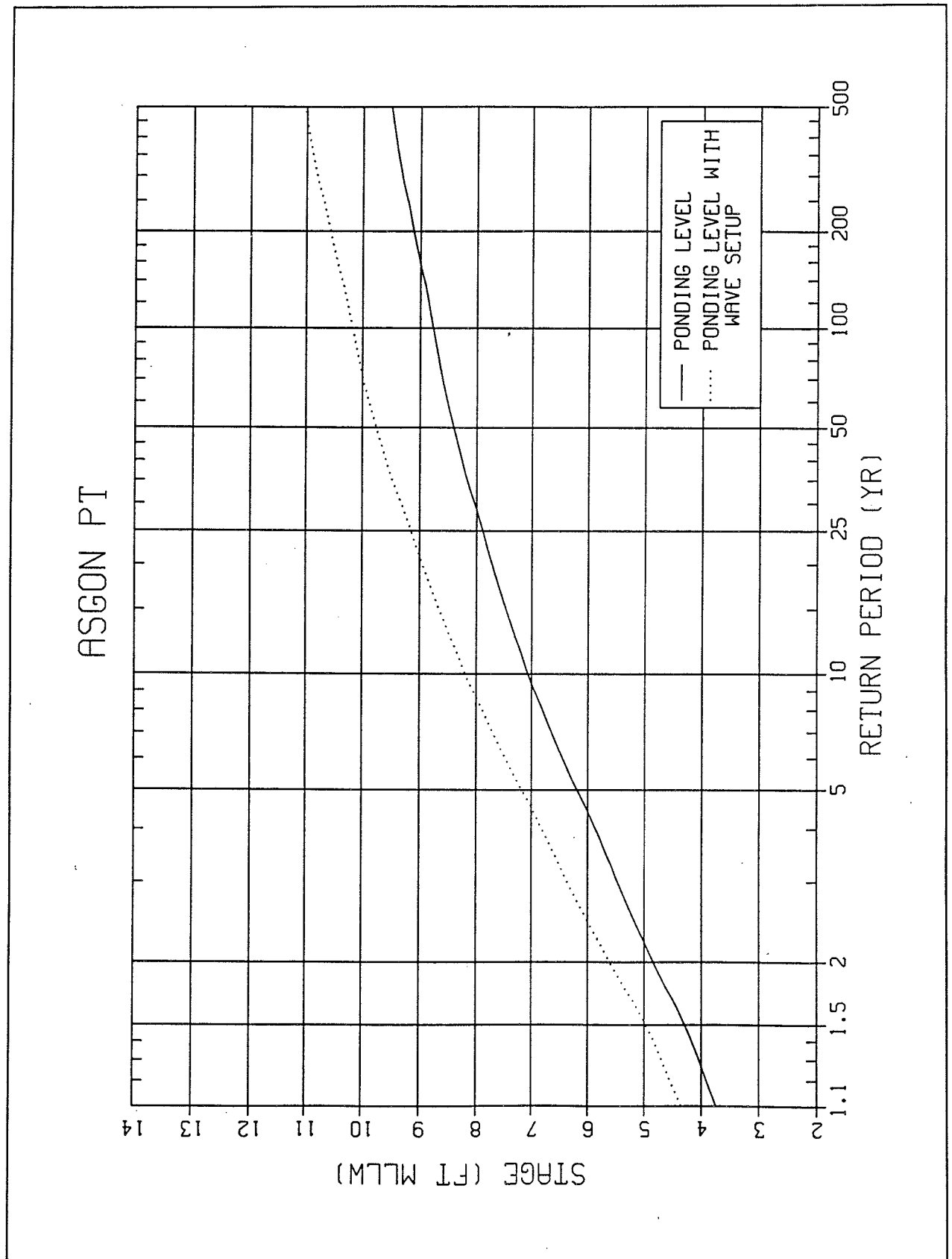


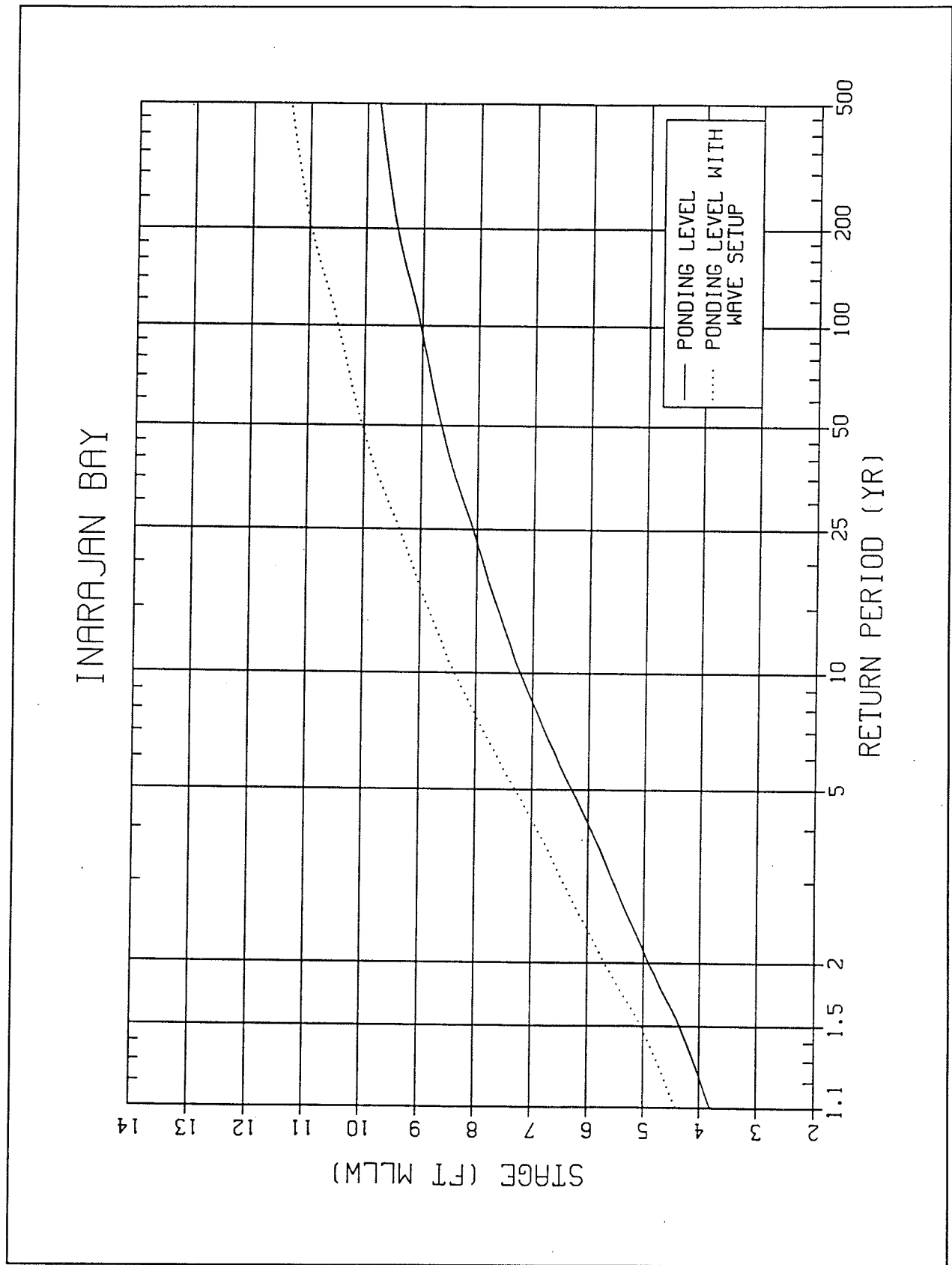


ACHO PT

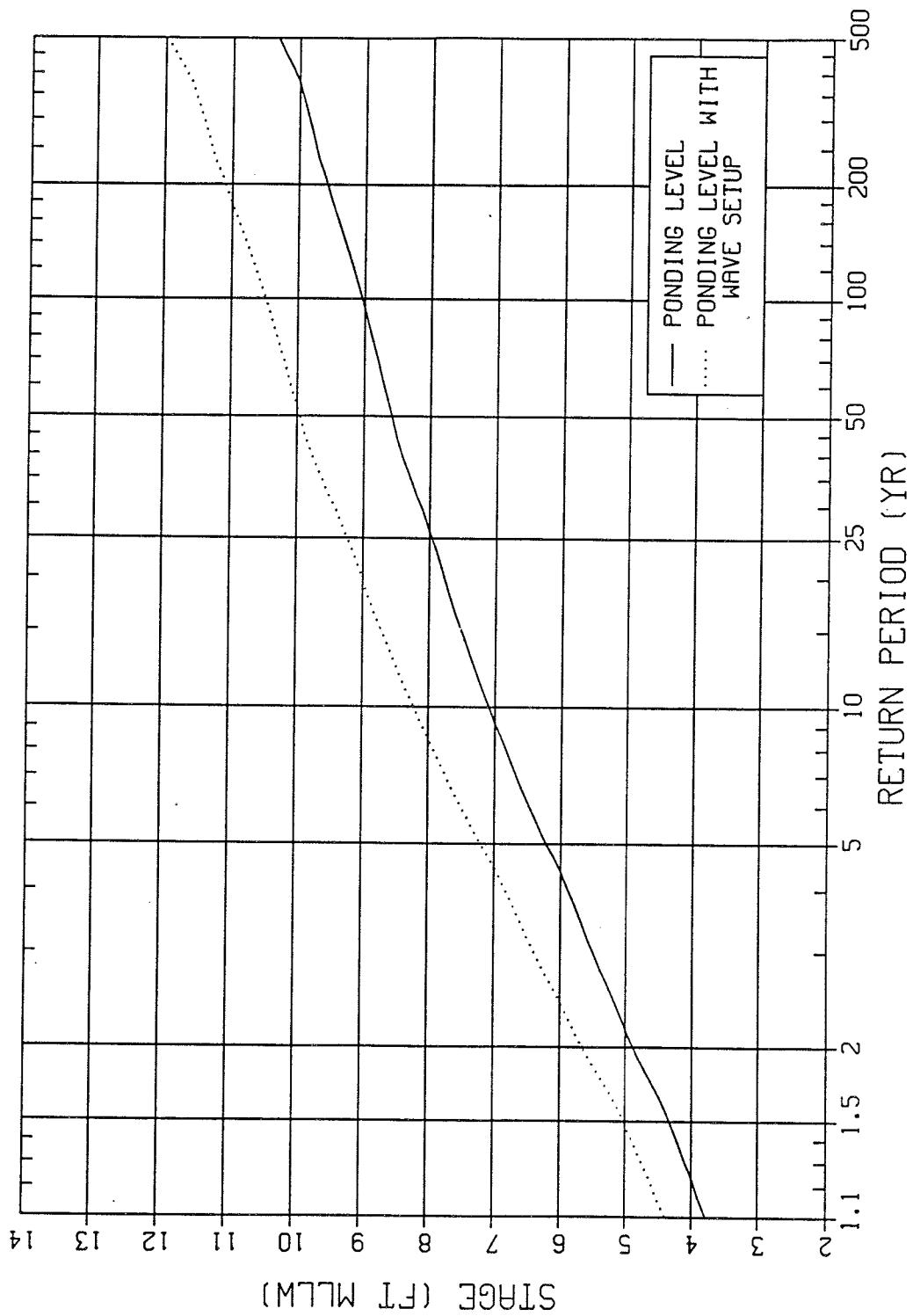








GUAIFAN



Appendix B

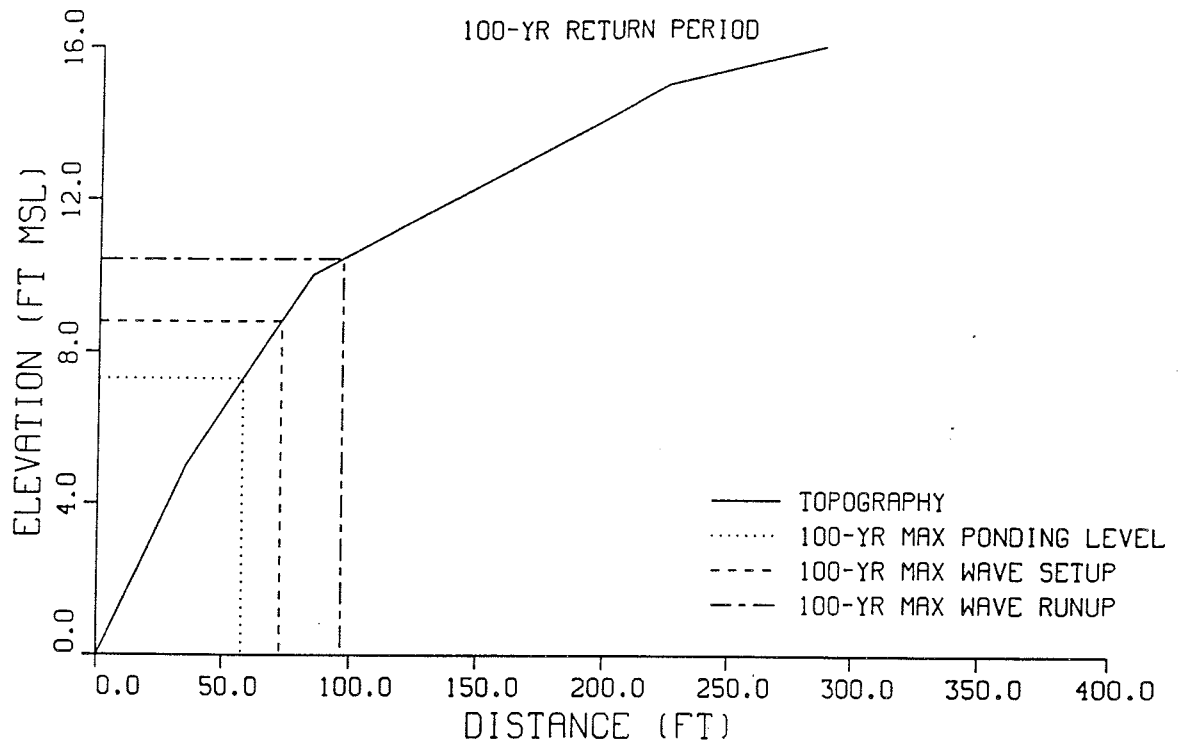
Wave Setup and Runup Profile

Figures

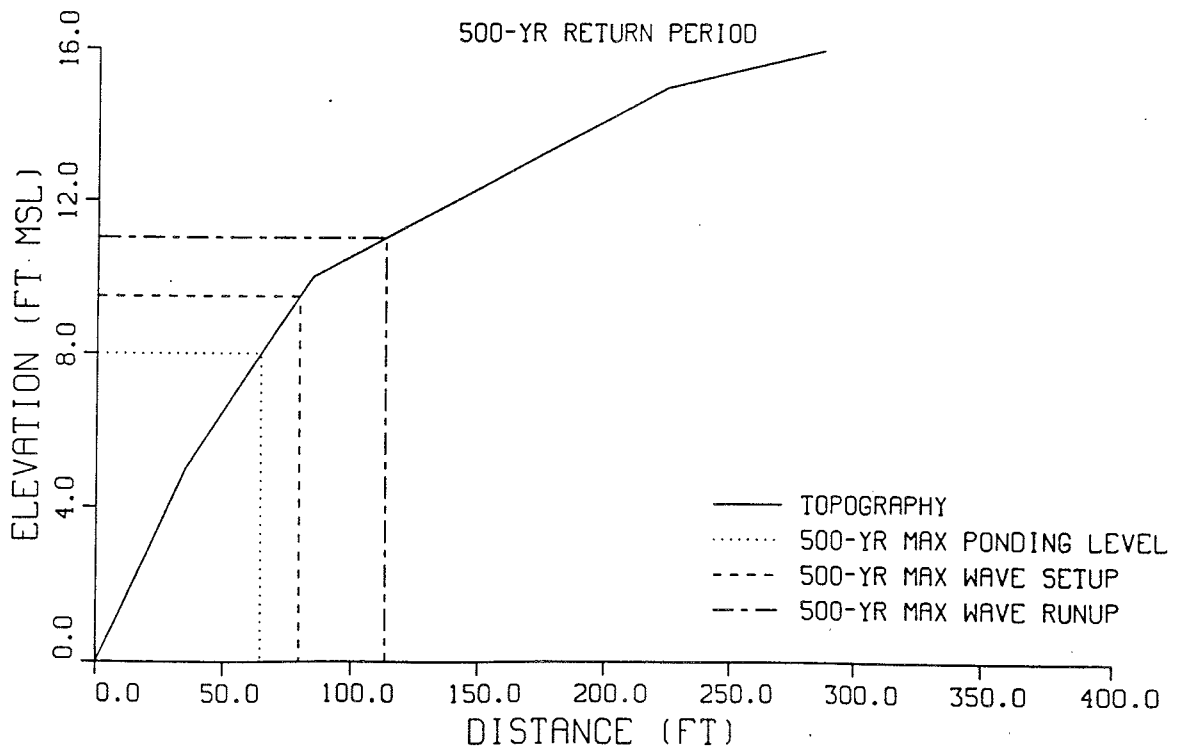
SOUTHERN GUAM TYPHOON ANALYSIS

PROFILE 1-1

100-YR RETURN PERIOD



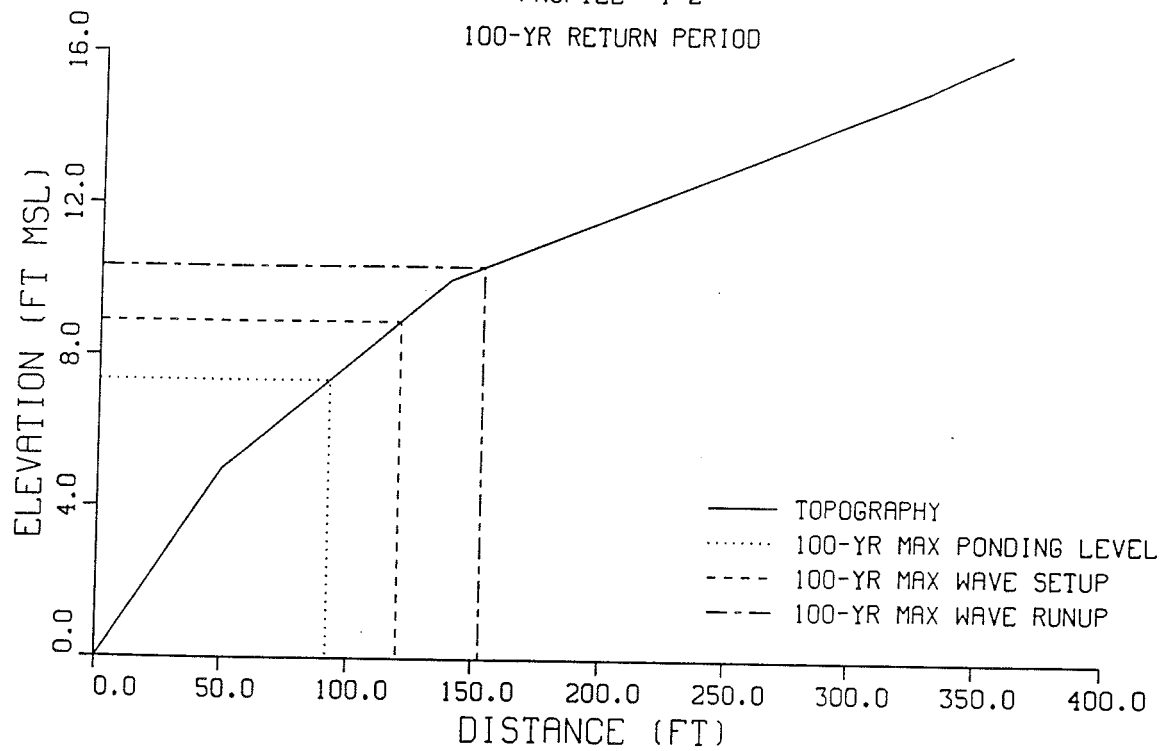
500-YR RETURN PERIOD



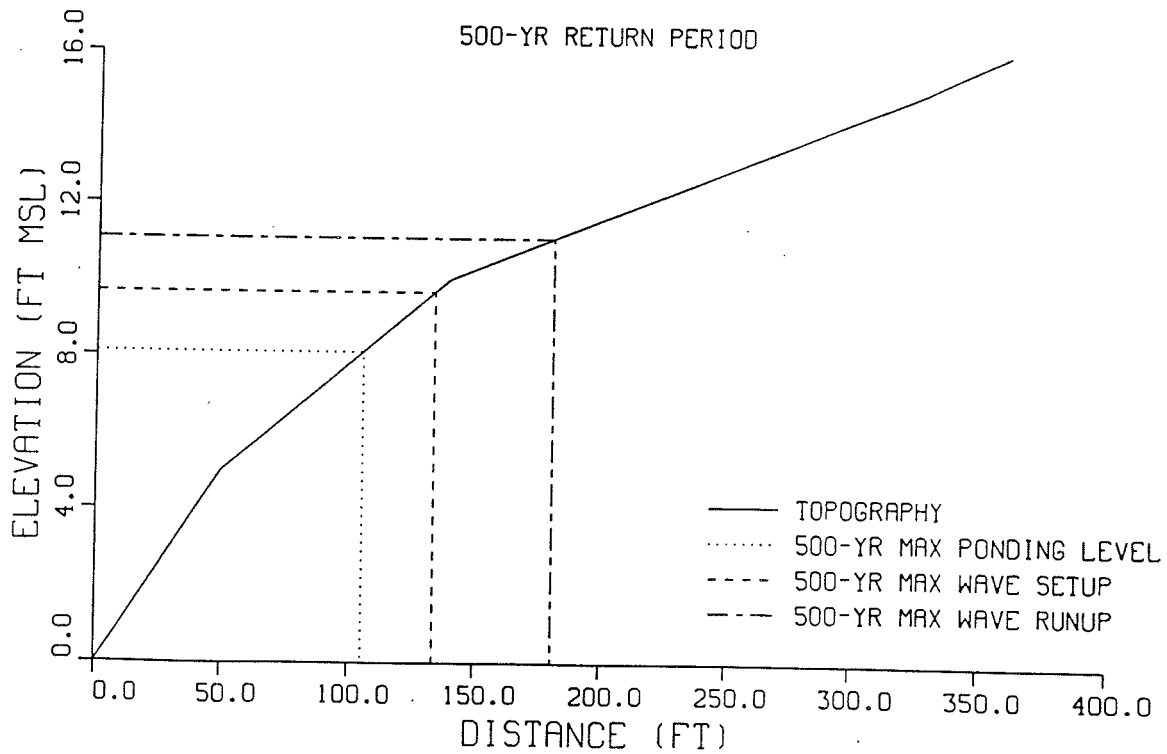
SOUTHERN GUAM TYPHOON ANALYSIS

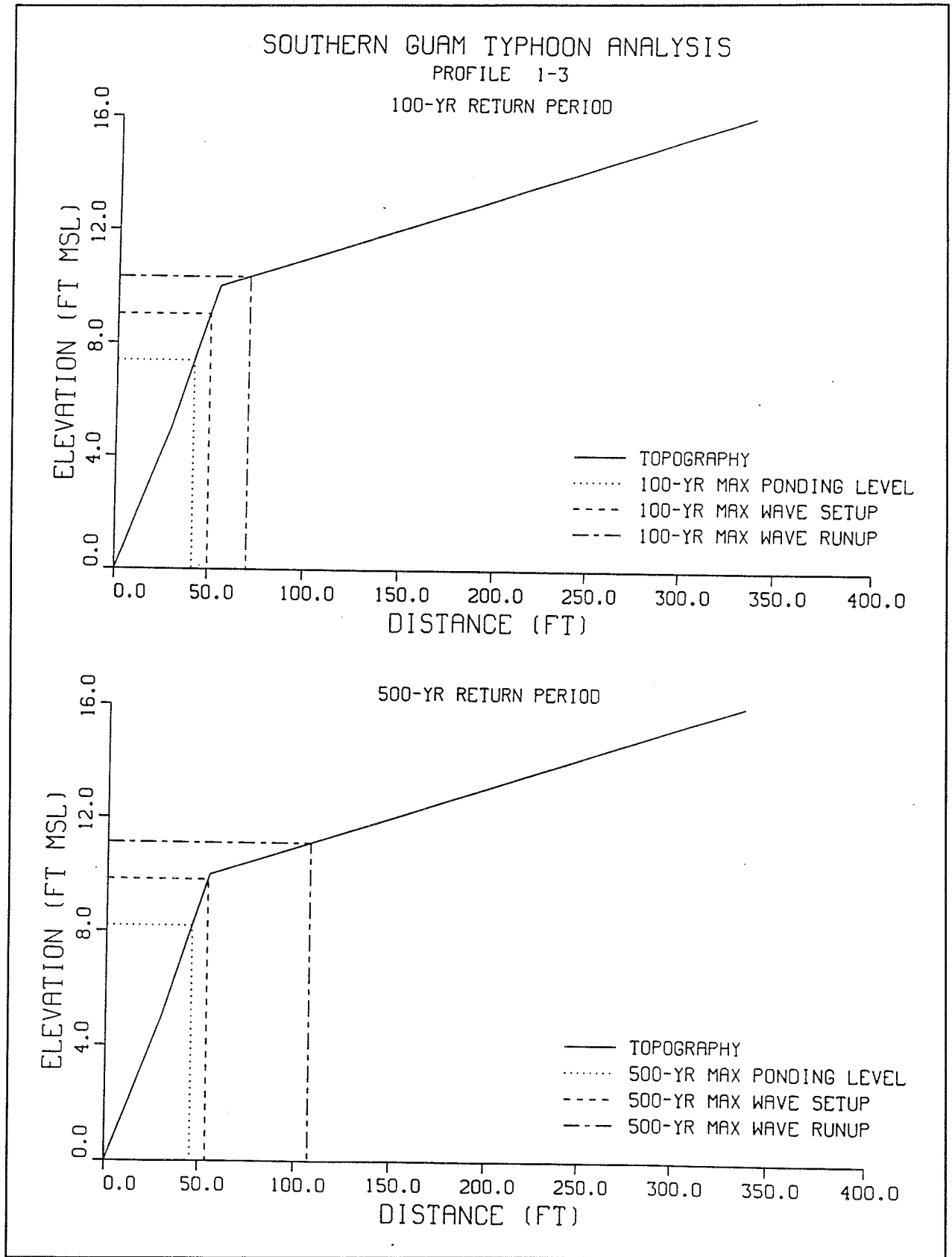
PROFILE 1-2

100-YR RETURN PERIOD



500-YR RETURN PERIOD

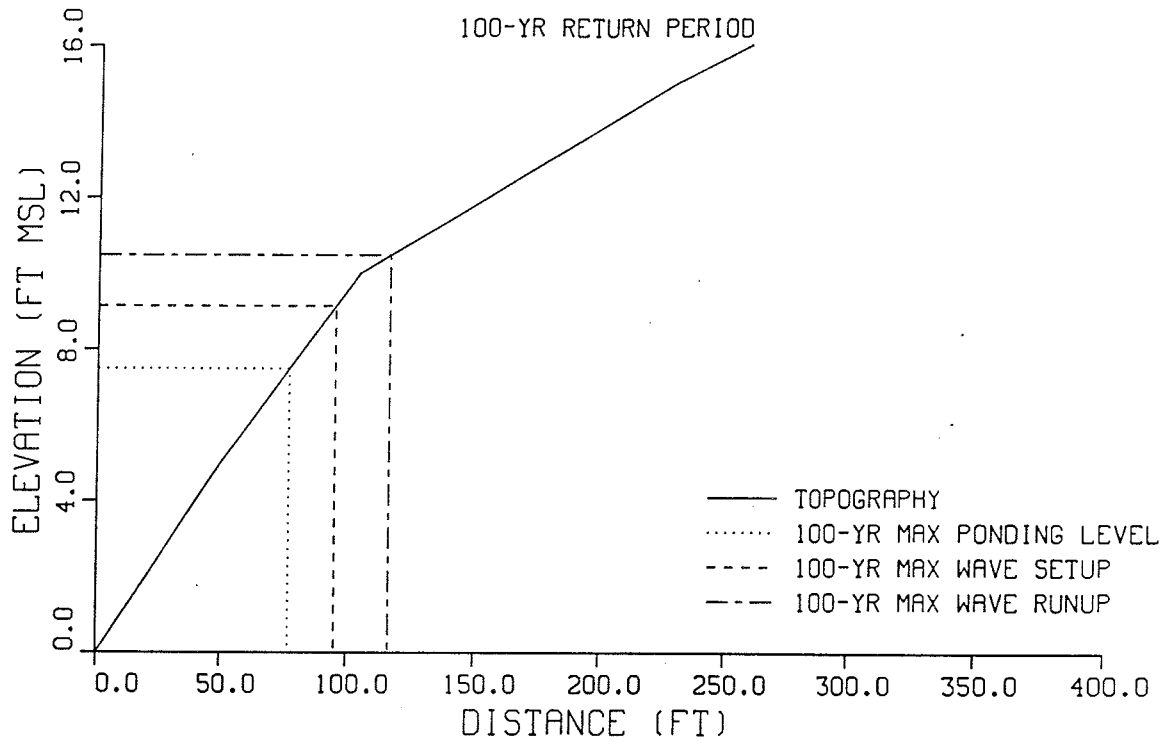




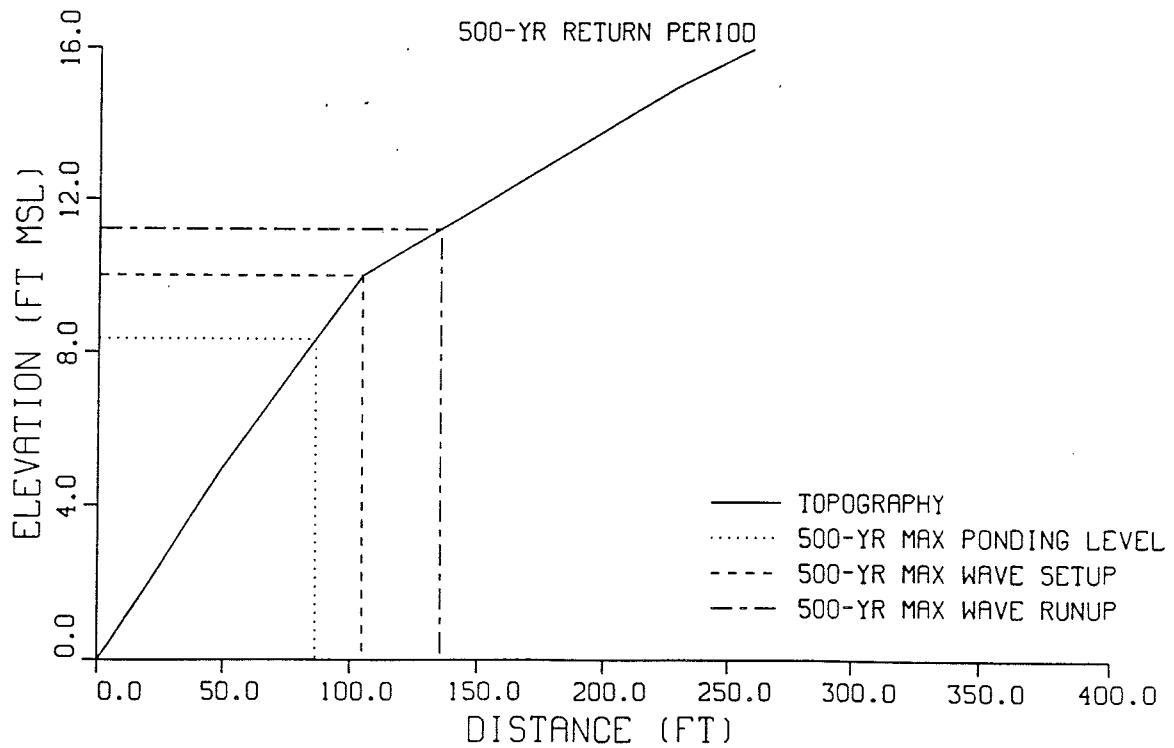
SOUTHERN GUAM TYPHOON ANALYSIS

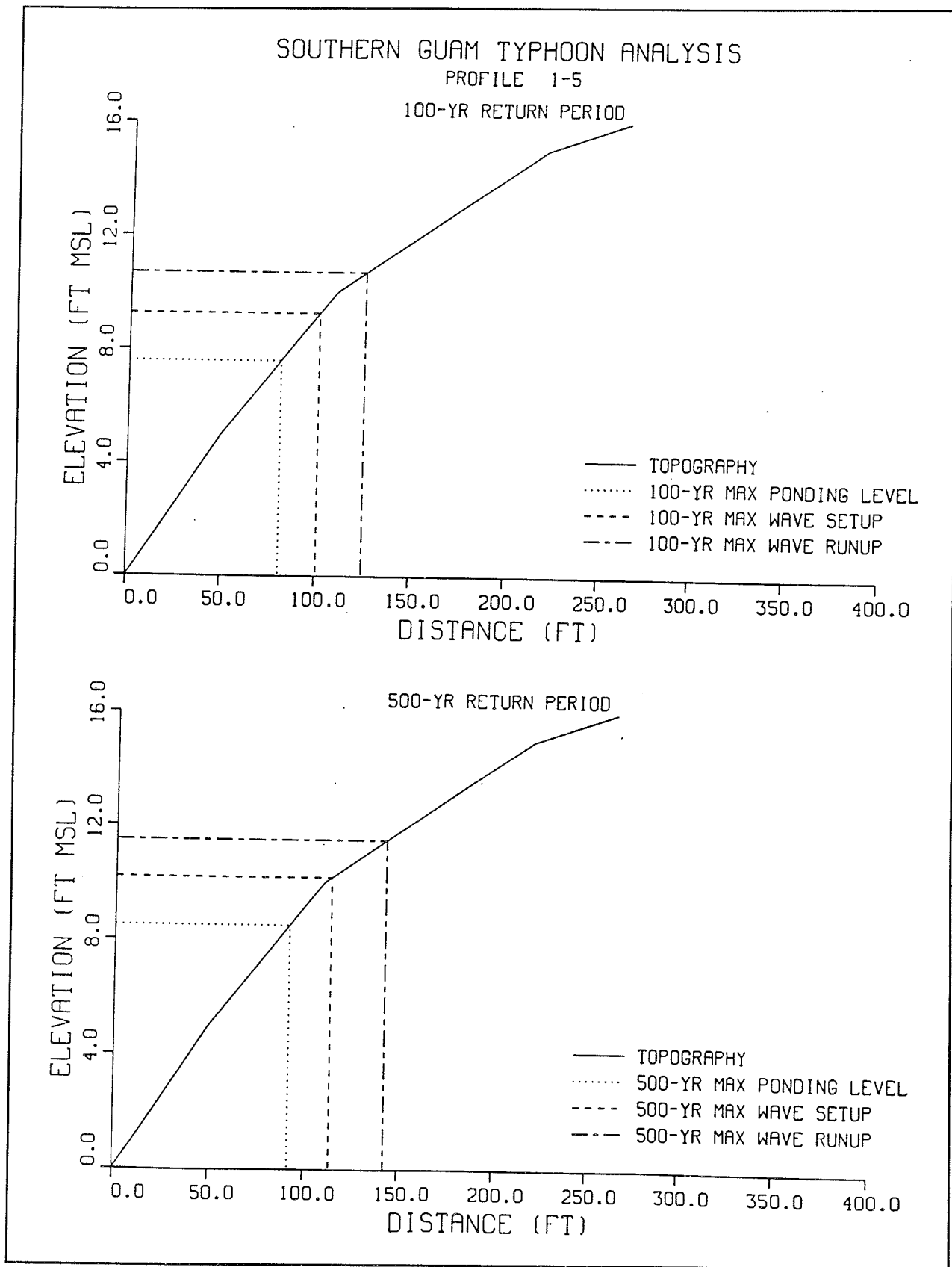
PROFILE 1-4

100-YR RETURN PERIOD



500-YR RETURN PERIOD

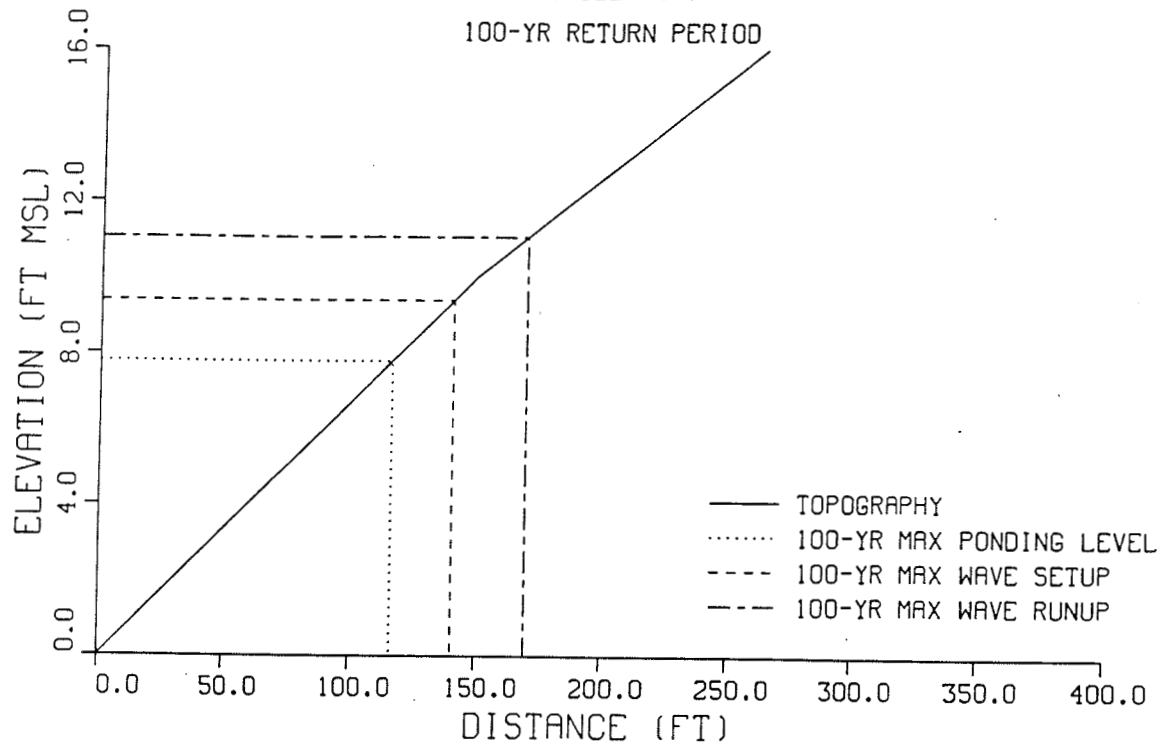




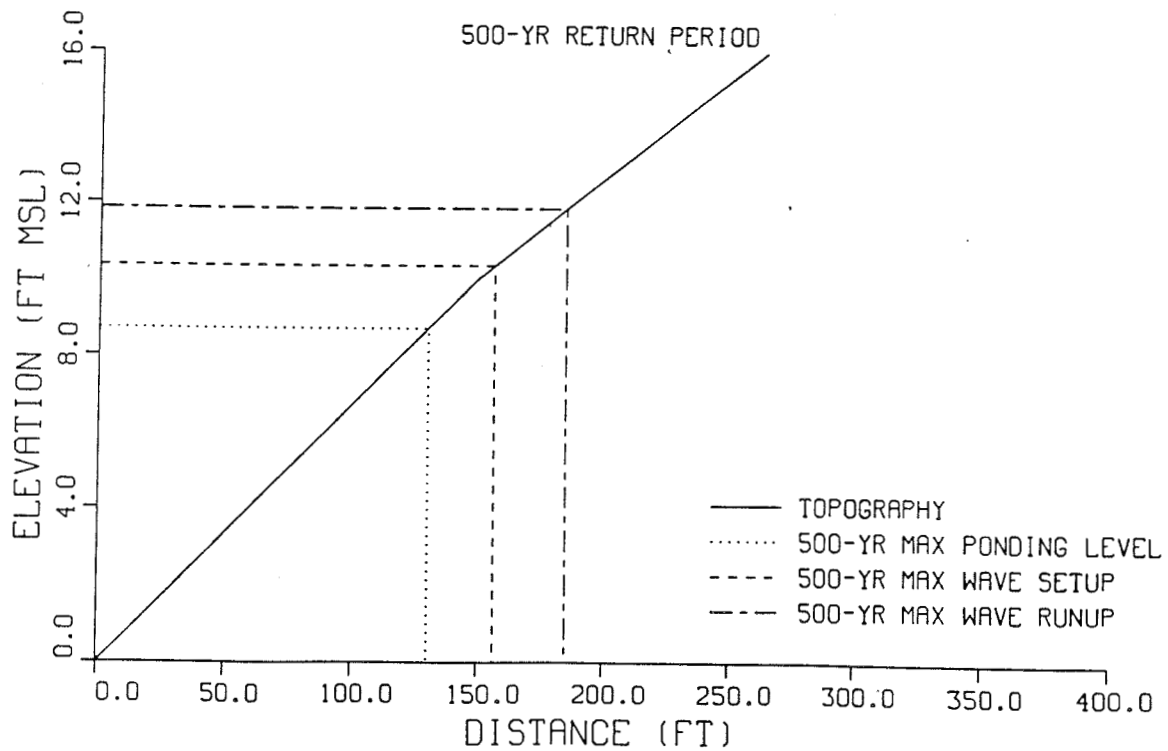
SOUTHERN GUAM TYPHOON ANALYSIS

PROFILE 1-6

100-YR RETURN PERIOD



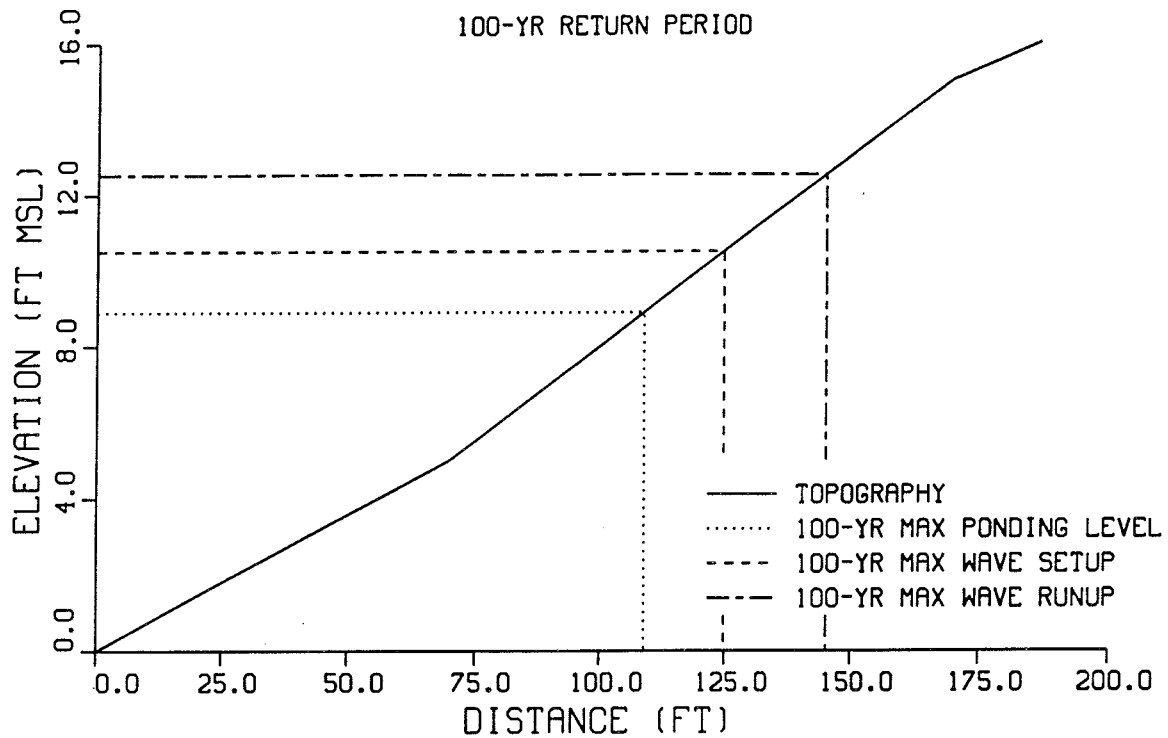
500-YR RETURN PERIOD



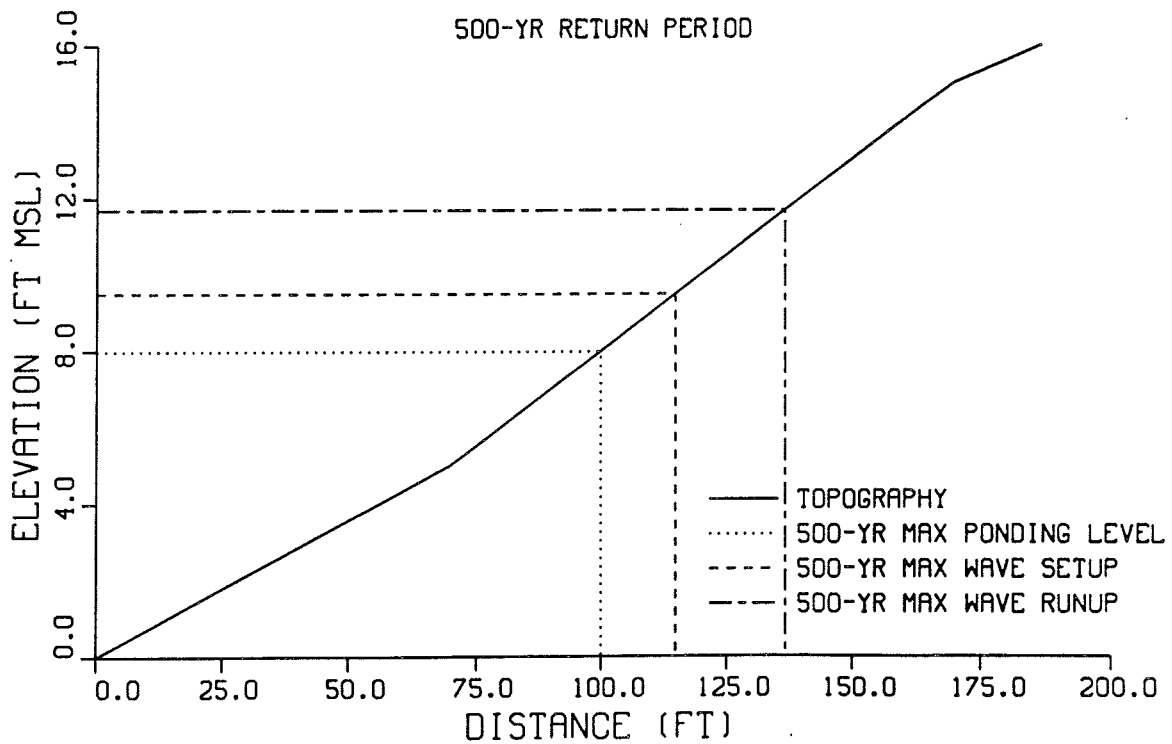
SOUTHERN GUAM TYPHOON ANALYSIS

PROFILE 2-1

100-YR RETURN PERIOD



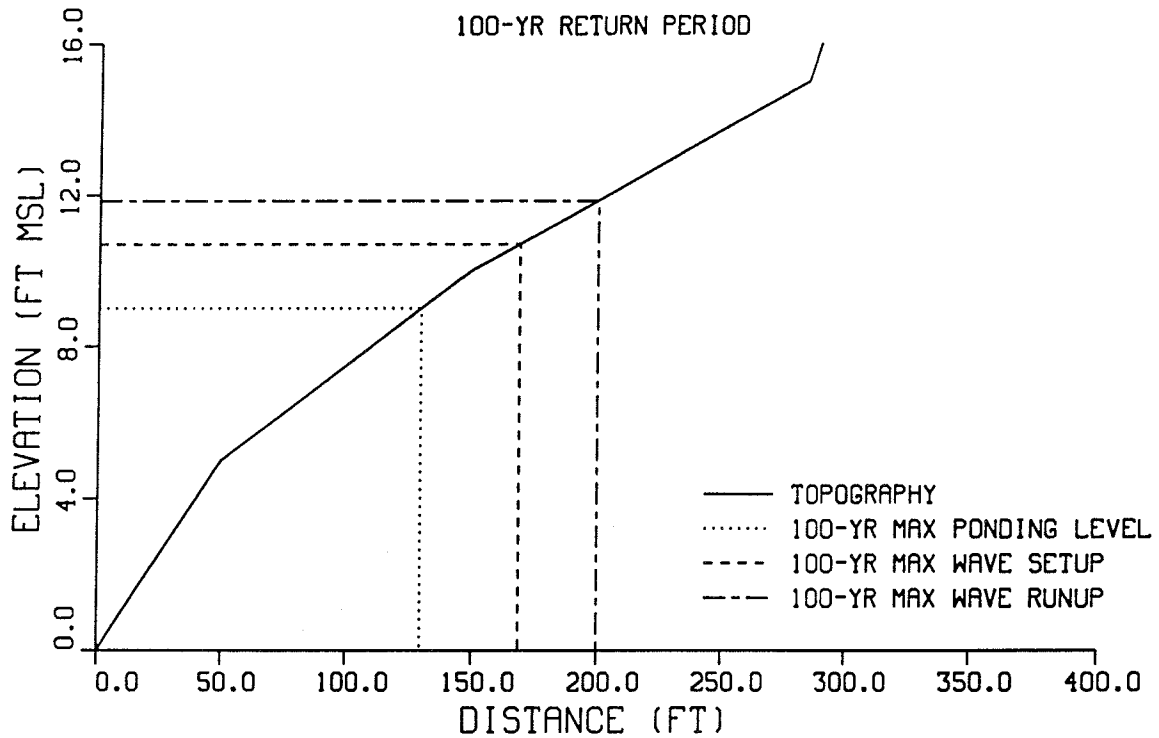
500-YR RETURN PERIOD



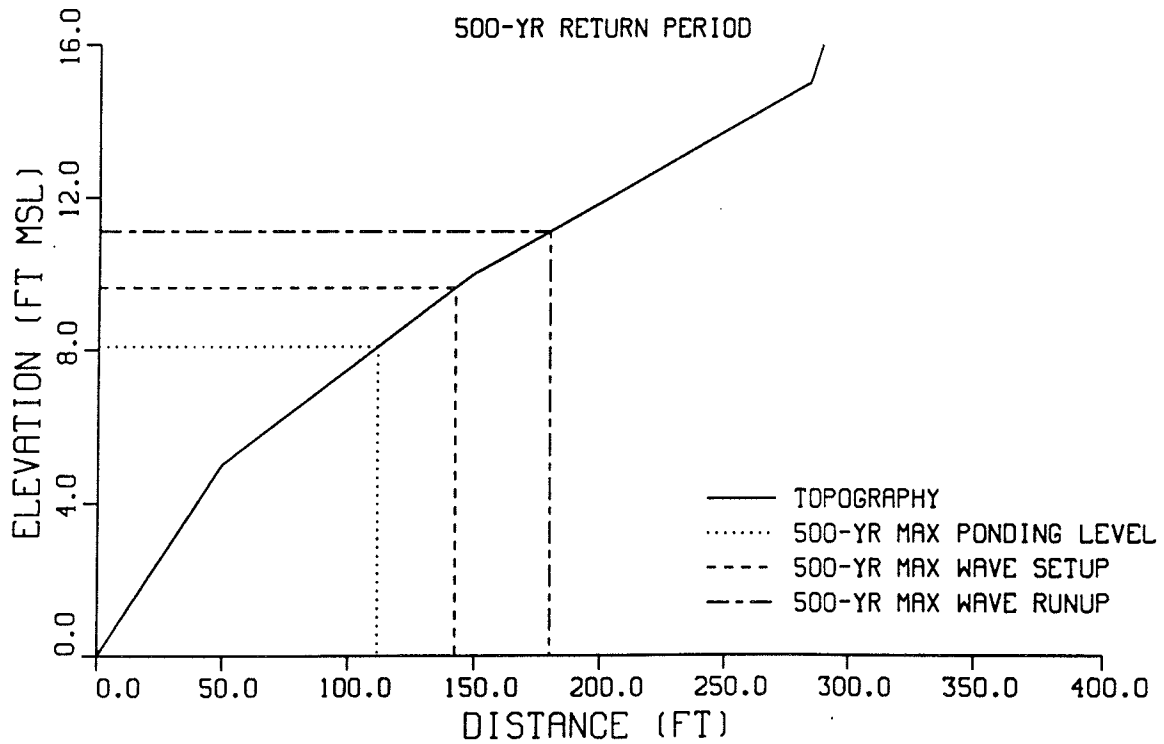
SOUTHERN GUAM TYPHOON ANALYSIS

PROFILE 2-2

100-YR RETURN PERIOD



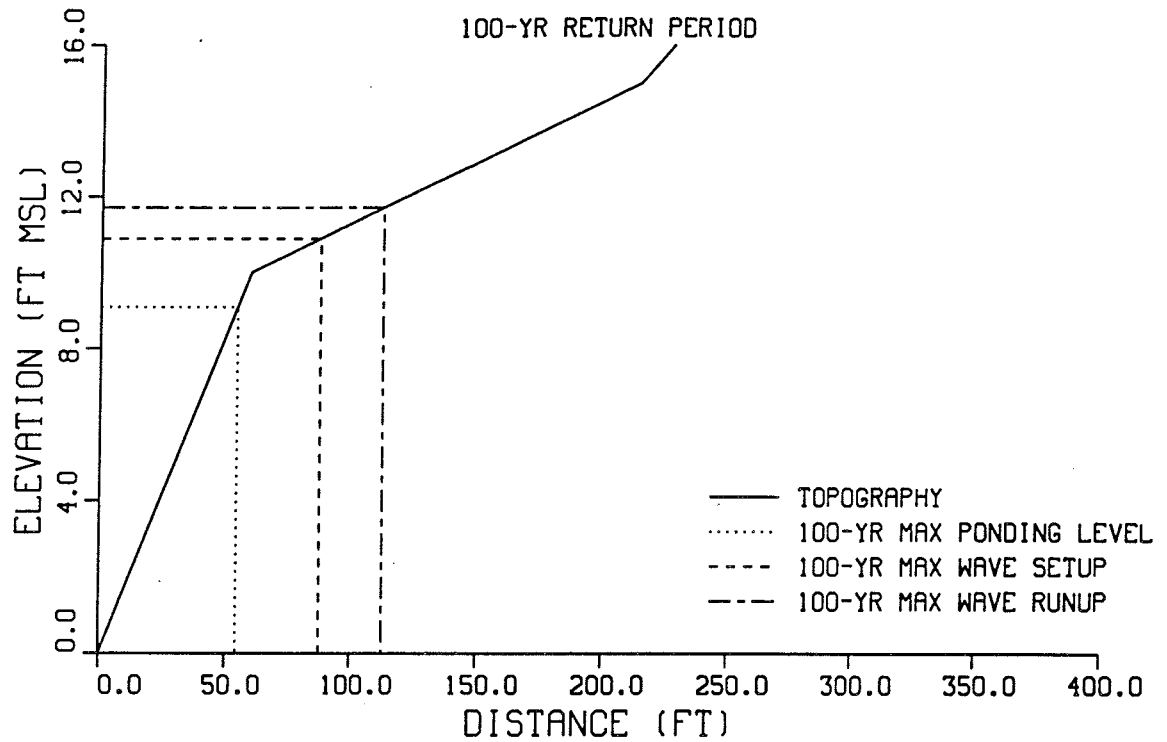
500-YR RETURN PERIOD



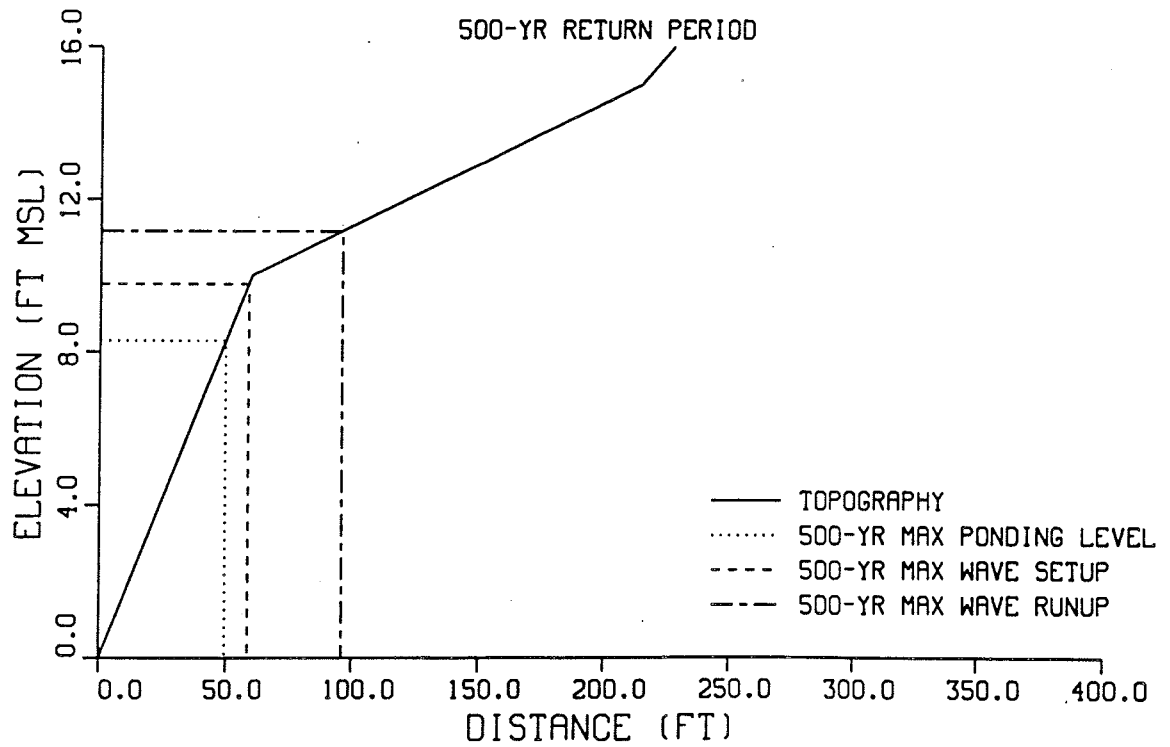
SOUTHERN GUAM TYPHOON ANALYSIS

PROFILE 2-3

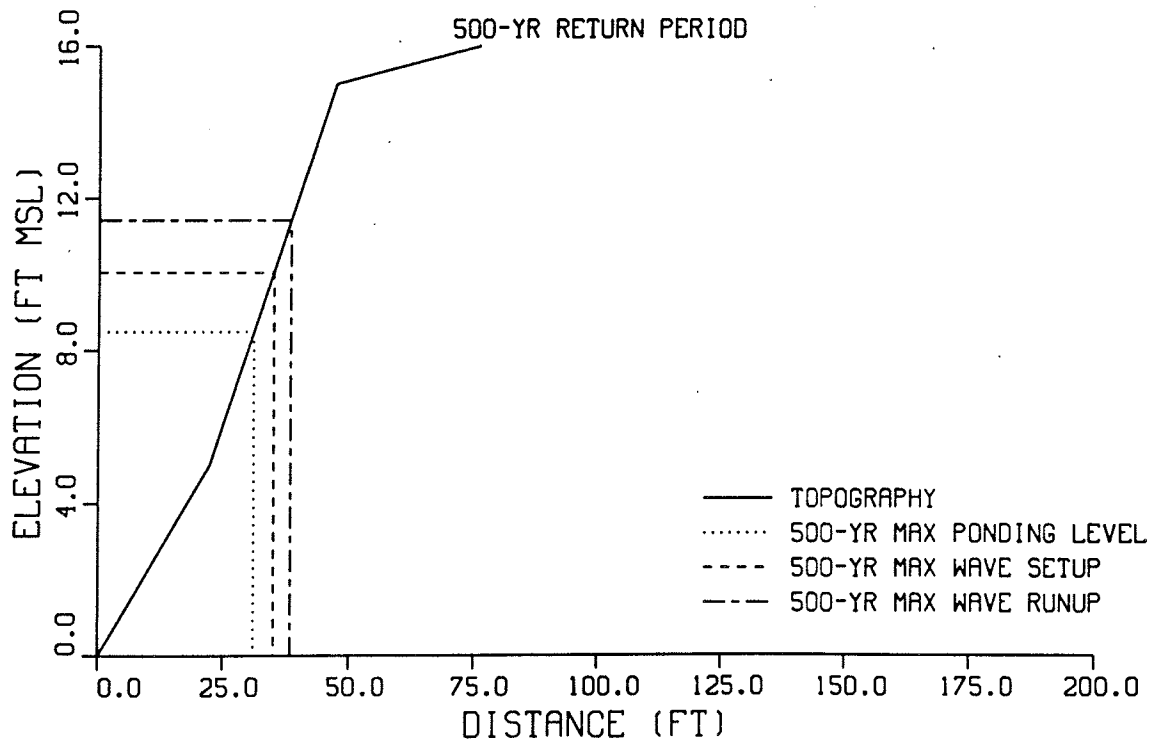
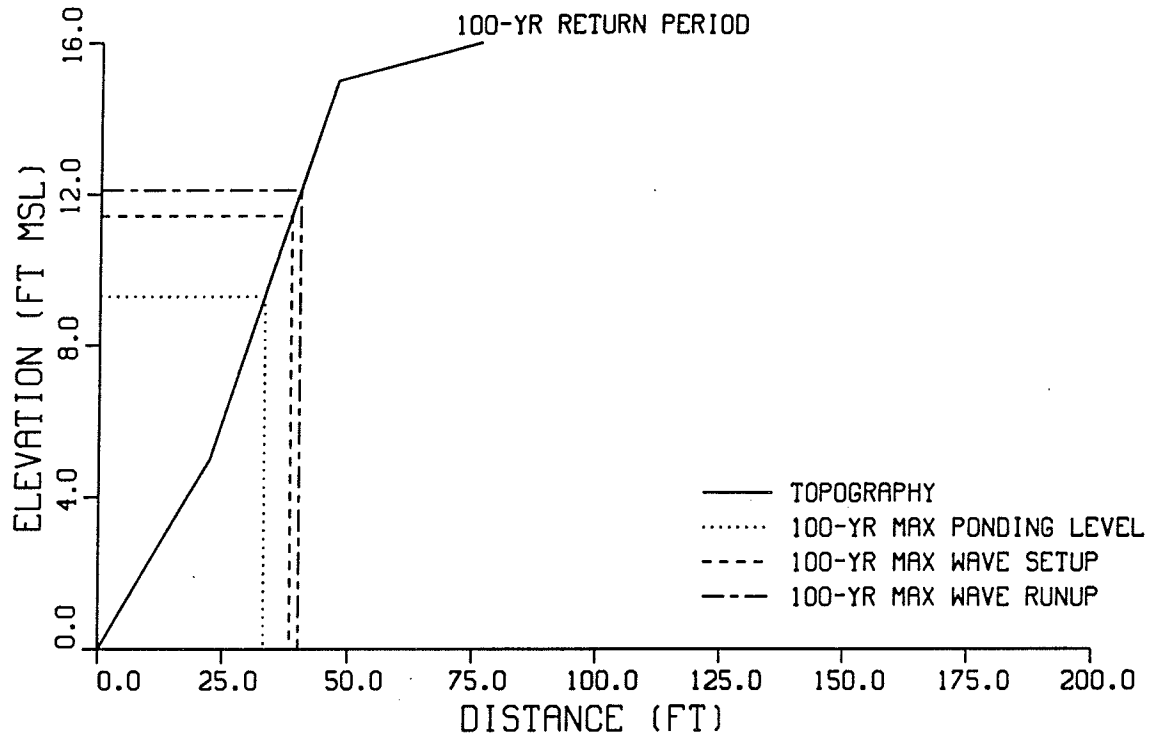
100-YR RETURN PERIOD



500-YR RETURN PERIOD



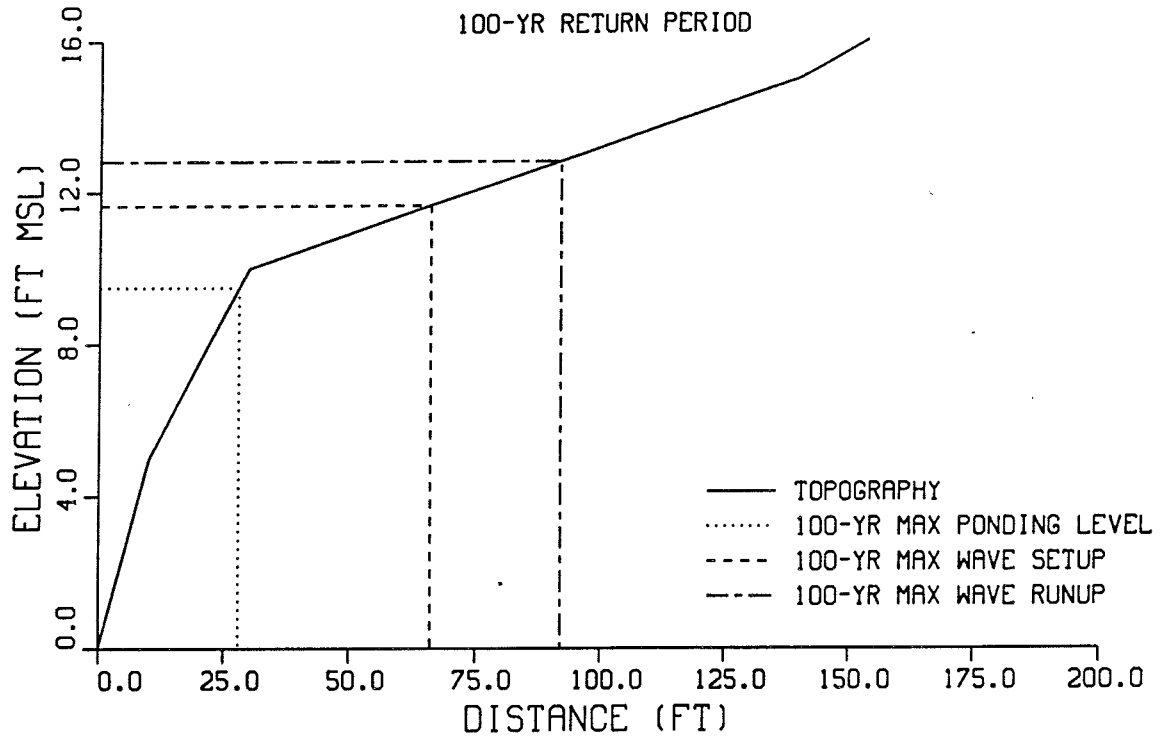
SOUTHERN GUAM TYPHOON ANALYSIS PROFILE 2-4



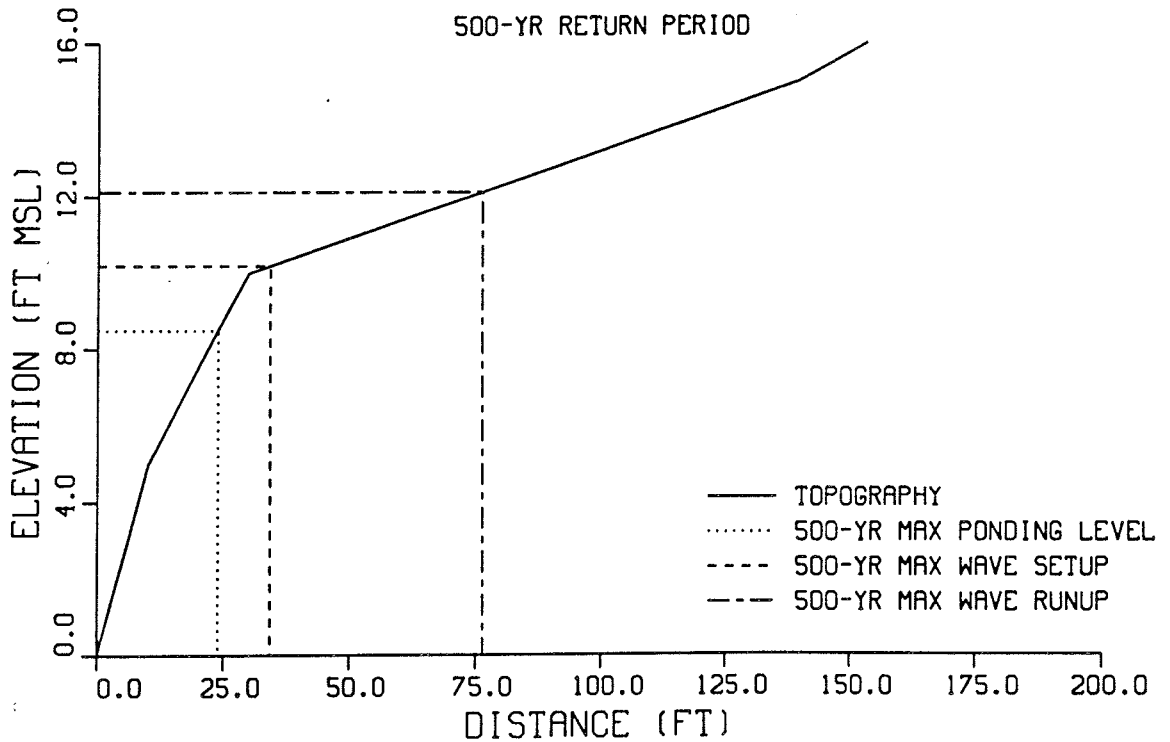
SOUTHERN GUAM TYPHOON ANALYSIS

PROFILE 2-5

100-YR RETURN PERIOD



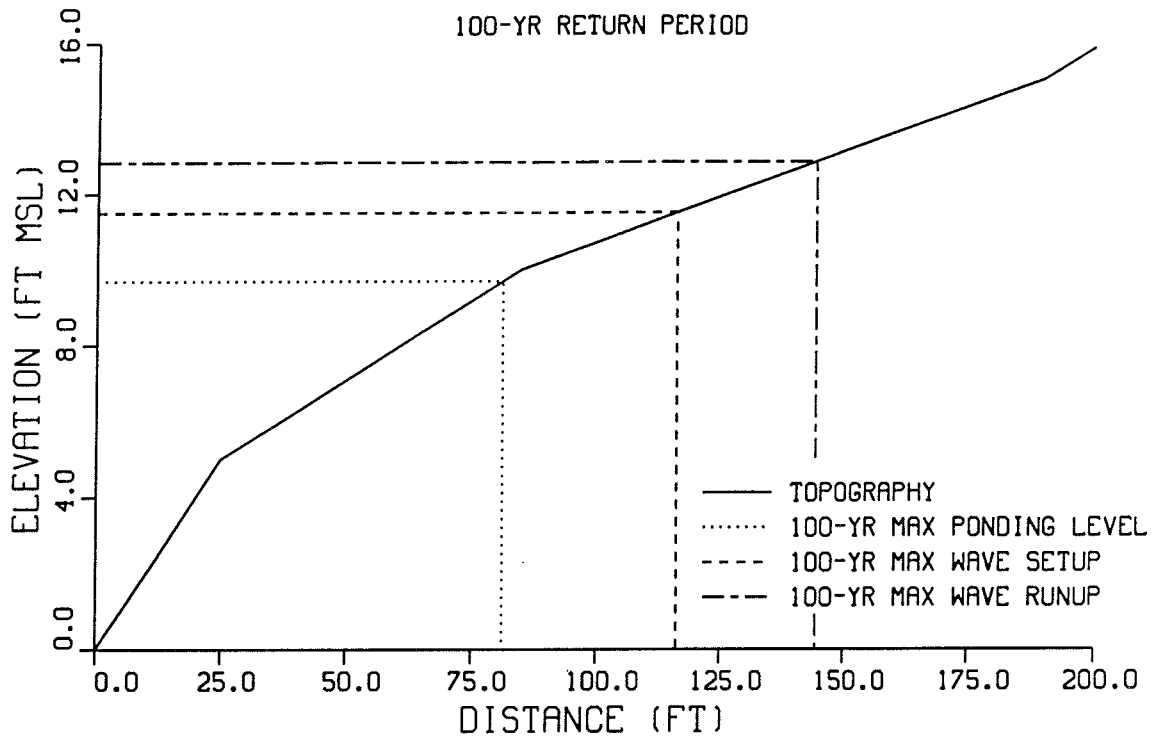
500-YR RETURN PERIOD



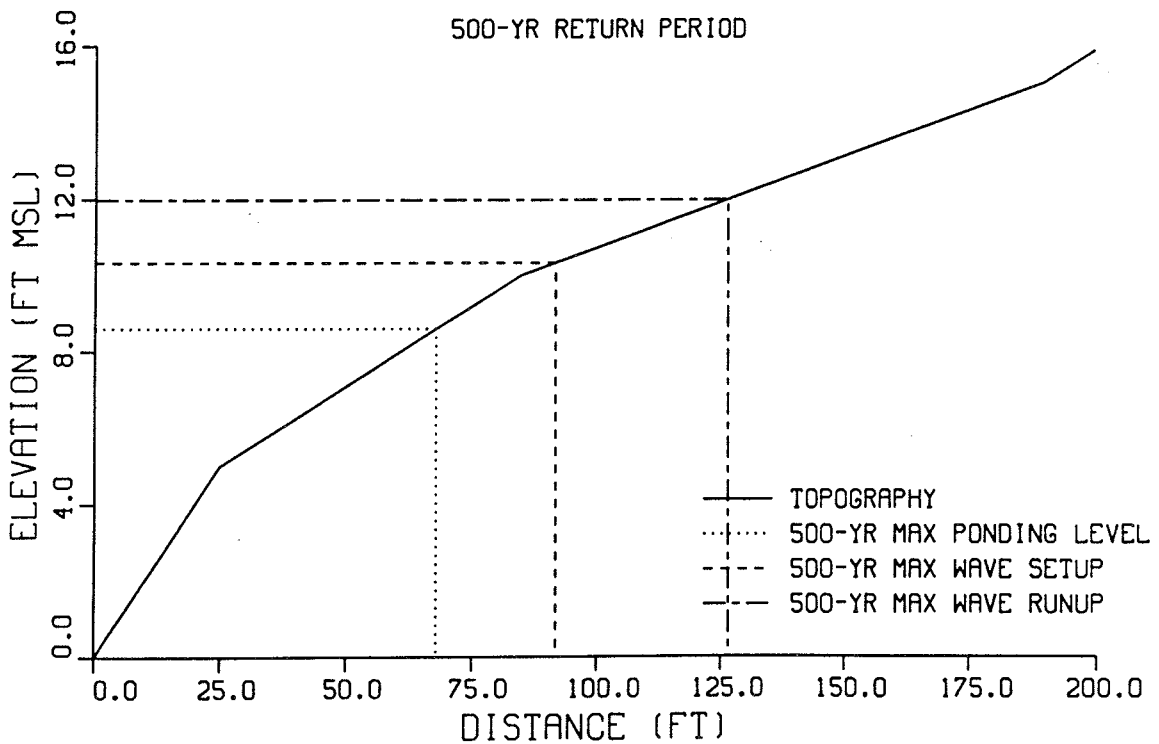
SOUTHERN GUAM TYPHOON ANALYSIS

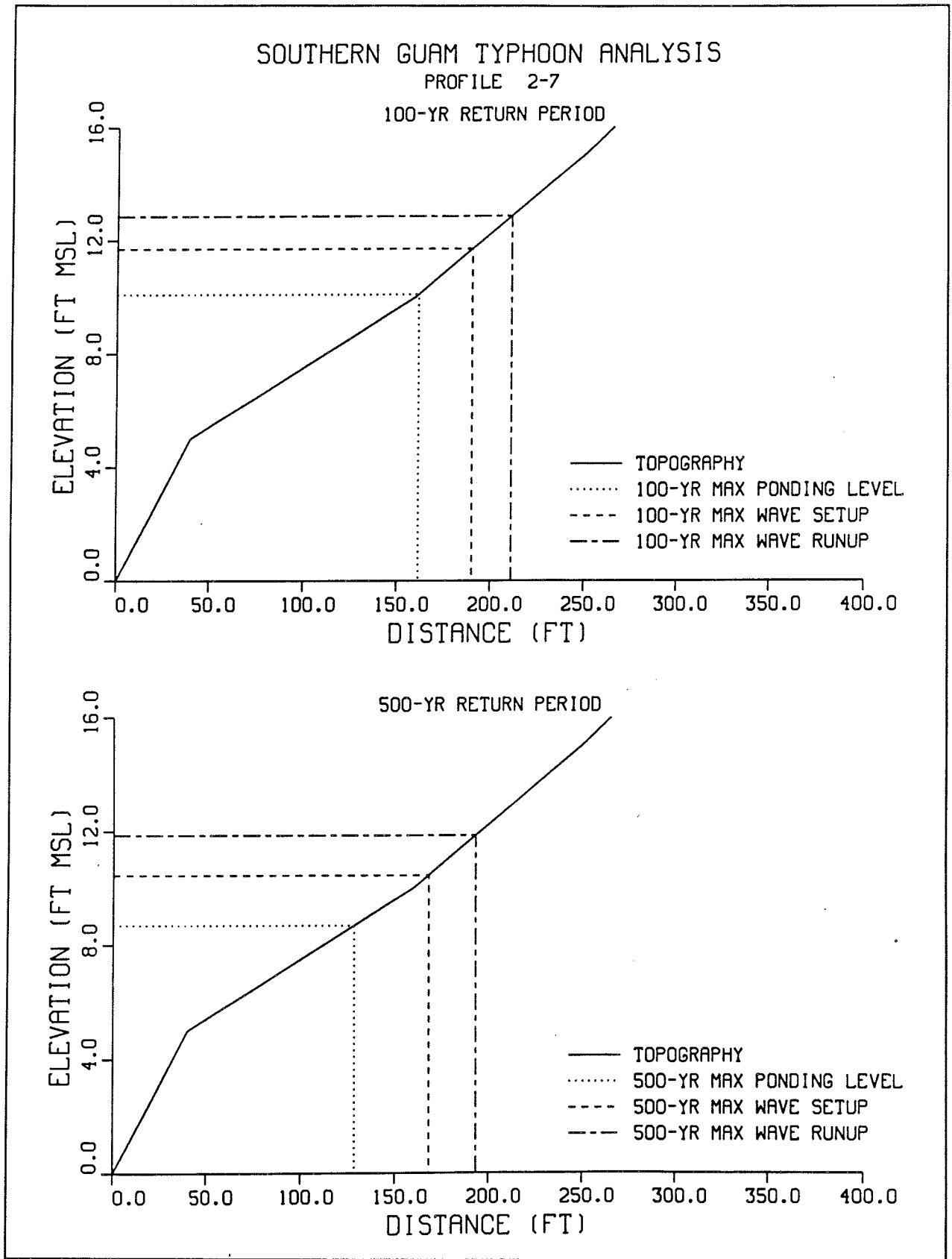
PROFILE 2-6

100-YR RETURN PERIOD



500-YR RETURN PERIOD

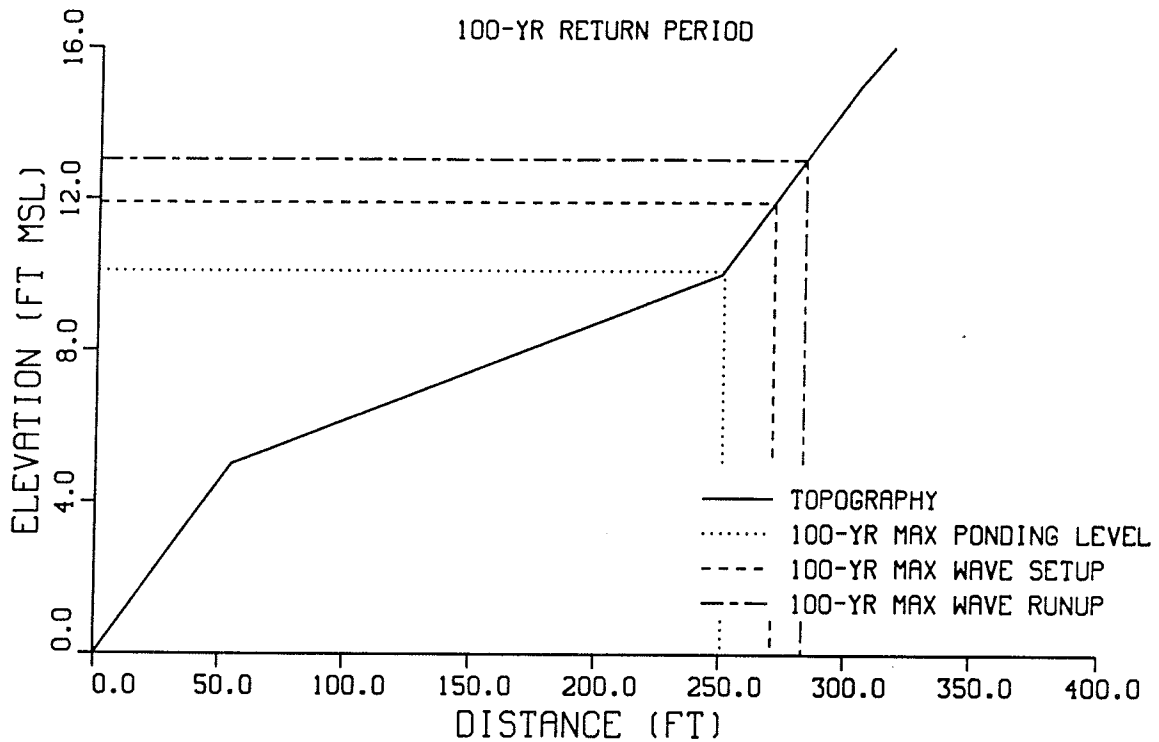




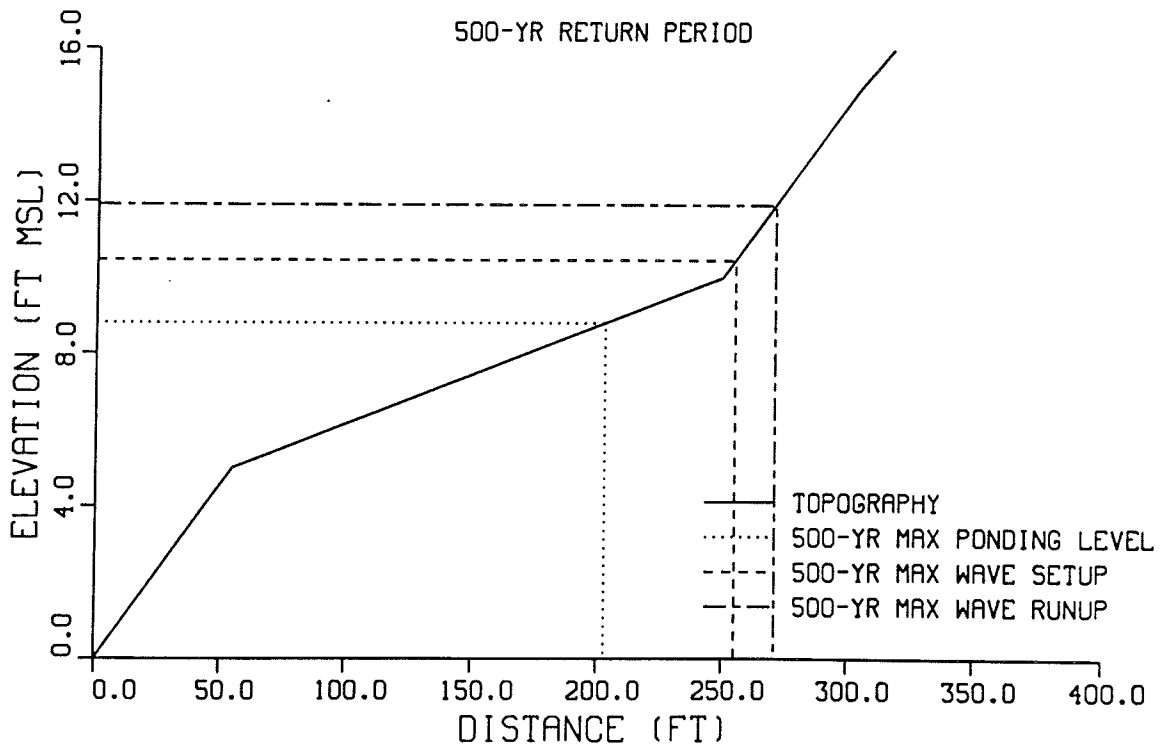
SOUTHERN GUAM TYPHOON ANALYSIS

PROFILE 3-1

100-YR RETURN PERIOD



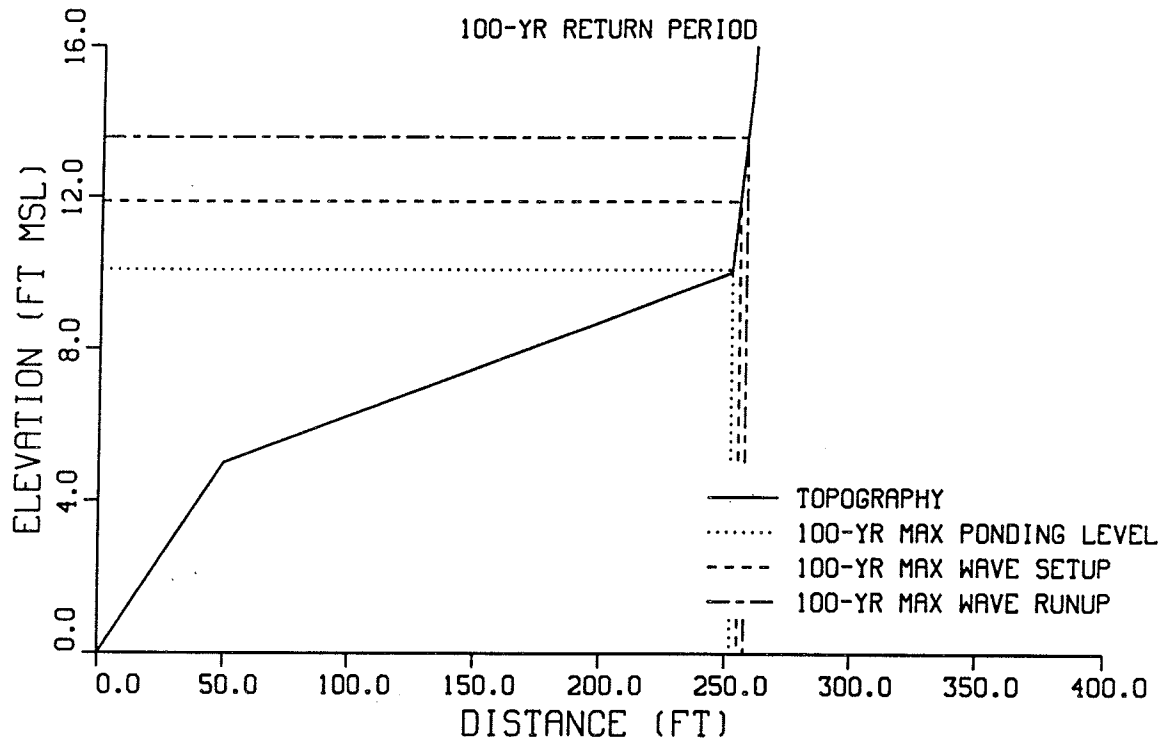
500-YR RETURN PERIOD



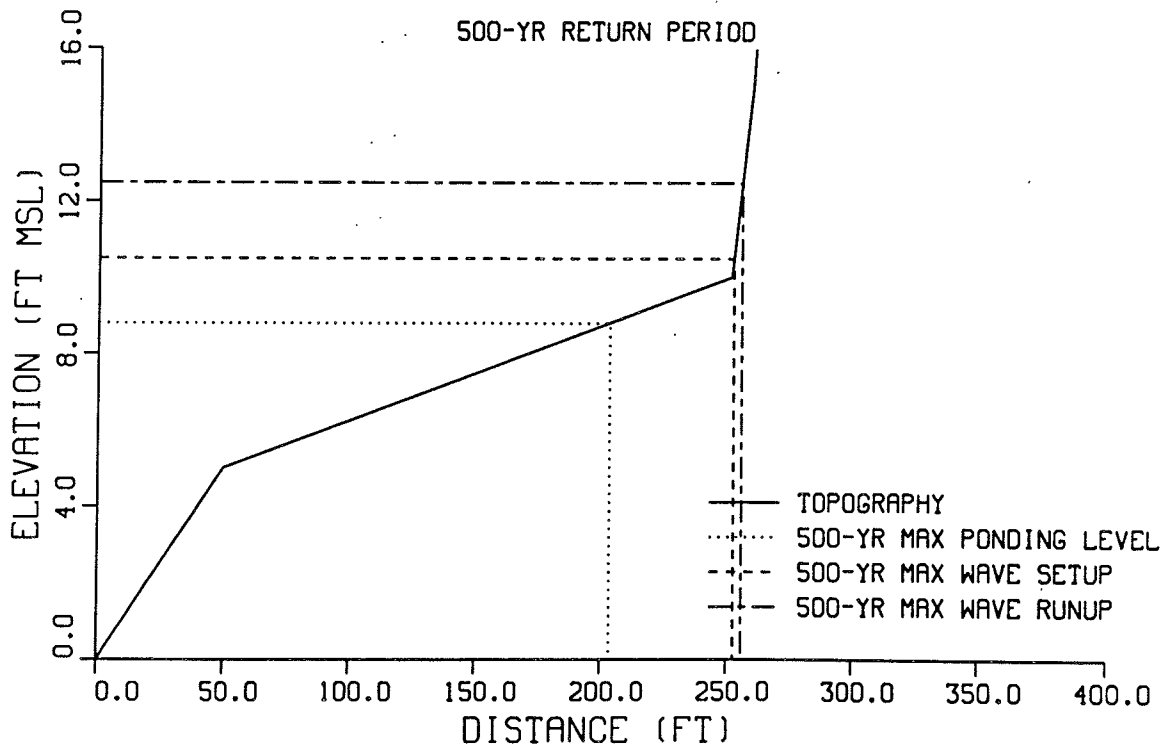
SOUTHERN GUAM TYPHOON ANALYSIS

PROFILE 3-2

100-YR RETURN PERIOD



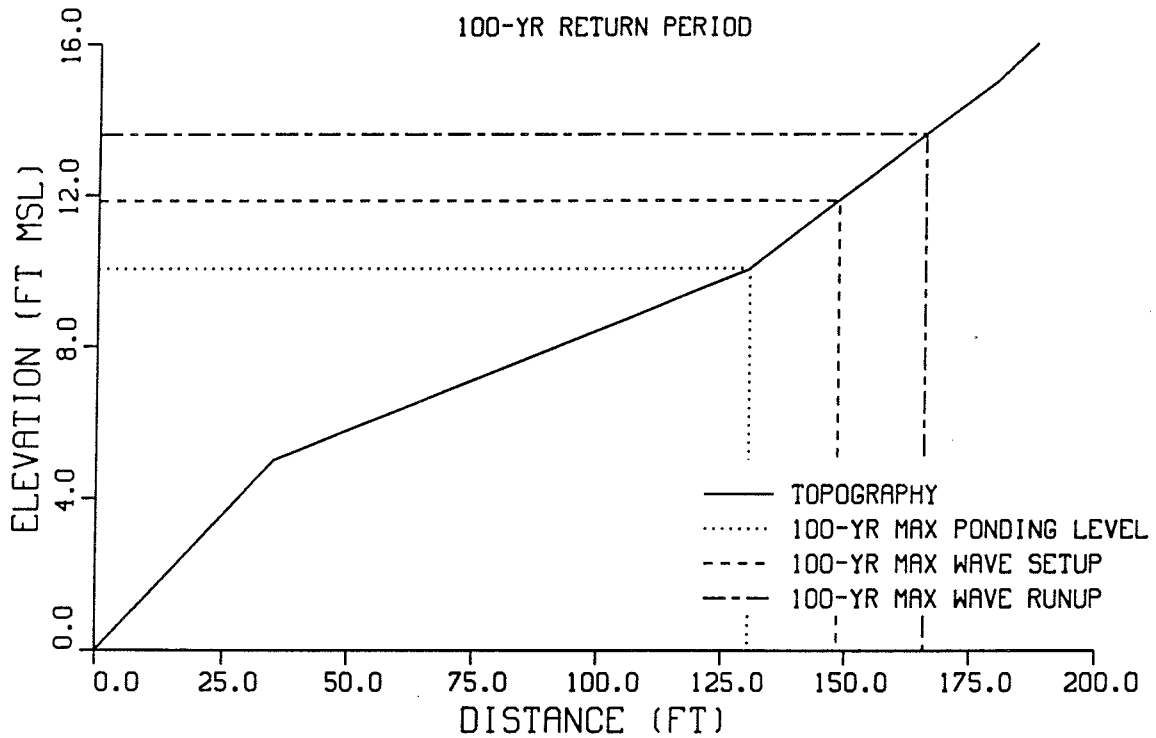
500-YR RETURN PERIOD



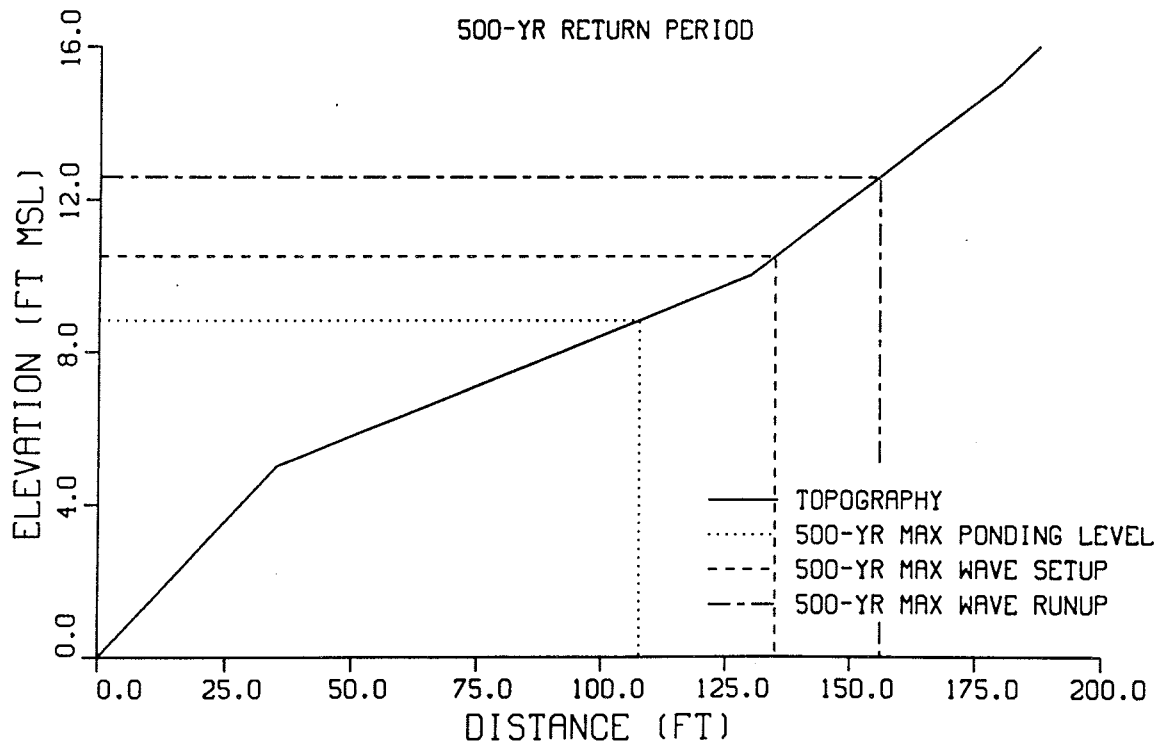
SOUTHERN GUAM TYPHOON ANALYSIS

PROFILE 3-3

100-YR RETURN PERIOD



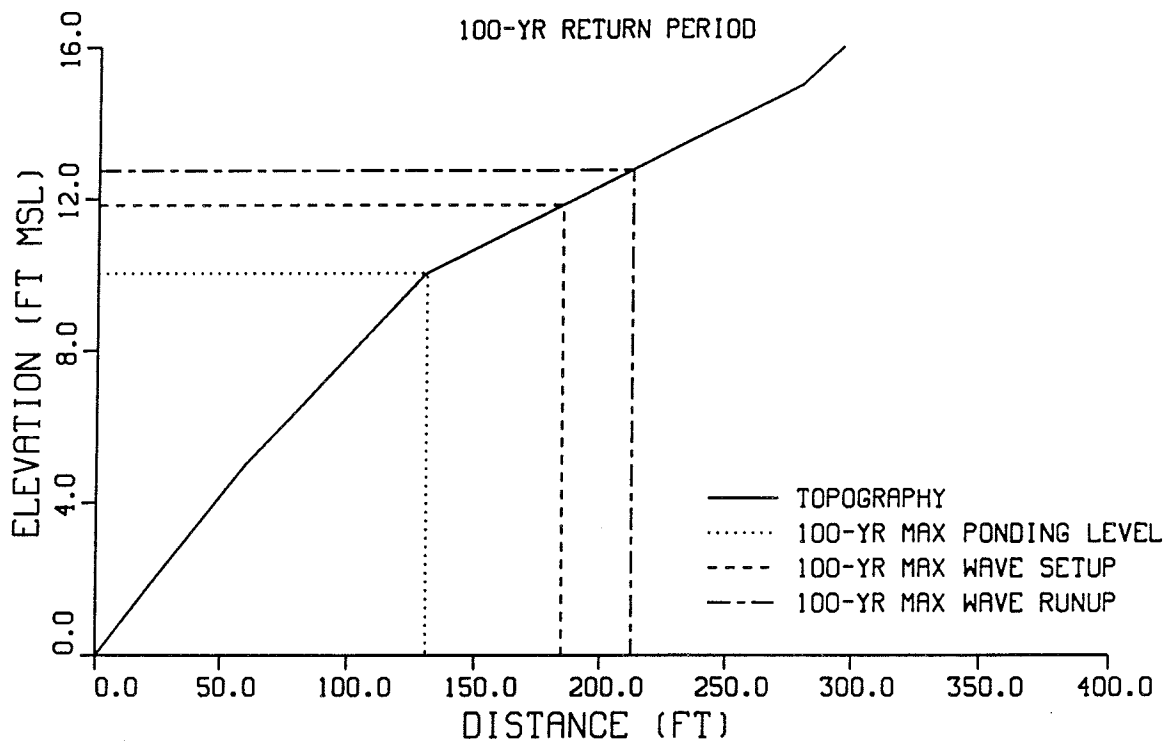
500-YR RETURN PERIOD



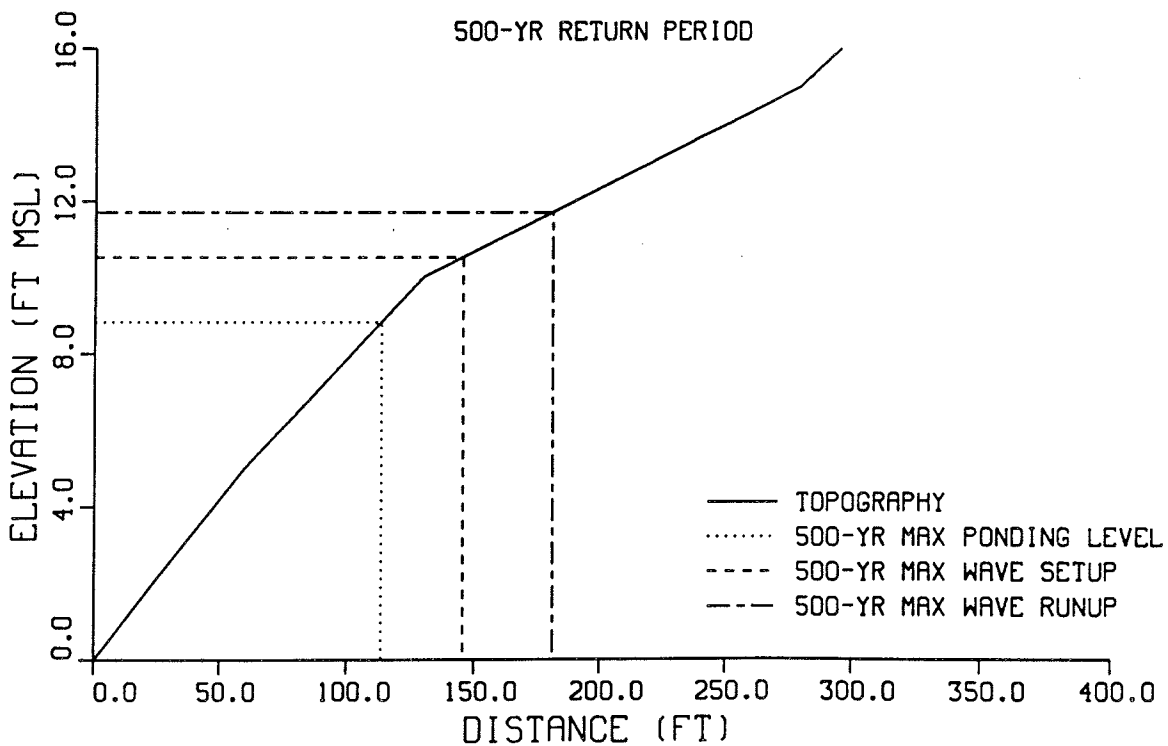
SOUTHERN GUAM TYPHOON ANALYSIS

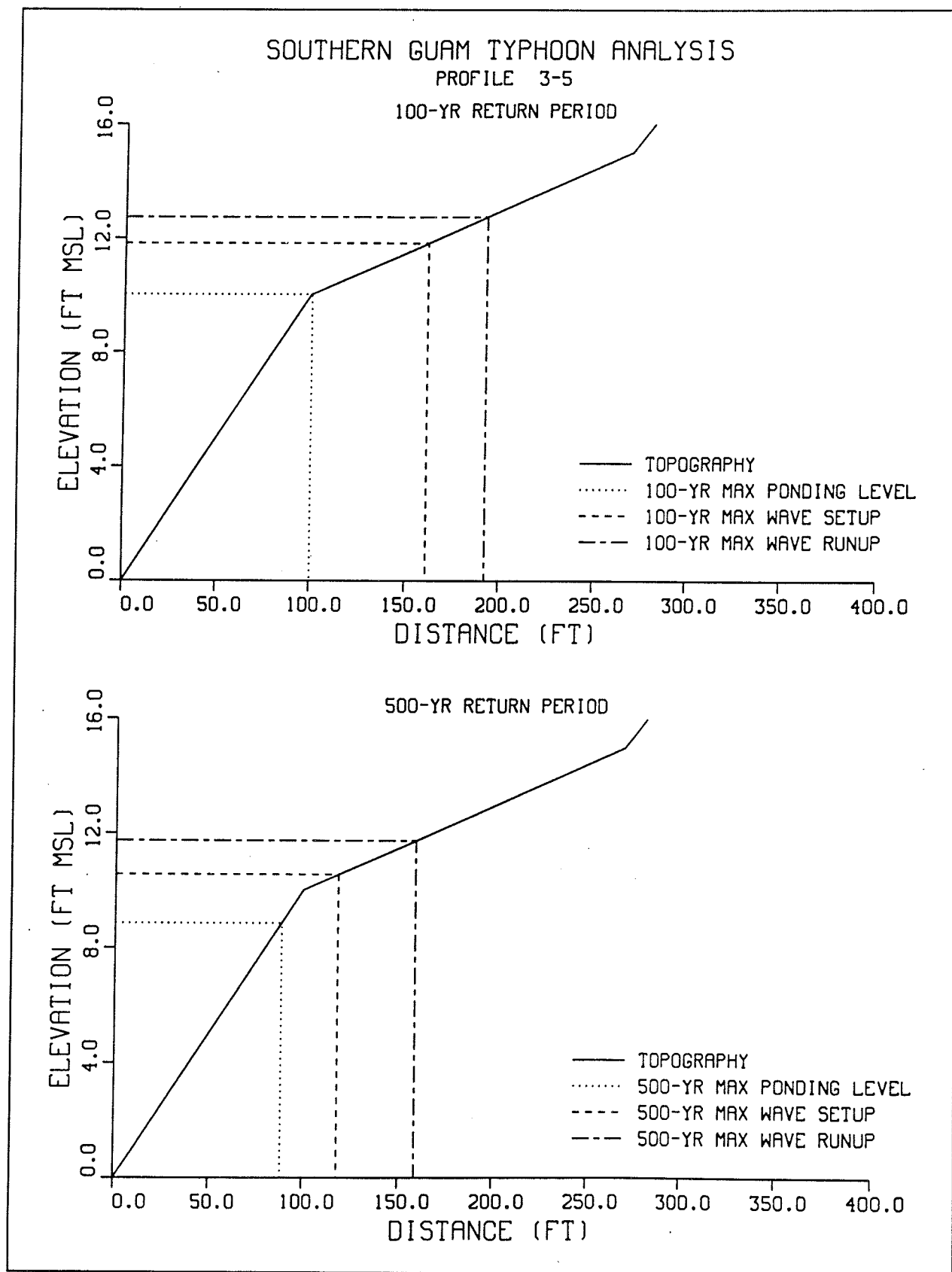
PROFILE 3-4

100-YR RETURN PERIOD



500-YR RETURN PERIOD

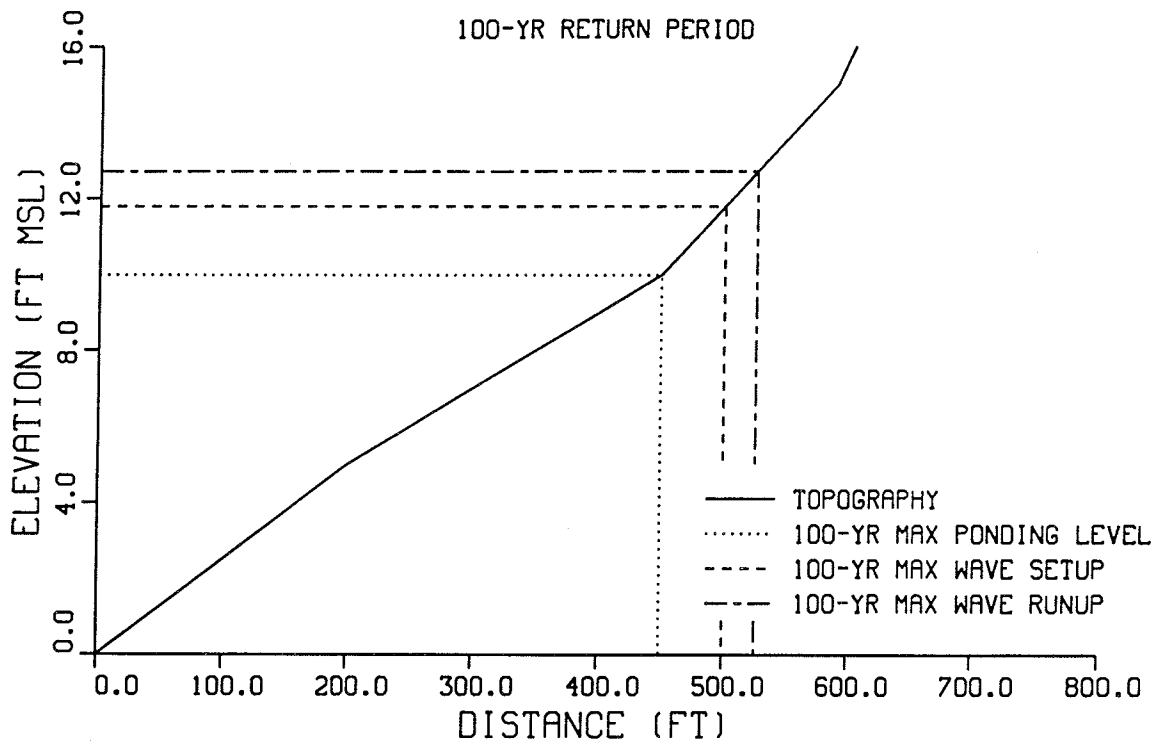




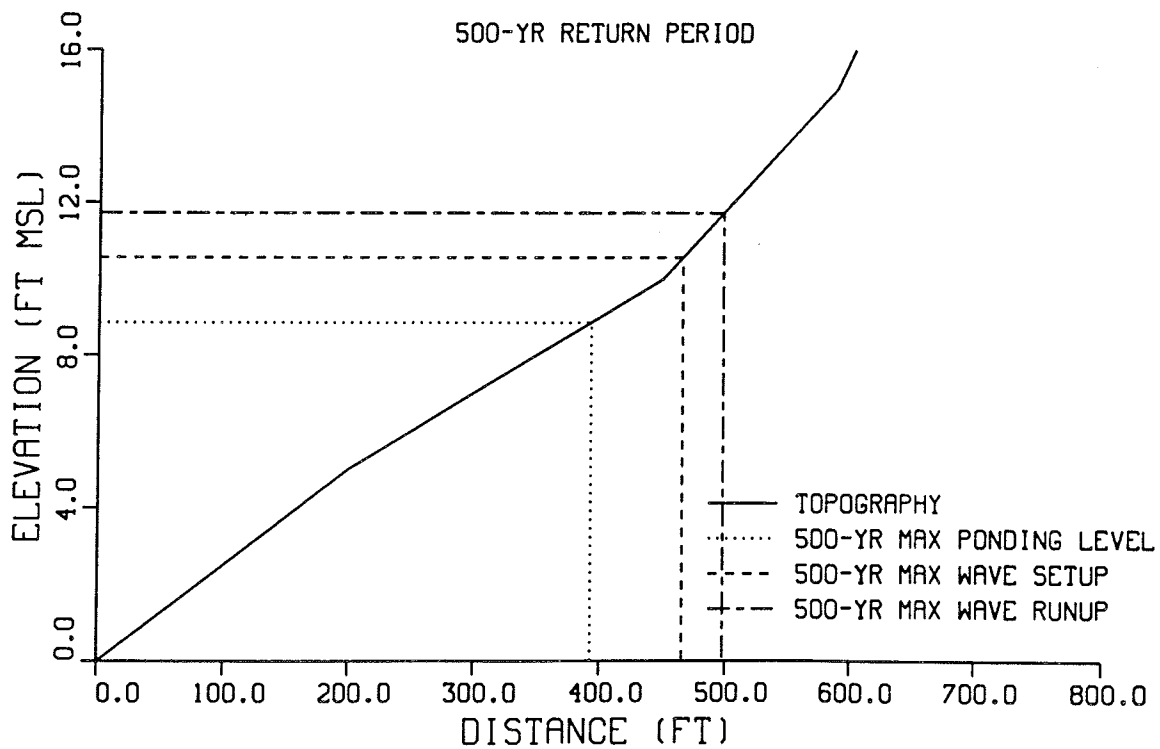
SOUTHERN GUAM TYPHOON ANALYSIS

PROFILE 3-6

100-YR RETURN PERIOD



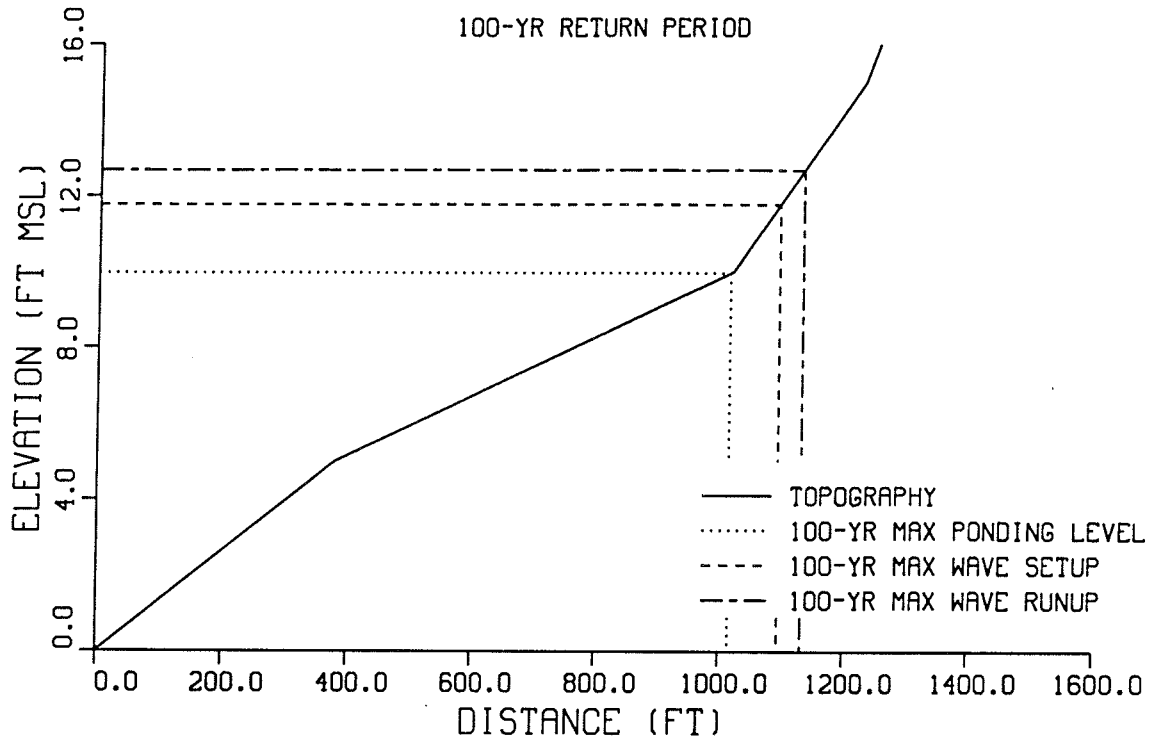
500-YR RETURN PERIOD



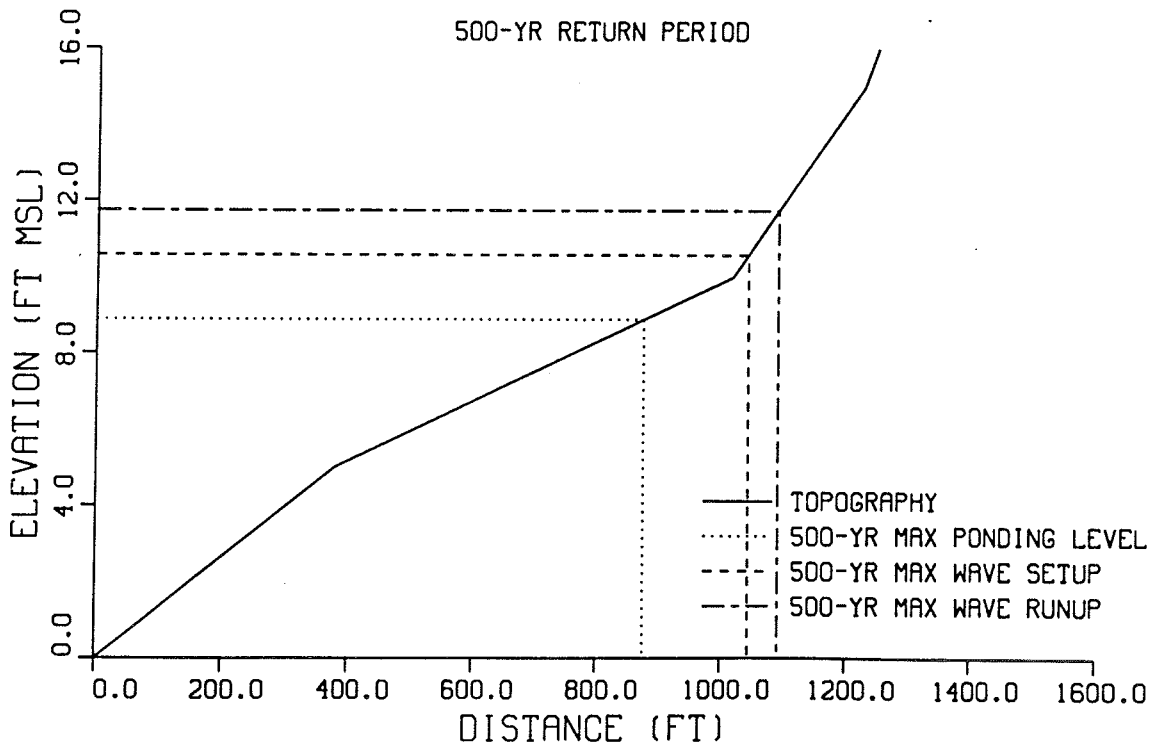
SOUTHERN GUAM TYPHOON ANALYSIS

PROFILE 4-1

100-YR RETURN PERIOD



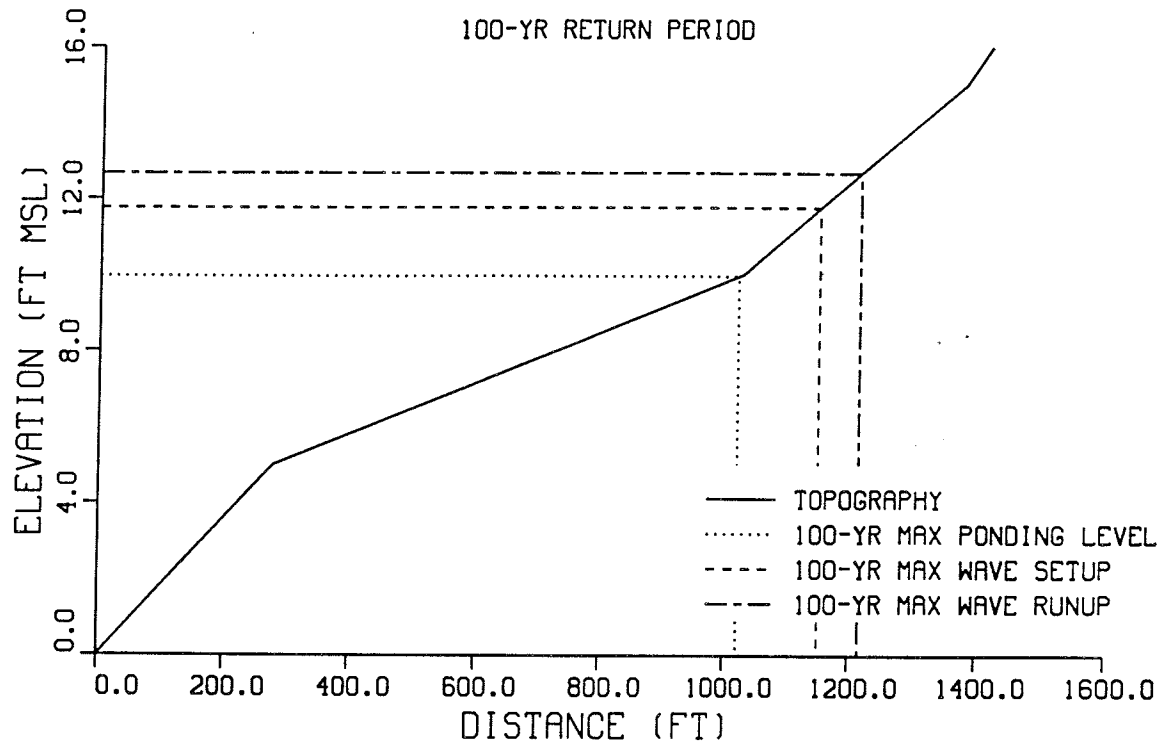
500-YR RETURN PERIOD



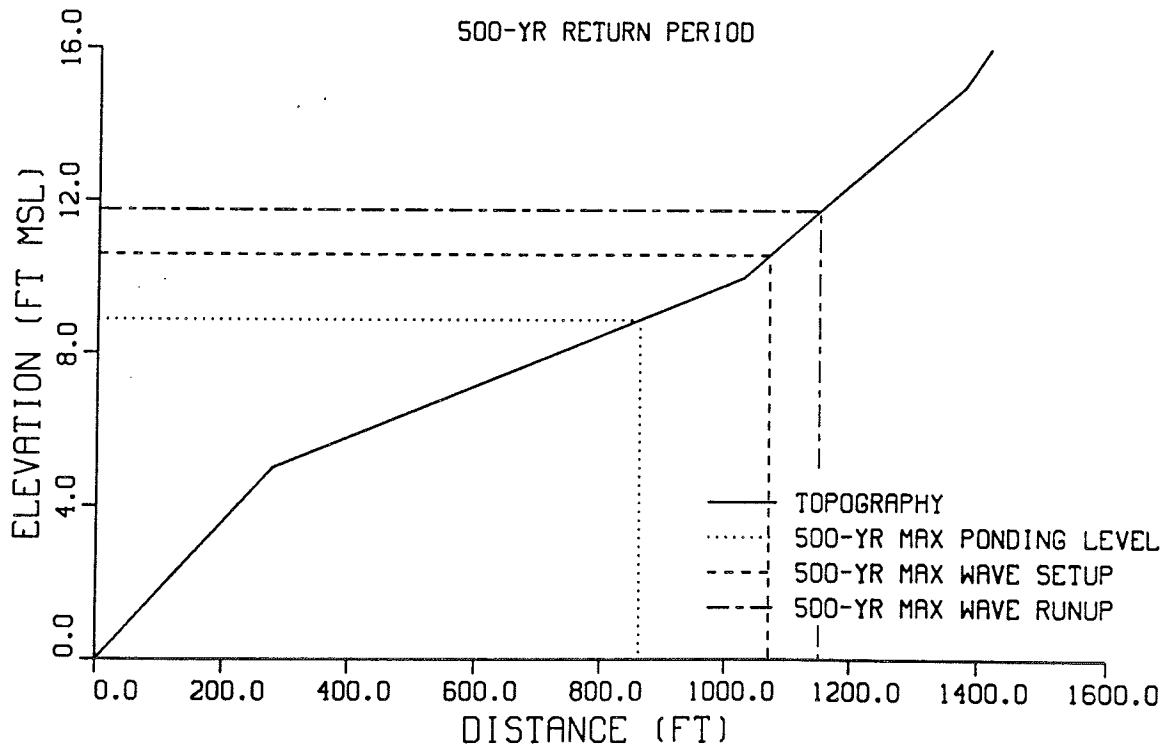
SOUTHERN GUAM TYPHOON ANALYSIS

PROFILE 4-2

100-YR RETURN PERIOD



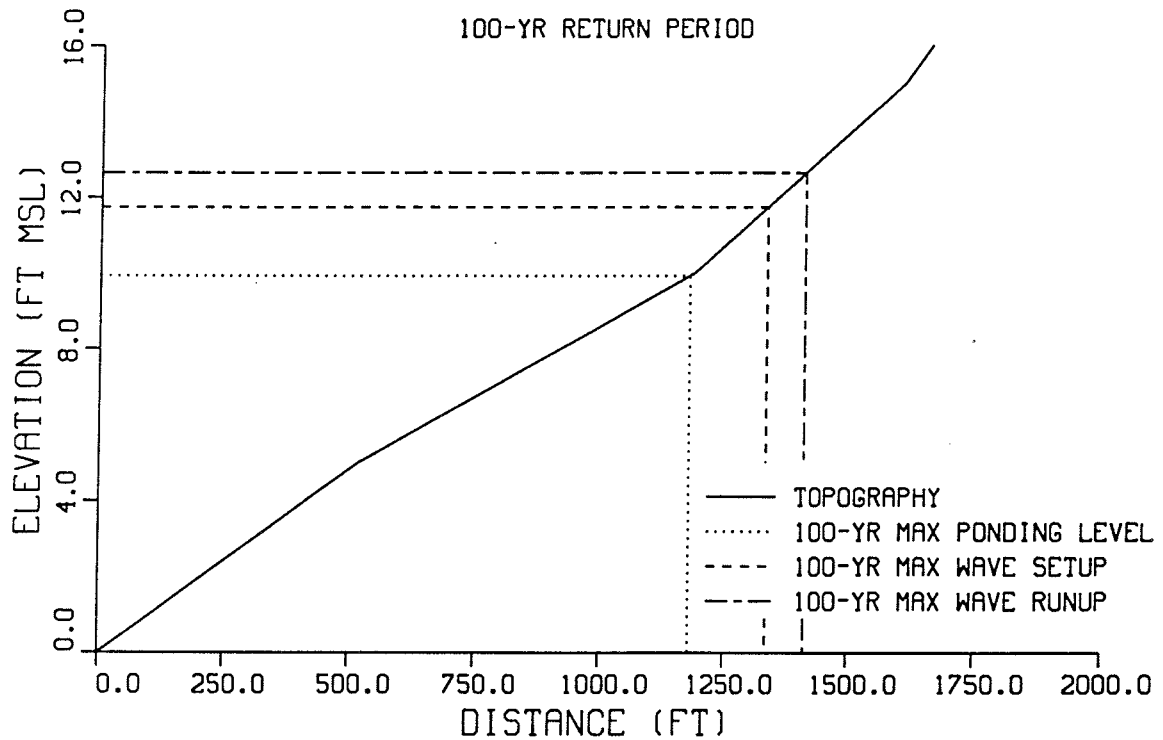
500-YR RETURN PERIOD



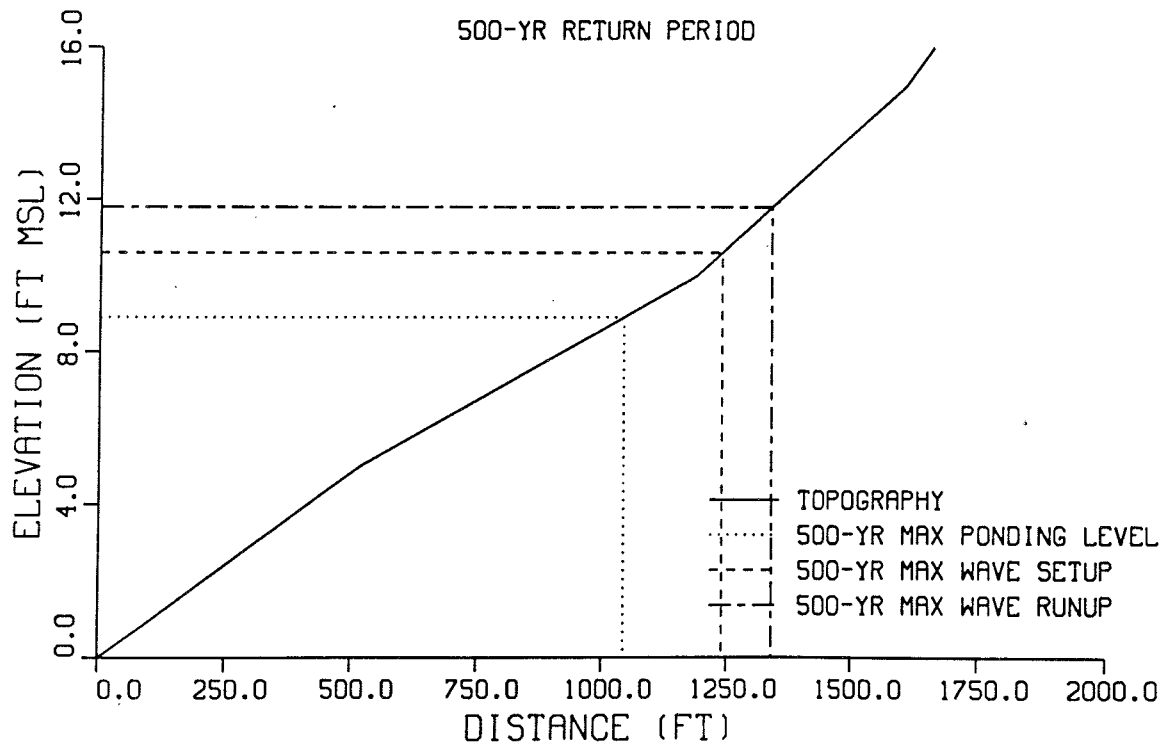
SOUTHERN GUAM TYPHOON ANALYSIS

PROFILE 4-3

100-YR RETURN PERIOD



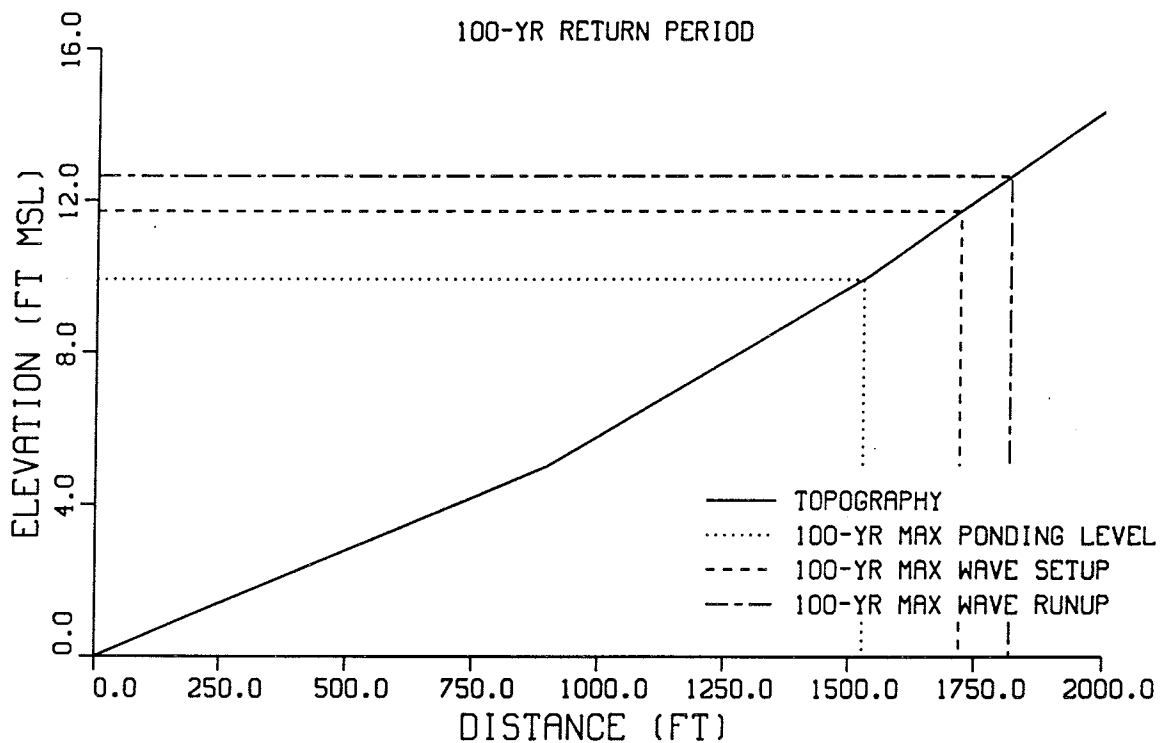
500-YR RETURN PERIOD



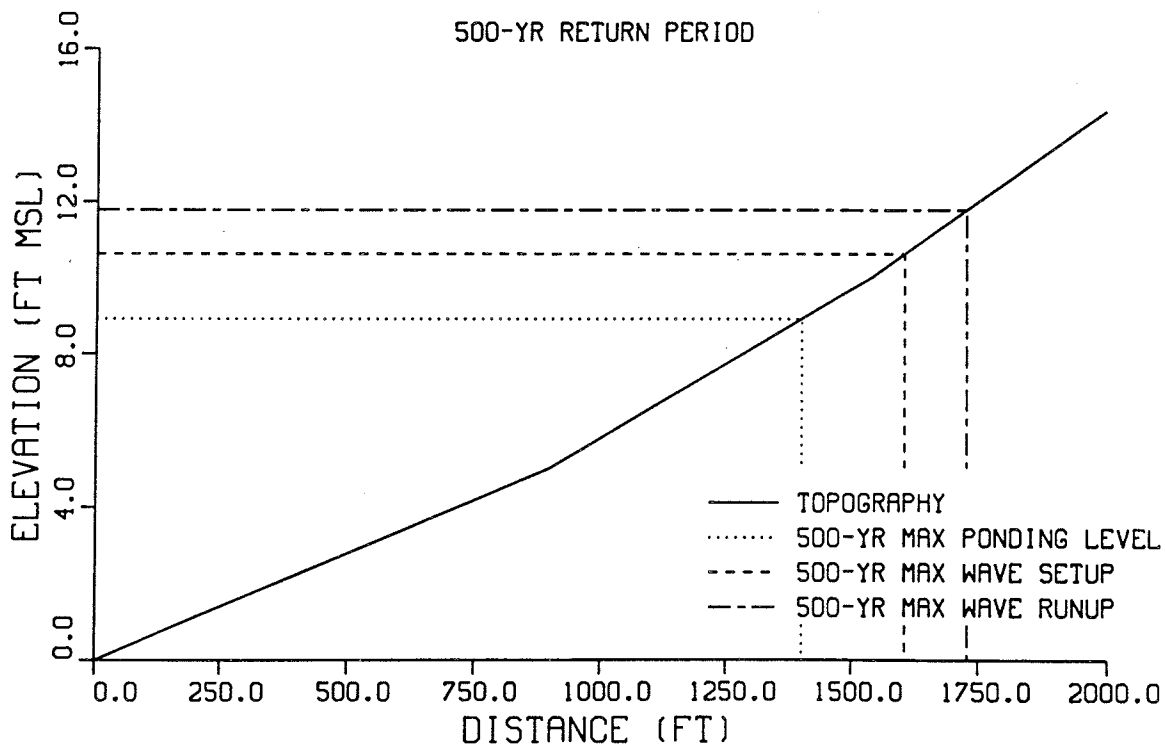
SOUTHERN GUAM TYPHOON ANALYSIS

PROFILE 4-4

100-YR RETURN PERIOD



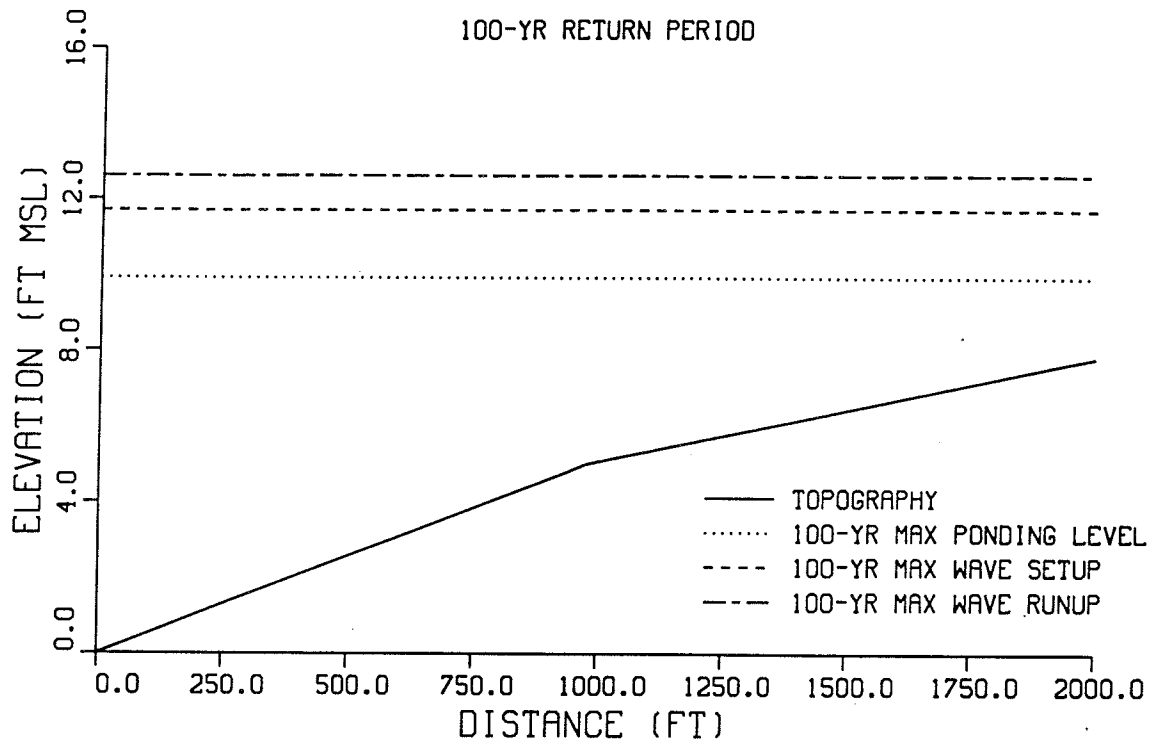
500-YR RETURN PERIOD



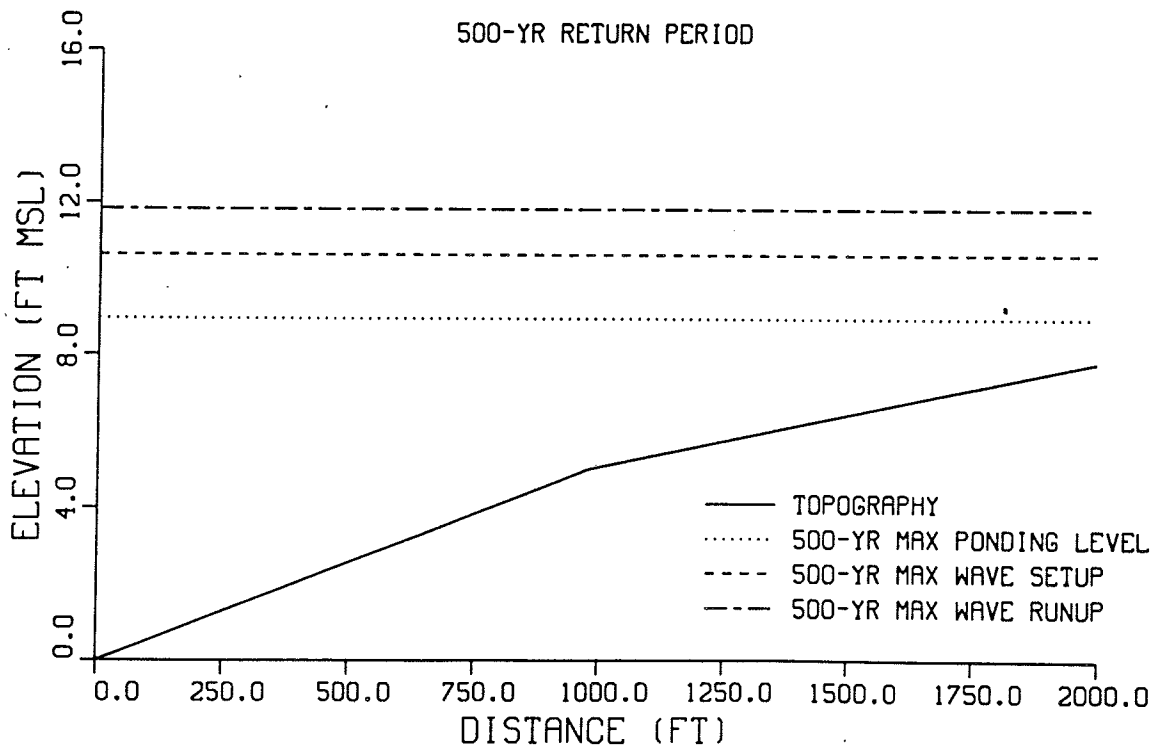
SOUTHERN GUAM TYPHOON ANALYSIS

PROFILE 4-5

100-YR RETURN PERIOD



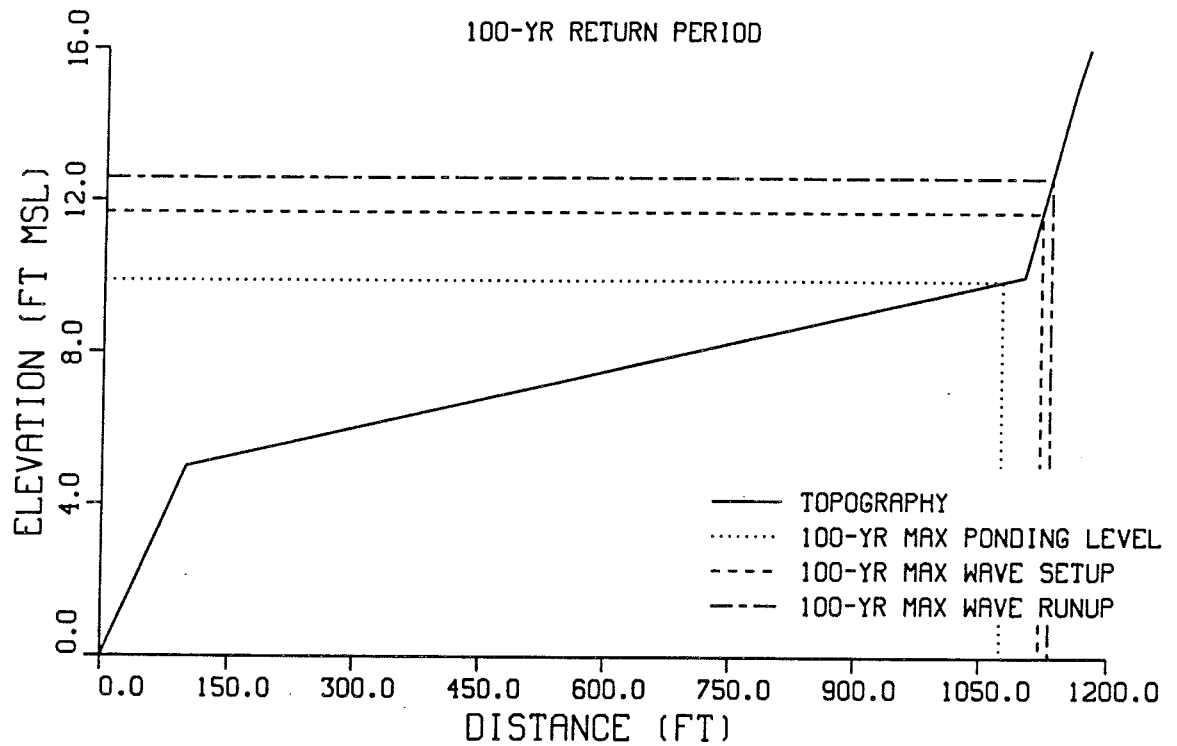
500-YR RETURN PERIOD



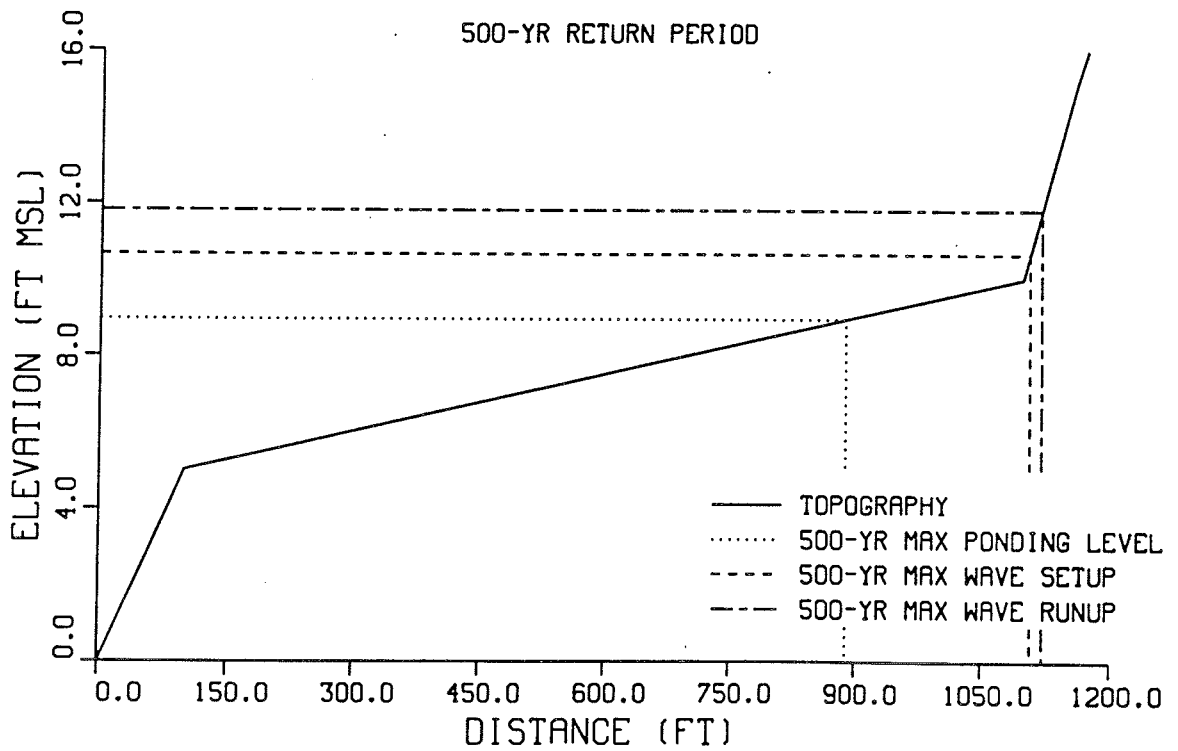
SOUTHERN GUAM TYPHOON ANALYSIS

PROFILE 4-6

100-YR RETURN PERIOD



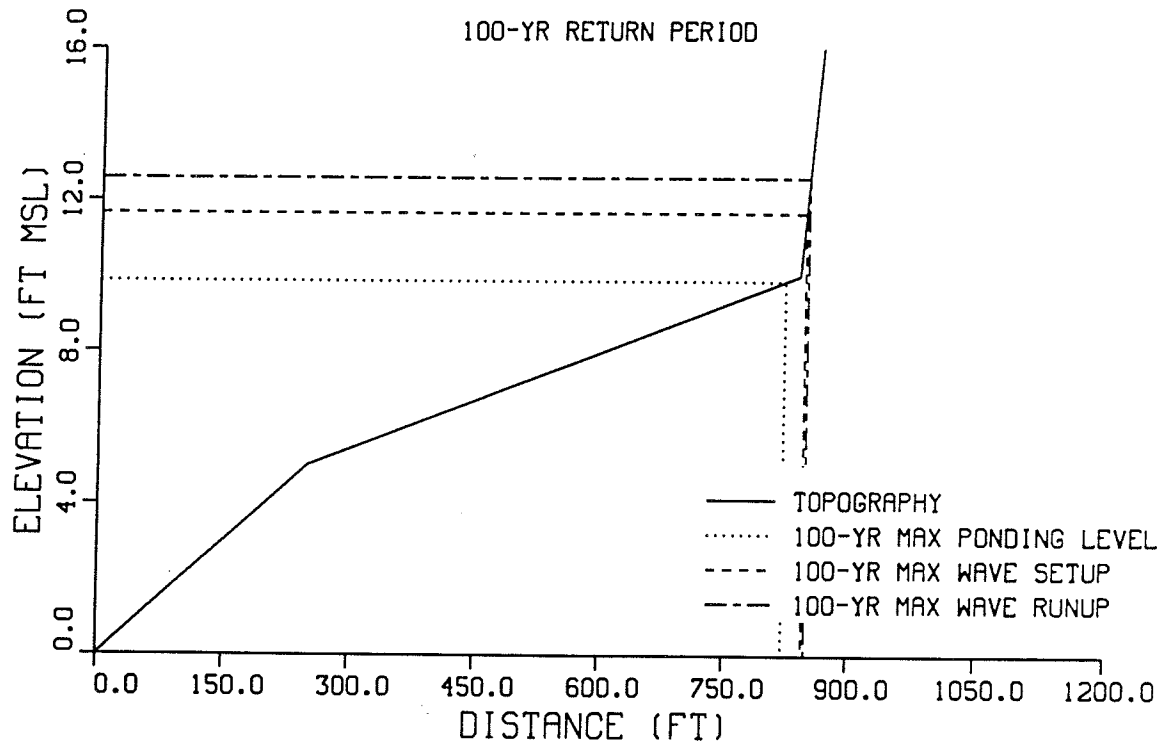
500-YR RETURN PERIOD



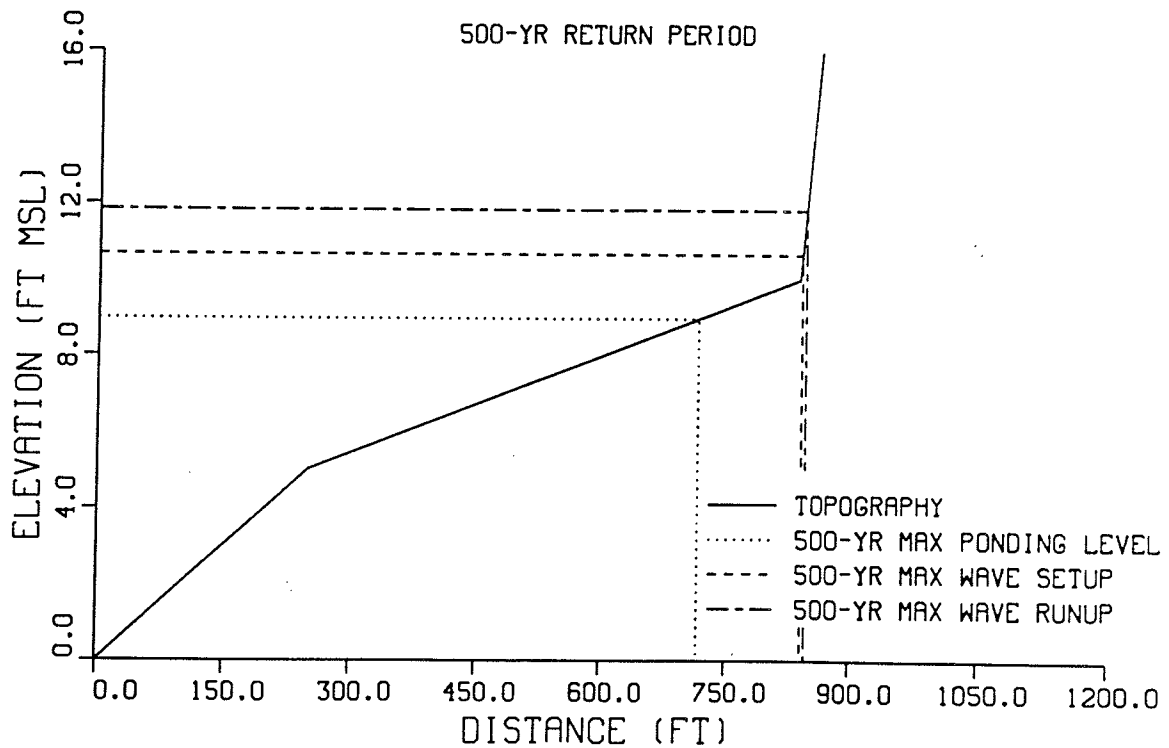
SOUTHERN GUAM TYPHOON ANALYSIS

PROFILE 4-7

100-YR RETURN PERIOD



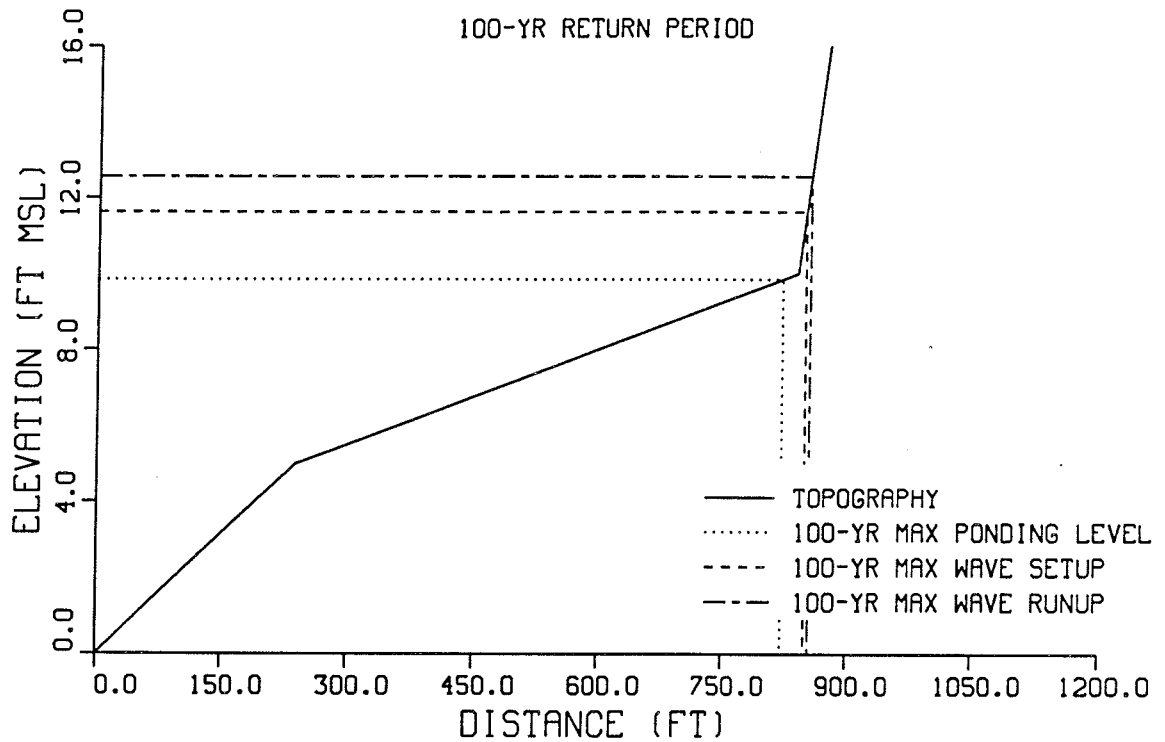
500-YR RETURN PERIOD



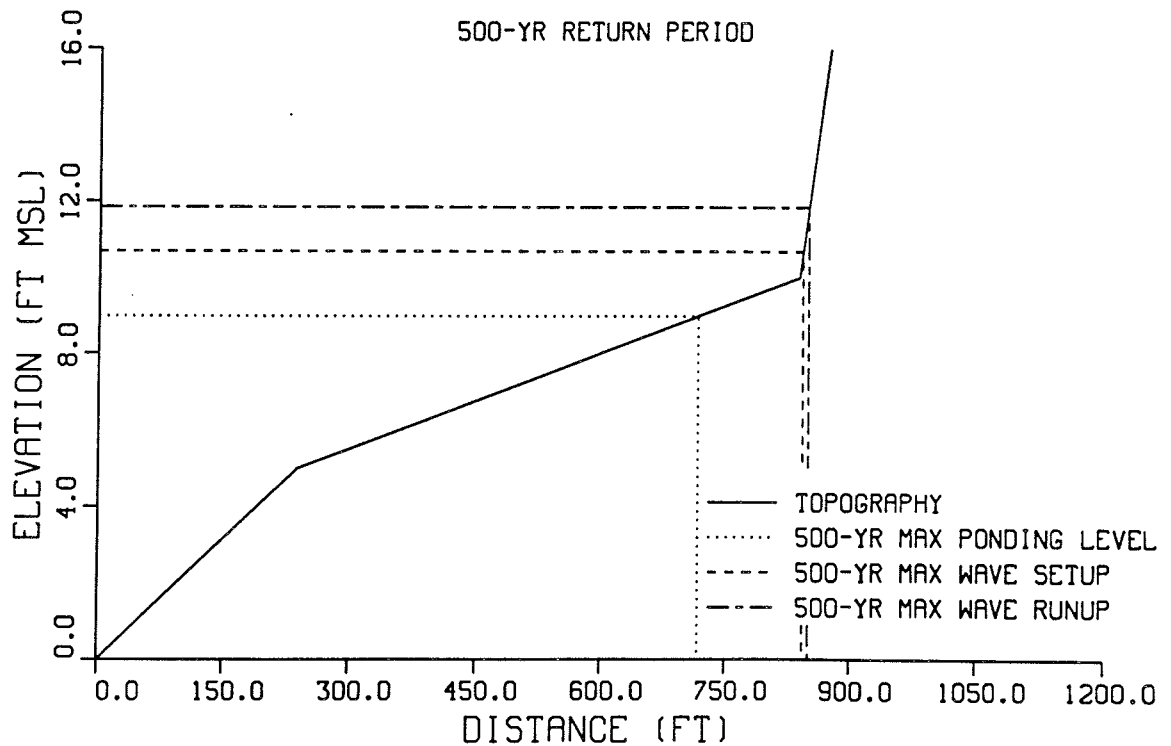
SOUTHERN GUAM TYPHOON ANALYSIS

PROFILE 4-8

100-YR RETURN PERIOD



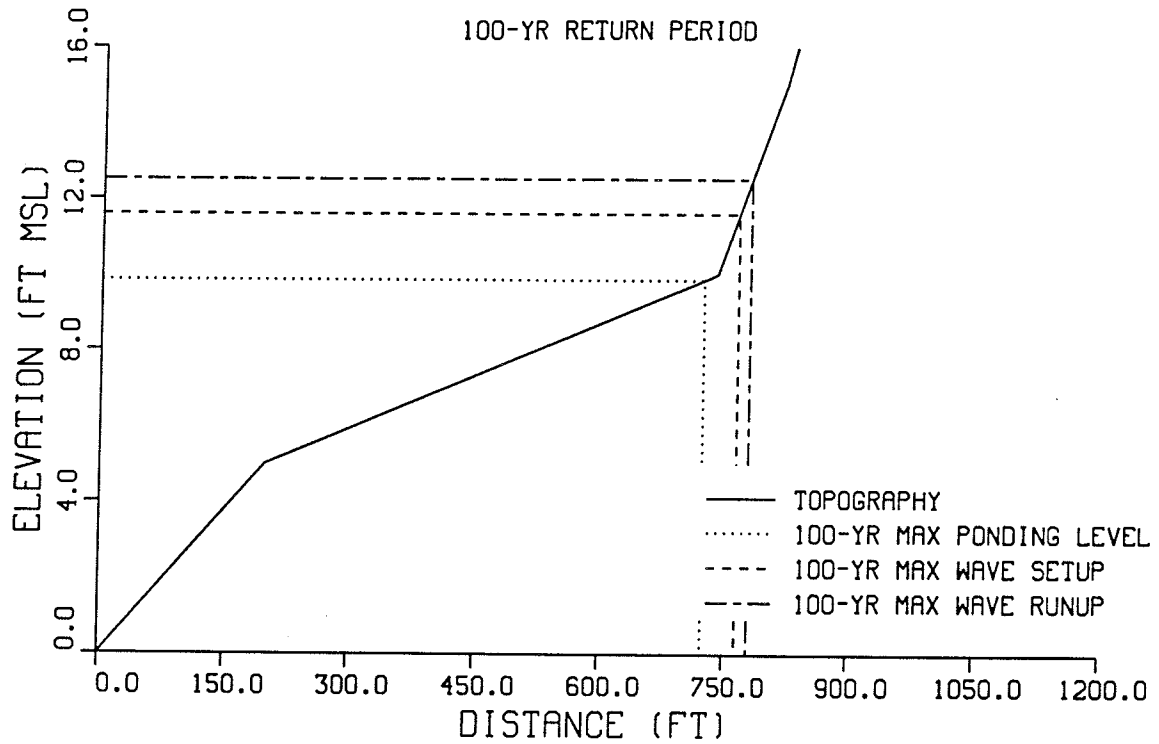
500-YR RETURN PERIOD



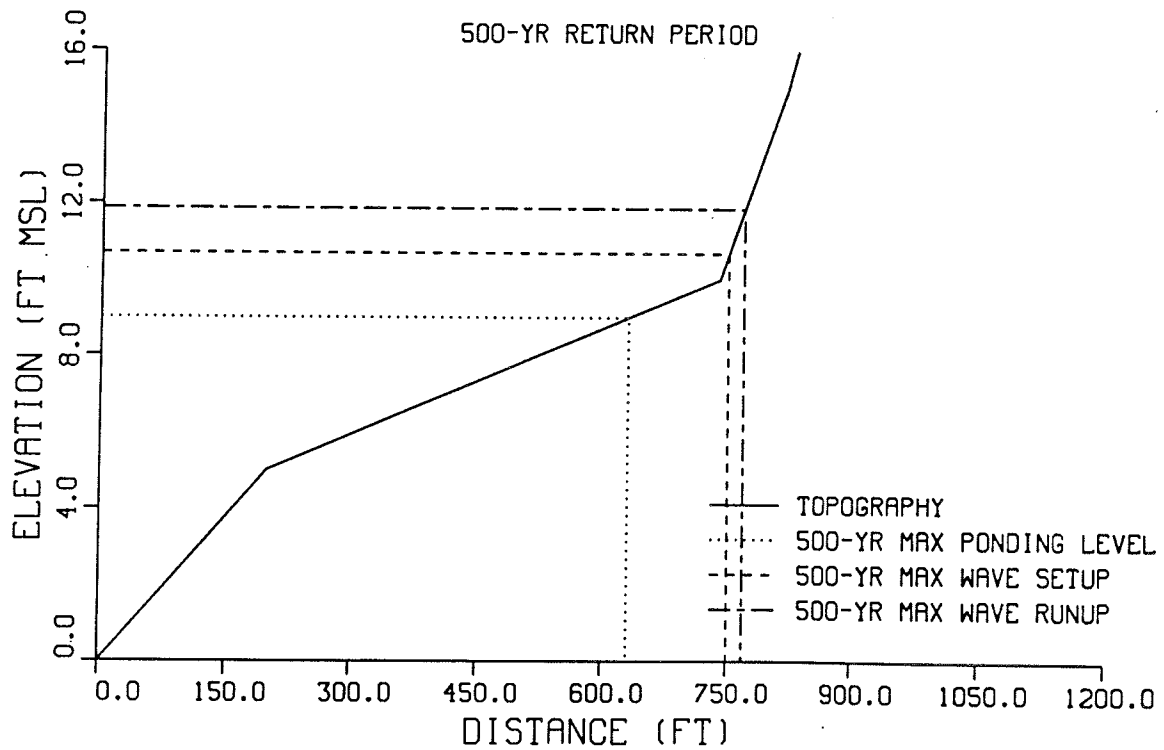
SOUTHERN GUAM TYPHOON ANALYSIS

PROFILE 4-9

100-YR RETURN PERIOD



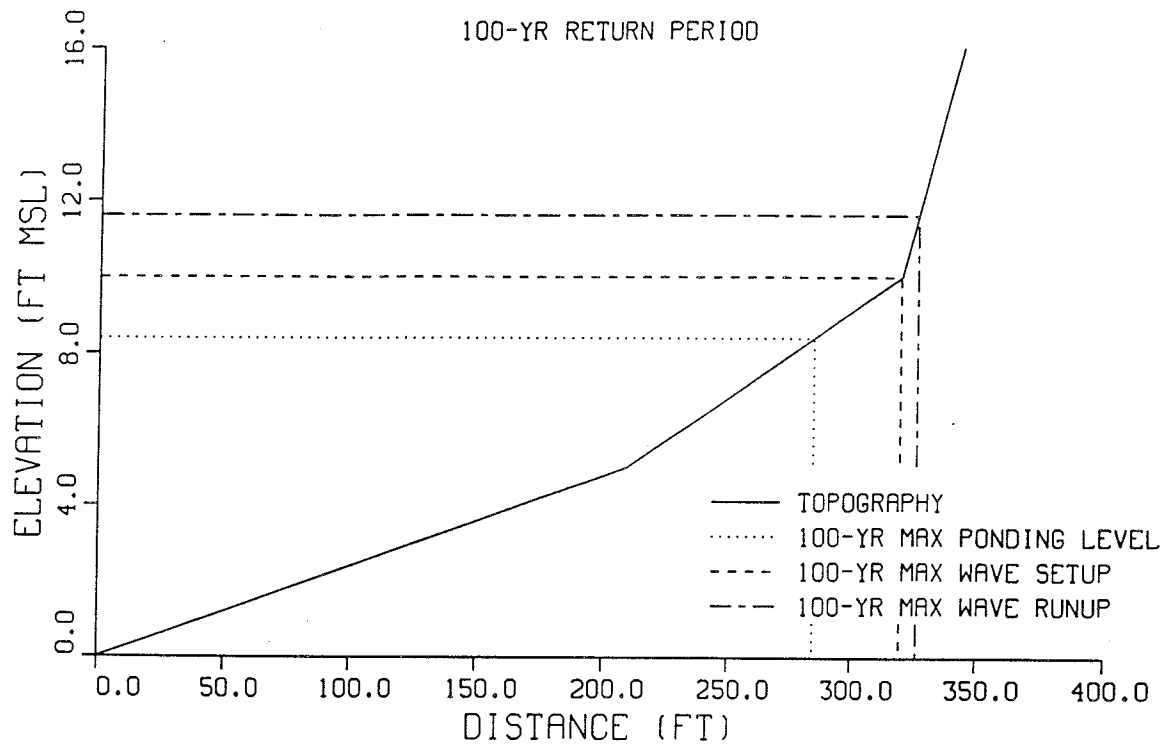
500-YR RETURN PERIOD



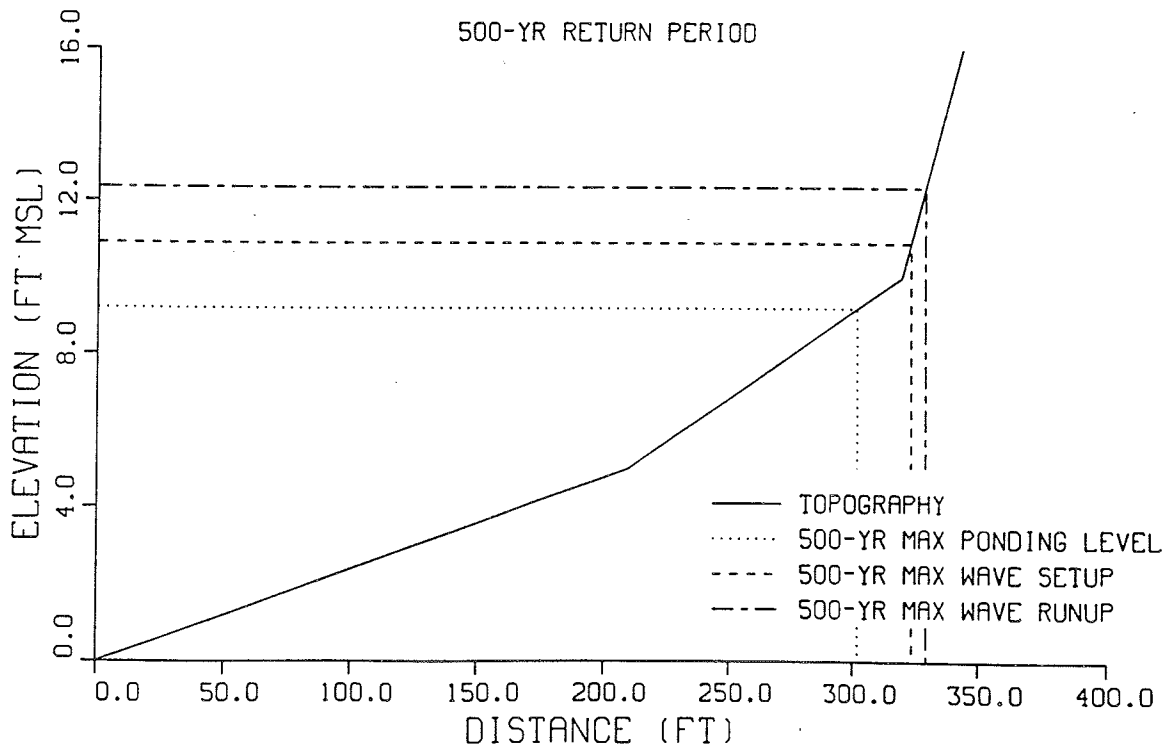
SOUTHERN GUAM TYPHOON ANALYSIS

PROFILE 5-1

100-YR RETURN PERIOD



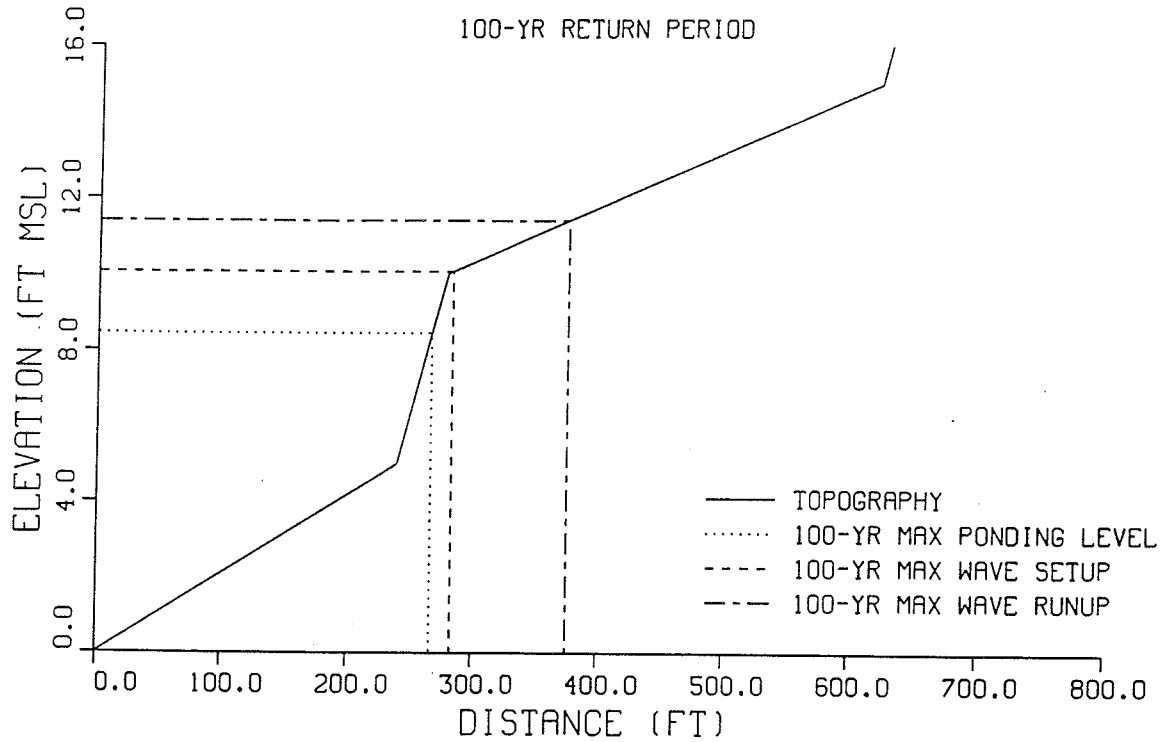
500-YR RETURN PERIOD



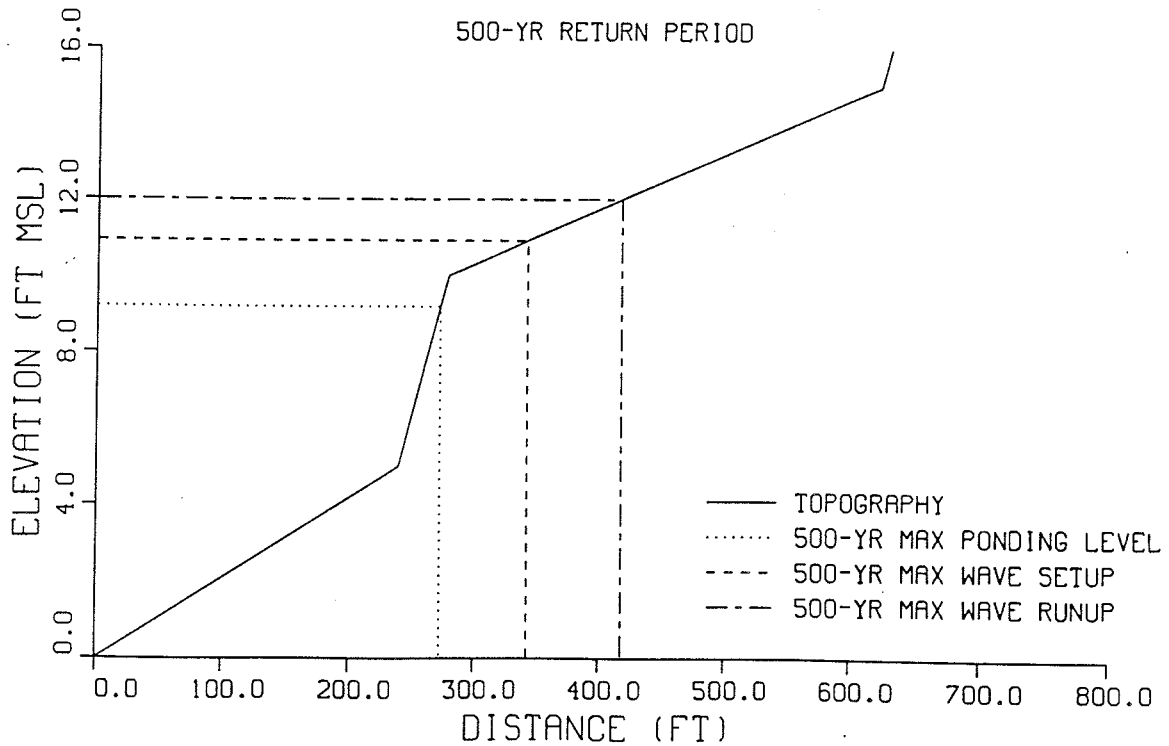
SOUTHERN GUAM TYPHOON ANALYSIS

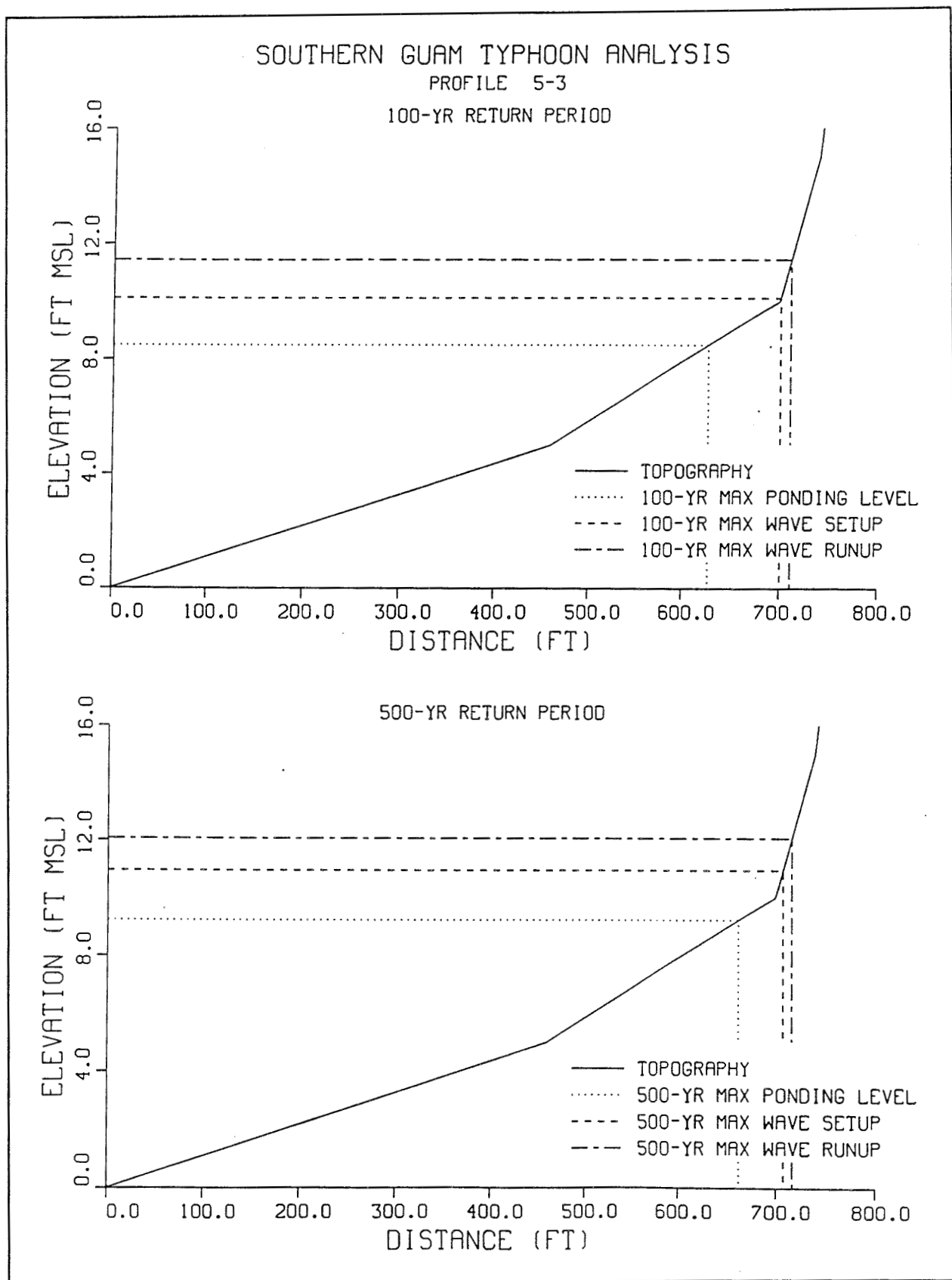
PROFILE 5-2

100-YR RETURN PERIOD



500-YR RETURN PERIOD

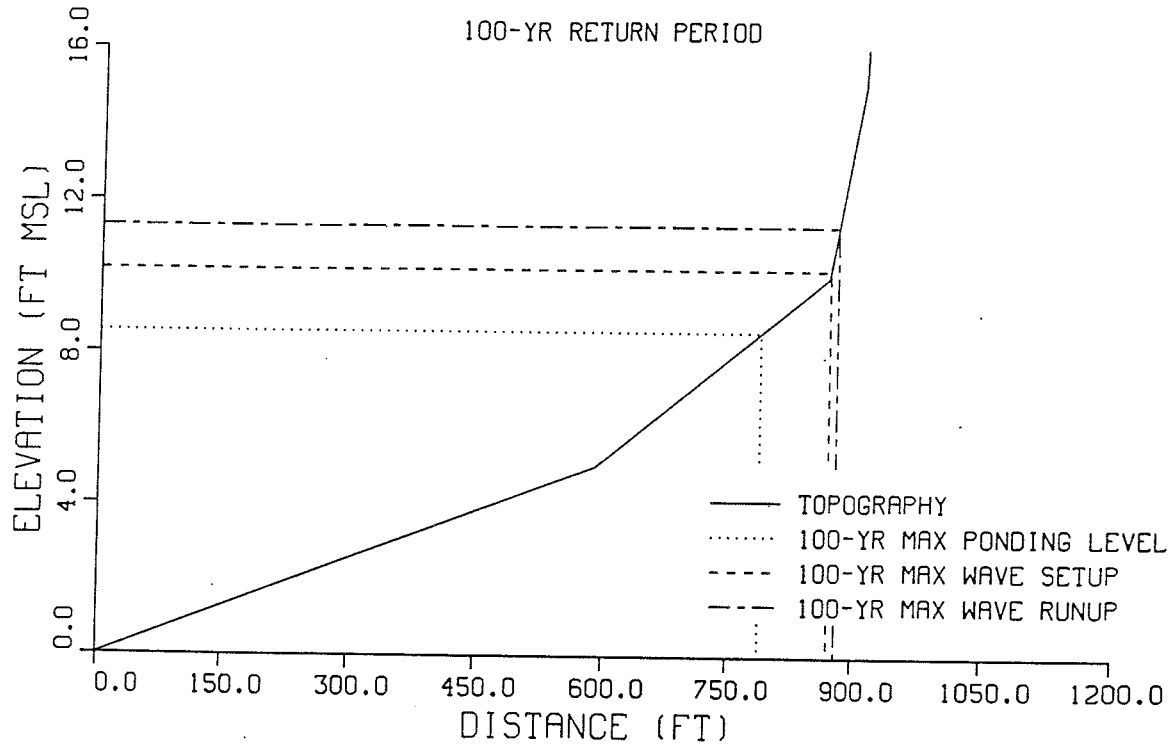




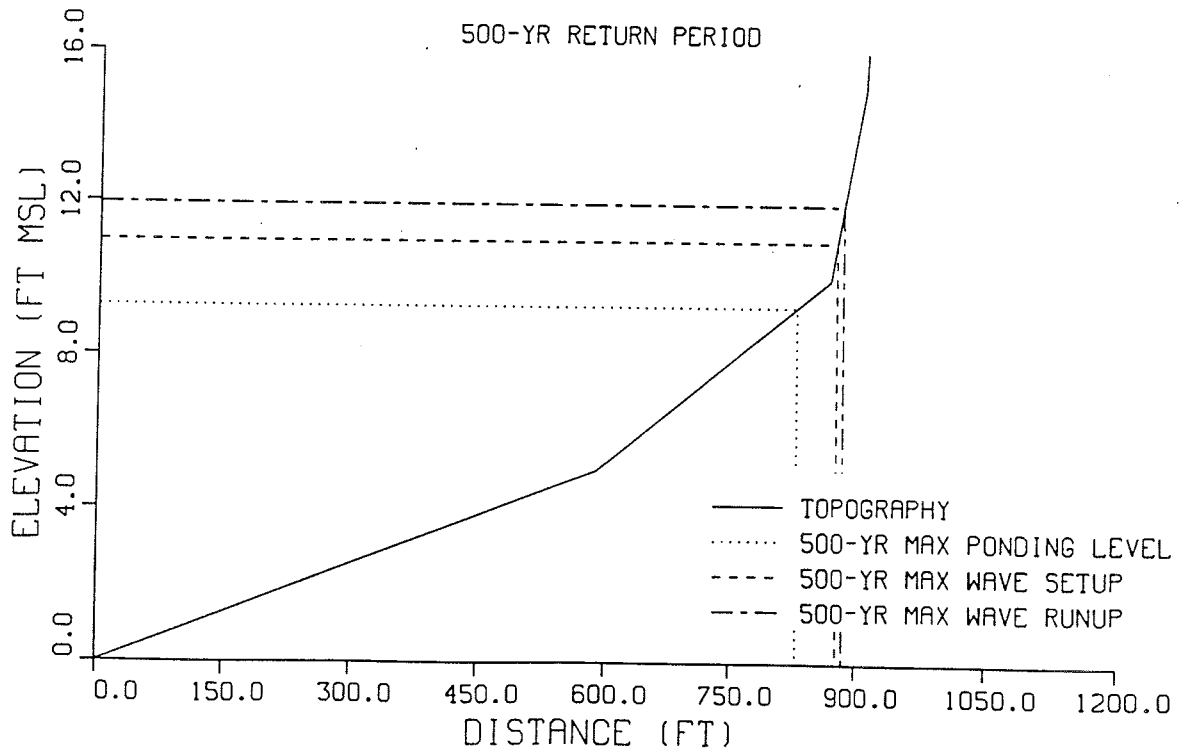
SOUTHERN GUAM TYPHOON ANALYSIS

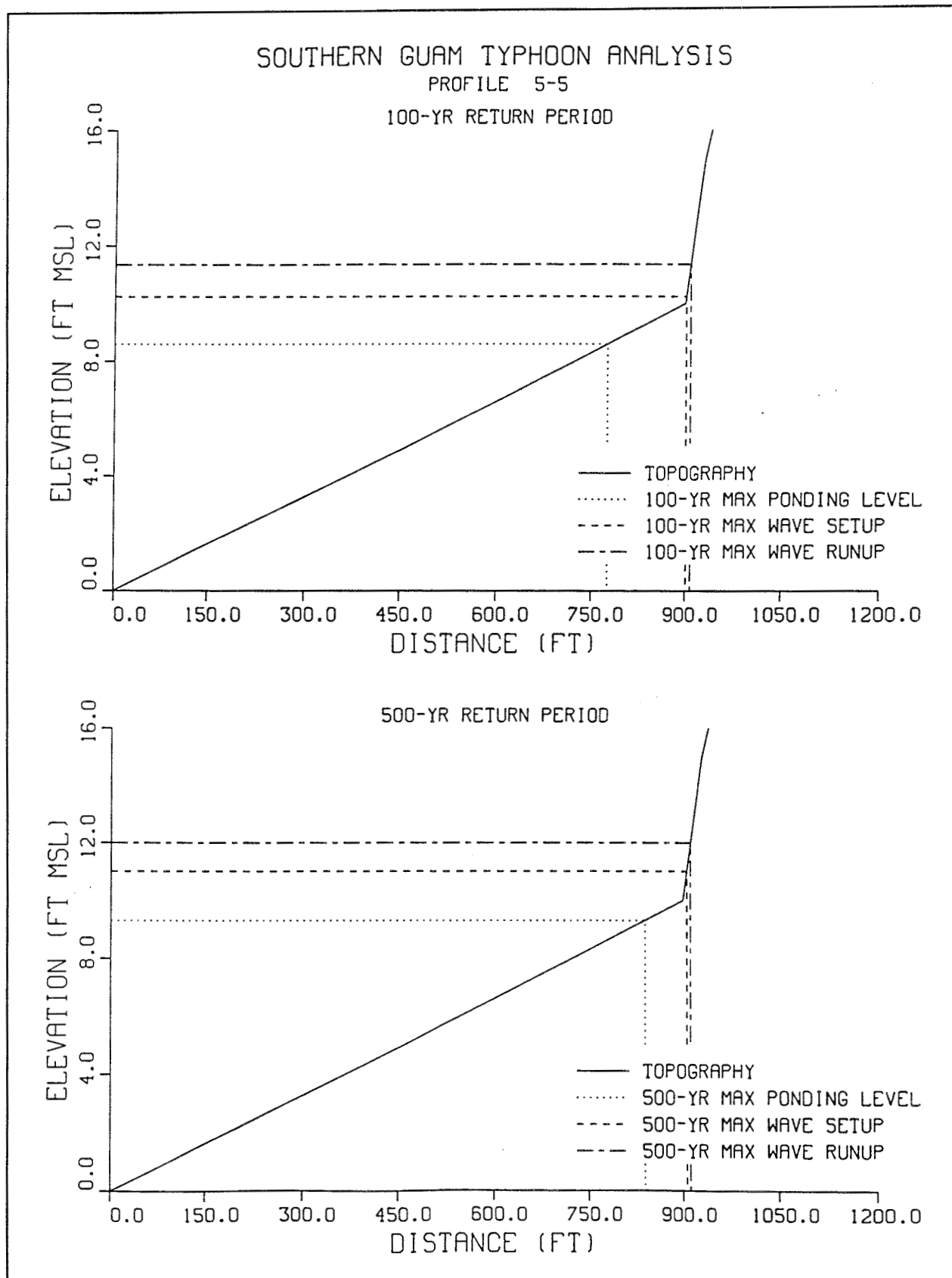
PROFILE 5-4

100-YR RETURN PERIOD



500-YR RETURN PERIOD

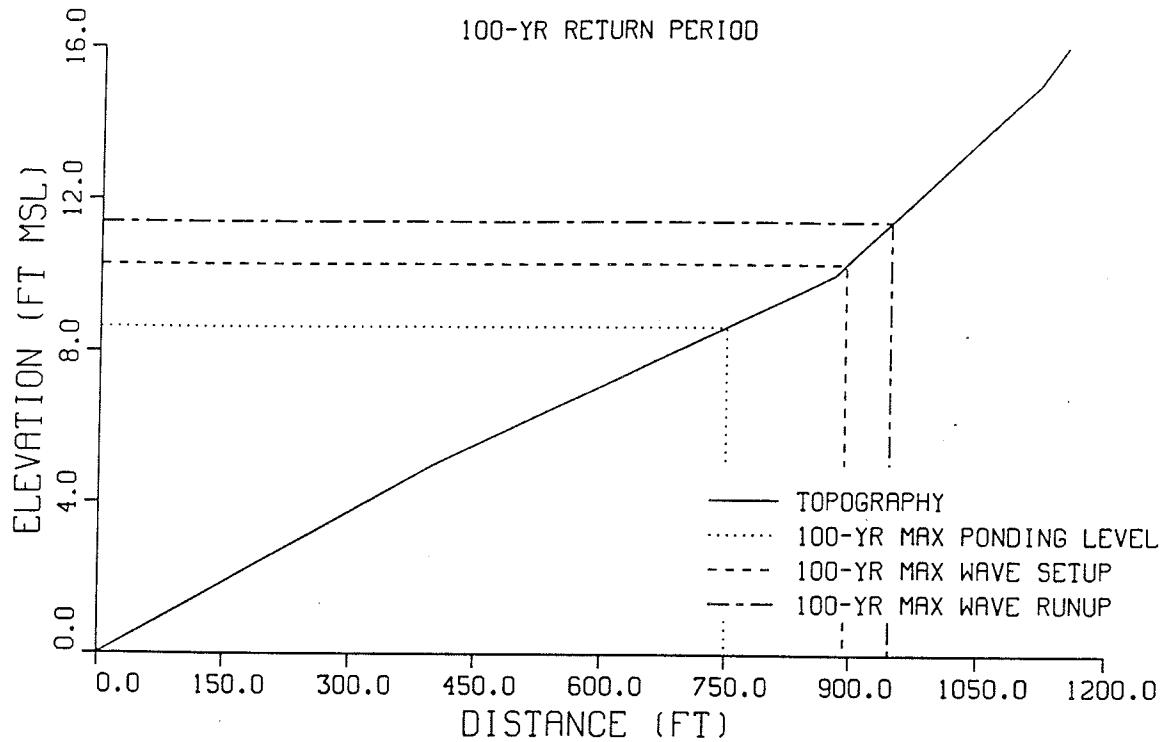




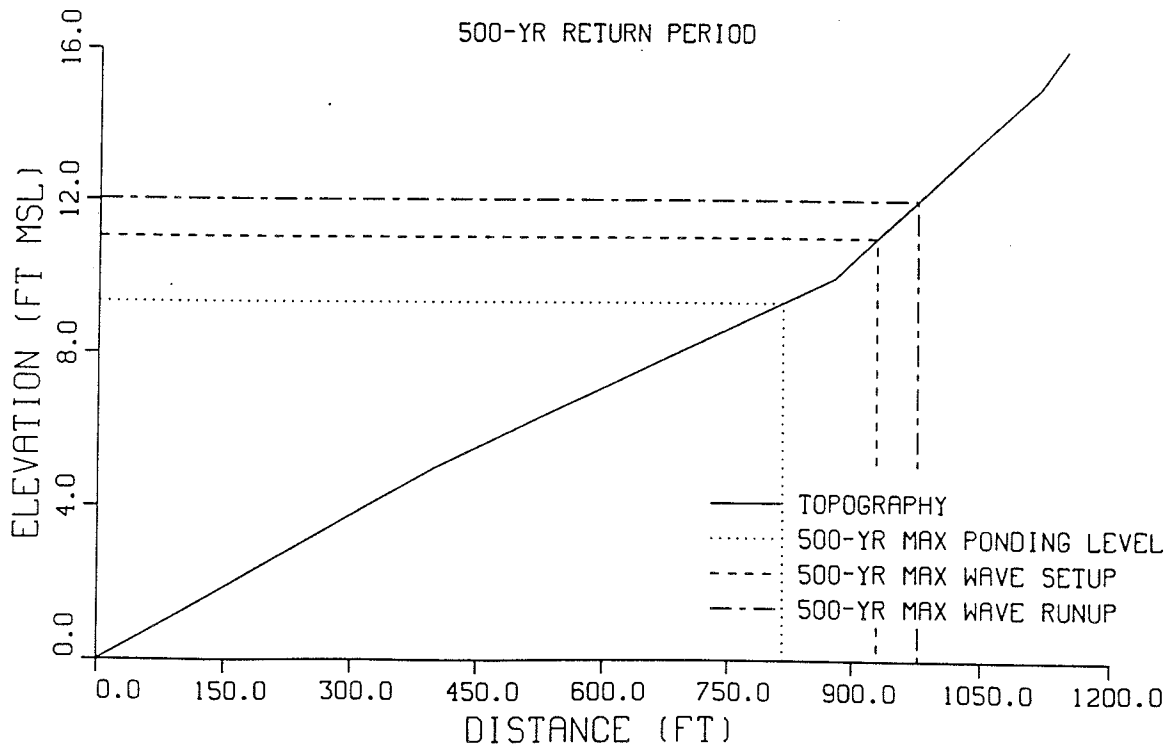
SOUTHERN GUAM TYPHOON ANALYSIS

PROFILE 5-6

100-YR RETURN PERIOD



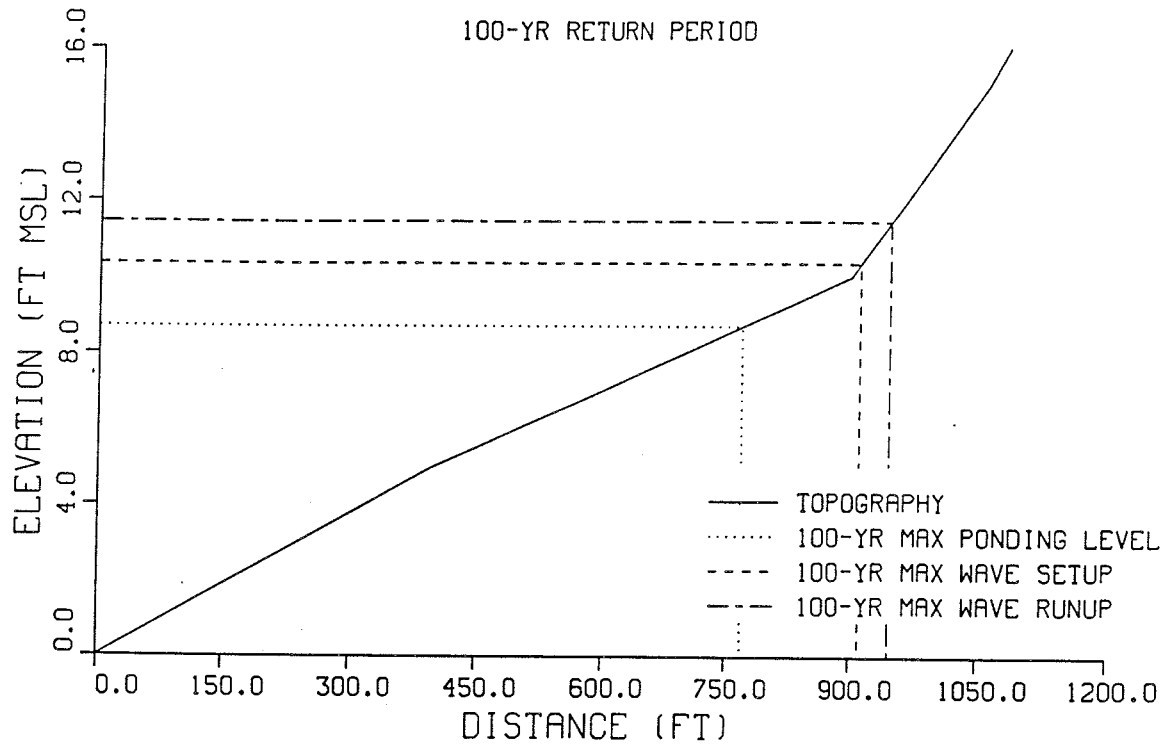
500-YR RETURN PERIOD



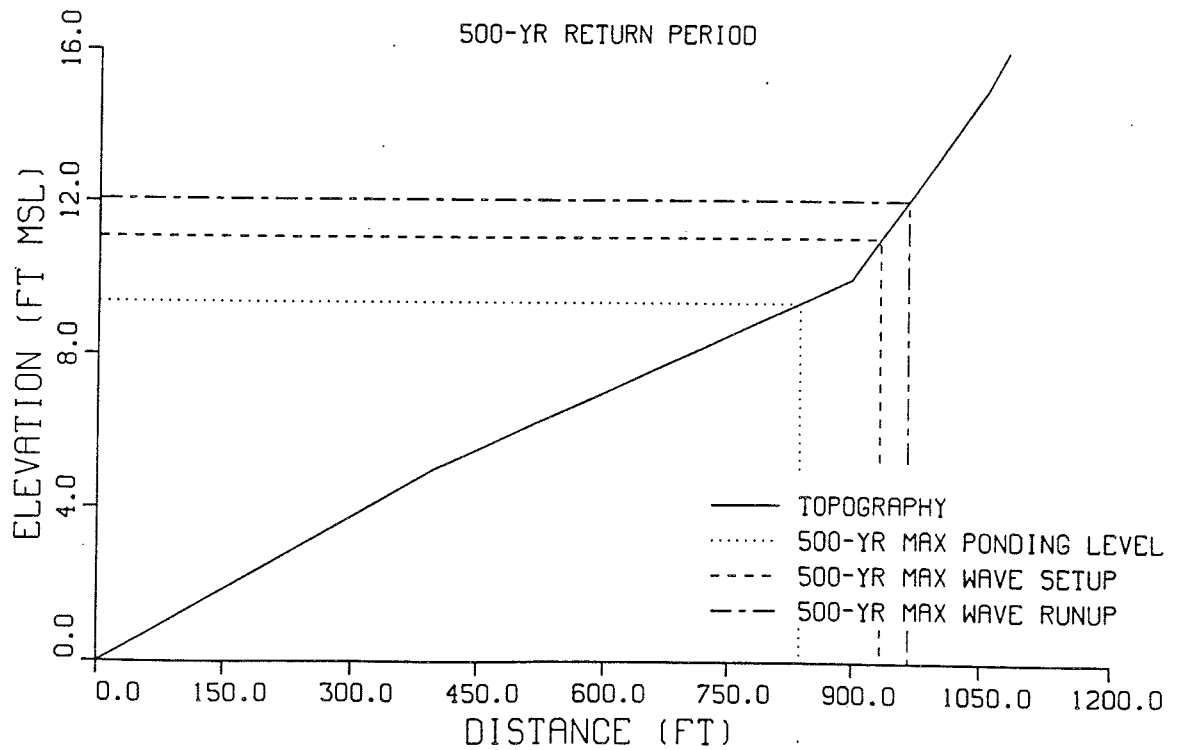
SOUTHERN GUAM TYPHOON ANALYSIS

PROFILE 5-7

100-YR RETURN PERIOD



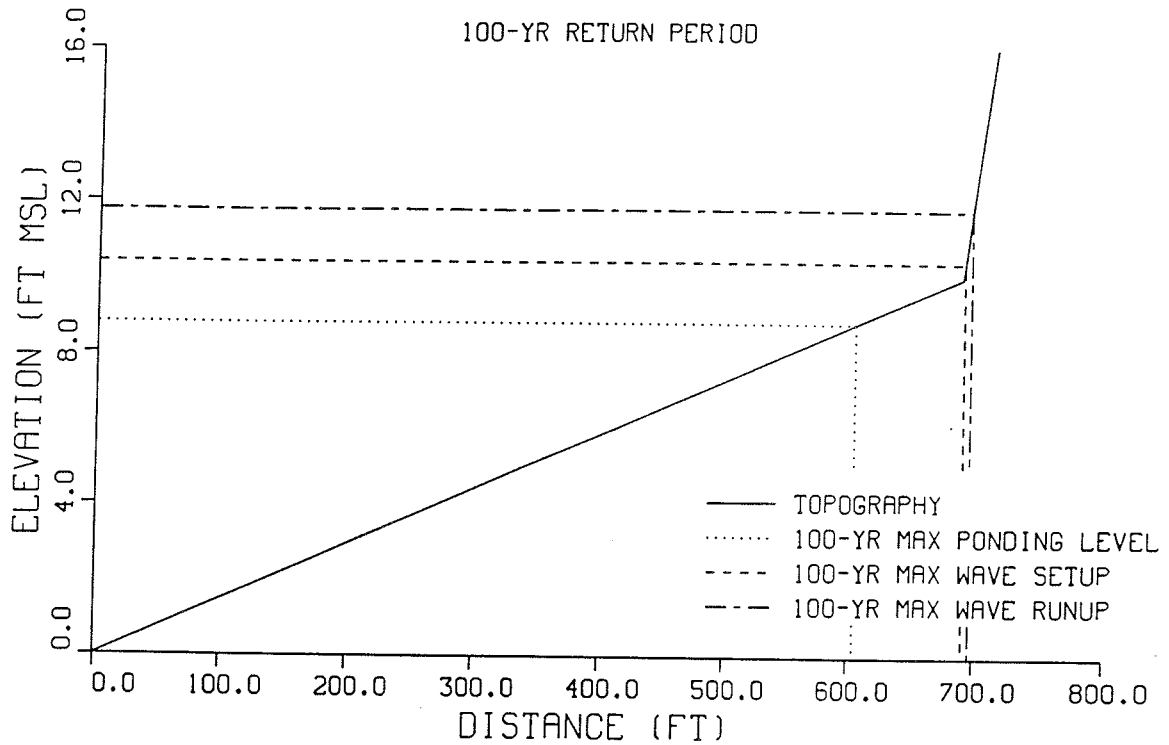
500-YR RETURN PERIOD



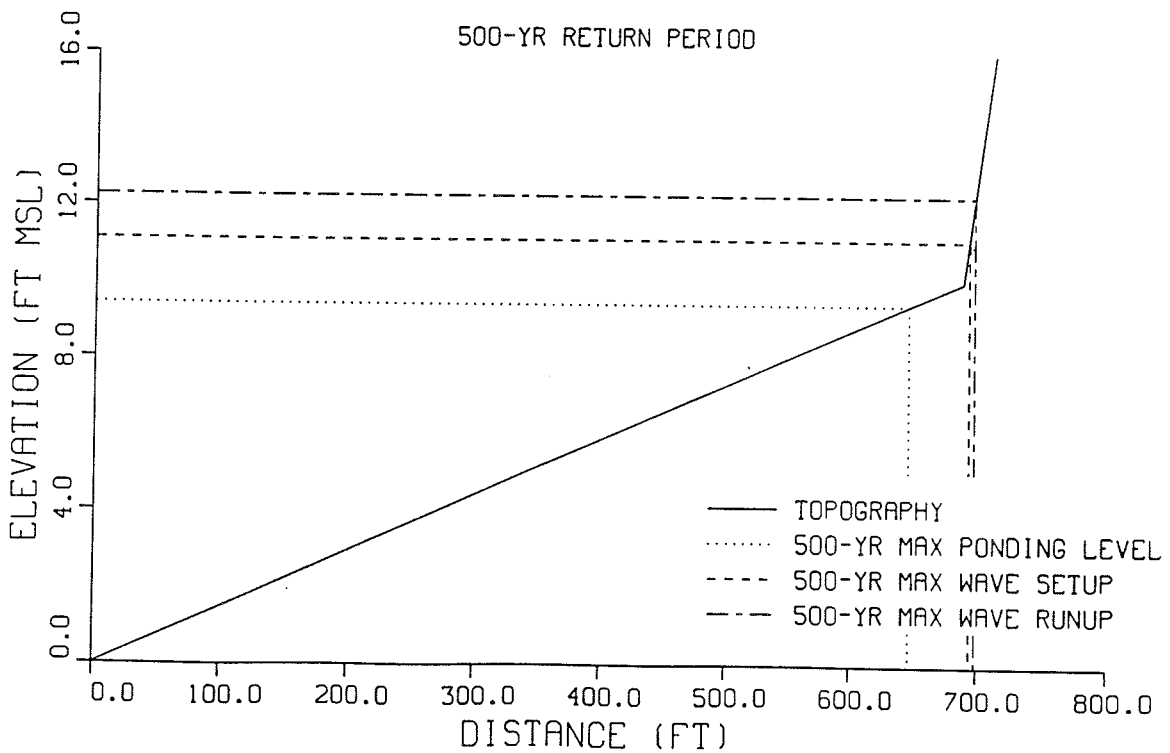
SOUTHERN GUAM TYPHOON ANALYSIS

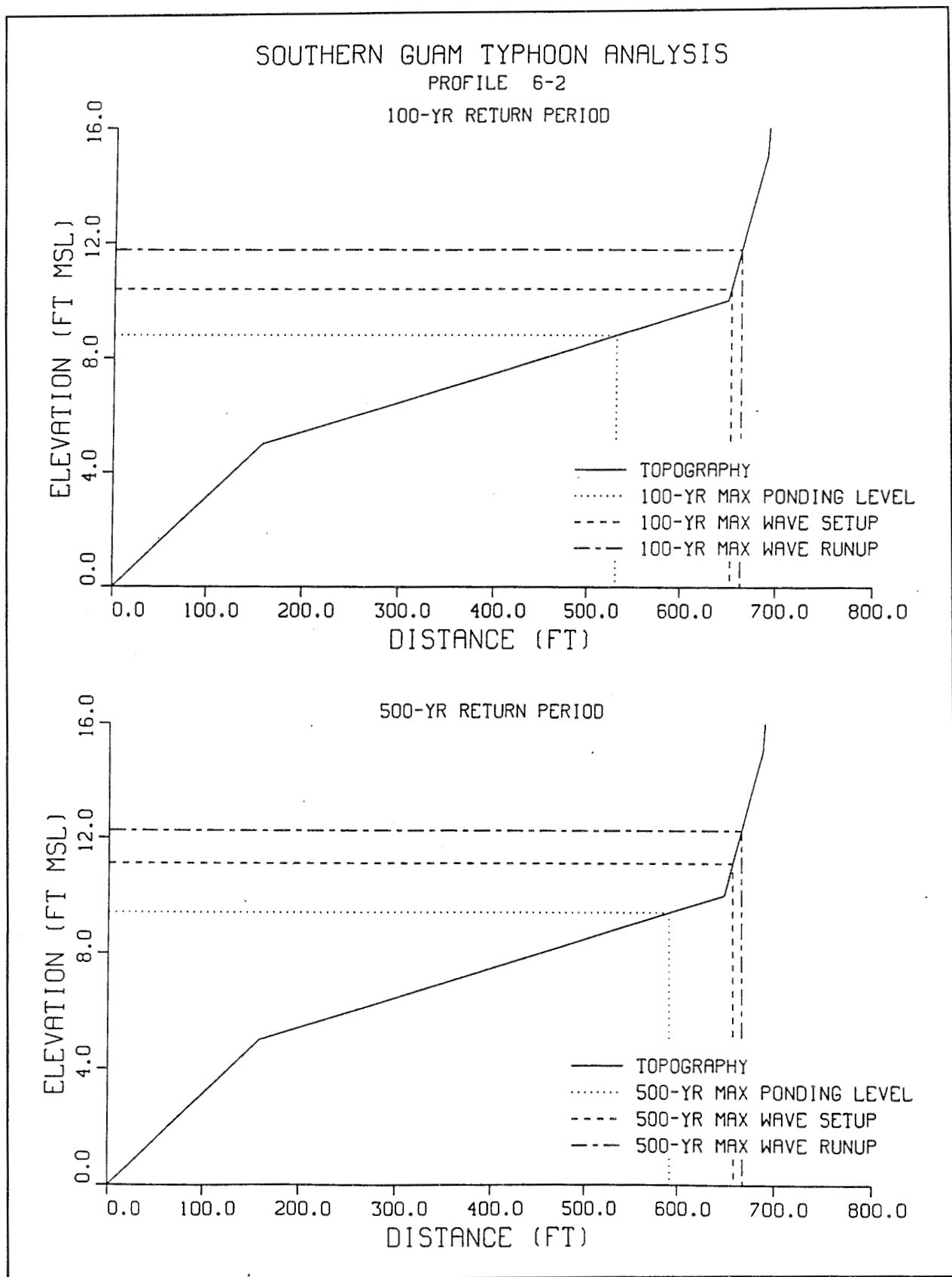
PROFILE 6-1

100-YR RETURN PERIOD



500-YR RETURN PERIOD

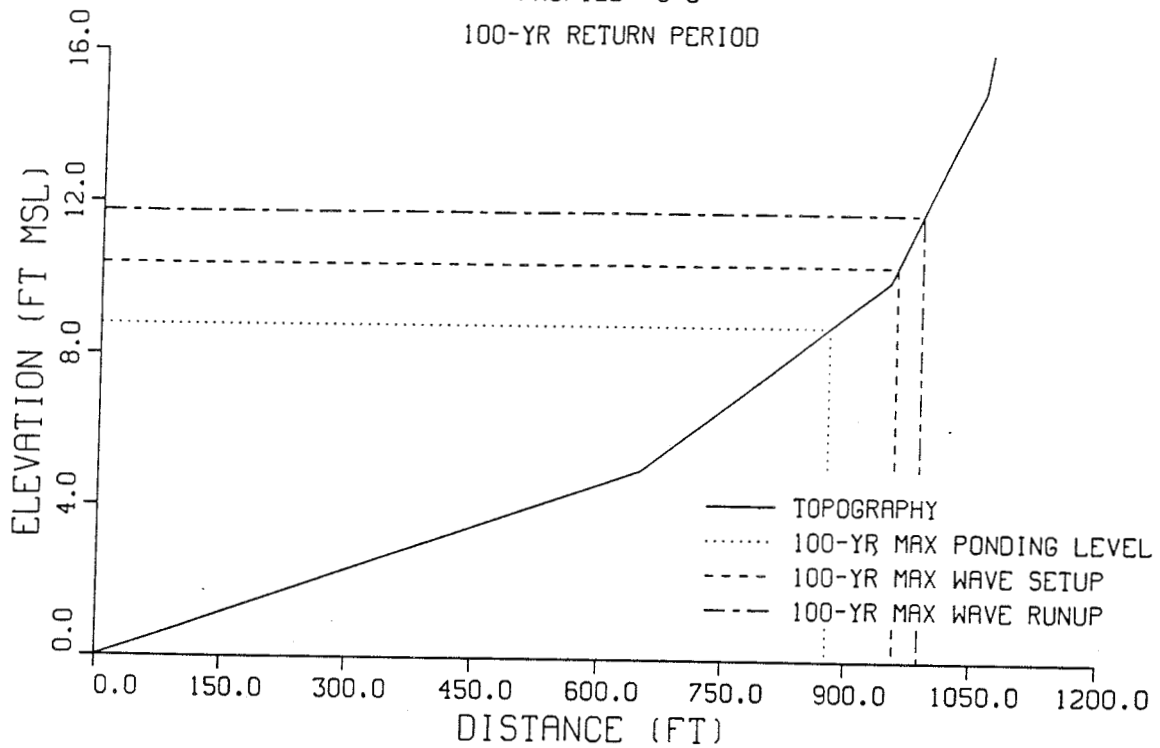




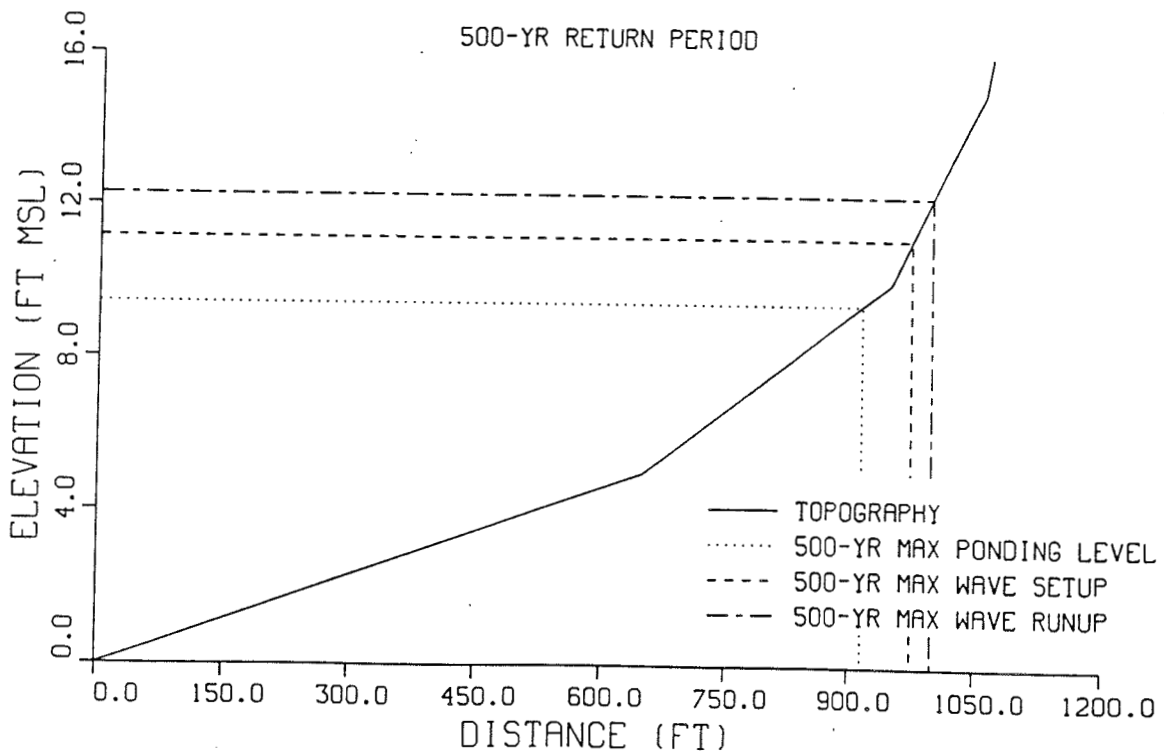
SOUTHERN GUAM TYPHOON ANALYSIS

PROFILE 6-3

100-YR RETURN PERIOD



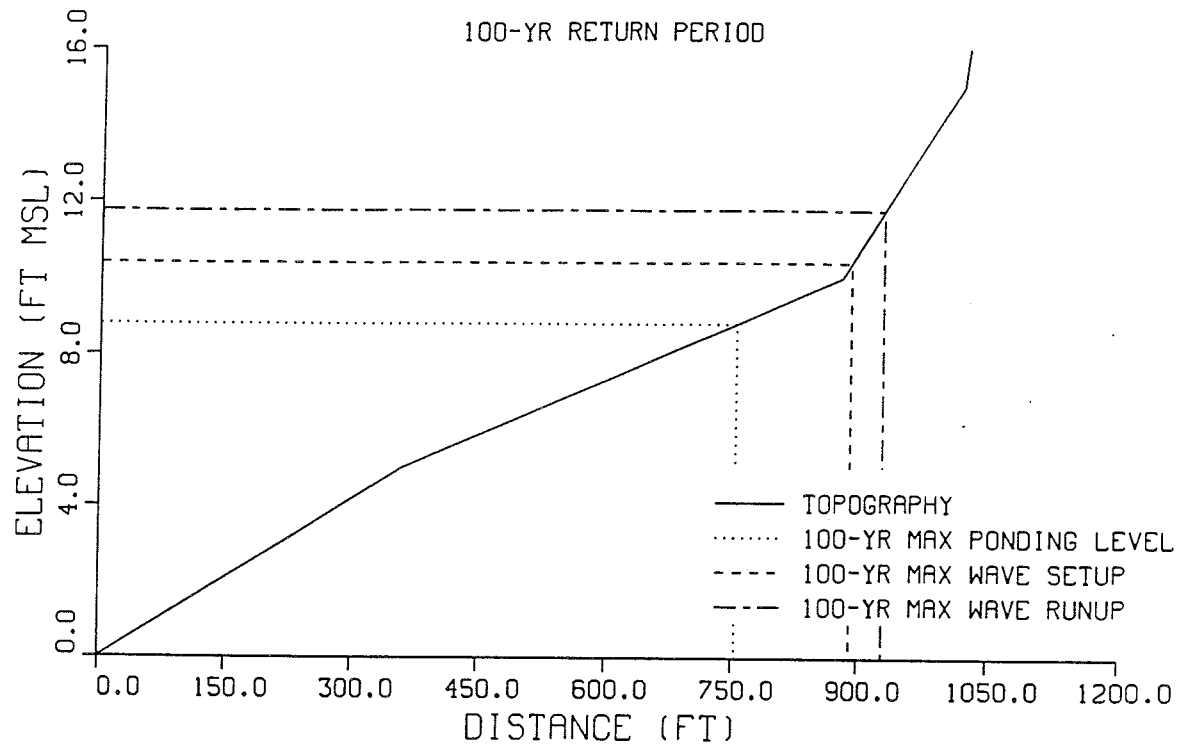
500-YR RETURN PERIOD



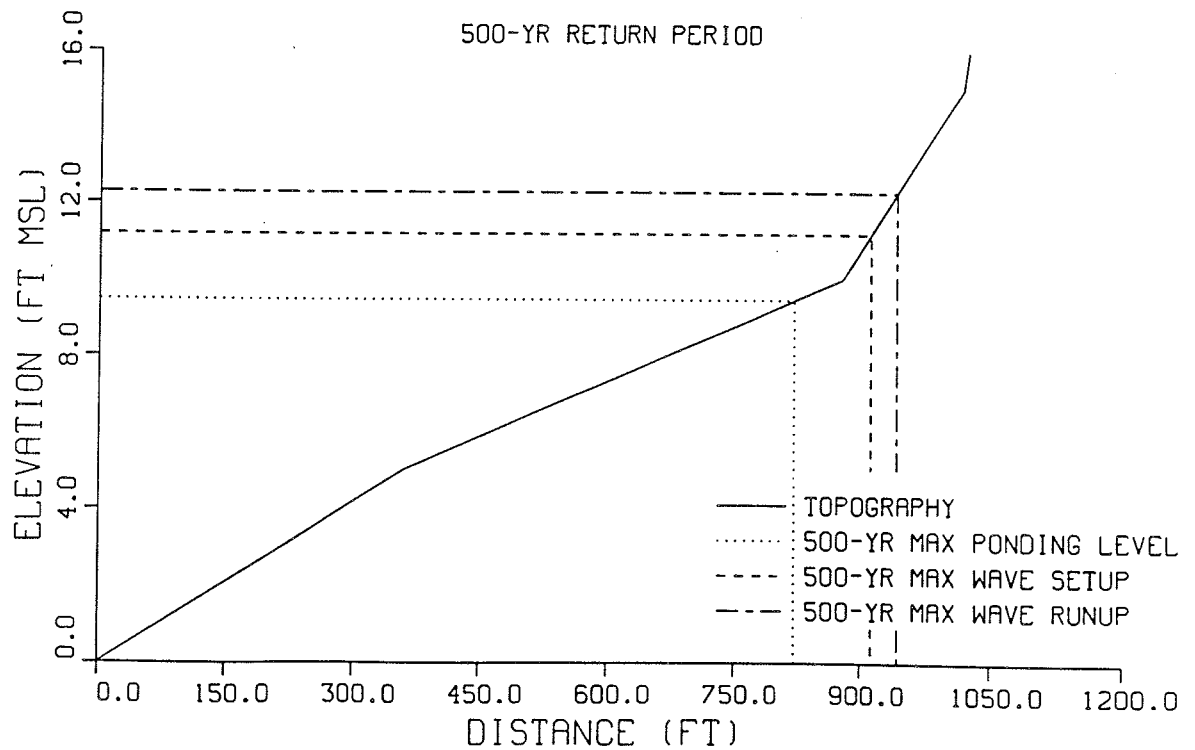
SOUTHERN GUAM TYPHOON ANALYSIS

PROFILE 6-4

100-YR RETURN PERIOD



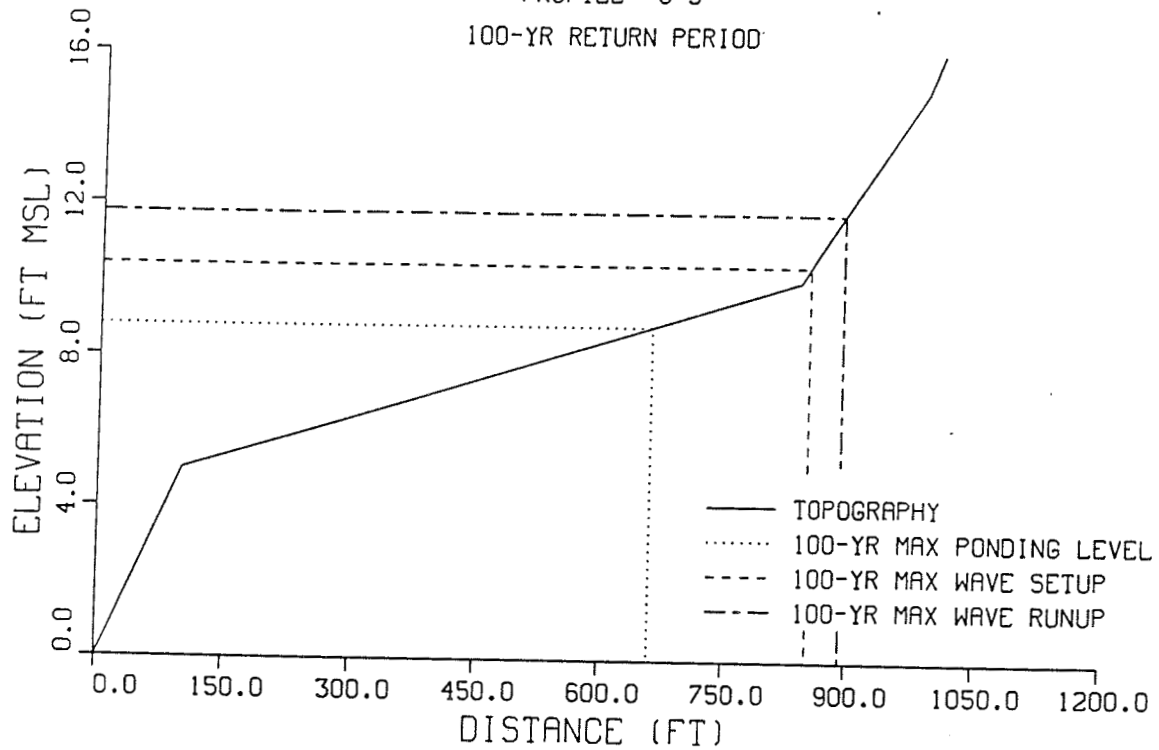
500-YR RETURN PERIOD



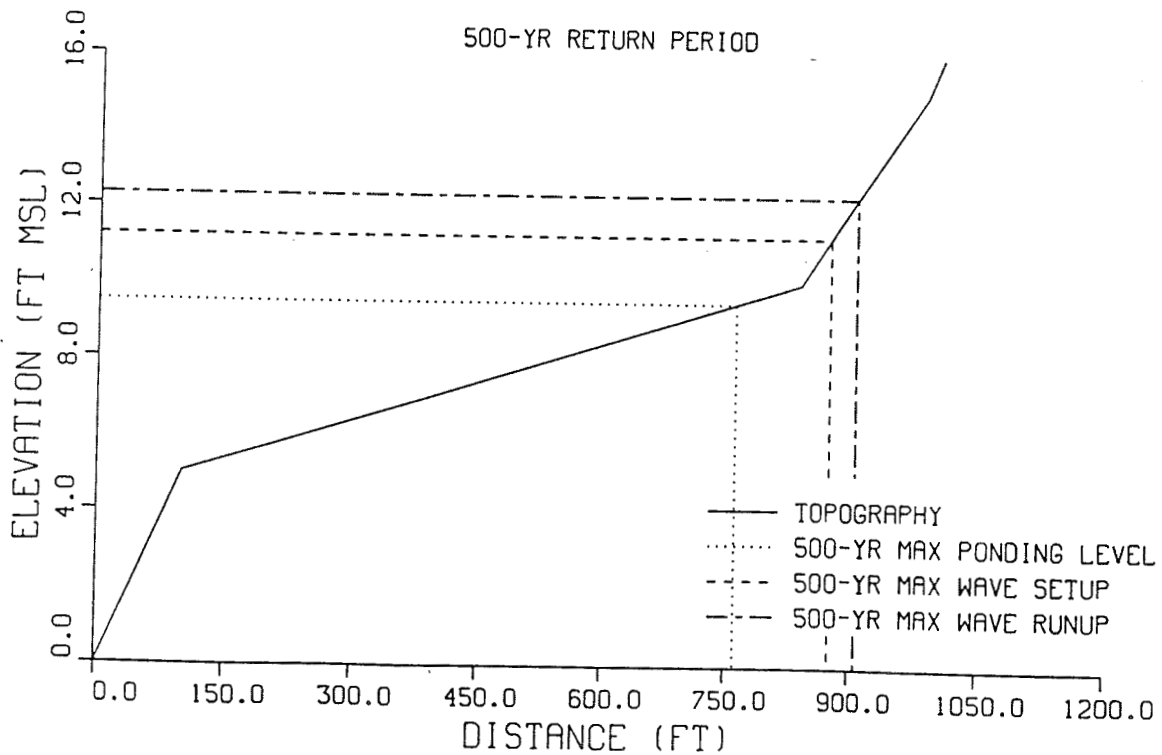
SOUTHERN GUAM TYPHOON ANALYSIS

PROFILE 6-5

100-YR RETURN PERIOD



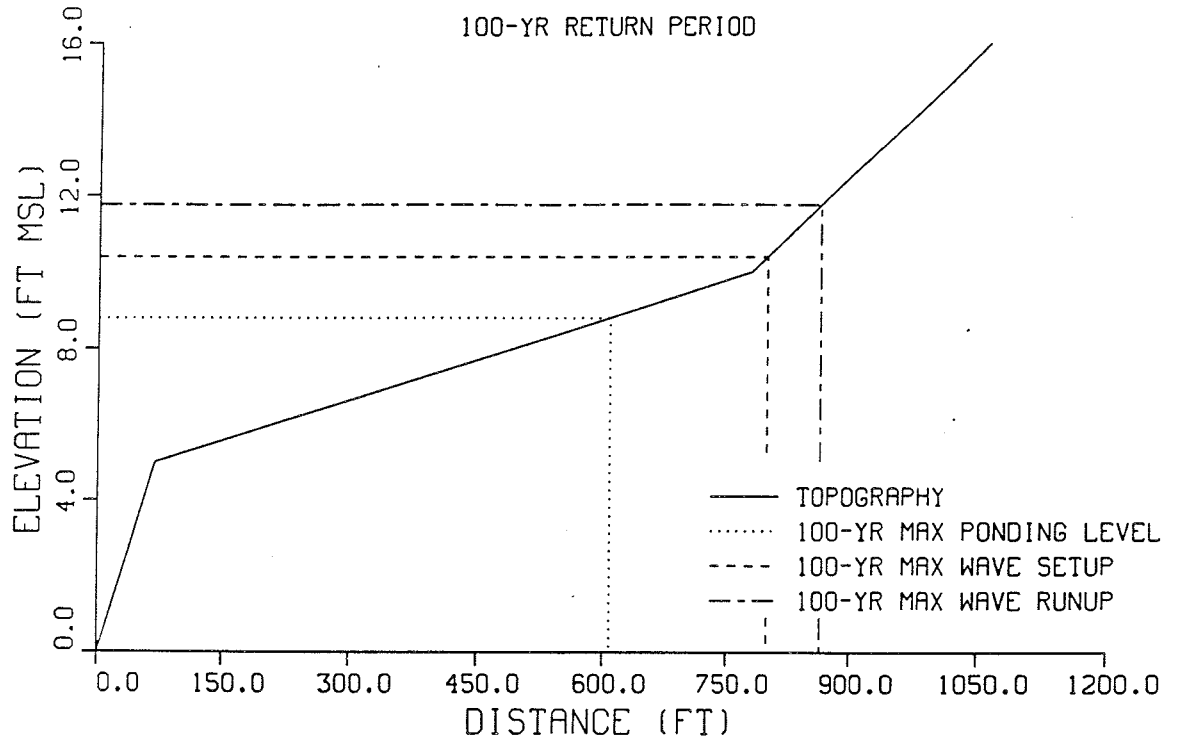
500-YR RETURN PERIOD



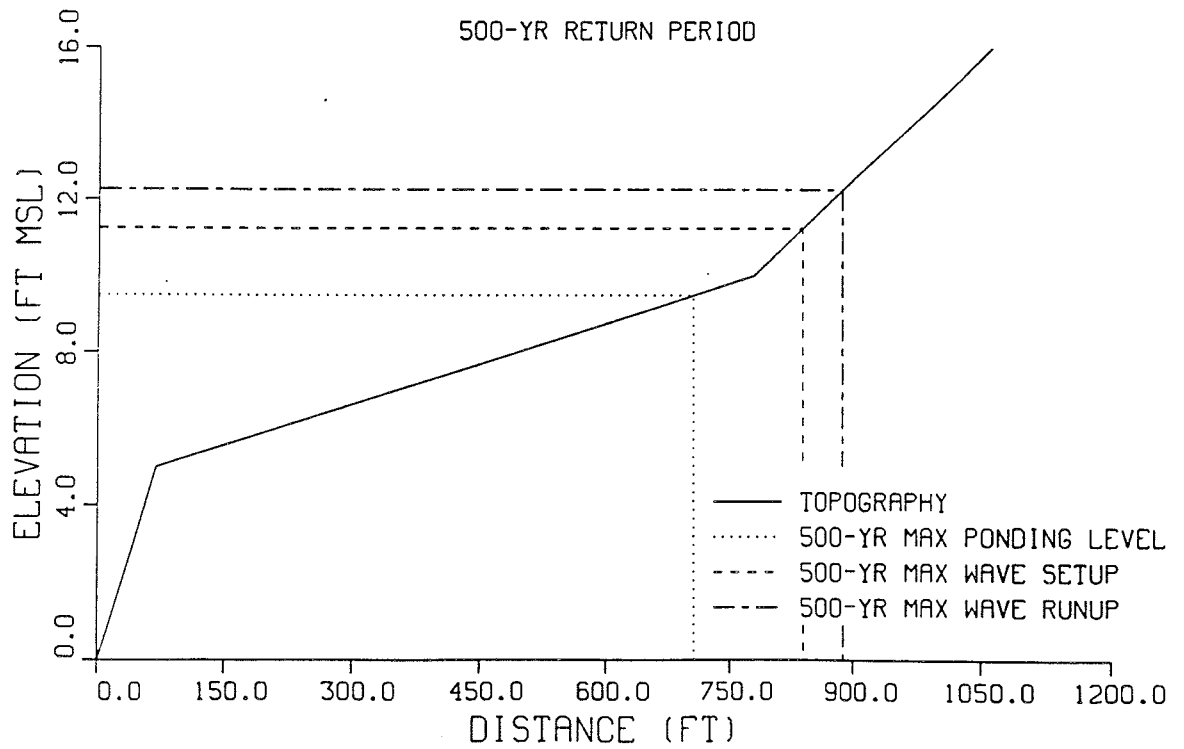
SOUTHERN GUAM TYPHOON ANALYSIS

PROFILE 6-6

100-YR RETURN PERIOD

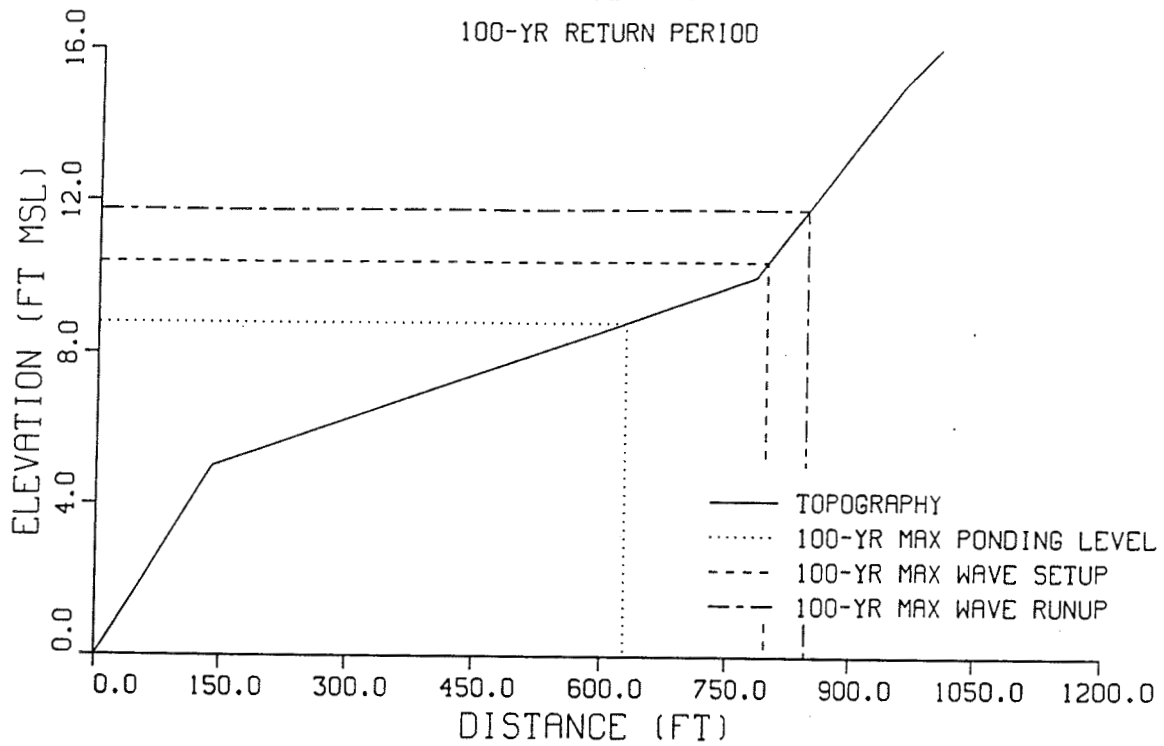


500-YR RETURN PERIOD

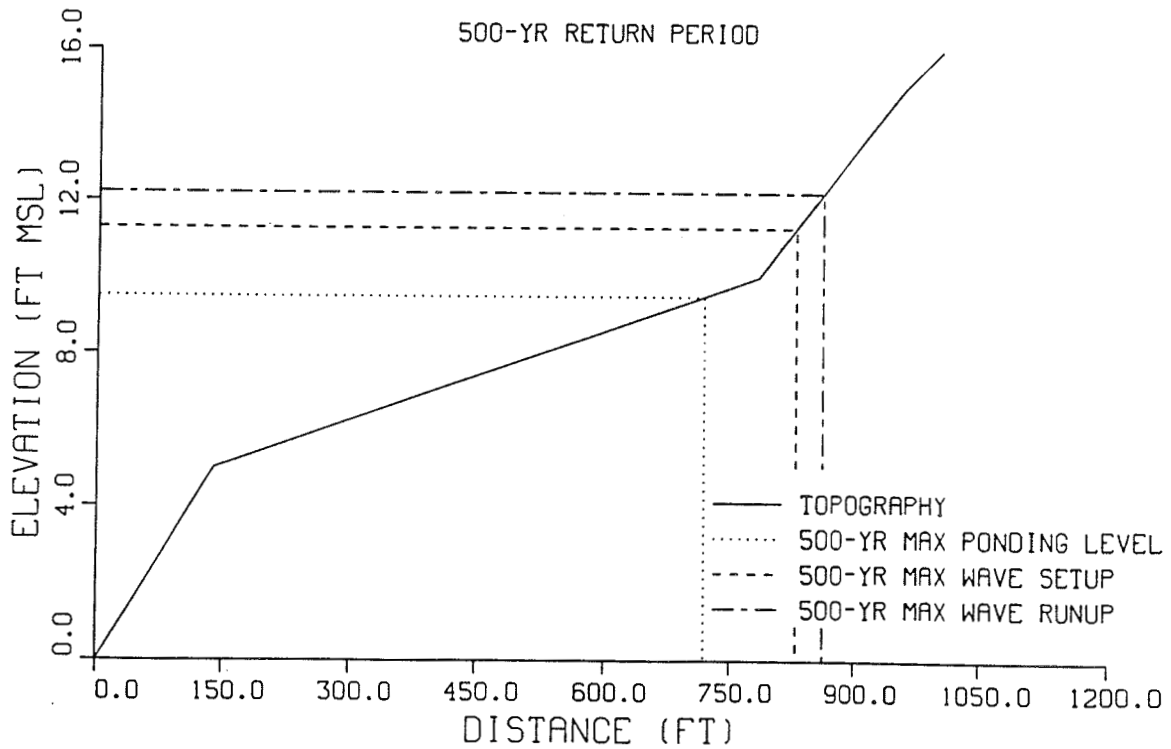


SOUTHERN GUAM TYPHOON ANALYSIS PROFILE 7-1

100-YR RETURN PERIOD



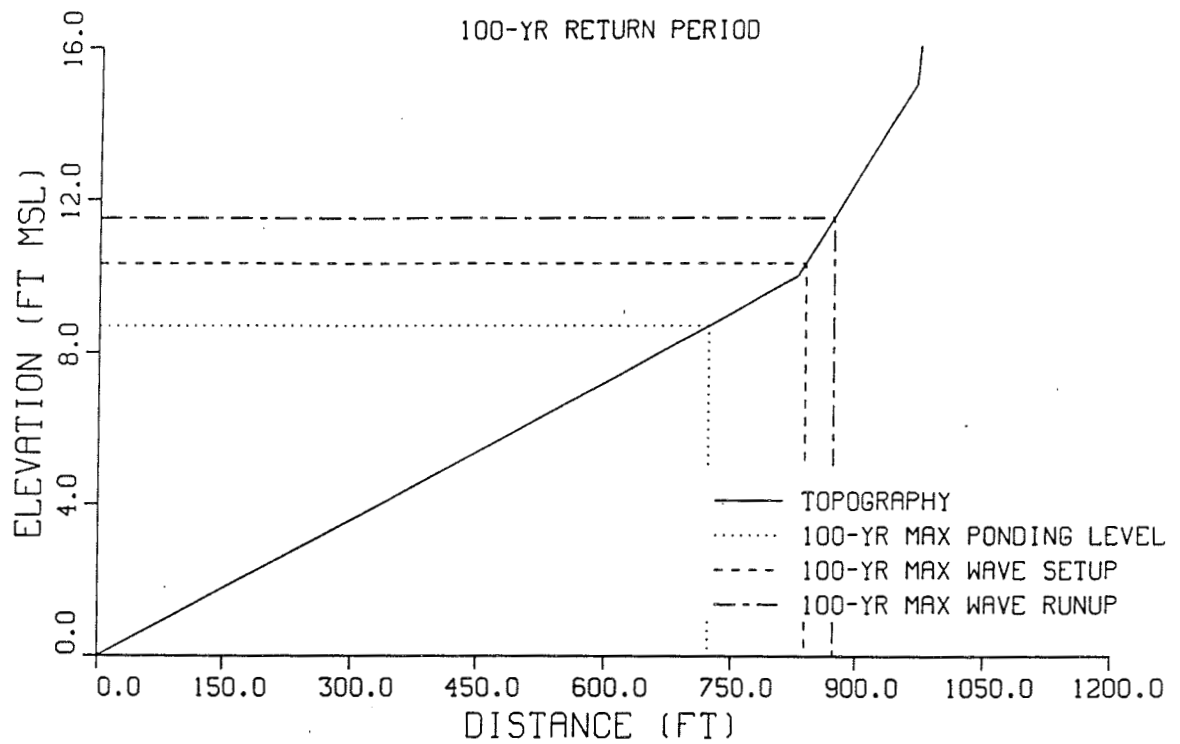
500-YR RETURN PERIOD



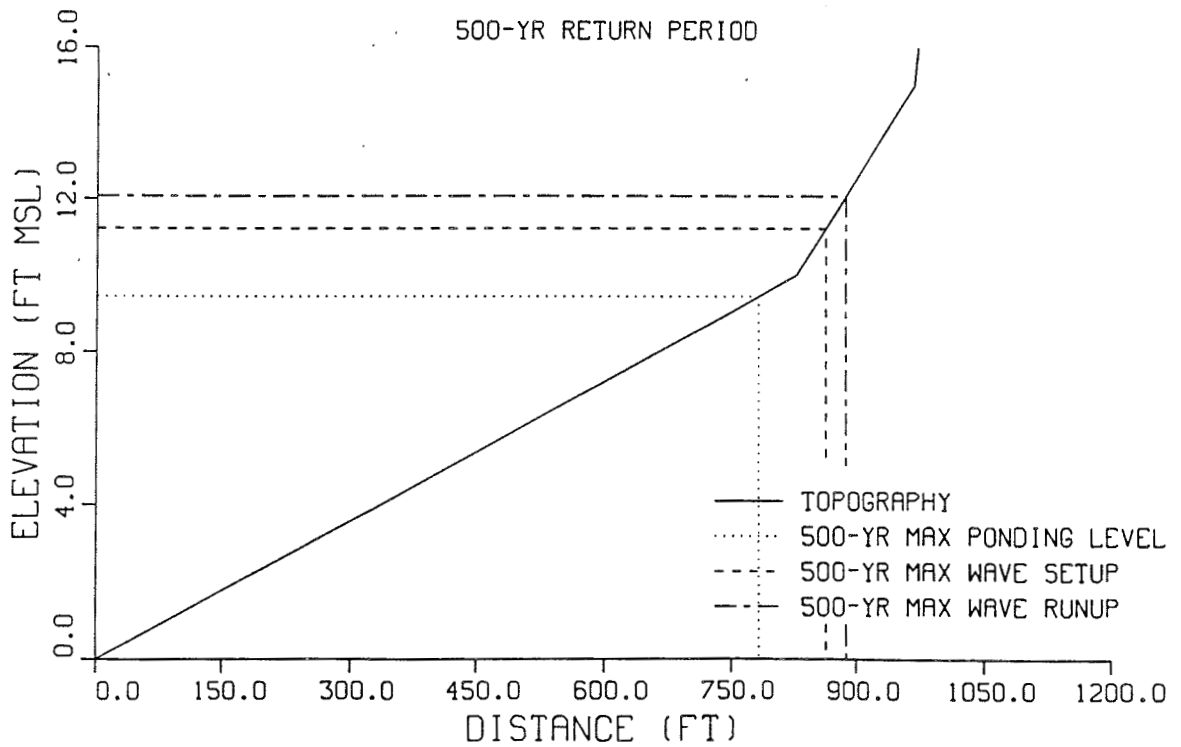
SOUTHERN GUAM TYPHOON ANALYSIS

PROFILE 7-2

100-YR RETURN PERIOD



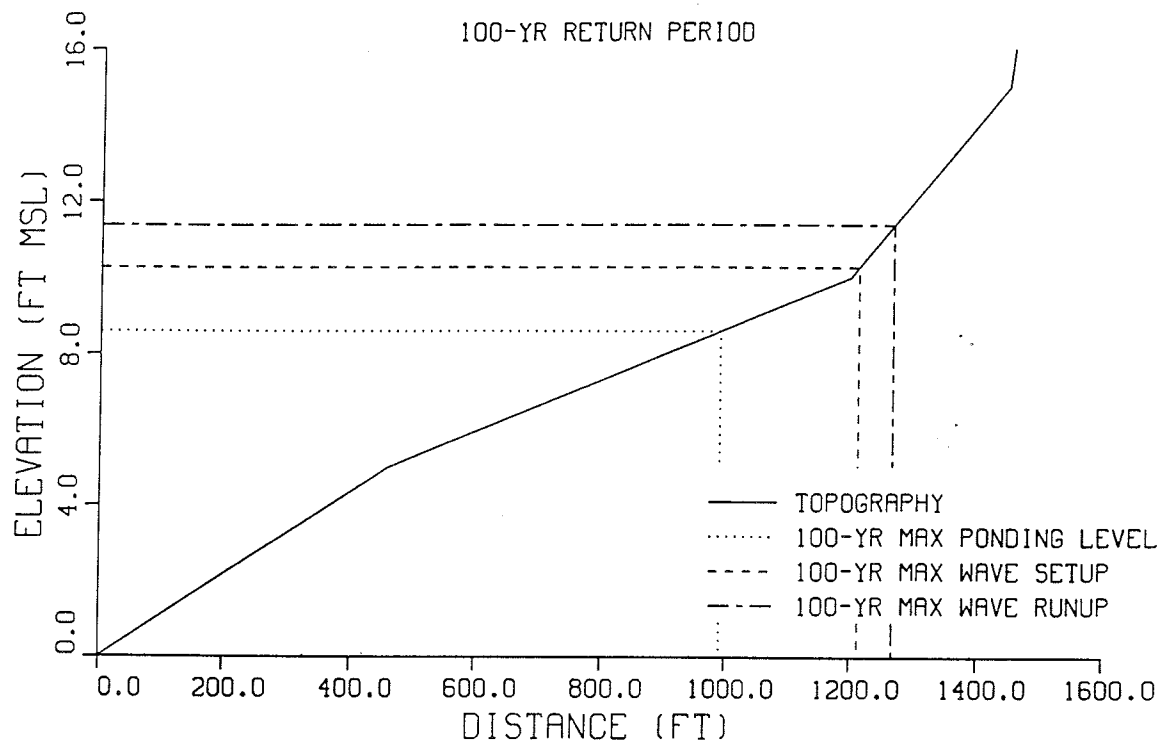
500-YR RETURN PERIOD



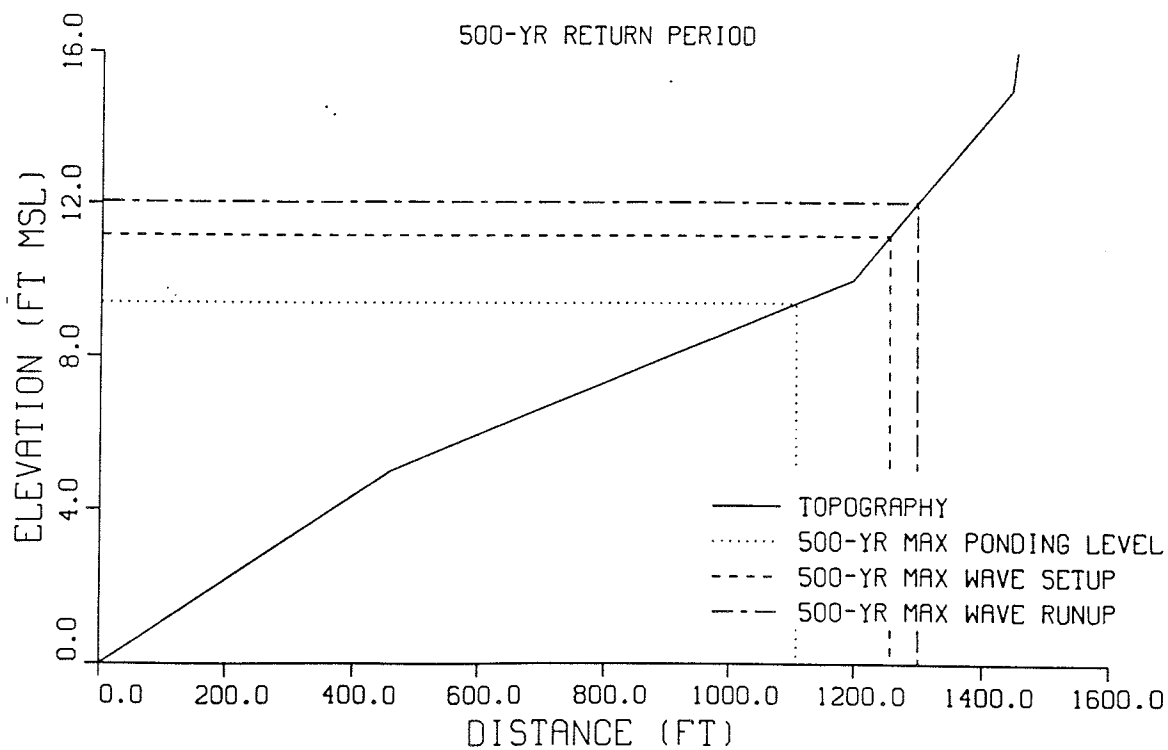
SOUTHERN GUAM TYPHOON ANALYSIS

PROFILE 7-3

100-YR RETURN PERIOD



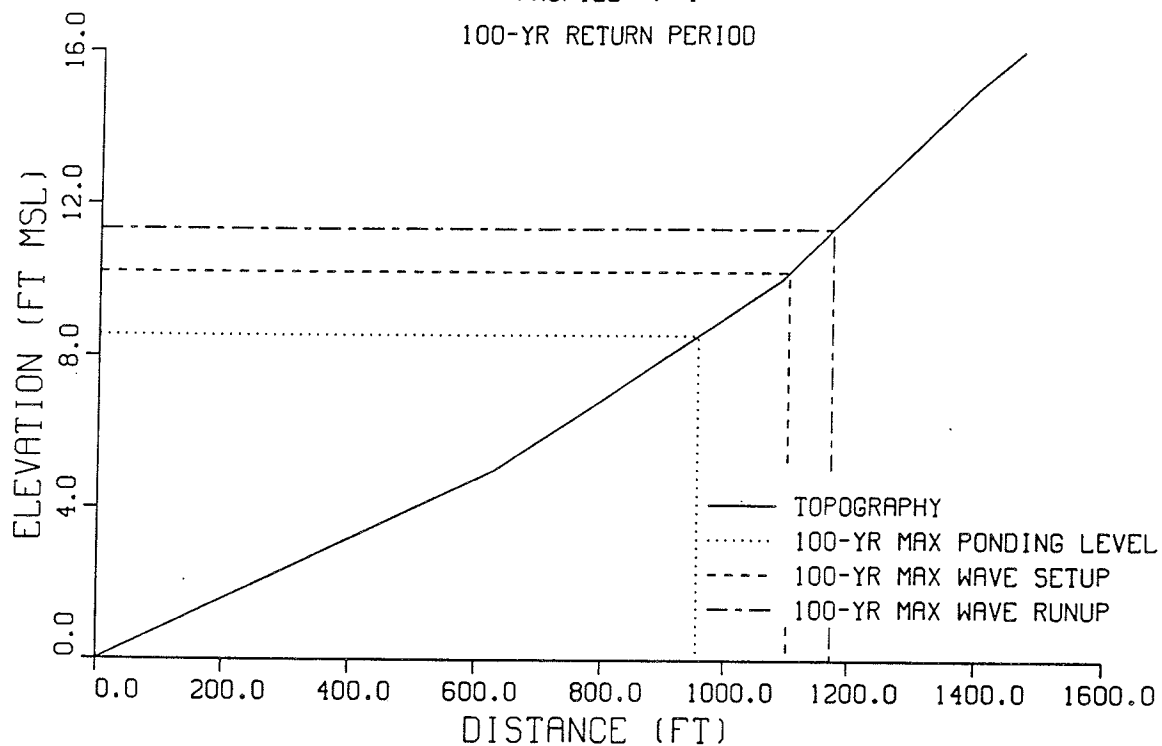
500-YR RETURN PERIOD



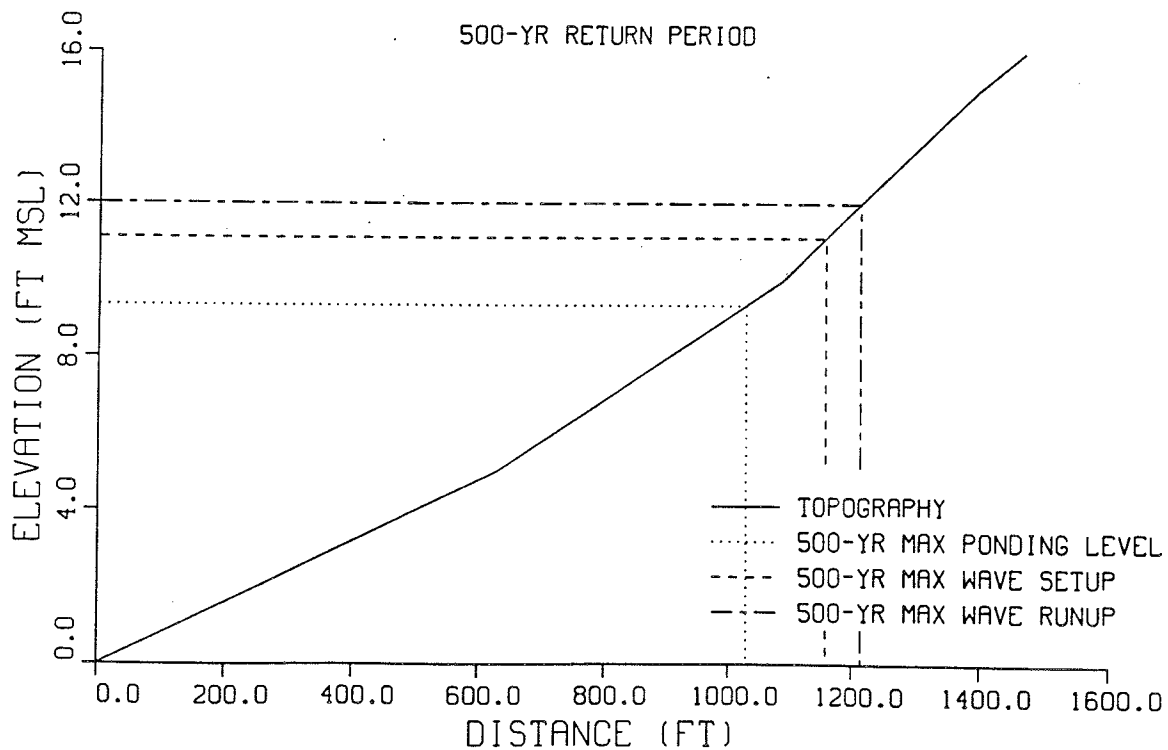
SOUTHERN GUAM TYPHOON ANALYSIS

PROFILE 7-4

100-YR RETURN PERIOD



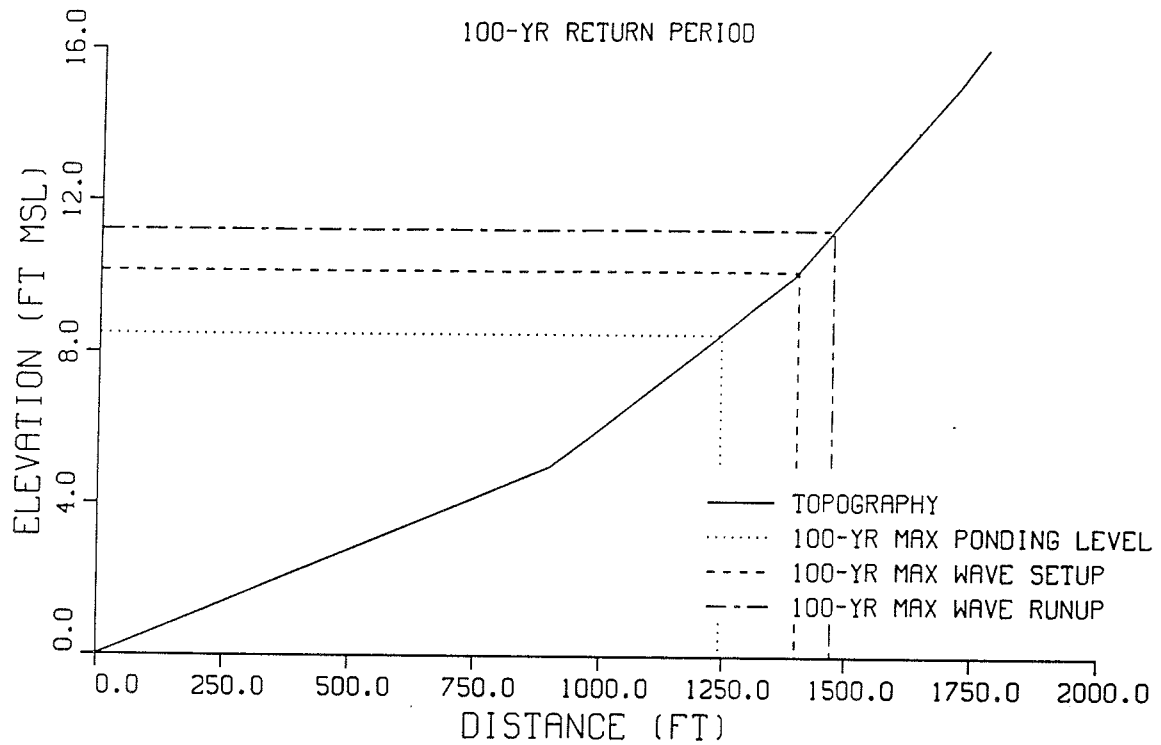
500-YR RETURN PERIOD



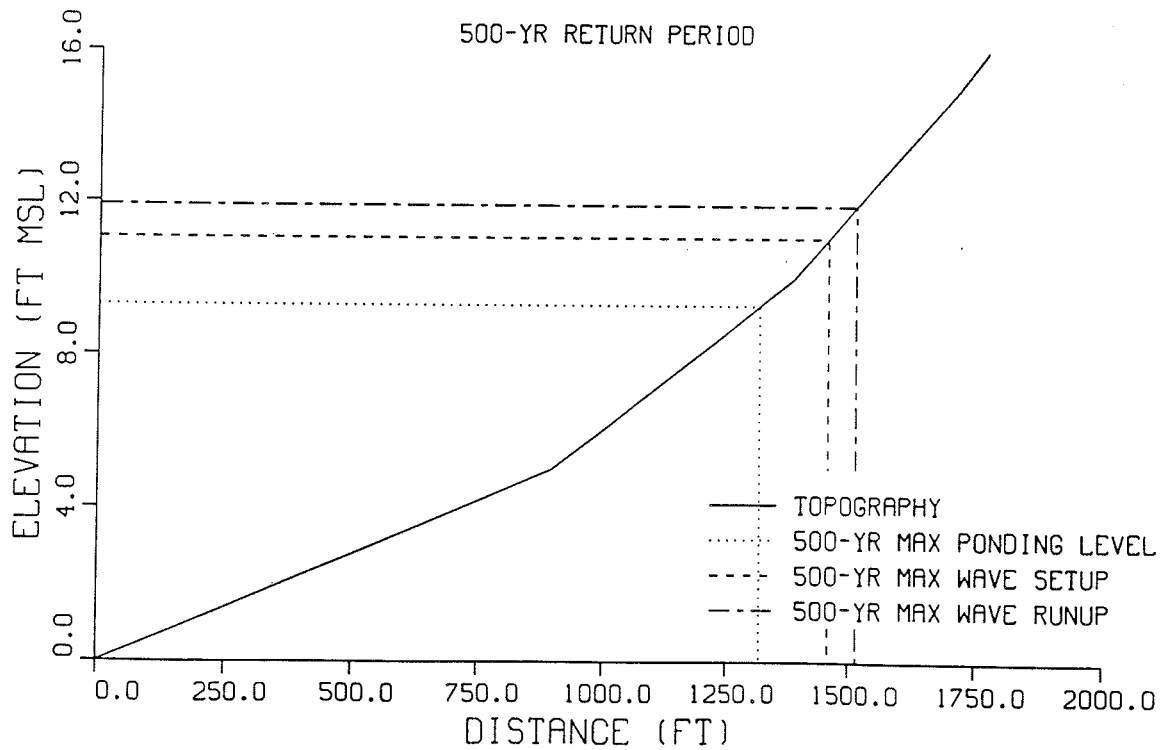
SOUTHERN GUAM TYPHOON ANALYSIS

PROFILE 7-5

100-YR RETURN PERIOD



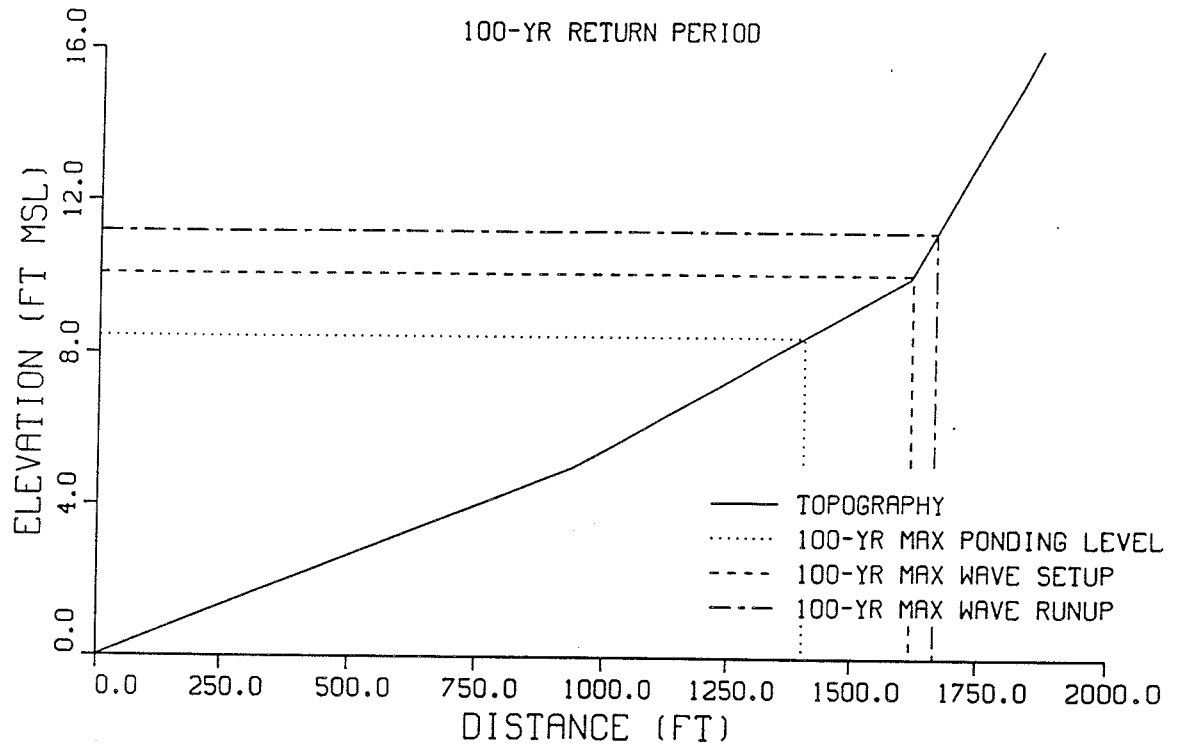
500-YR RETURN PERIOD



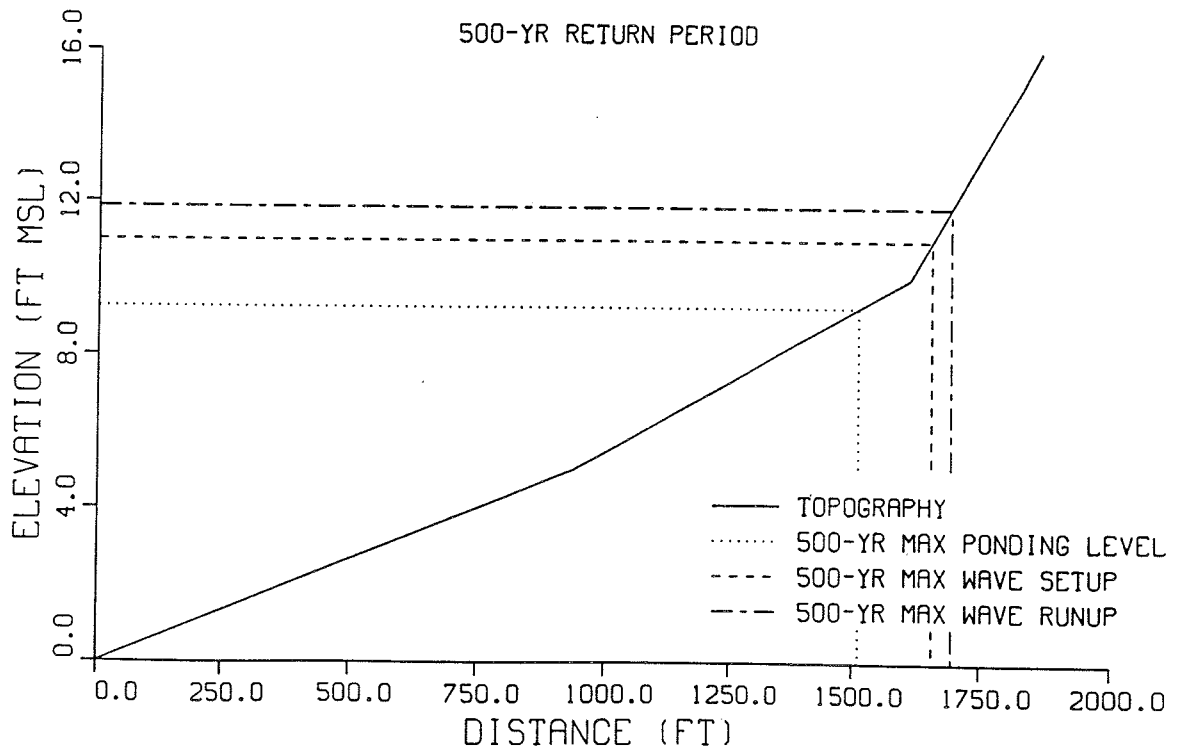
SOUTHERN GUAM TYPHOON ANALYSIS

PROFILE 7-6

100-YR RETURN PERIOD



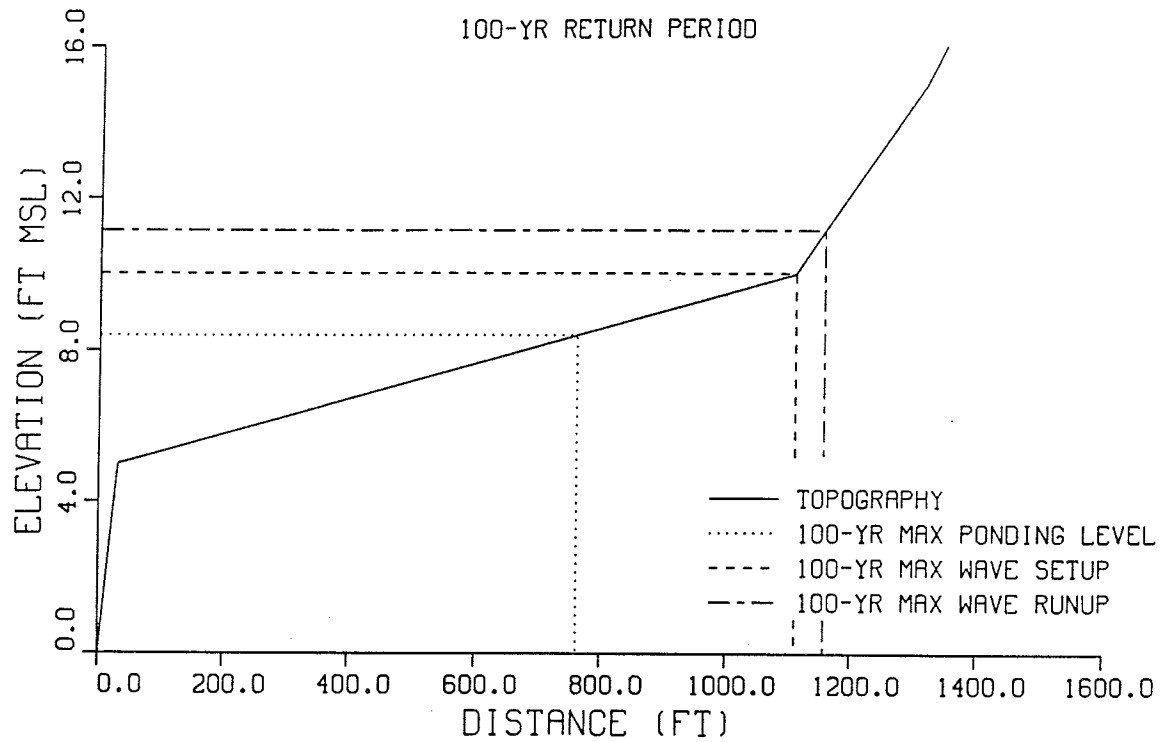
500-YR RETURN PERIOD



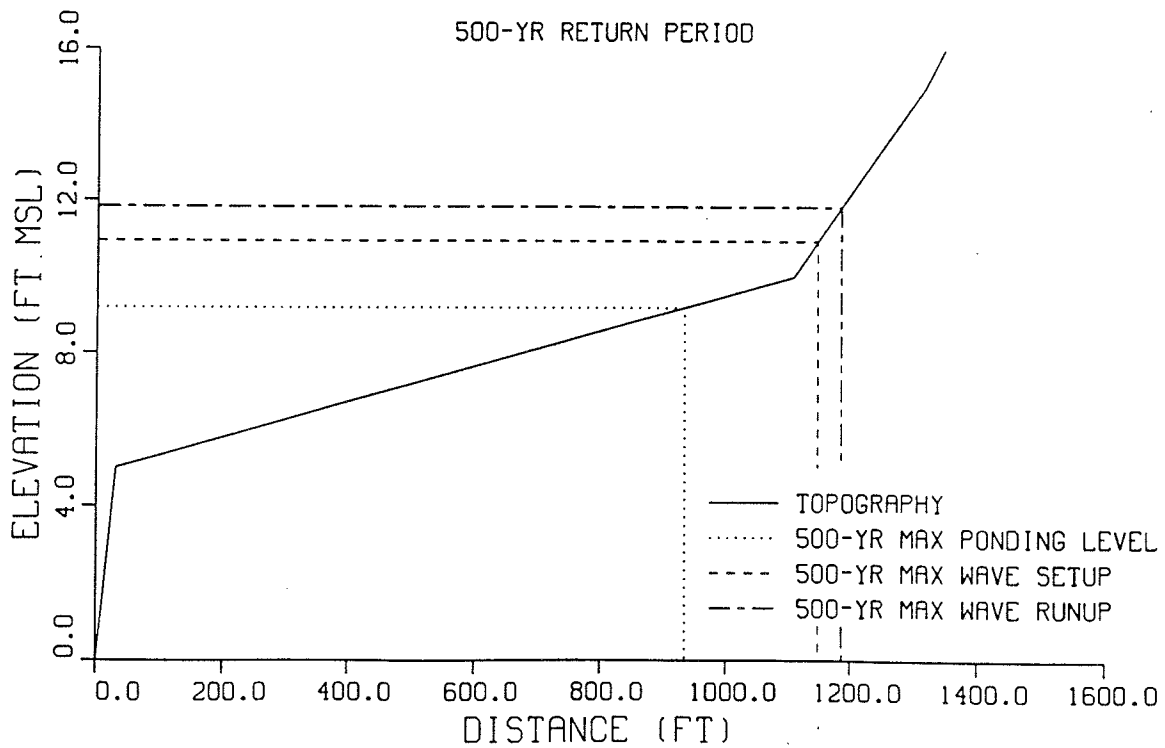
SOUTHERN GUAM TYPHOON ANALYSIS

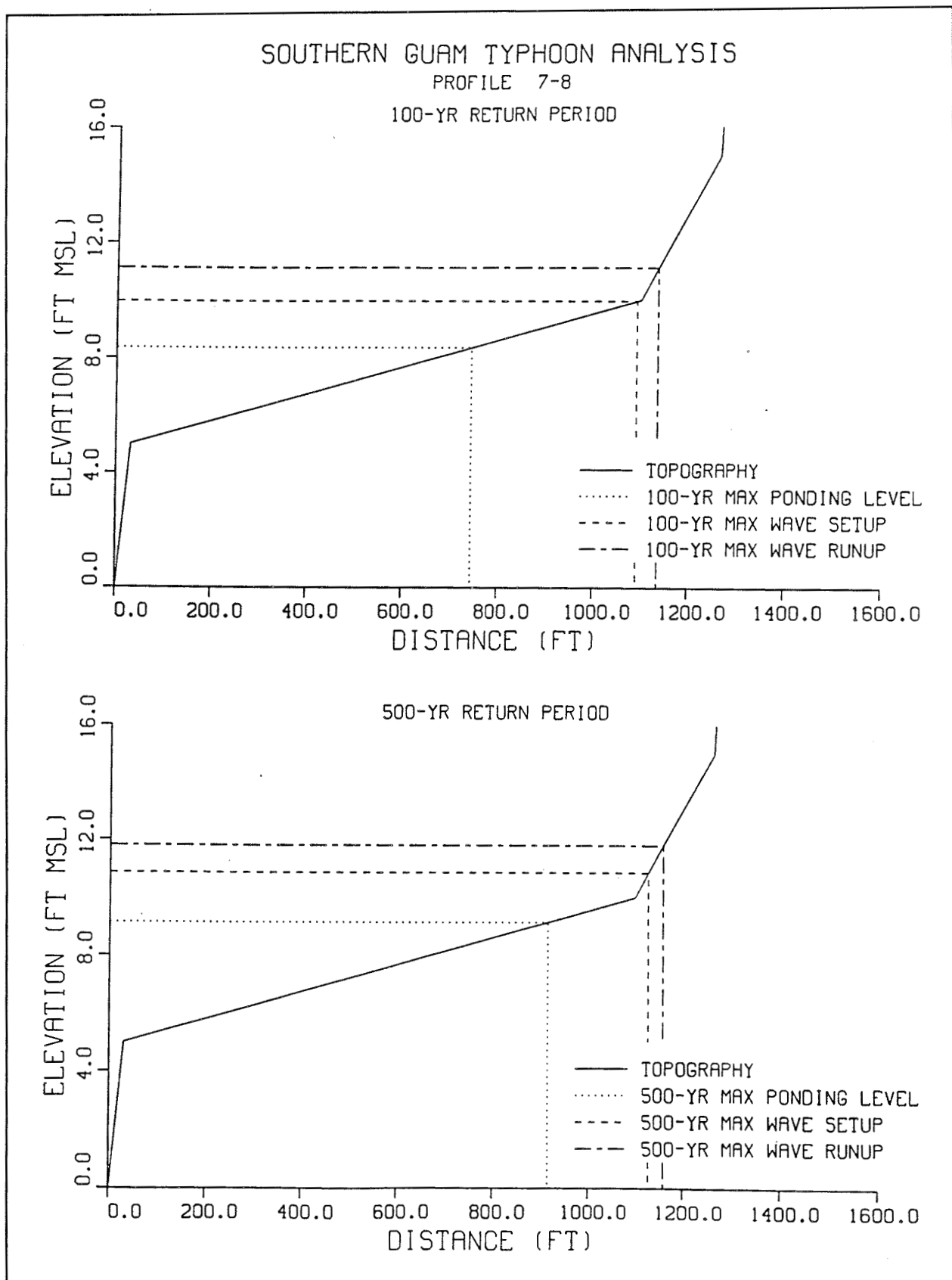
PROFILE 7-7

100-YR RETURN PERIOD



500-YR RETURN PERIOD

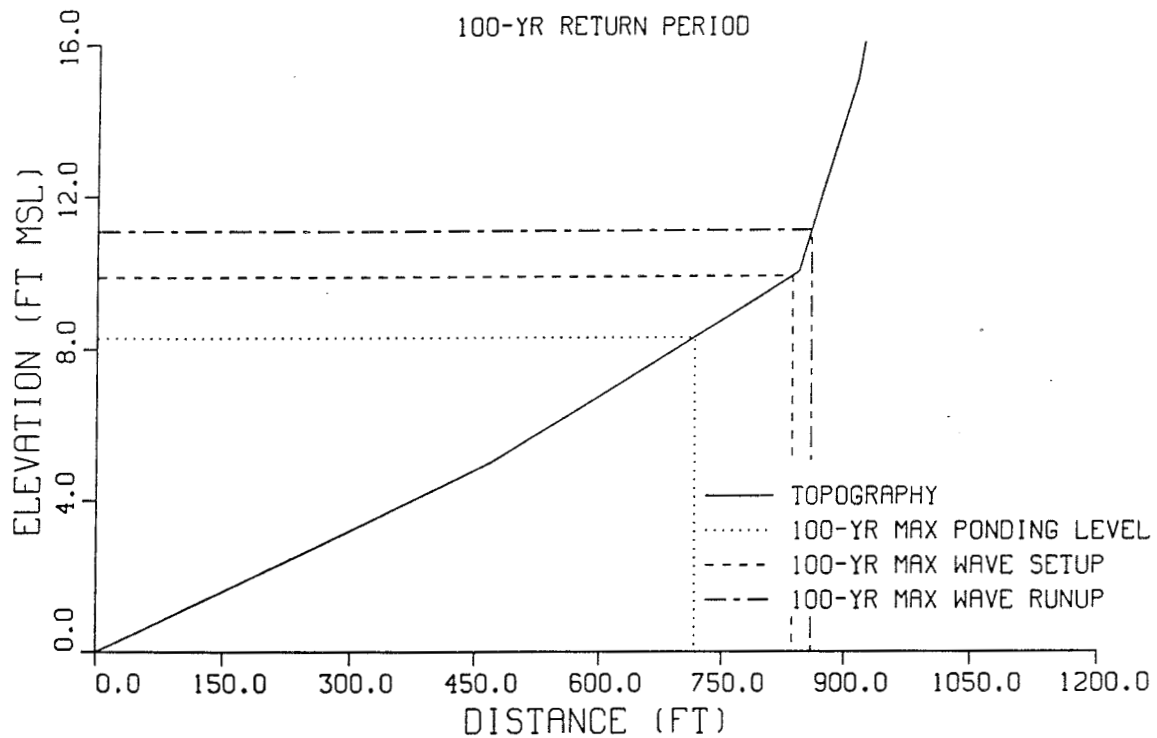




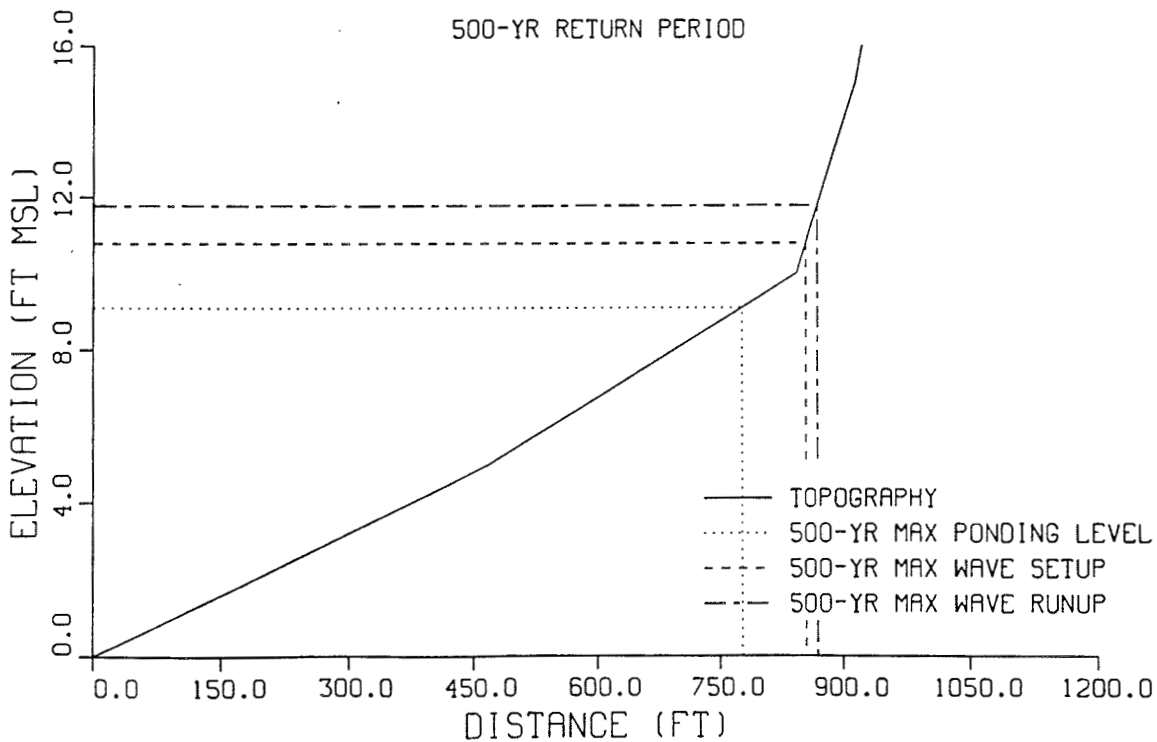
SOUTHERN GUAM TYPHOON ANALYSIS

PROFILE 8-1

100-YR RETURN PERIOD



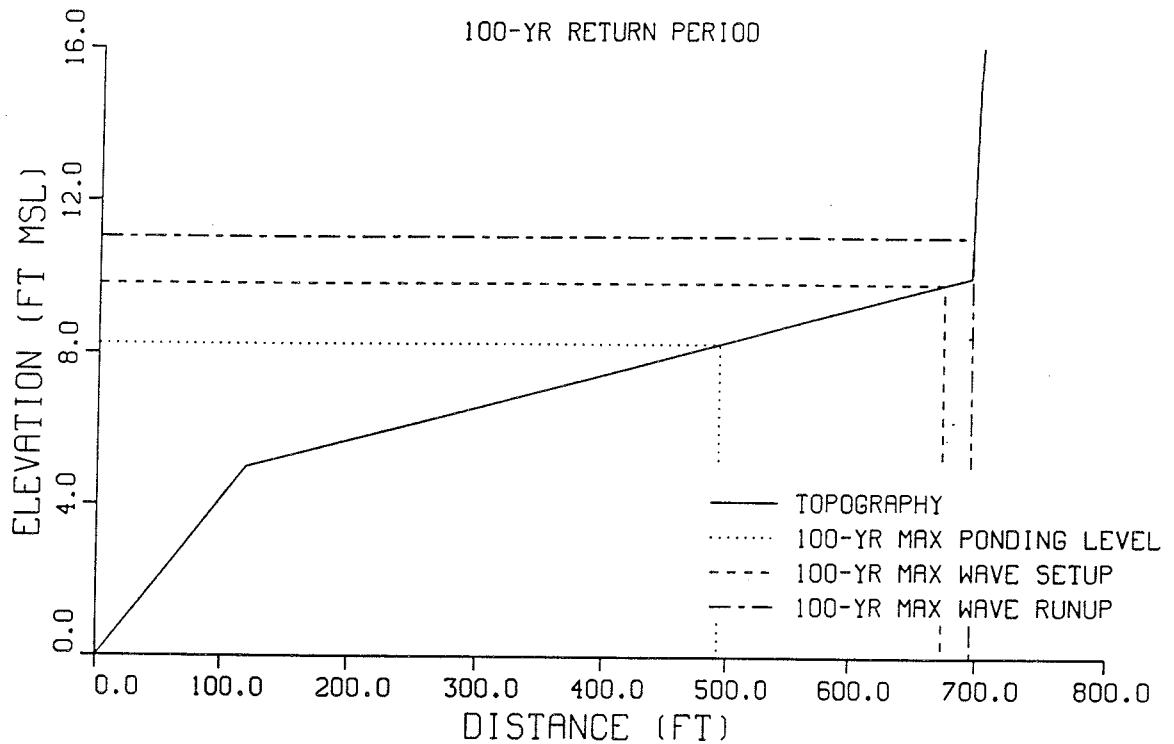
500-YR RETURN PERIOD



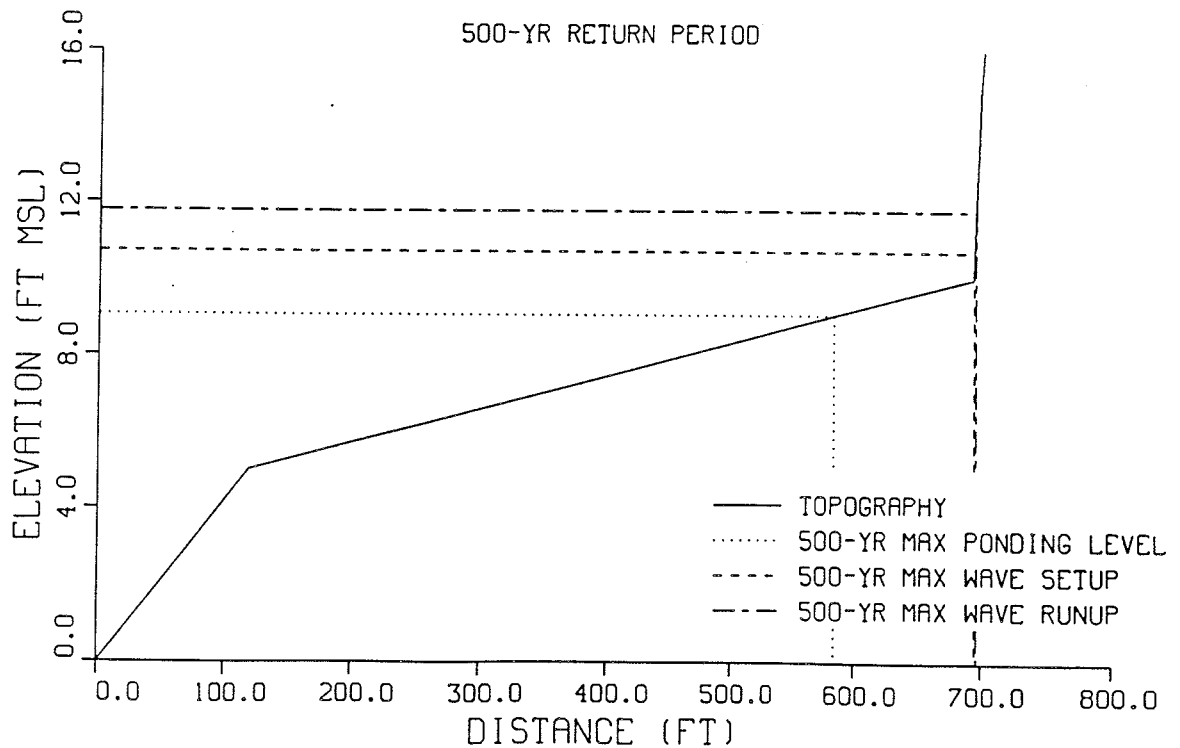
SOUTHERN GUAM TYPHOON ANALYSIS

PROFILE 8-2

100-YR RETURN PERIOD



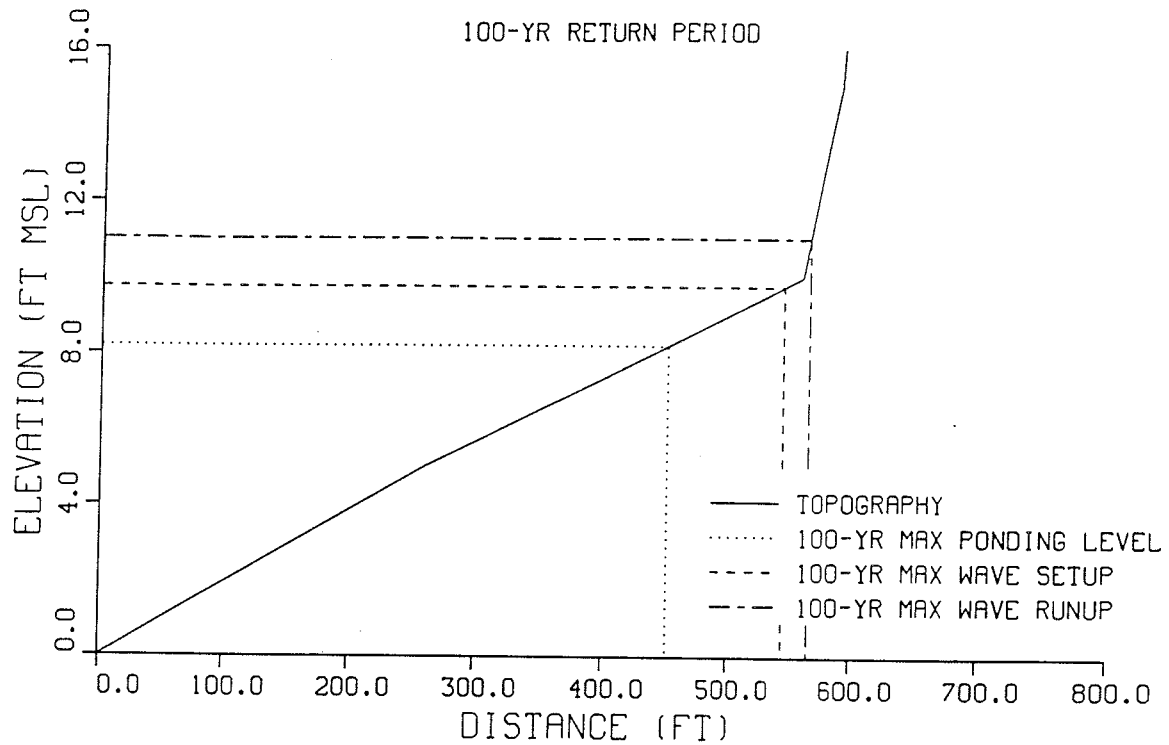
500-YR RETURN PERIOD



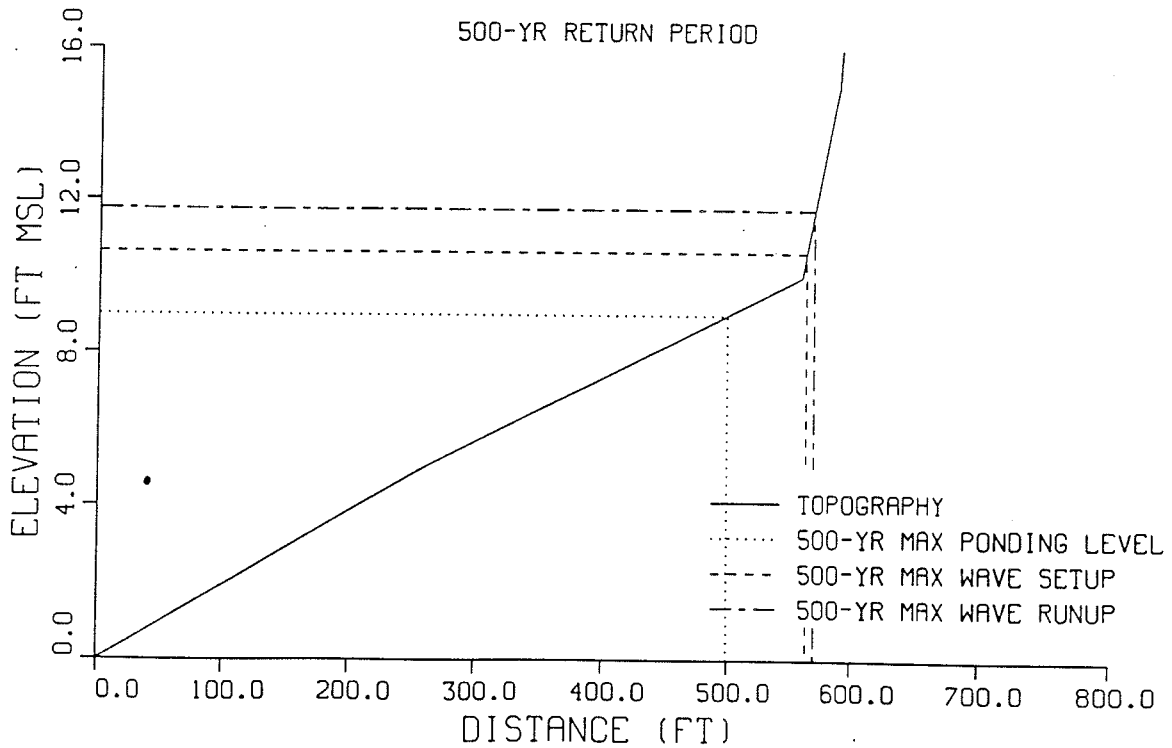
SOUTHERN GUAM TYPHOON ANALYSIS

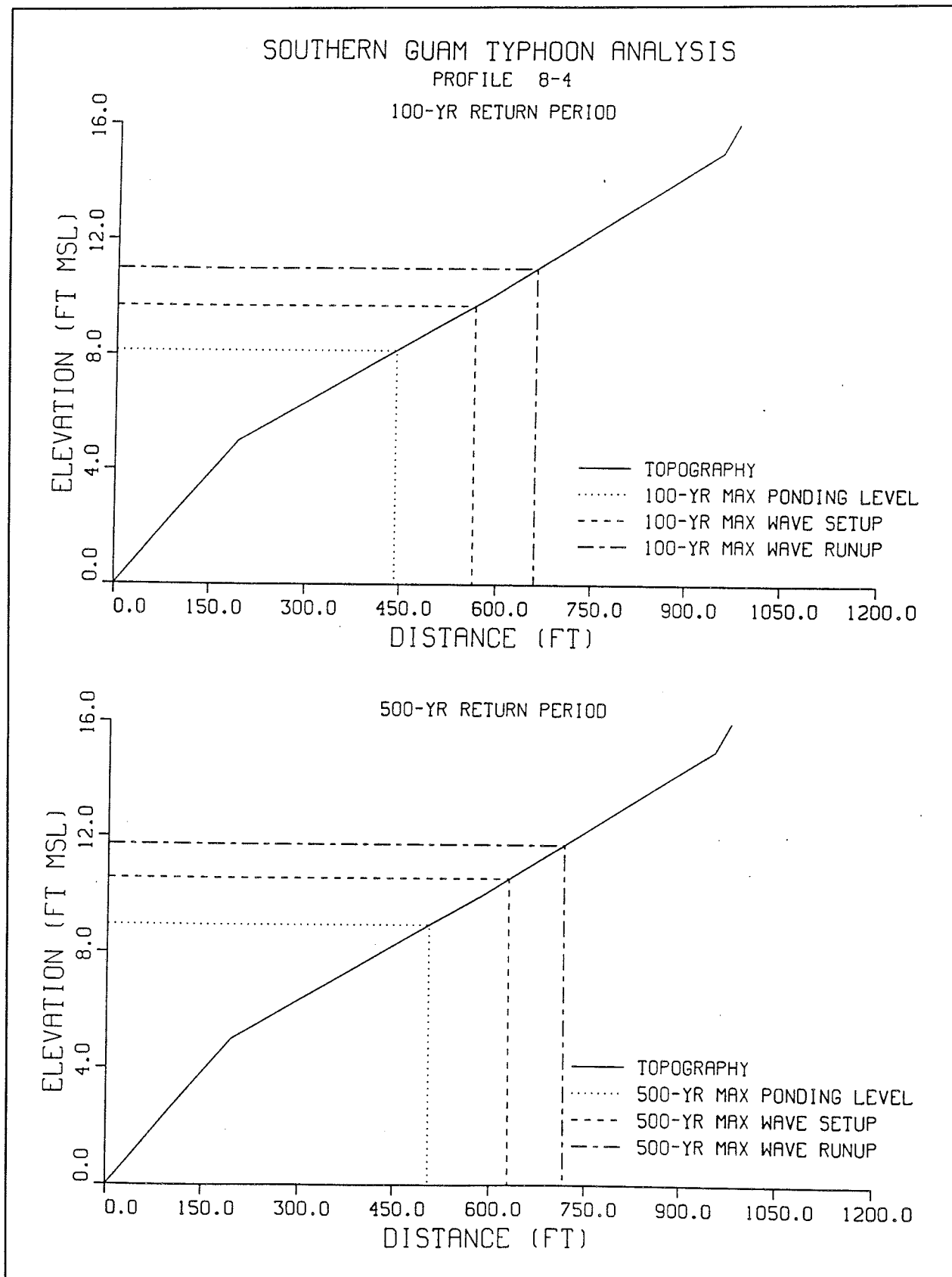
PROFILE 8-3

100-YR RETURN PERIOD



500-YR RETURN PERIOD

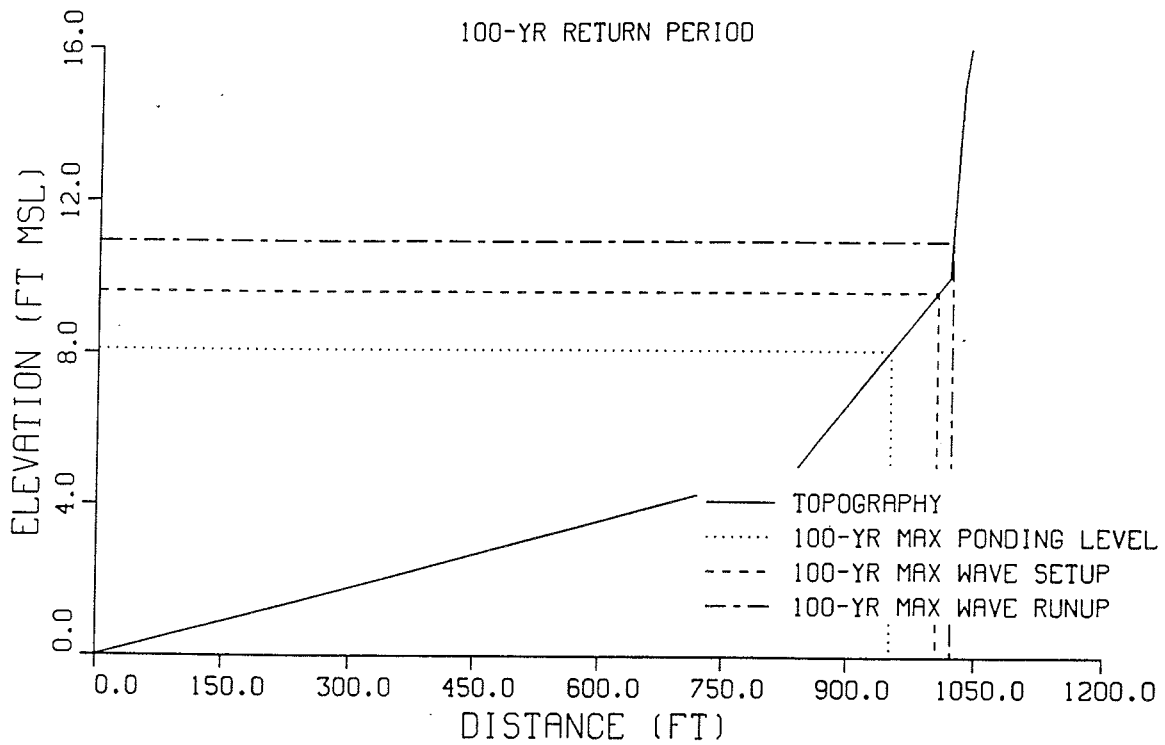




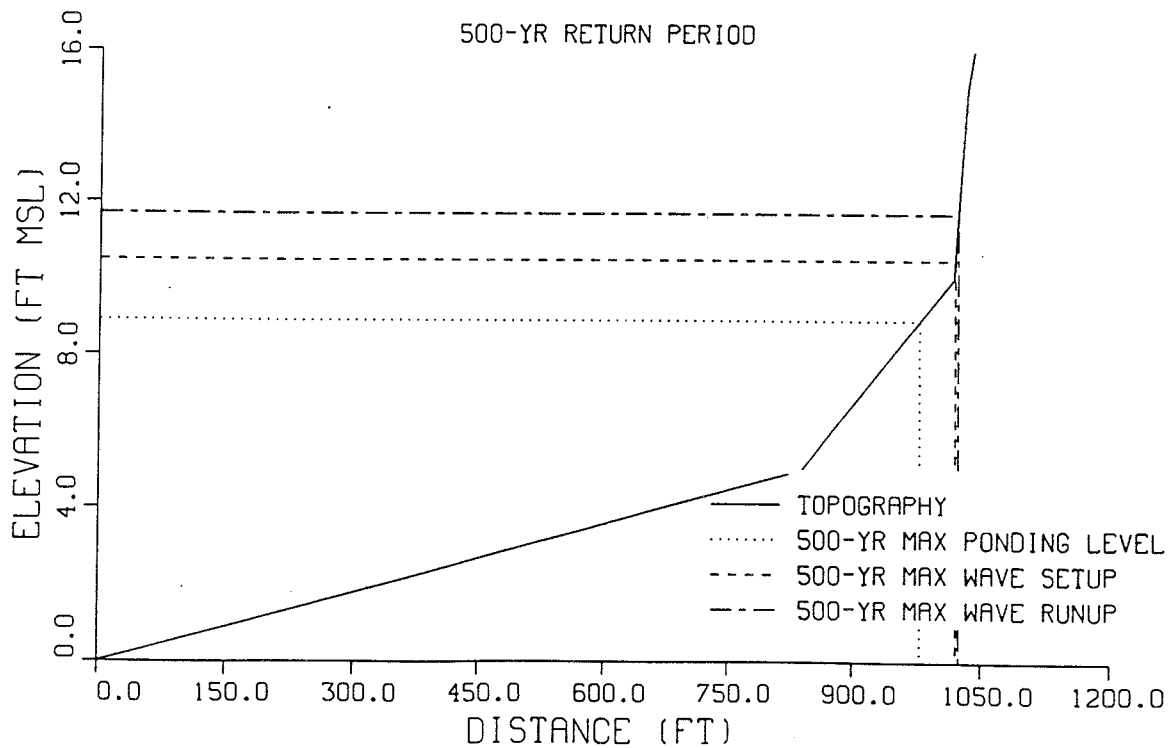
SOUTHERN GUAM TYPHOON ANALYSIS

PROFILE 8-5

100-YR RETURN PERIOD



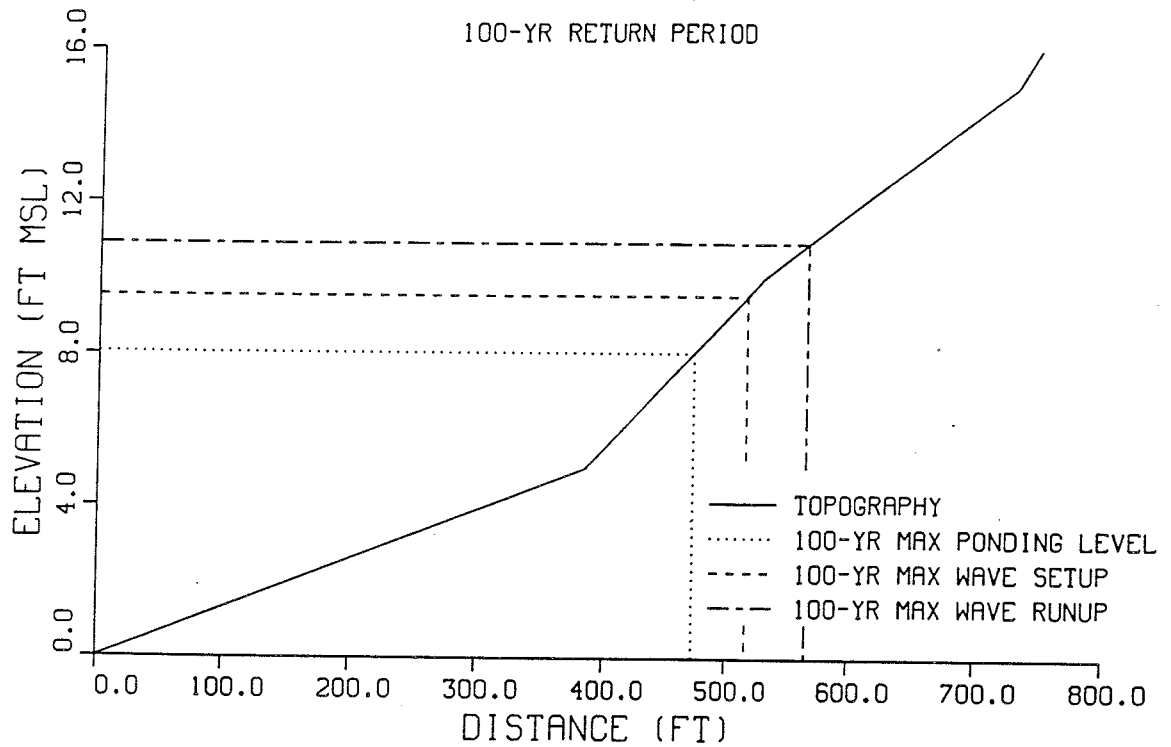
500-YR RETURN PERIOD



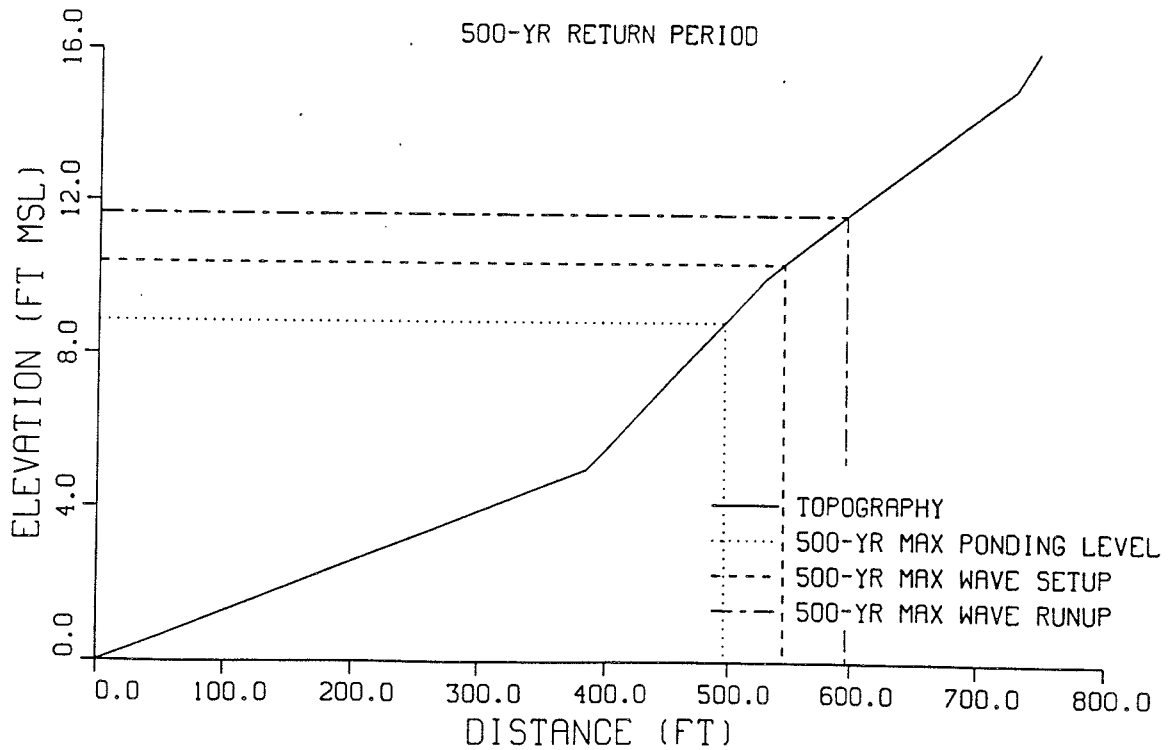
SOUTHERN GUAM TYPHOON ANALYSIS

PROFILE 8-6

100-YR RETURN PERIOD



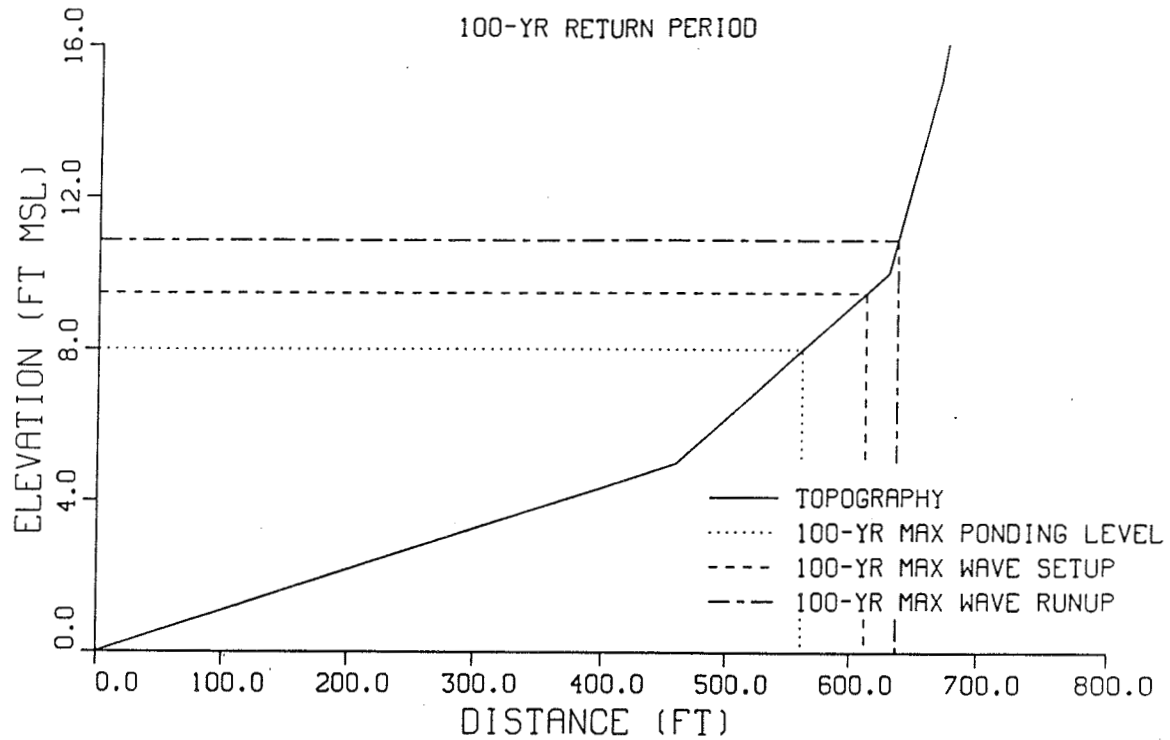
500-YR RETURN PERIOD



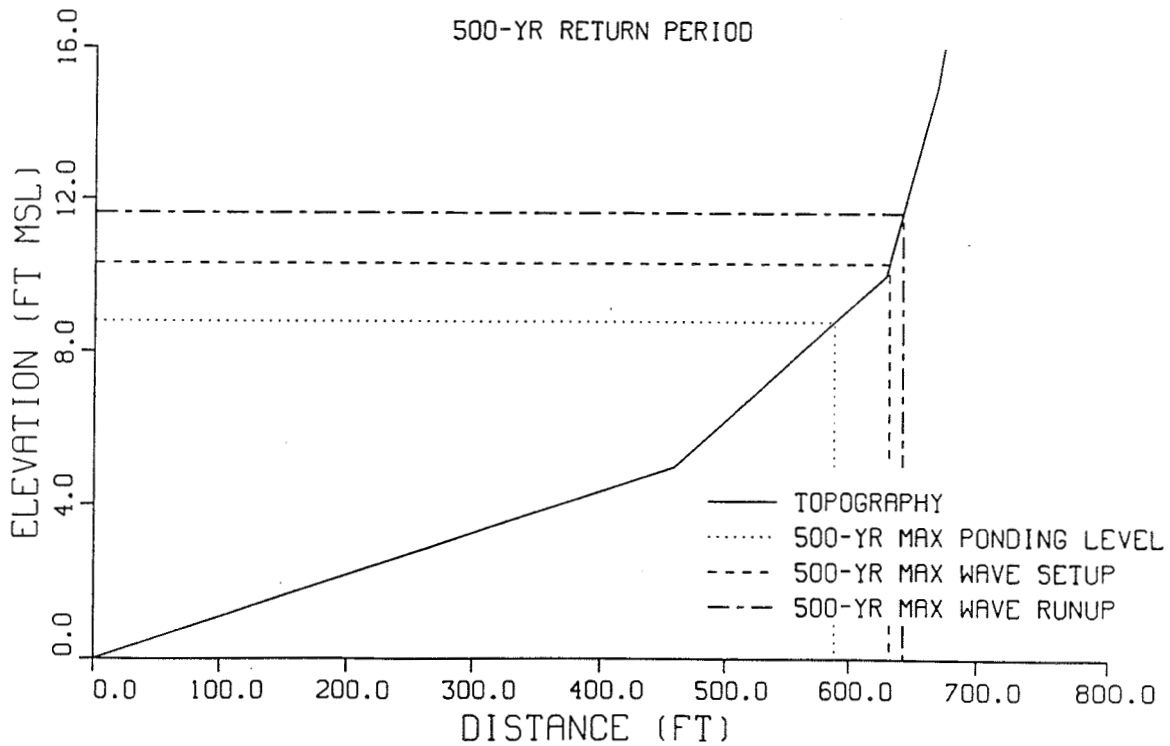
SOUTHERN GUAM TYPHOON ANALYSIS

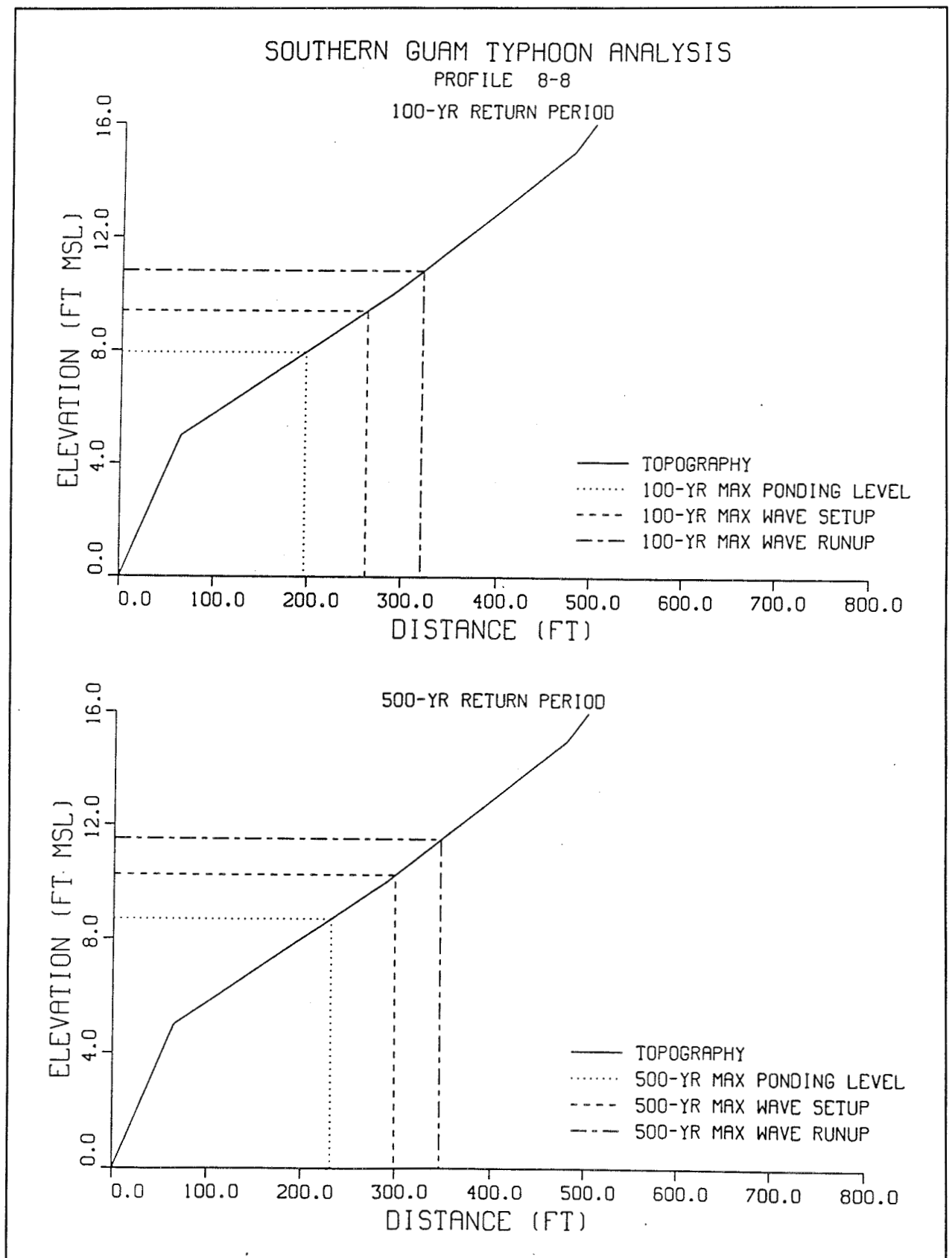
PROFILE 8-7

100-YR RETURN PERIOD



500-YR RETURN PERIOD

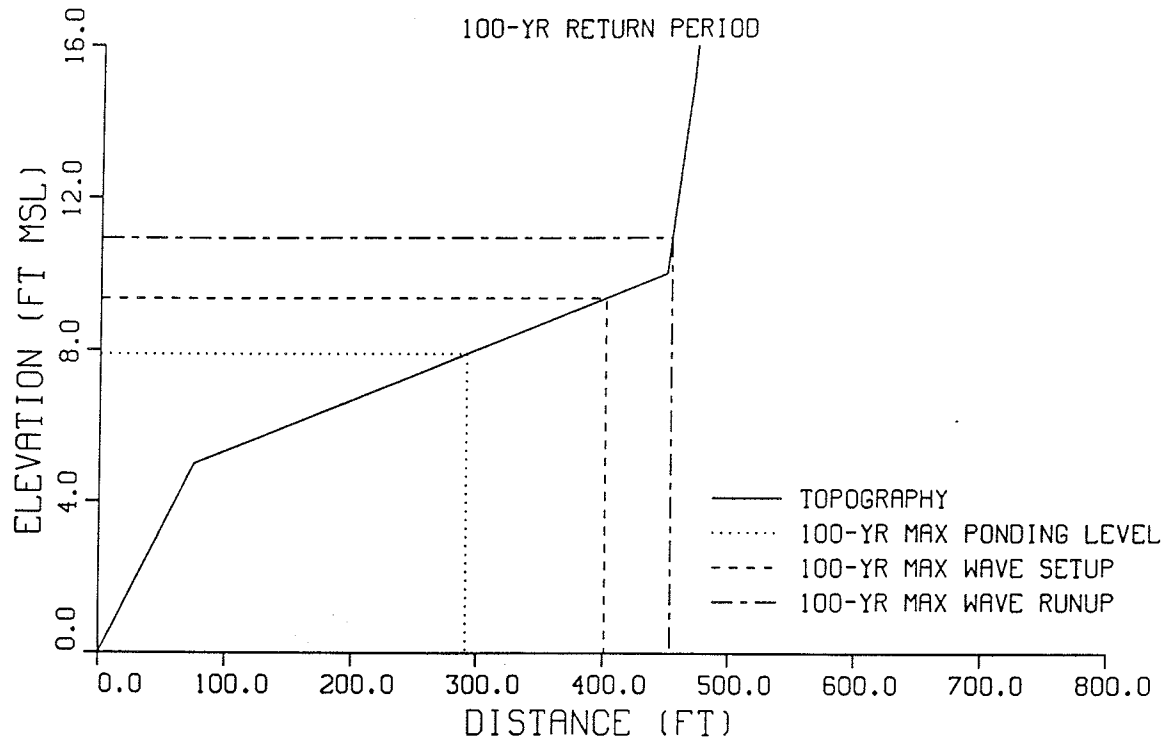




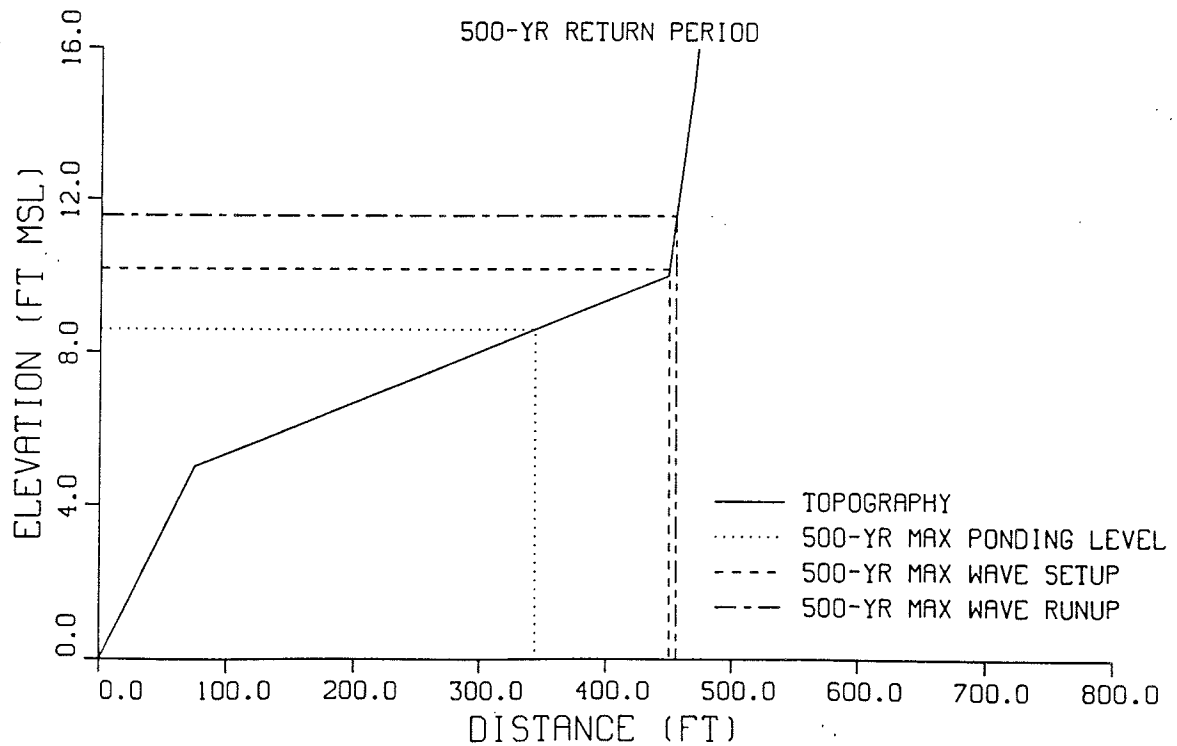
SOUTHERN GUAM TYPHOON ANALYSIS

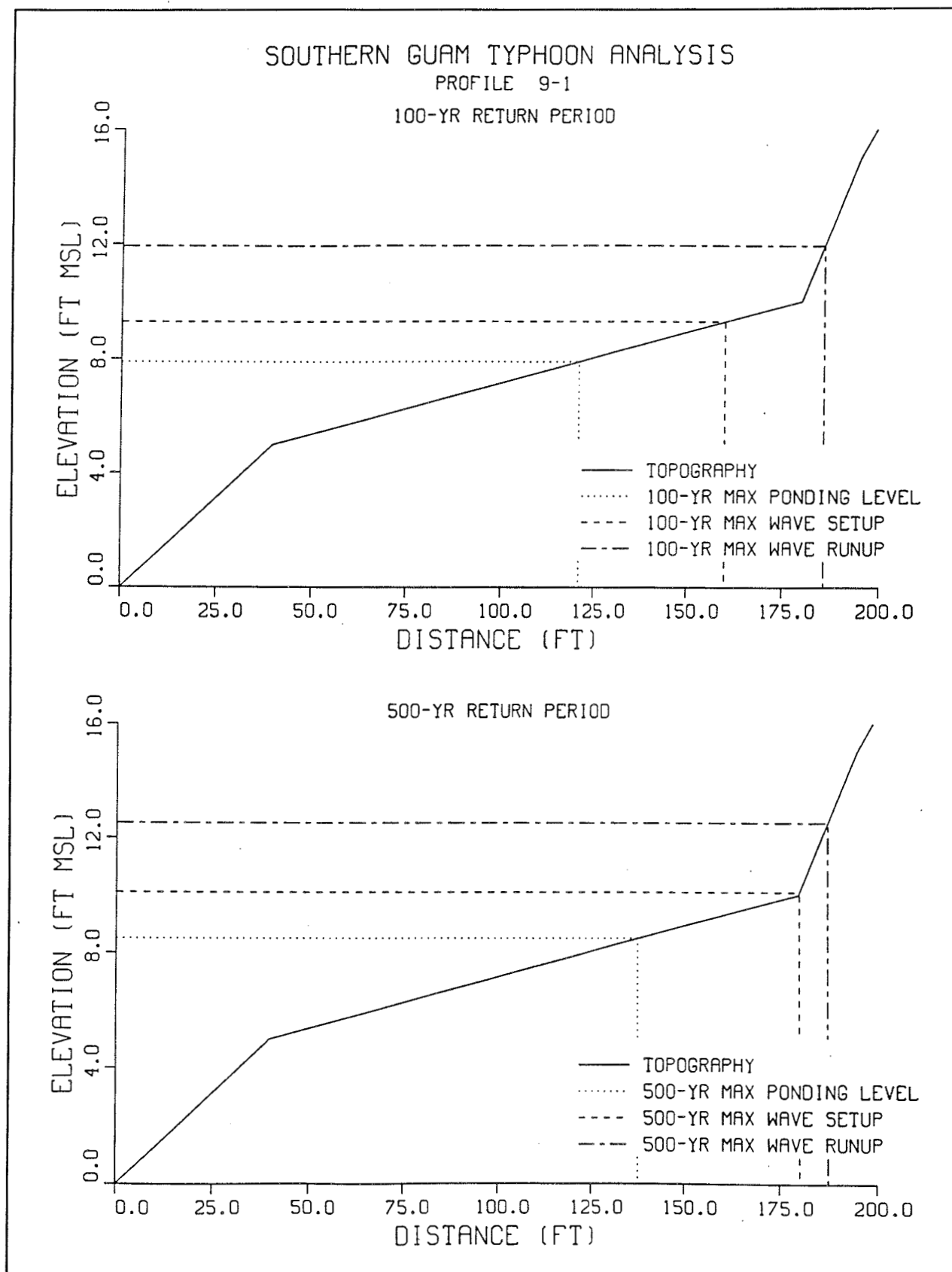
PROFILE 8-9

100-YR RETURN PERIOD



500-YR RETURN PERIOD

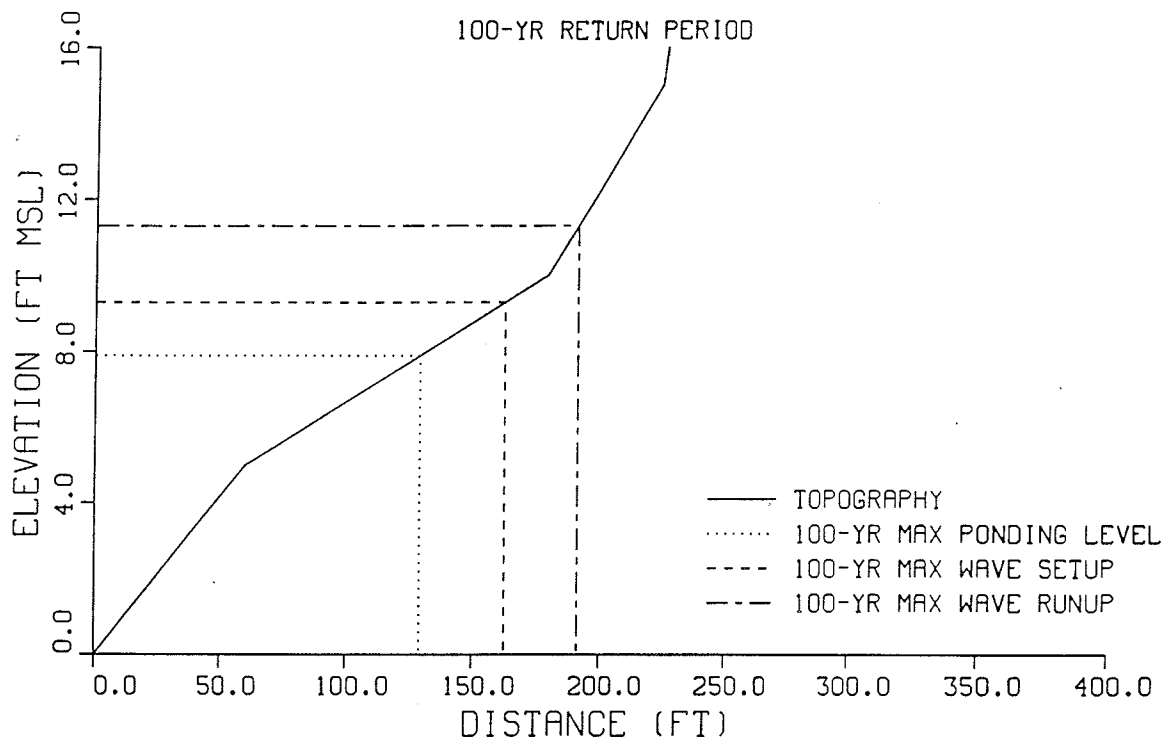




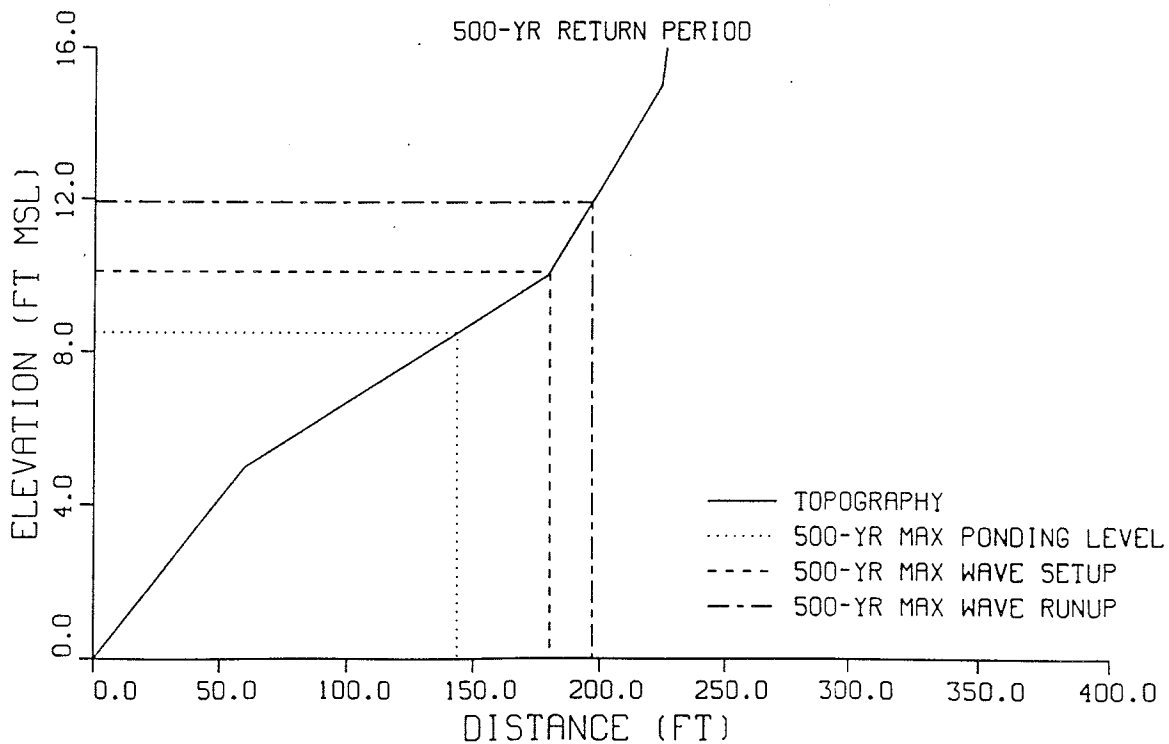
SOUTHERN GUAM TYPHOON ANALYSIS

PROFILE 9-2

100-YR RETURN PERIOD



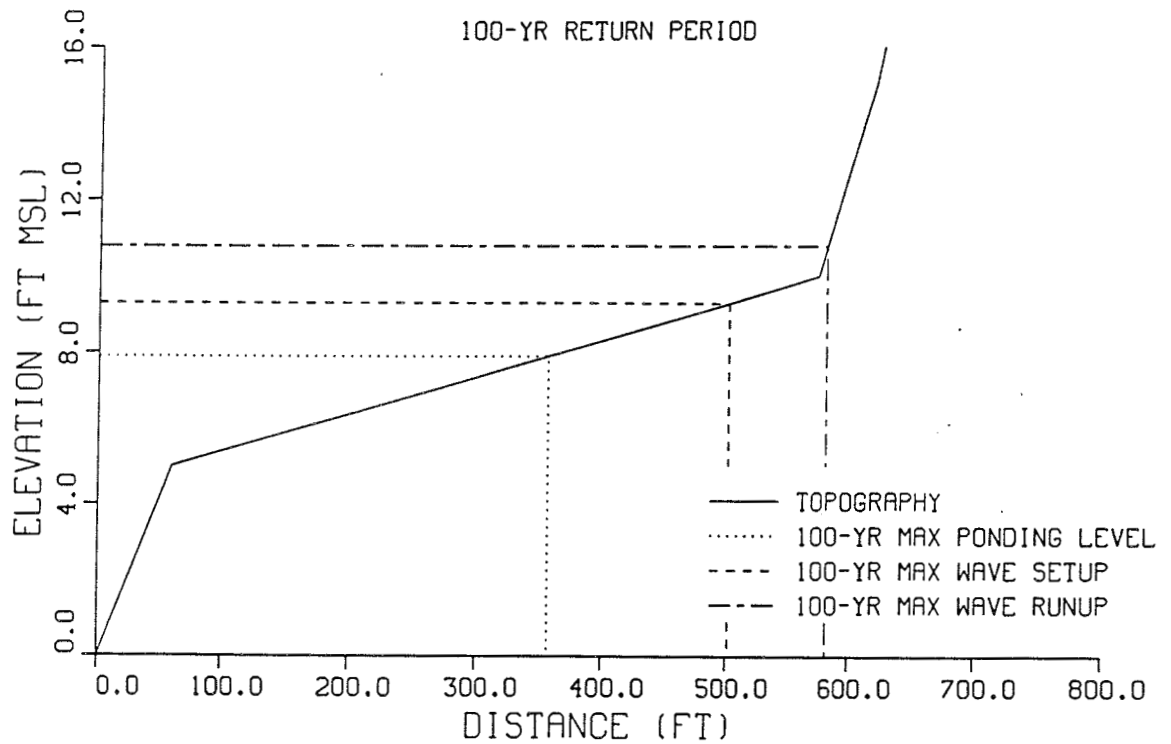
500-YR RETURN PERIOD



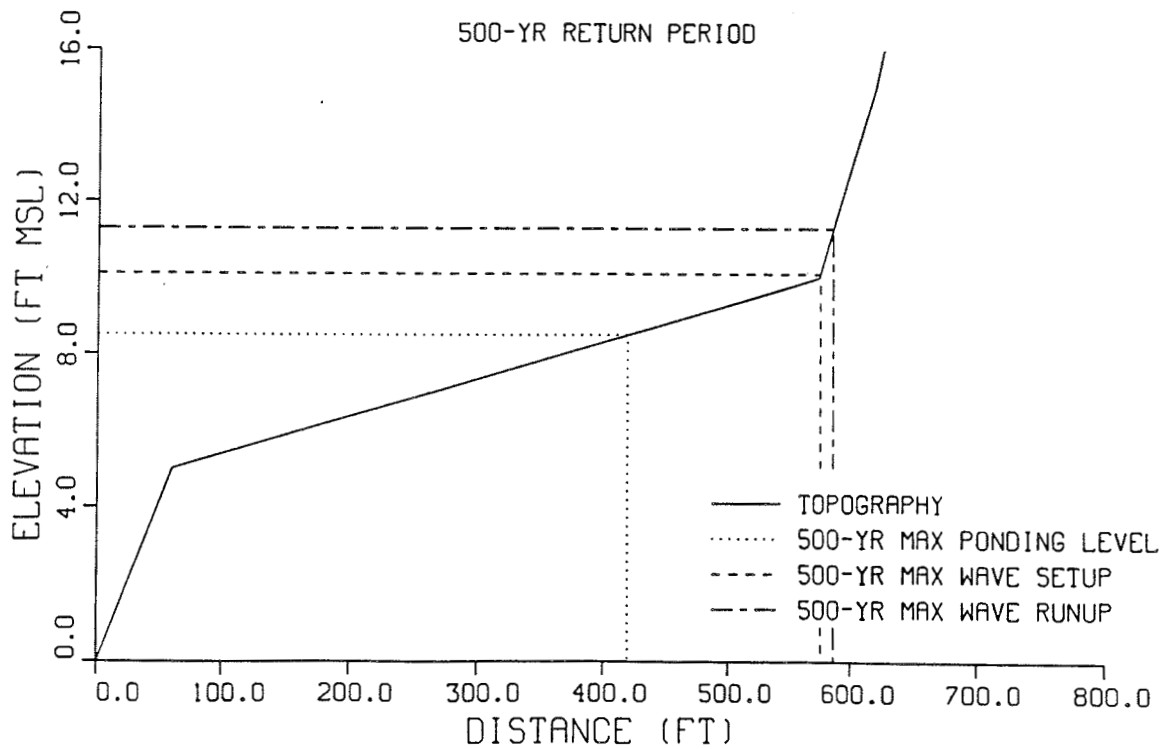
SOUTHERN GUAM TYPHOON ANALYSIS

PROFILE 9-3

100-YR RETURN PERIOD



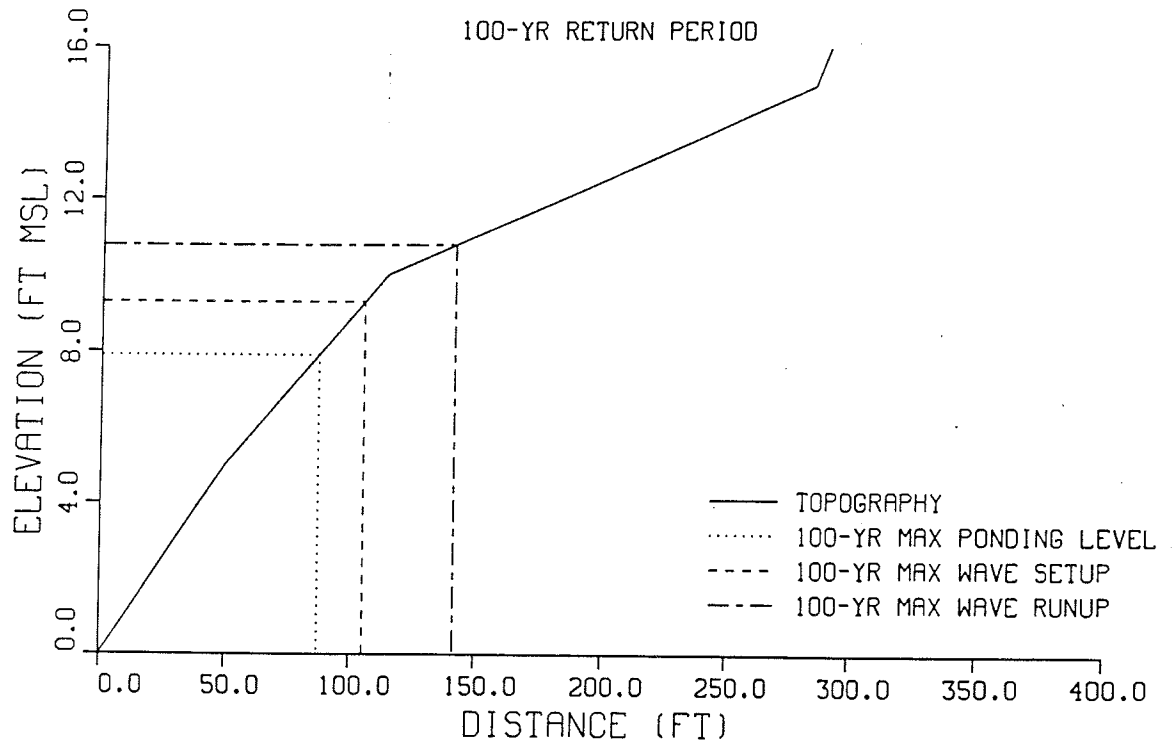
500-YR RETURN PERIOD



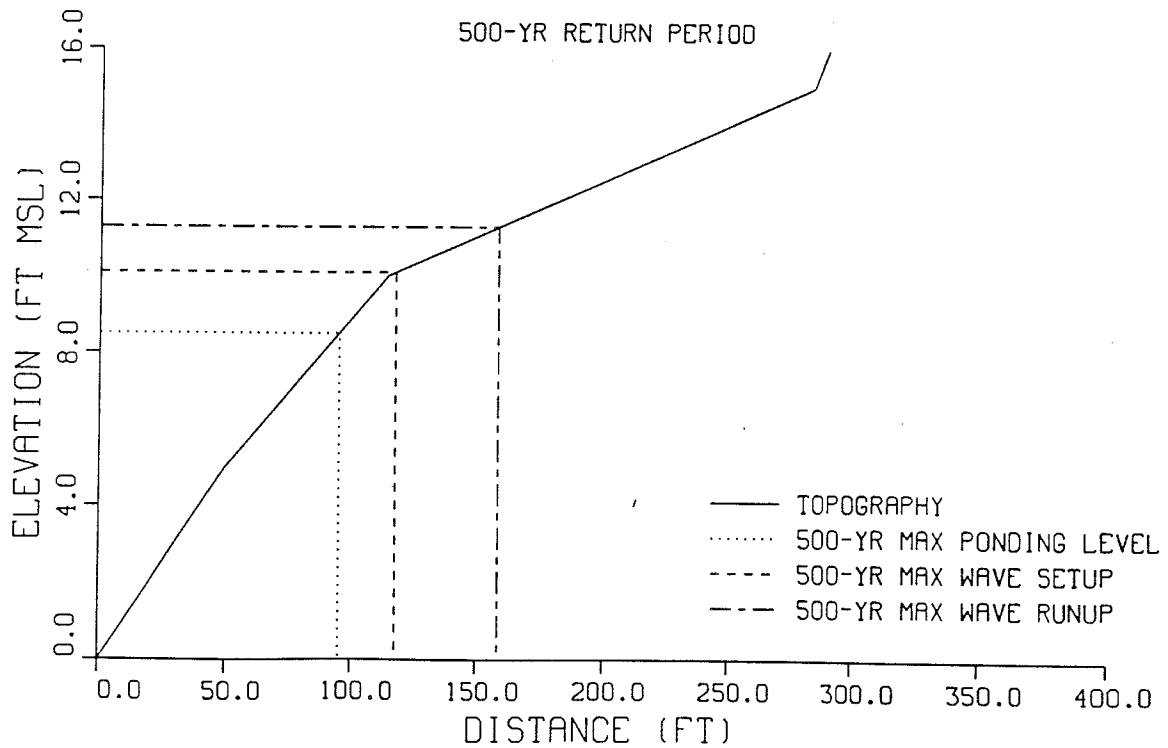
SOUTHERN GUAM TYPHOON ANALYSIS

PROFILE 9-4

100-YR RETURN PERIOD



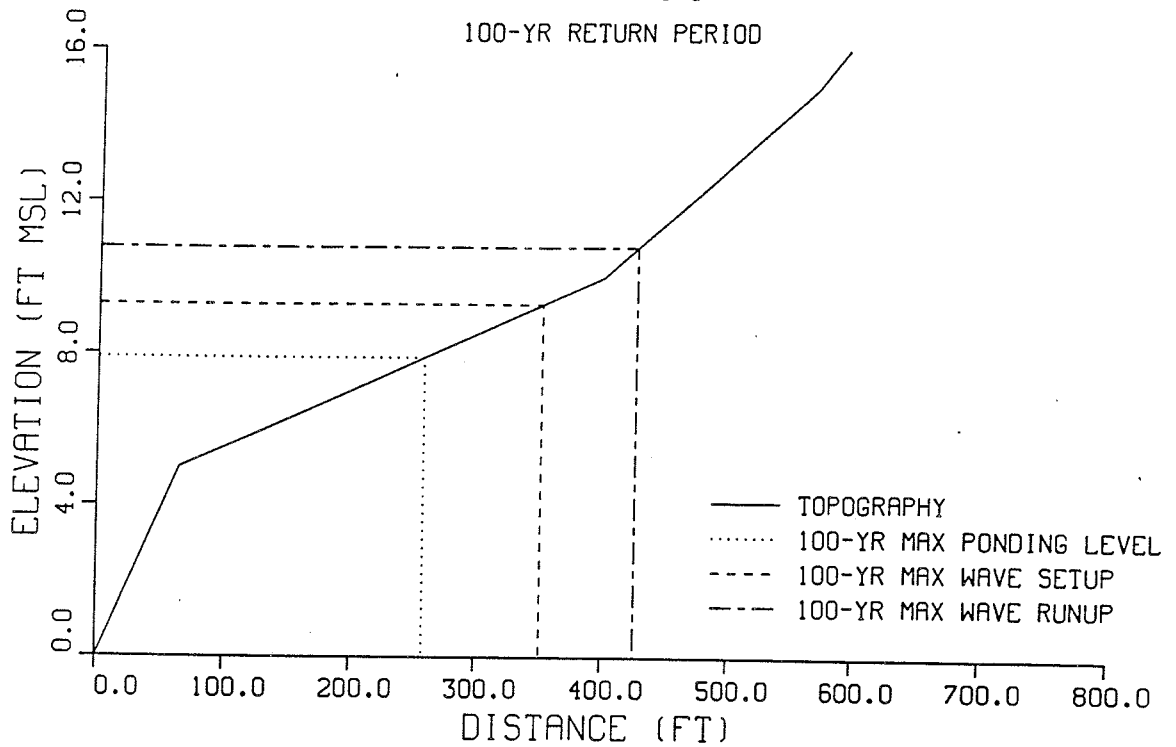
500-YR RETURN PERIOD



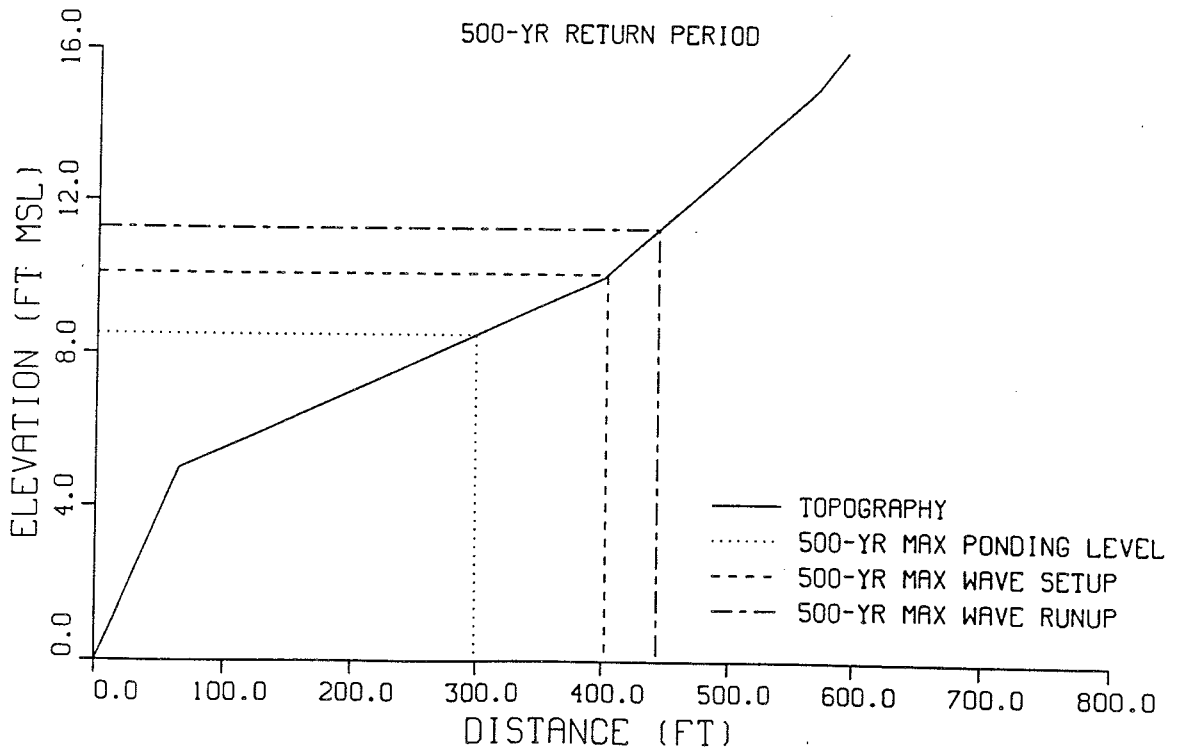
SOUTHERN GUAM TYPHOON ANALYSIS

PROFILE 9-5

100-YR RETURN PERIOD



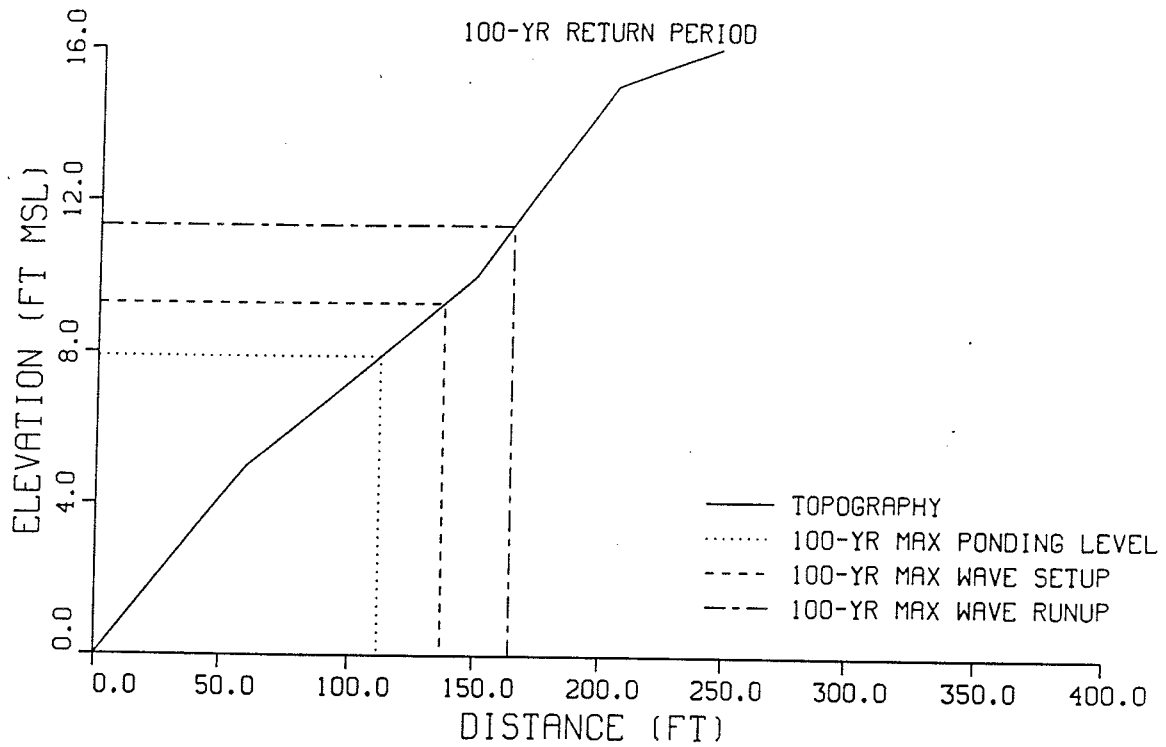
500-YR RETURN PERIOD



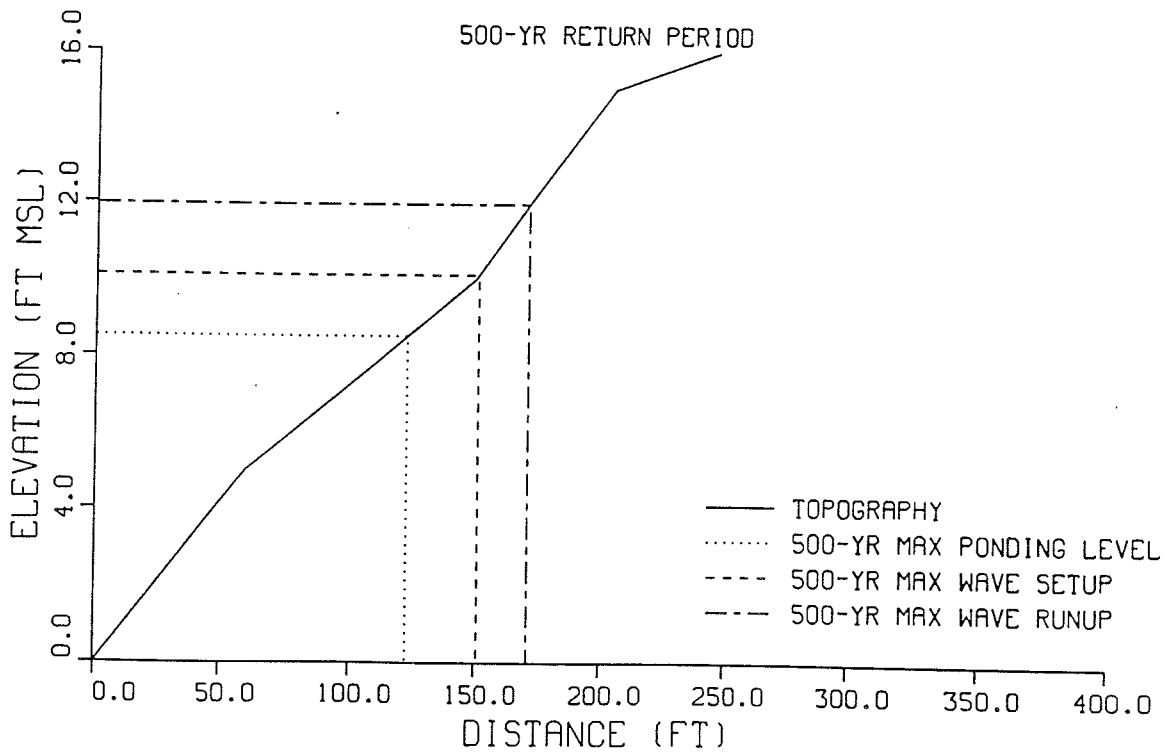
SOUTHERN GUAM TYPHOON ANALYSIS

PROFILE 9-6

100-YR RETURN PERIOD



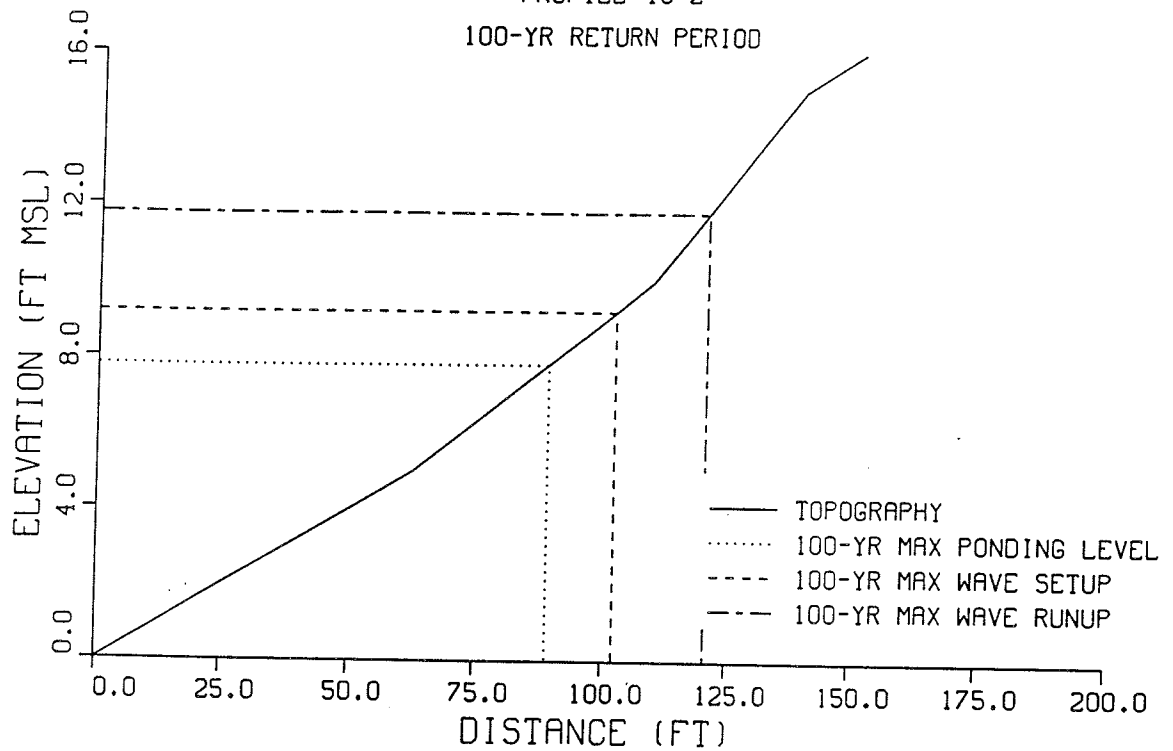
500-YR RETURN PERIOD



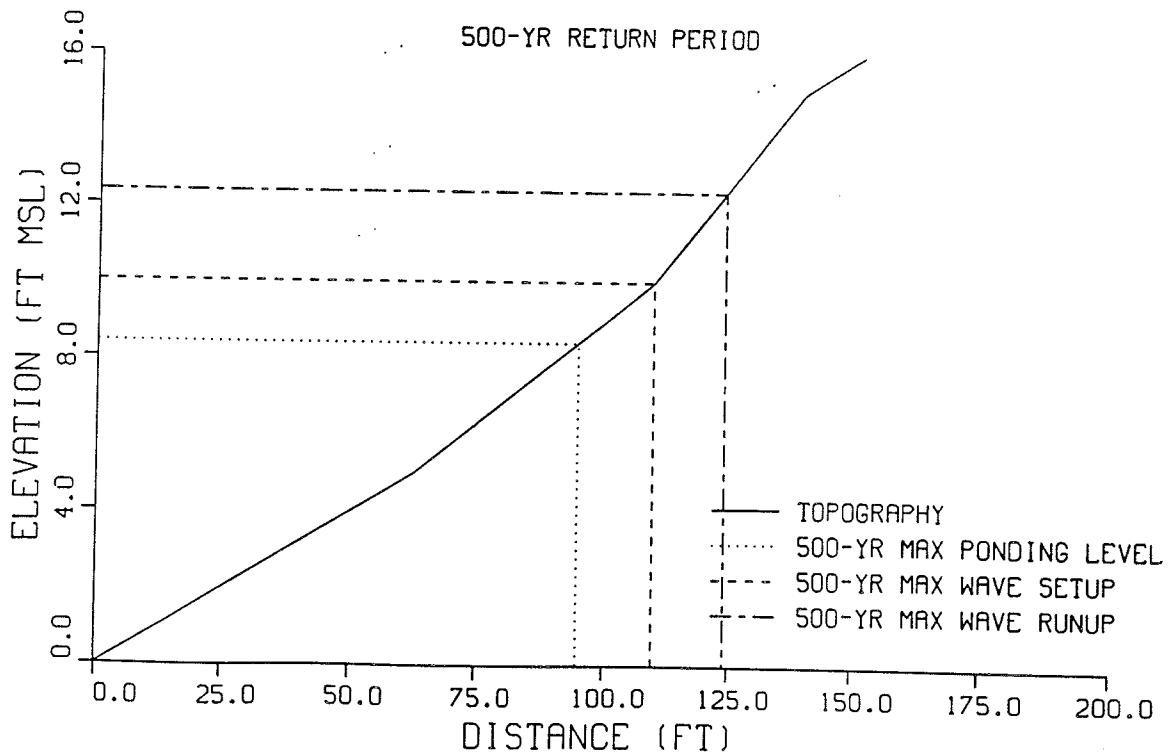
SOUTHERN GUAM TYPHOON ANALYSIS

PROFILE 10-2

100-YR RETURN PERIOD



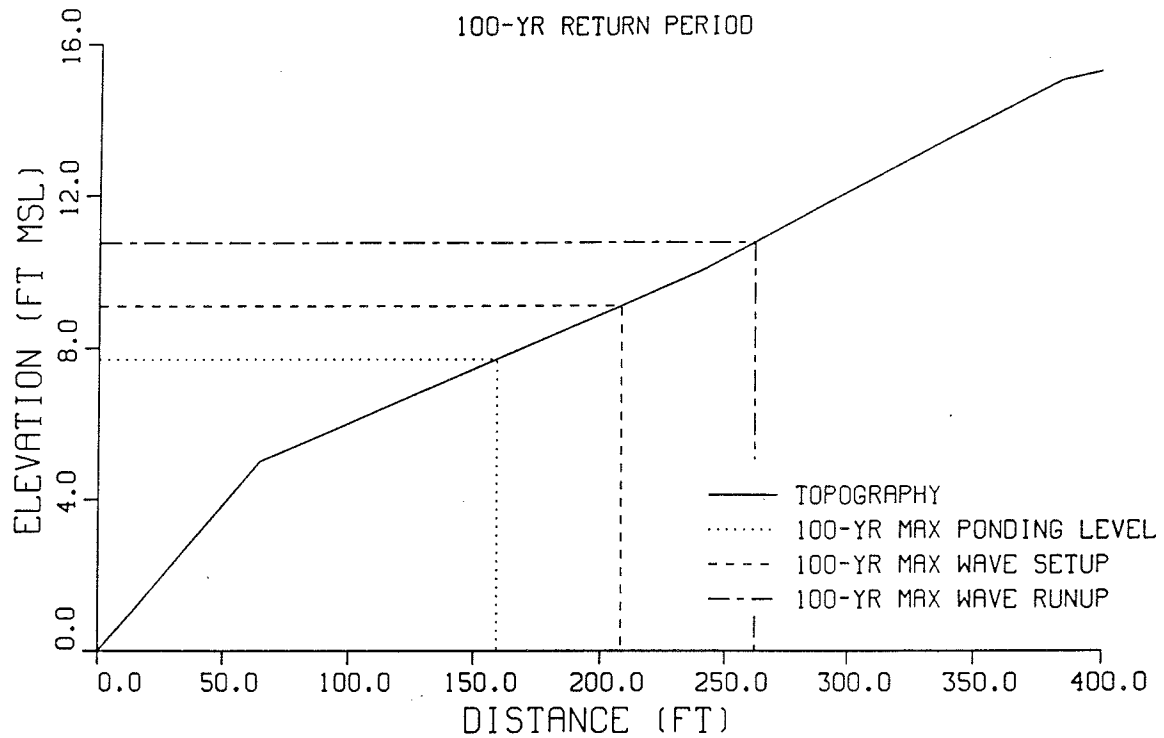
500-YR RETURN PERIOD



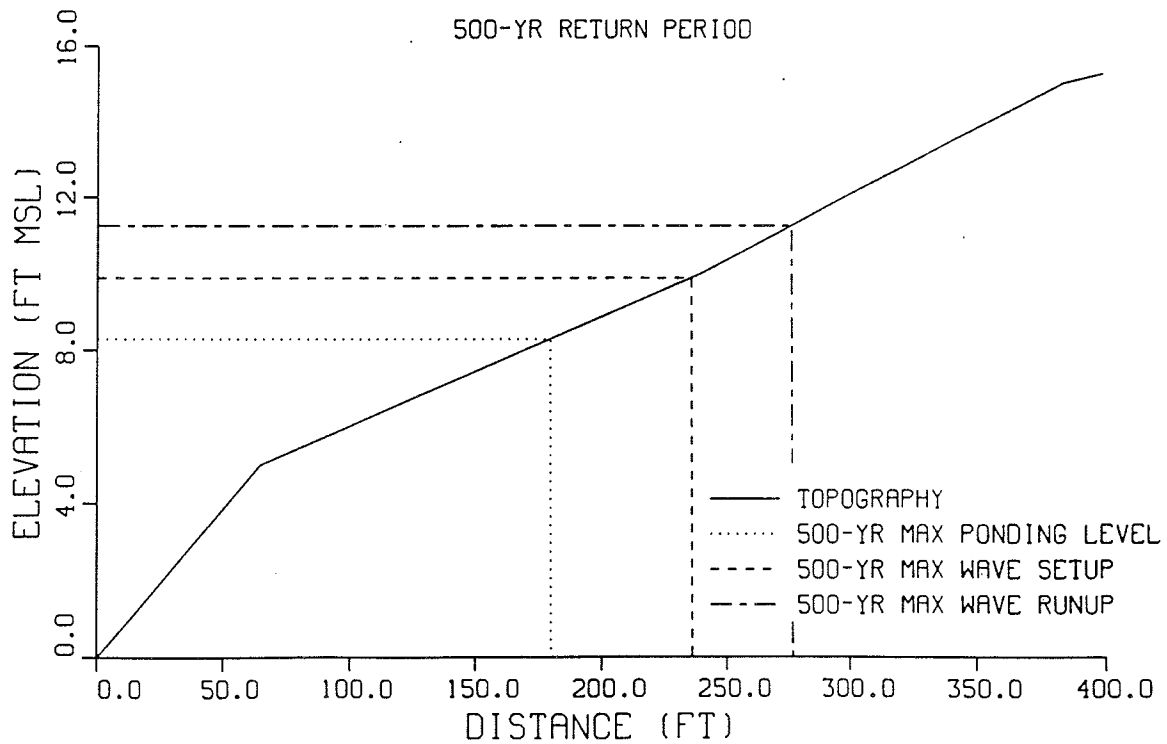
SOUTHERN GUAM TYPHOON ANALYSIS

PROFILE 10-3

100-YR RETURN PERIOD



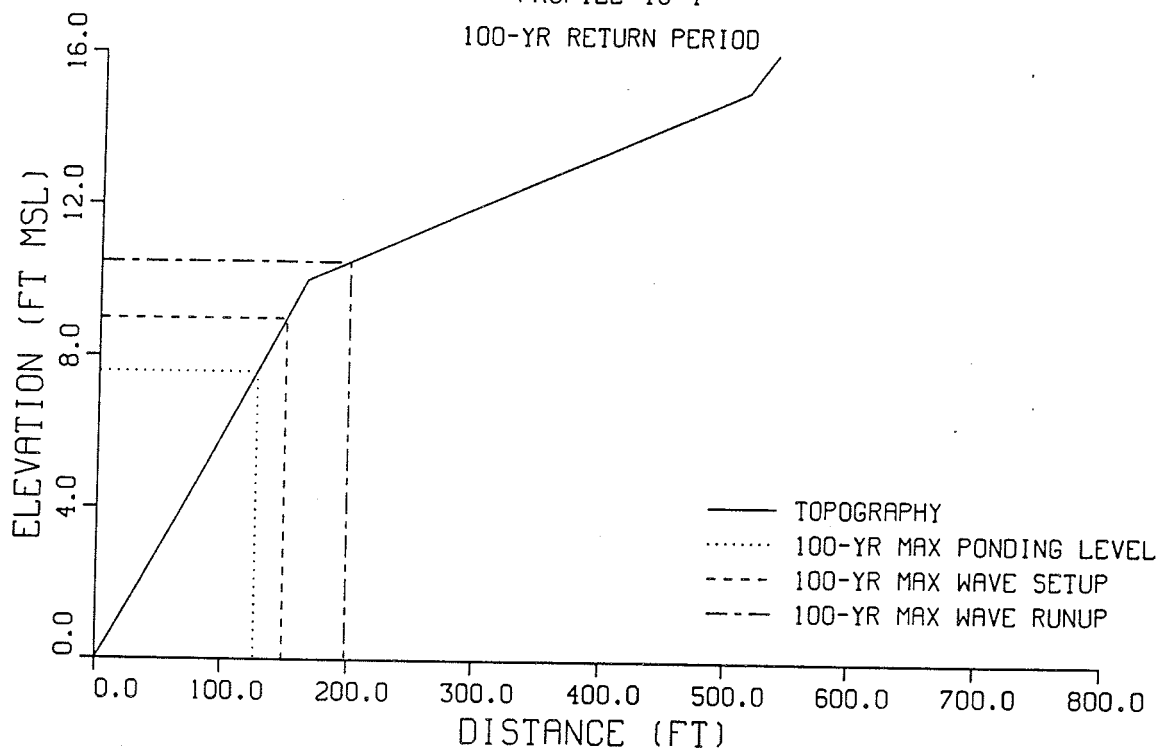
500-YR RETURN PERIOD



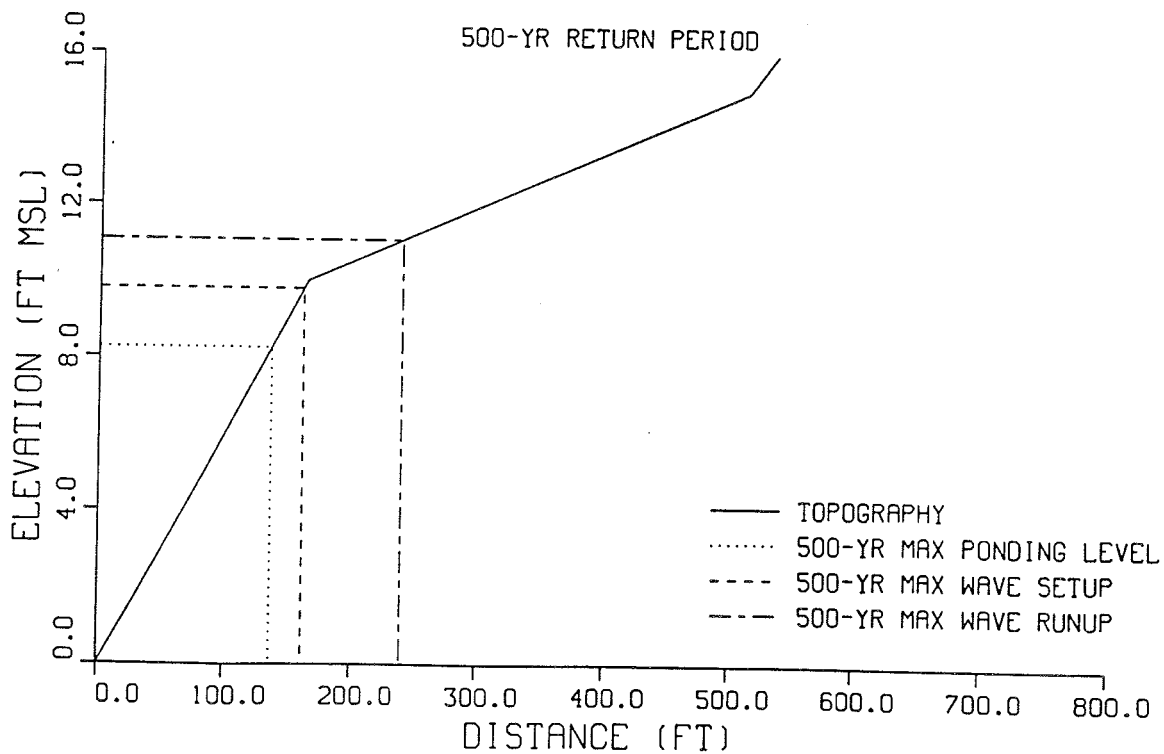
SOUTHERN GUAM TYPHOON ANALYSIS

PROFILE 10-4

100-YR RETURN PERIOD



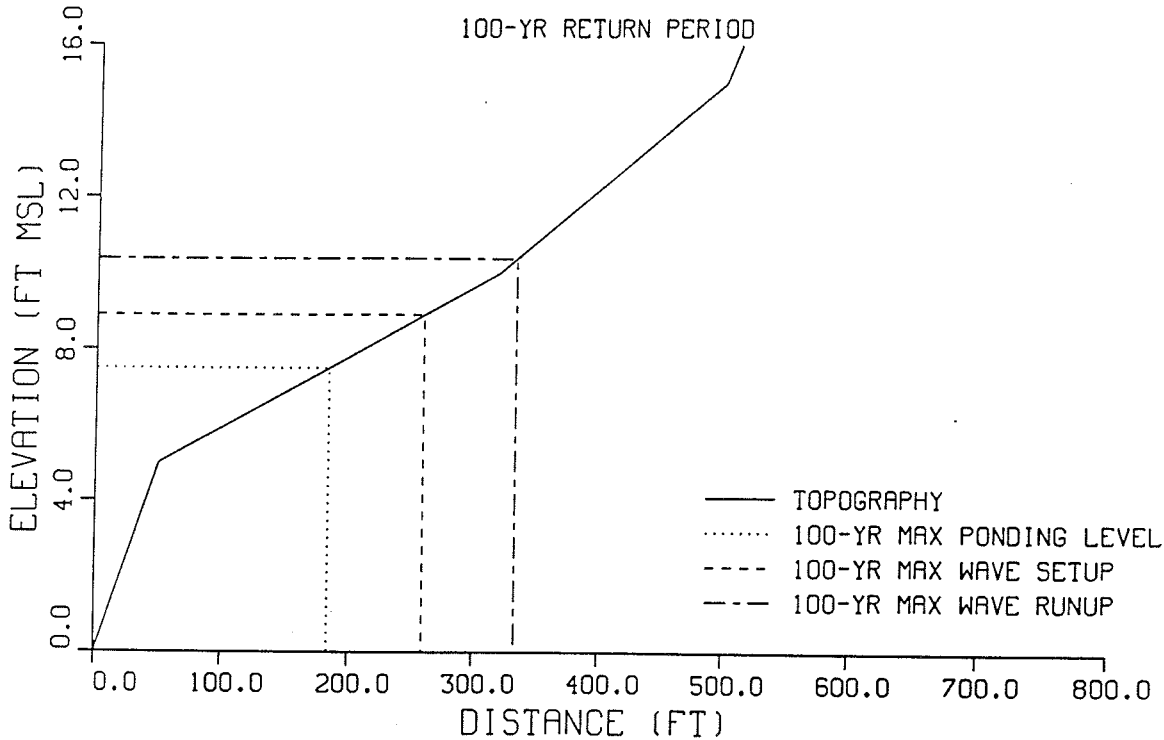
500-YR RETURN PERIOD



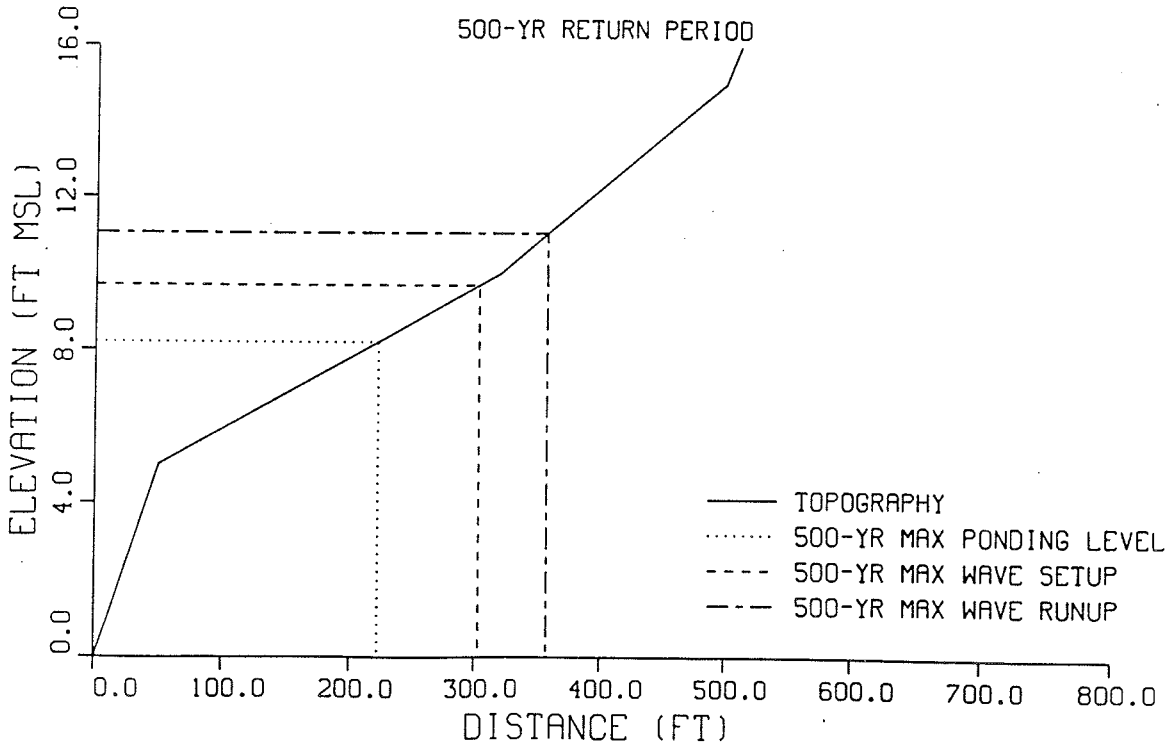
SOUTHERN GUAM TYPHOON ANALYSIS

PROFILE 11-1

100-YR RETURN PERIOD



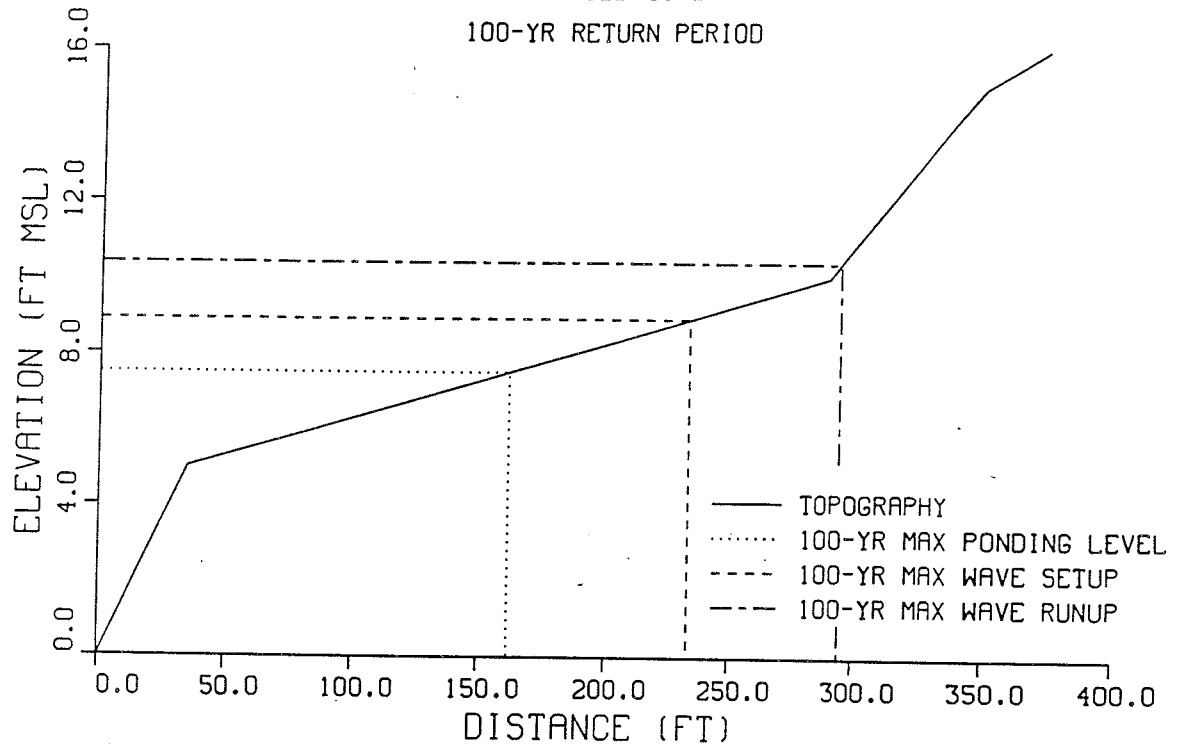
500-YR RETURN PERIOD



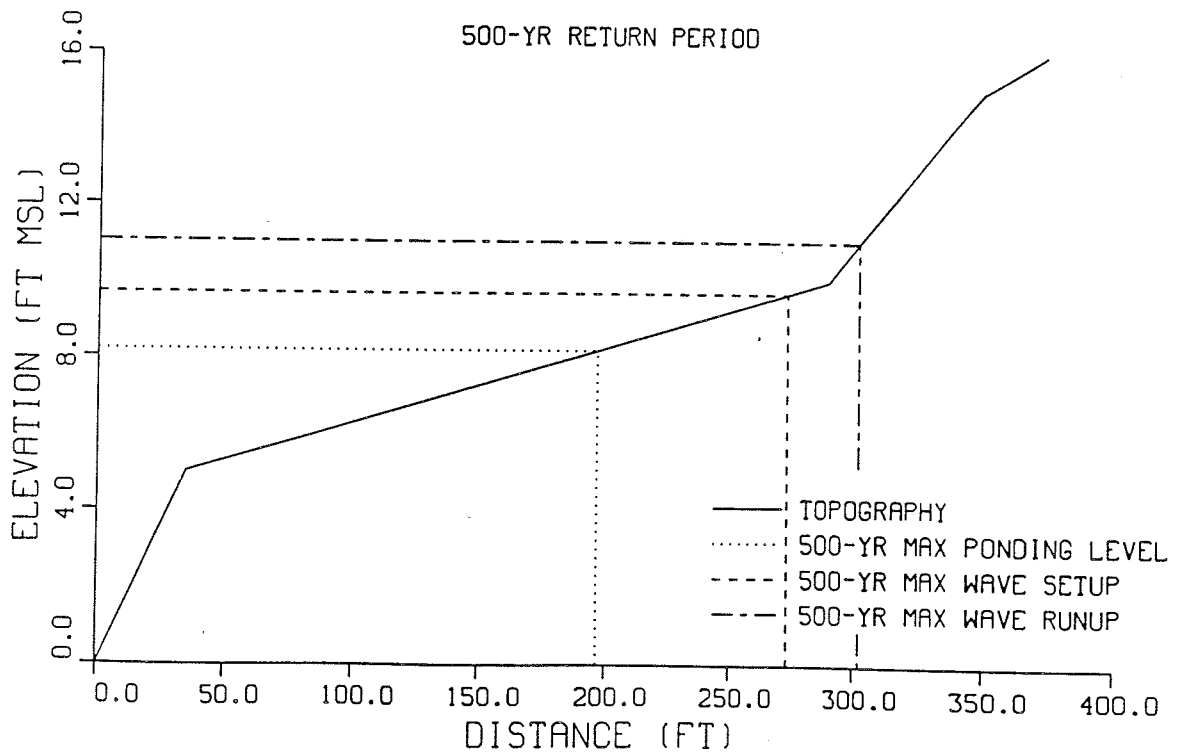
SOUTHERN GUAM TYPHOON ANALYSIS

PROFILE 11-2

100-YR RETURN PERIOD



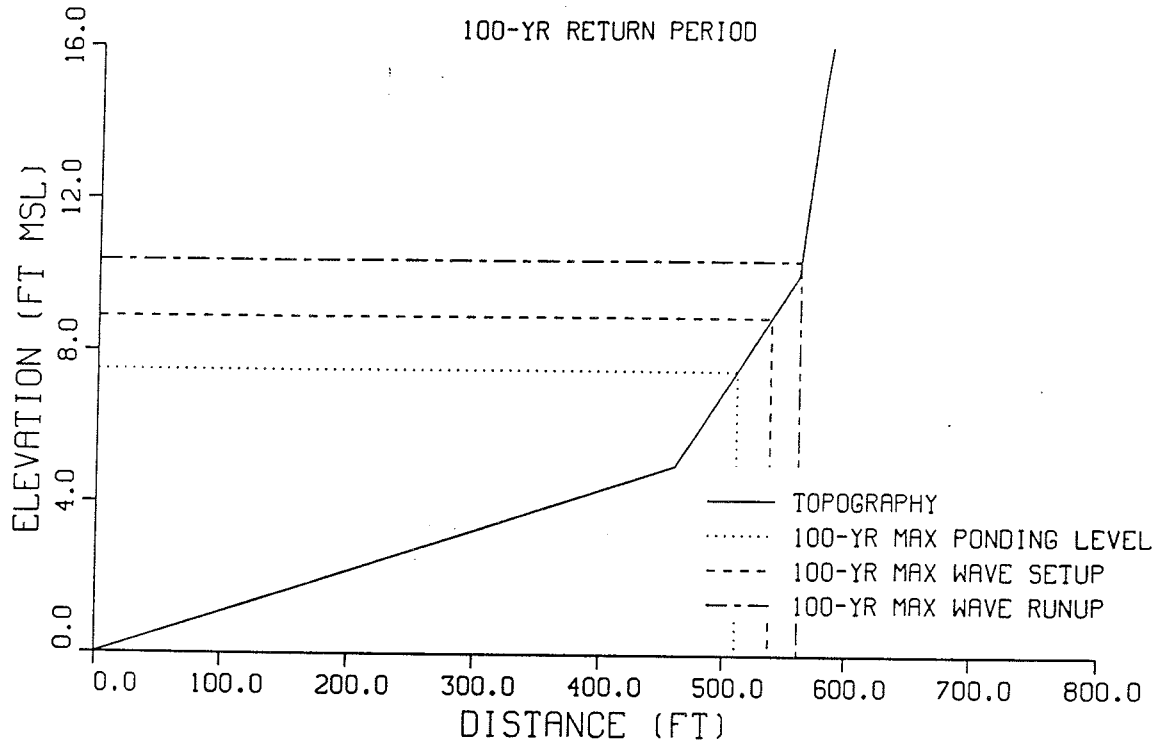
500-YR RETURN PERIOD



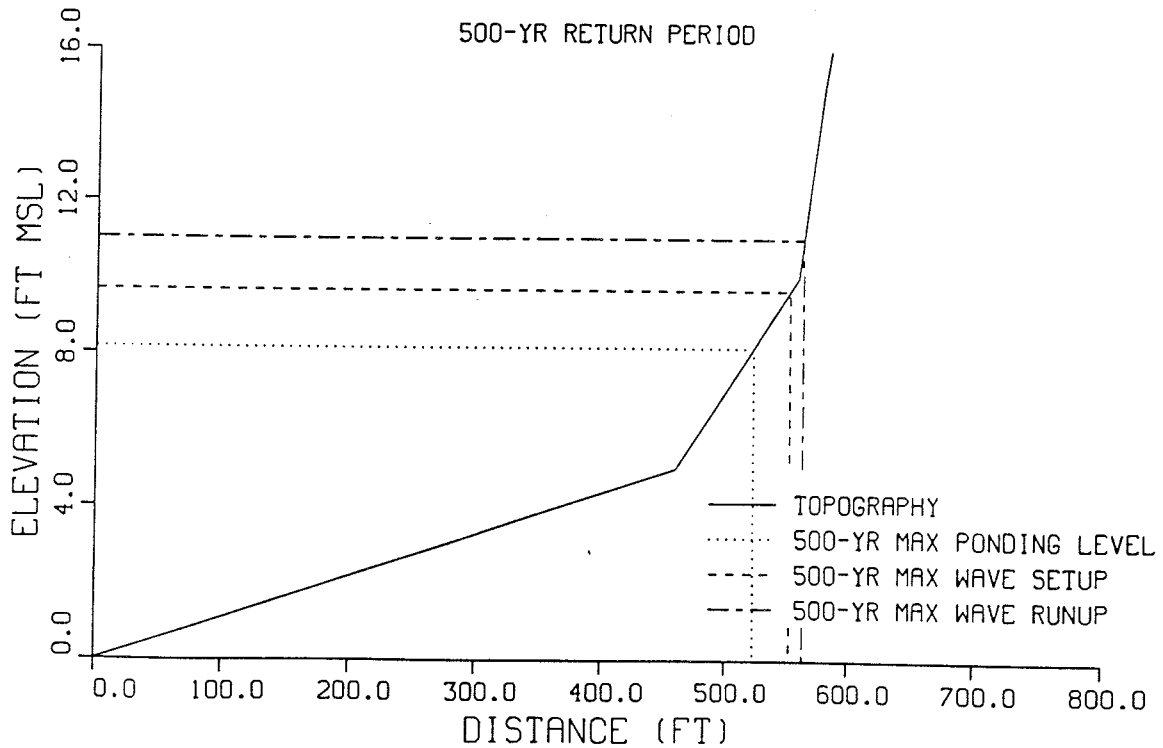
SOUTHERN GUAM TYPHOON ANALYSIS

PROFILE 11-3

100-YR RETURN PERIOD



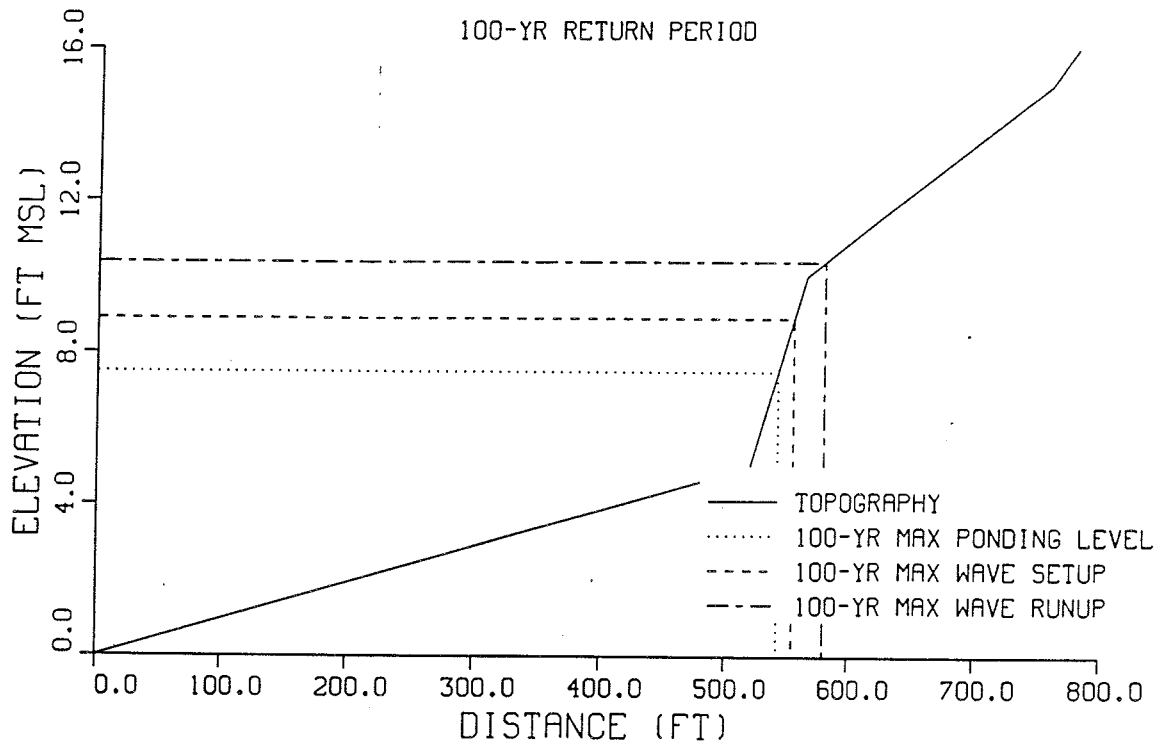
500-YR RETURN PERIOD



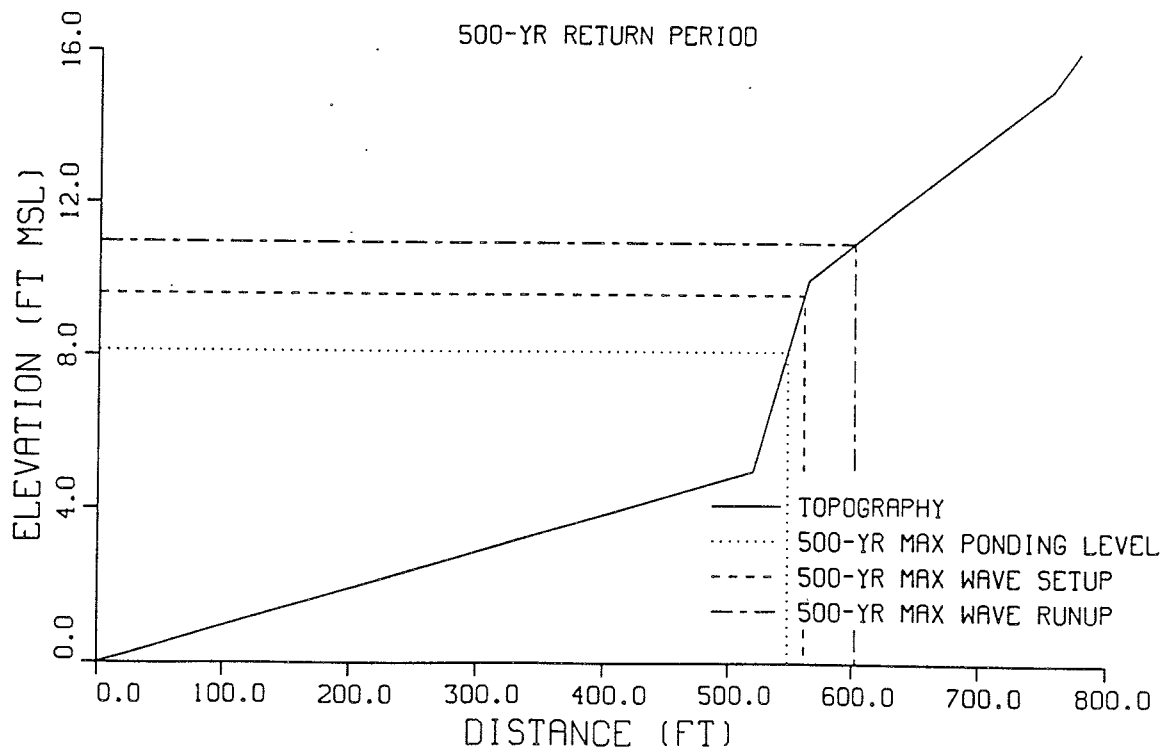
SOUTHERN GUAM TYPHOON ANALYSIS

PROFILE 11-5

100-YR RETURN PERIOD



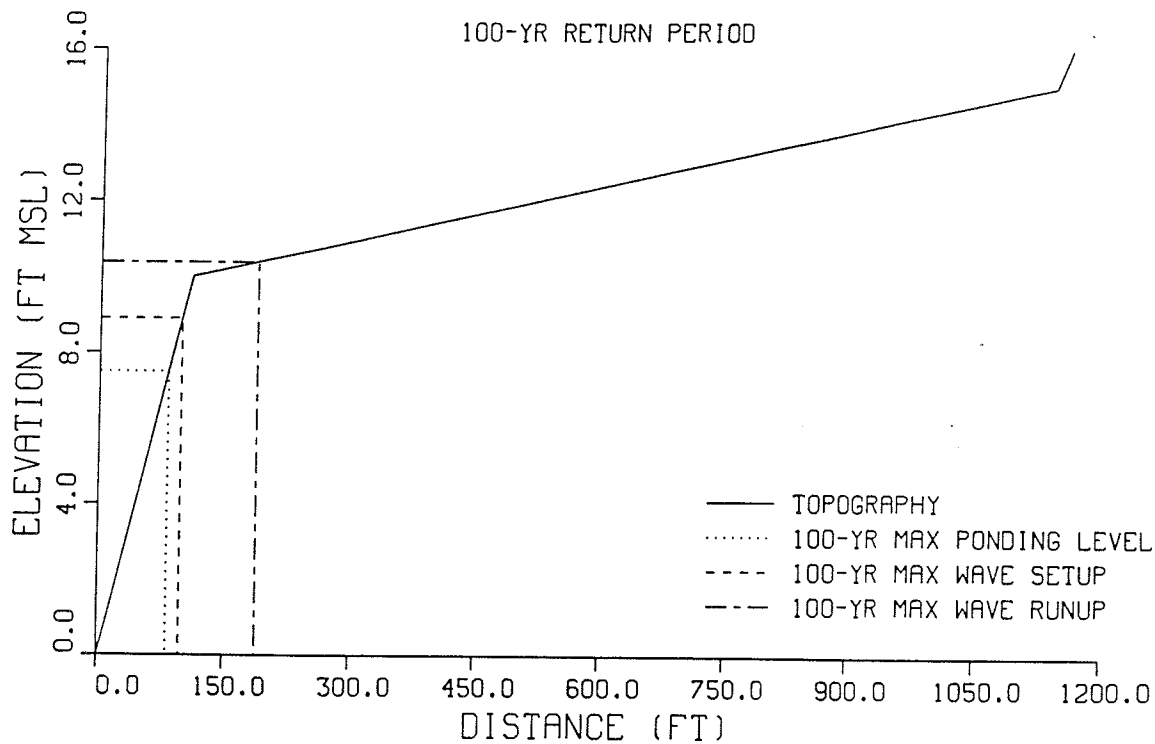
500-YR RETURN PERIOD



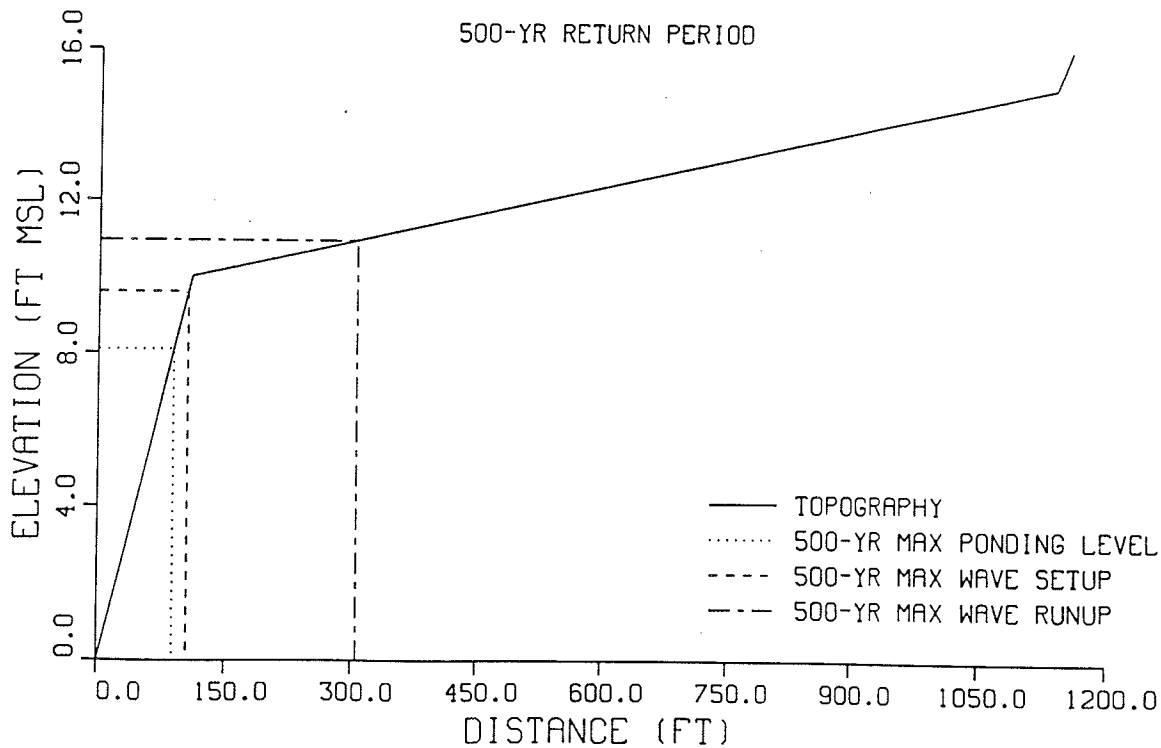
SOUTHERN GUAM TYPHOON ANALYSIS

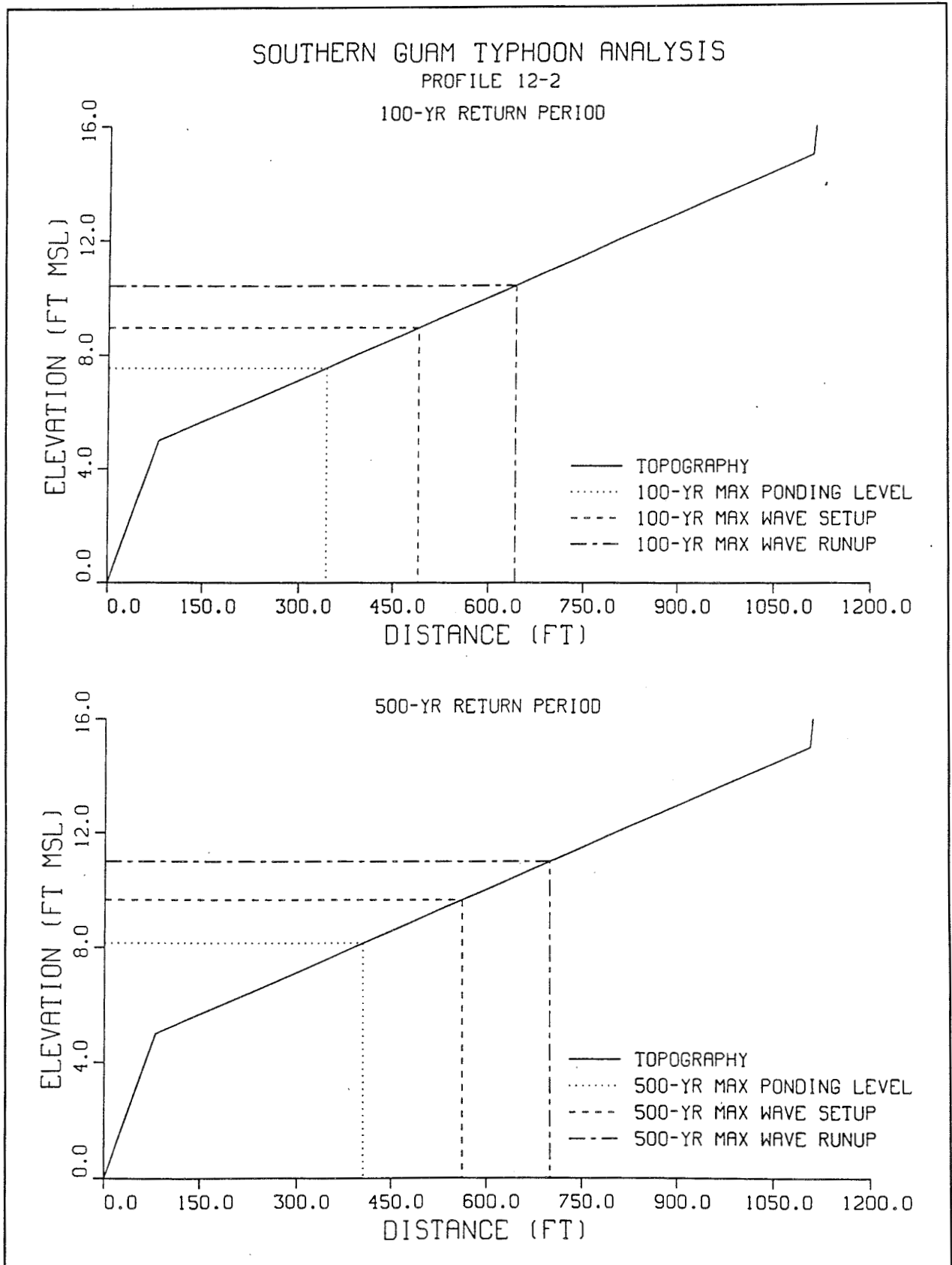
PROFILE 12-1

100-YR RETURN PERIOD



500-YR RETURN PERIOD

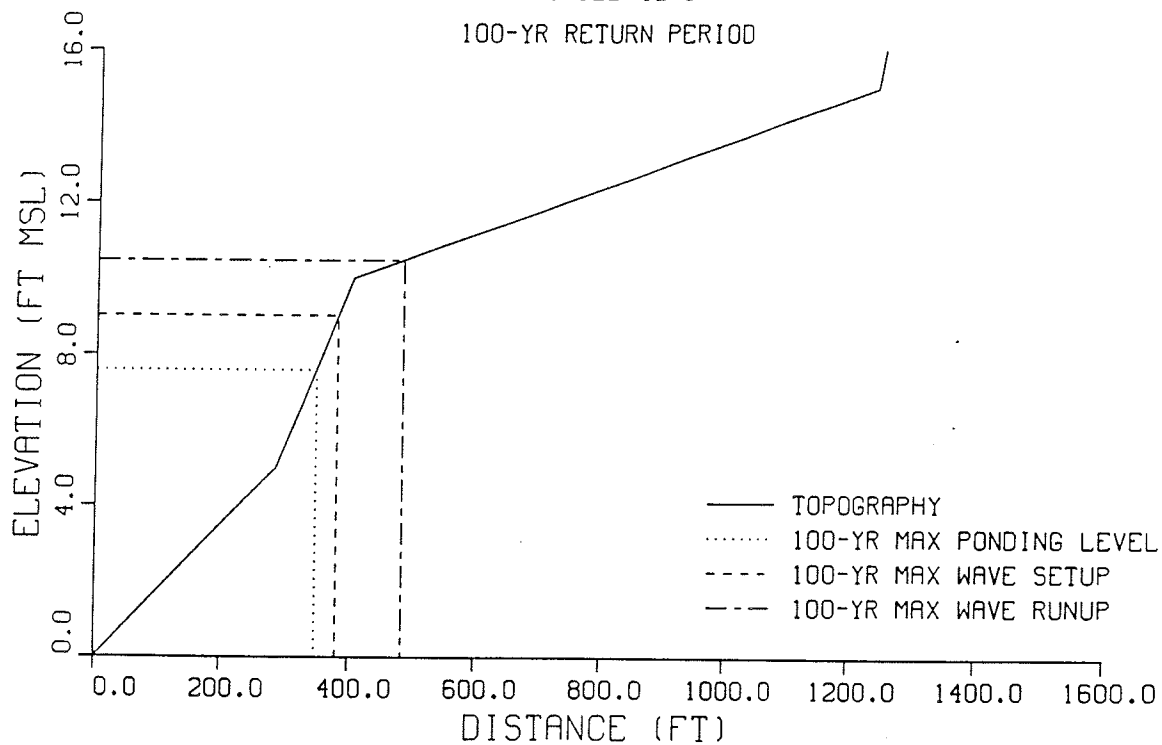




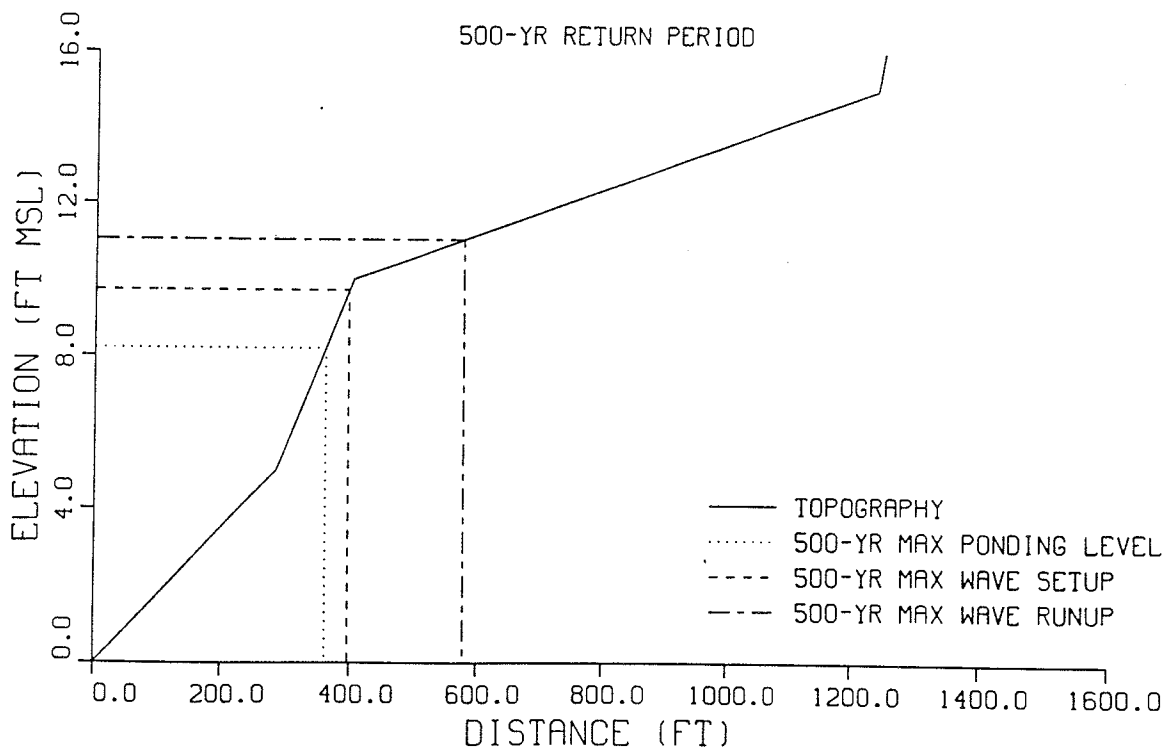
SOUTHERN GUAM TYPHOON ANALYSIS

PROFILE 12-3

100-YR RETURN PERIOD



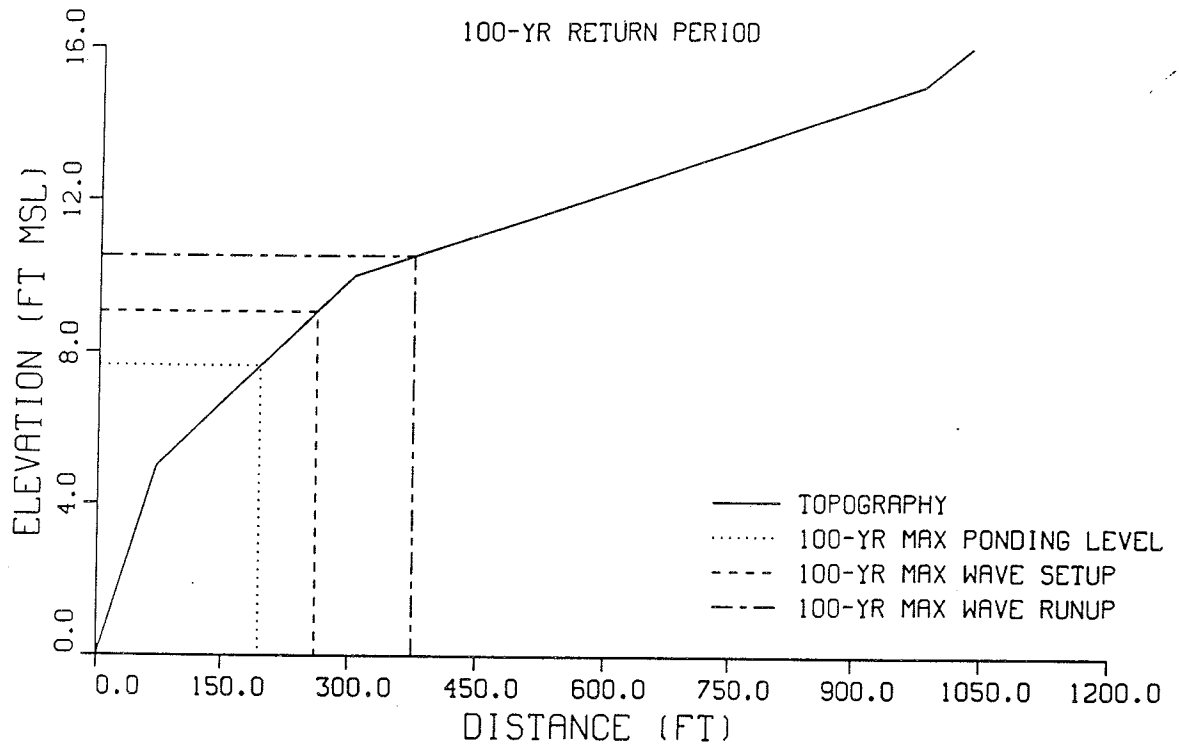
500-YR RETURN PERIOD



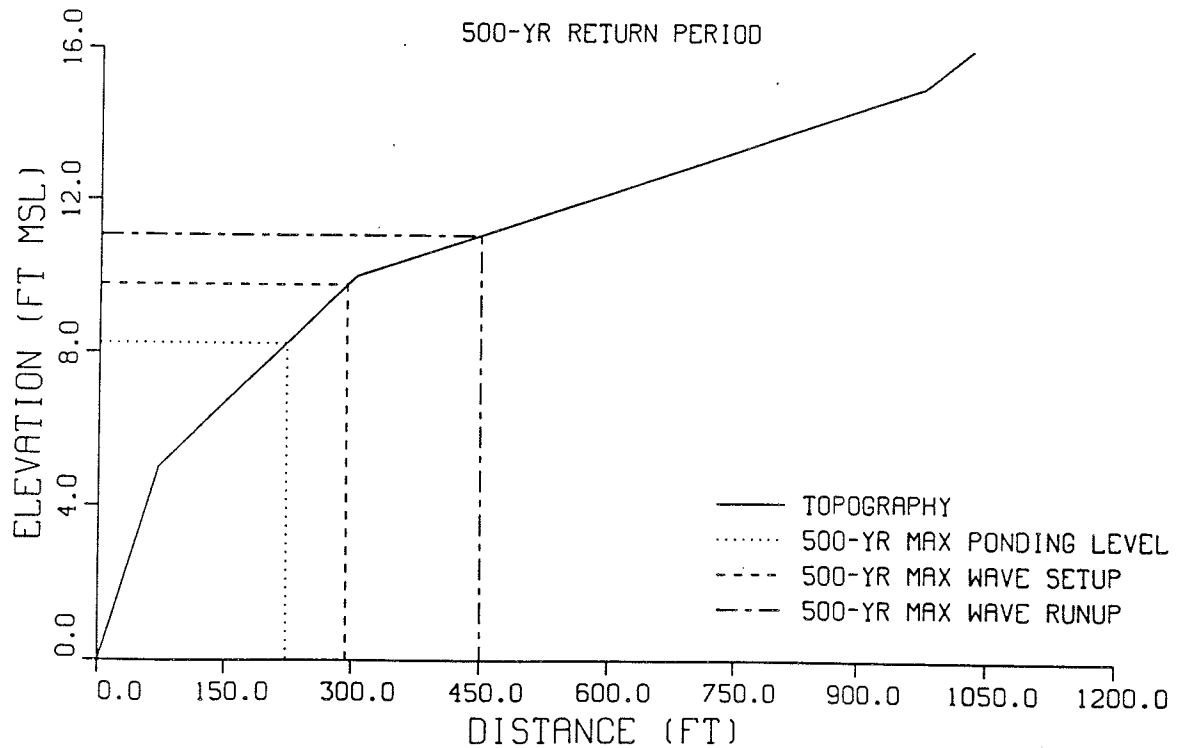
SOUTHERN GUAM TYPHOON ANALYSIS

PROFILE 12-4

100-YR RETURN PERIOD



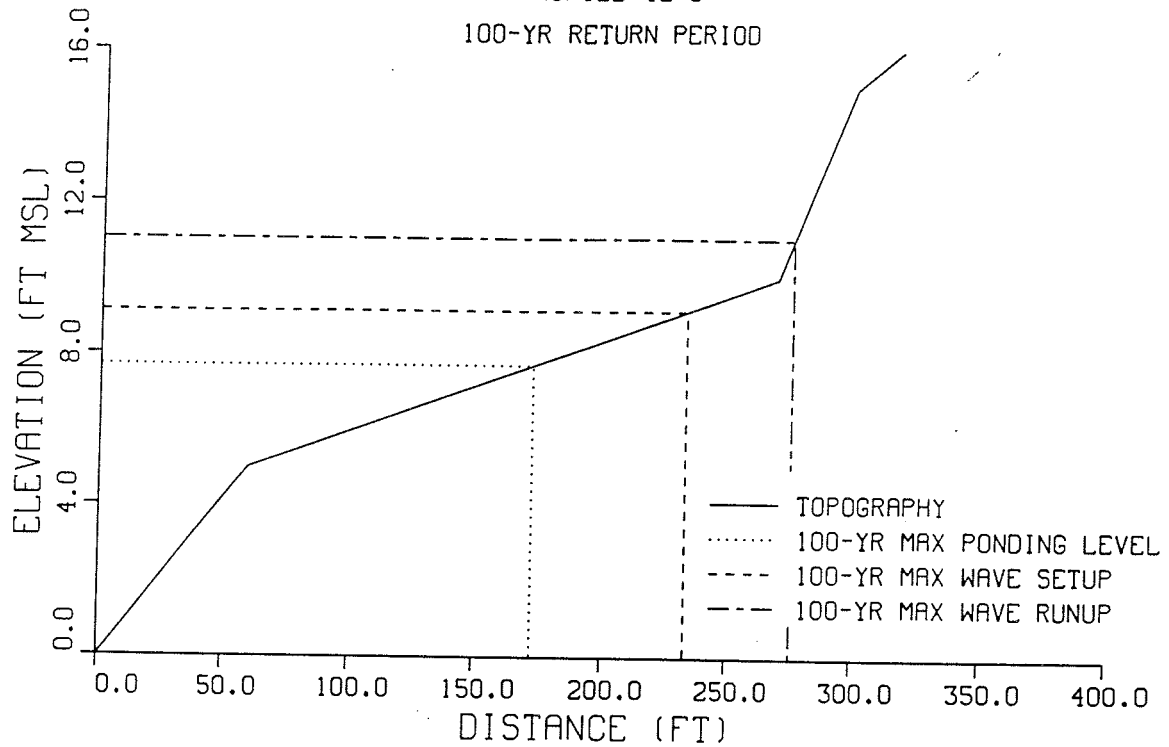
500-YR RETURN PERIOD



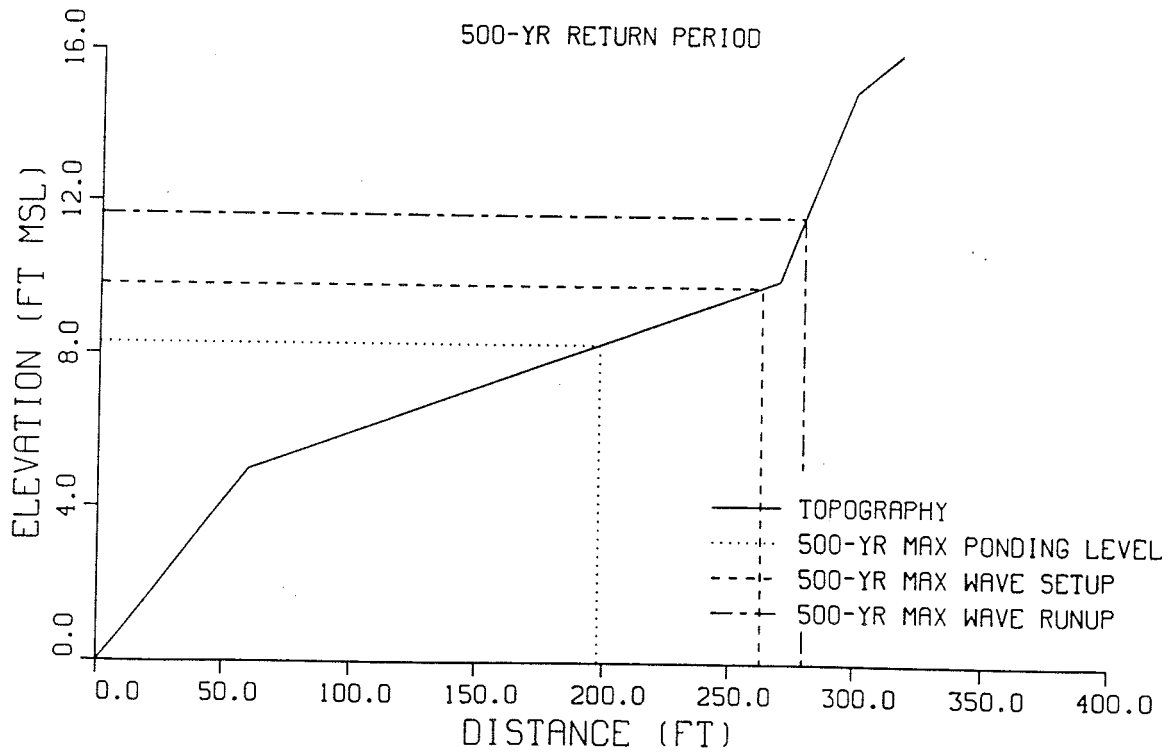
SOUTHERN GUAM TYPHOON ANALYSIS

PROFILE 12-5

100-YR RETURN PERIOD



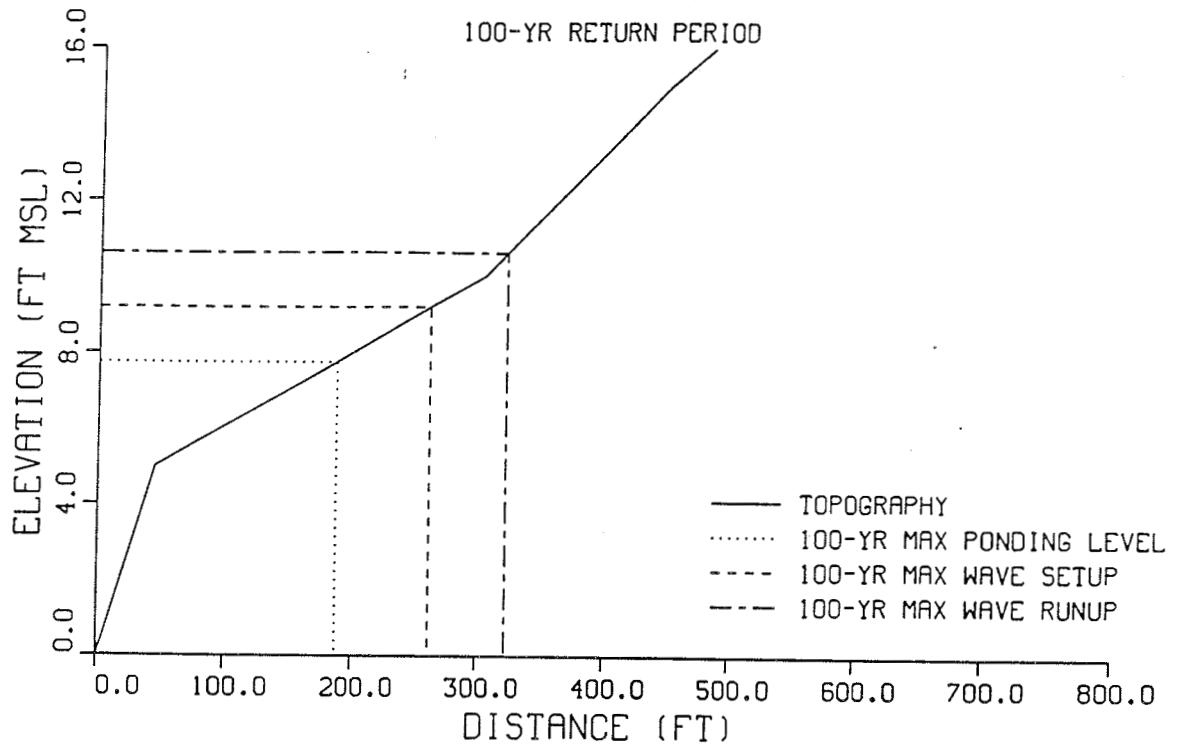
500-YR RETURN PERIOD



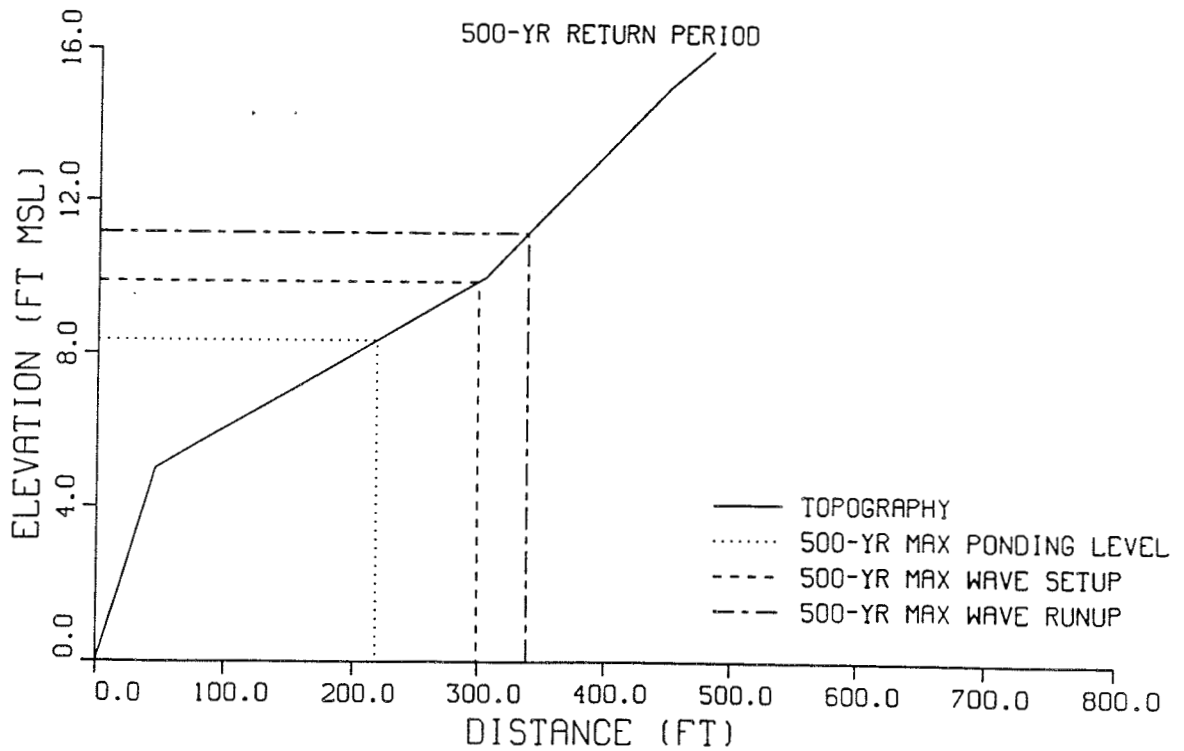
SOUTHERN GUAM TYPHOON ANALYSIS

PROFILE 12-6

100-YR RETURN PERIOD

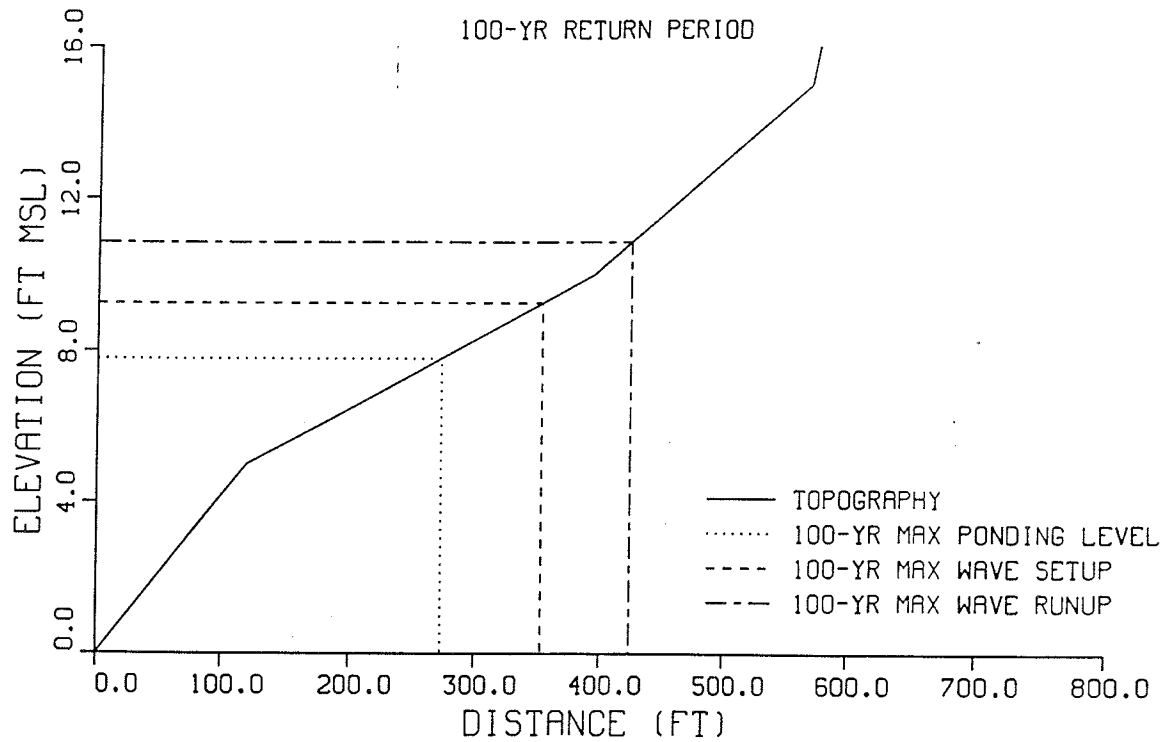


500-YR RETURN PERIOD

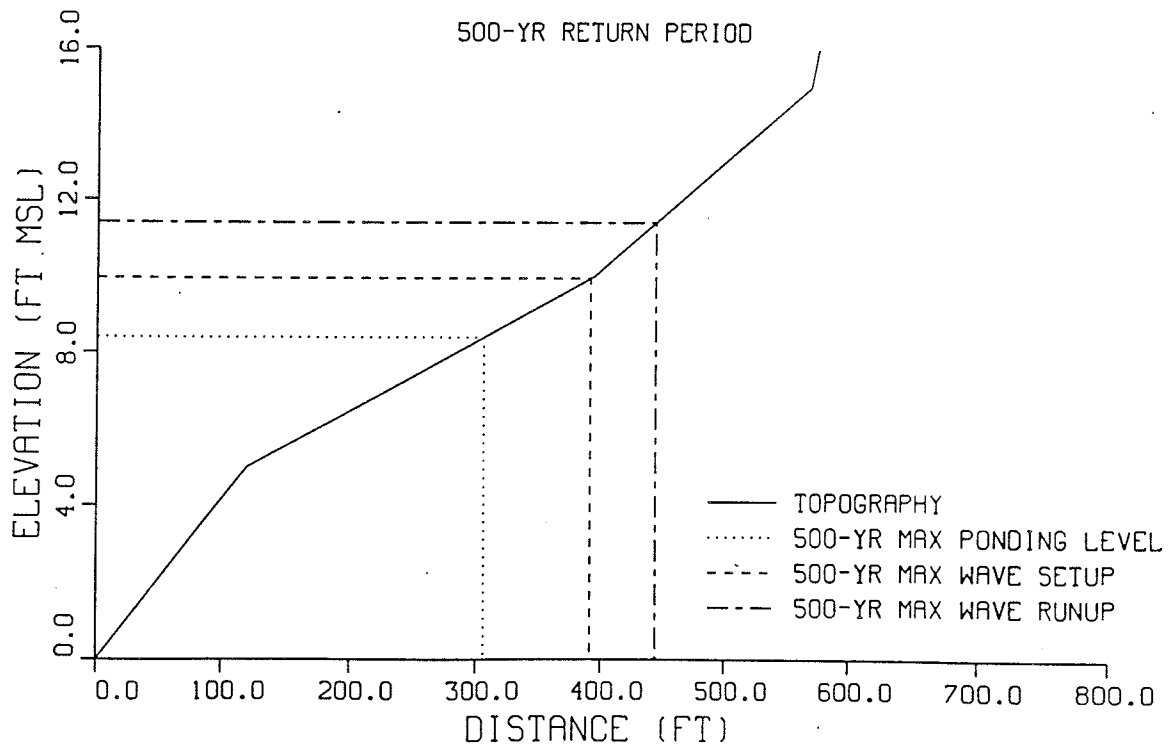


SOUTHERN GUAM TYPHOON ANALYSIS
PROFILE 12-7

100-YR RETURN PERIOD



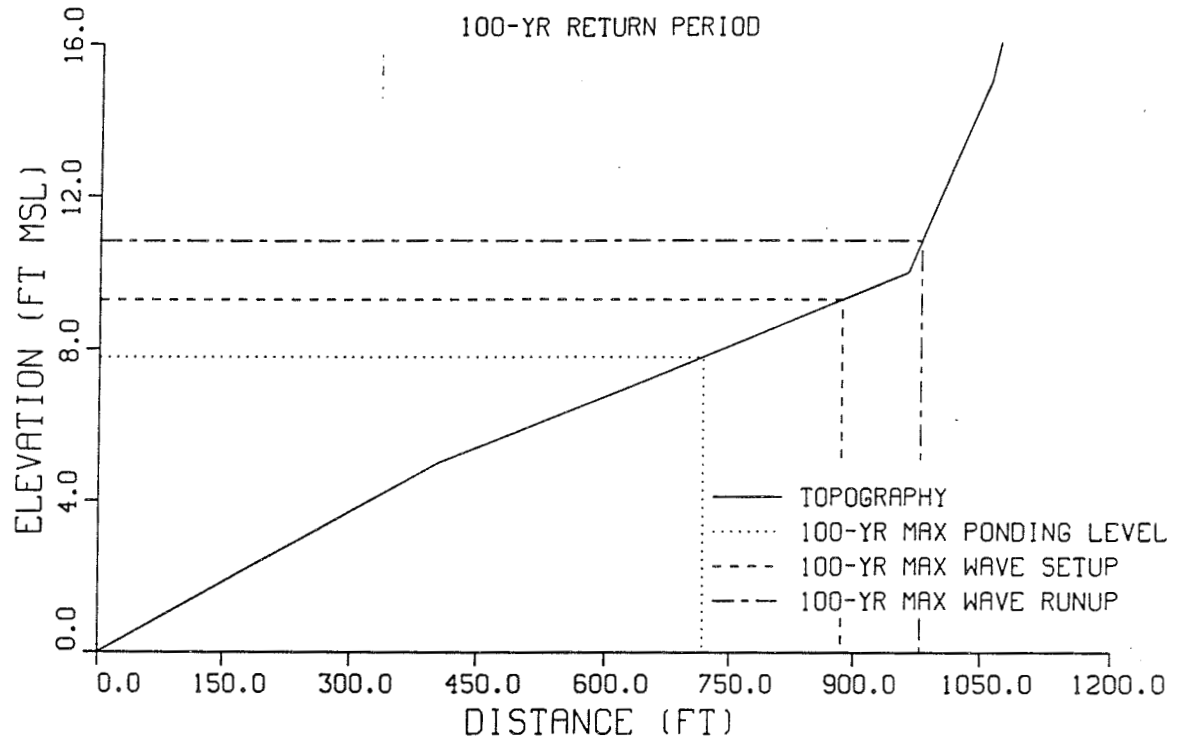
500-YR RETURN PERIOD



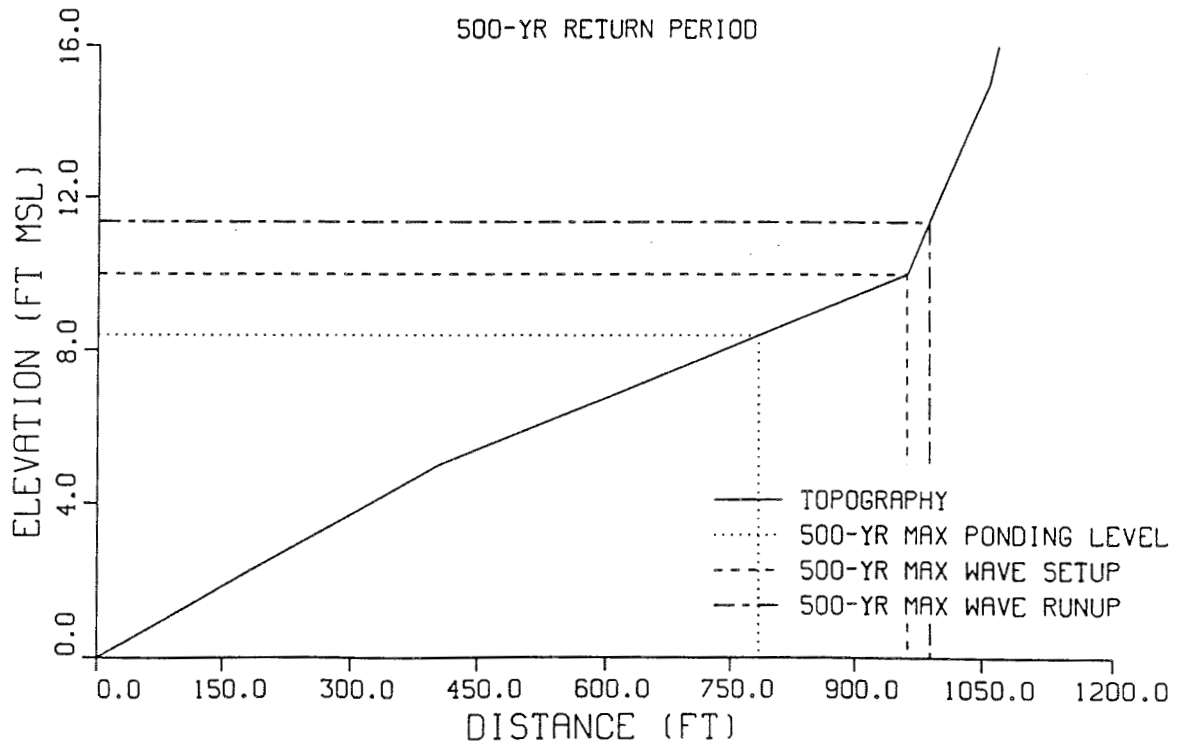
SOUTHERN GUAM TYPHOON ANALYSIS

PROFILE 13-1

100-YR RETURN PERIOD



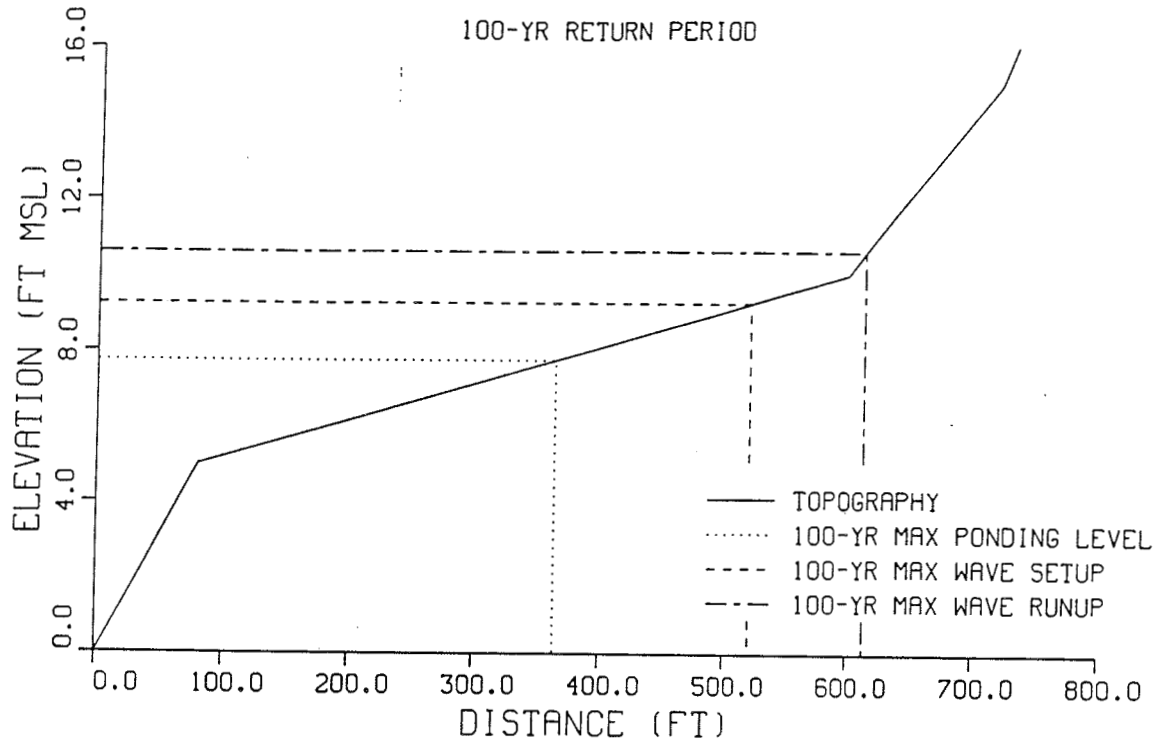
500-YR RETURN PERIOD



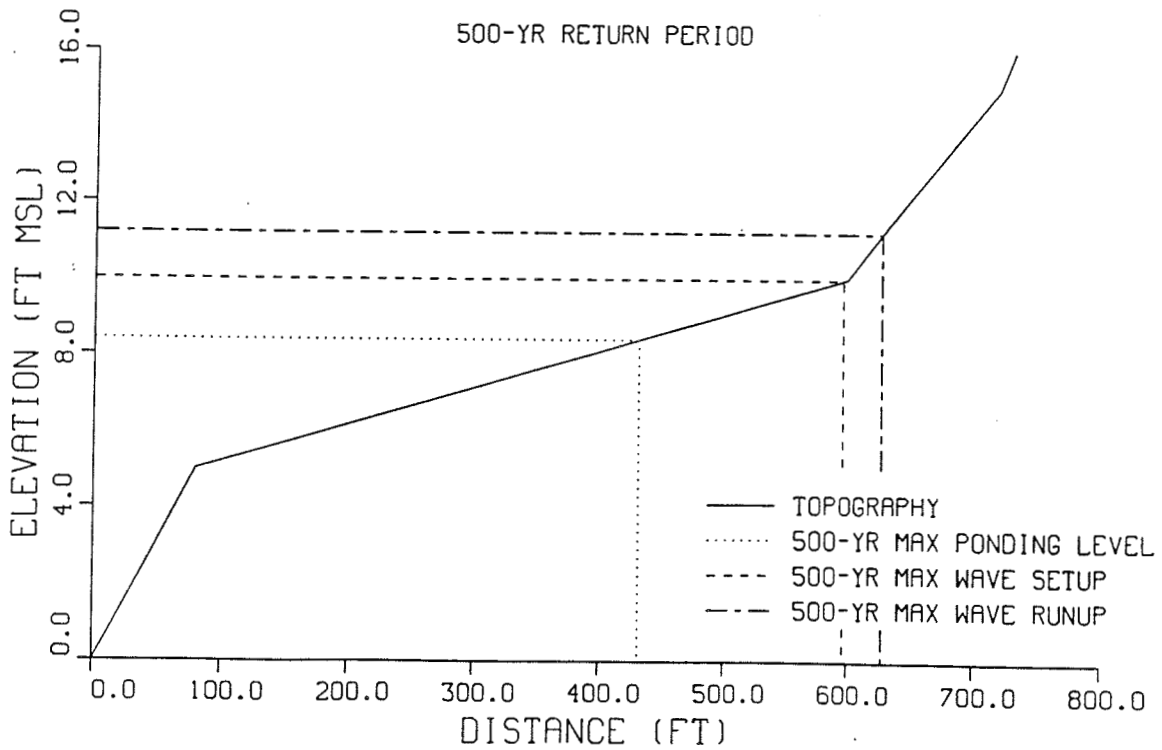
SOUTHERN GUAM TYPHOON ANALYSIS

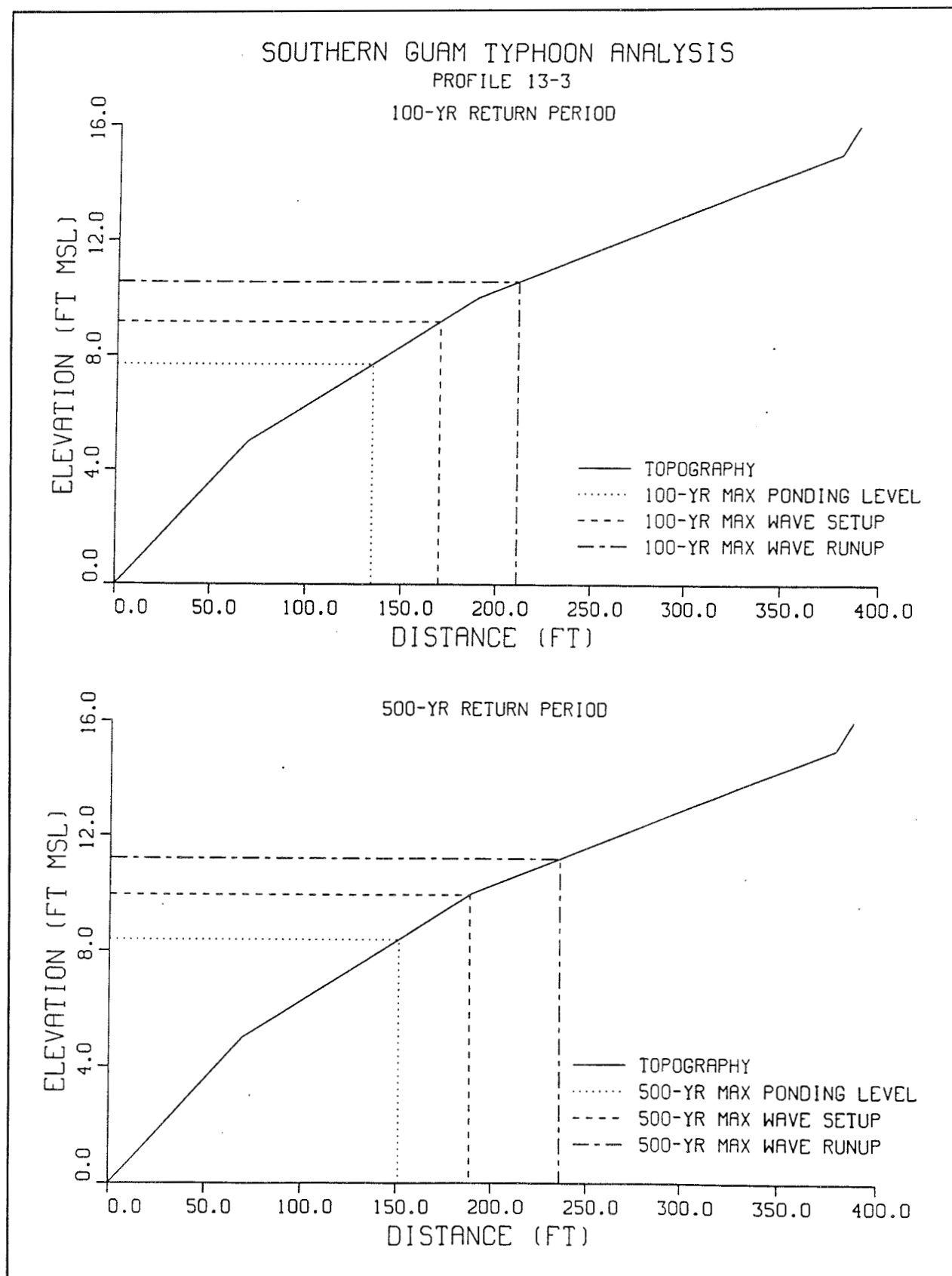
PROFILE 13-2

100-YR RETURN PERIOD



500-YR RETURN PERIOD

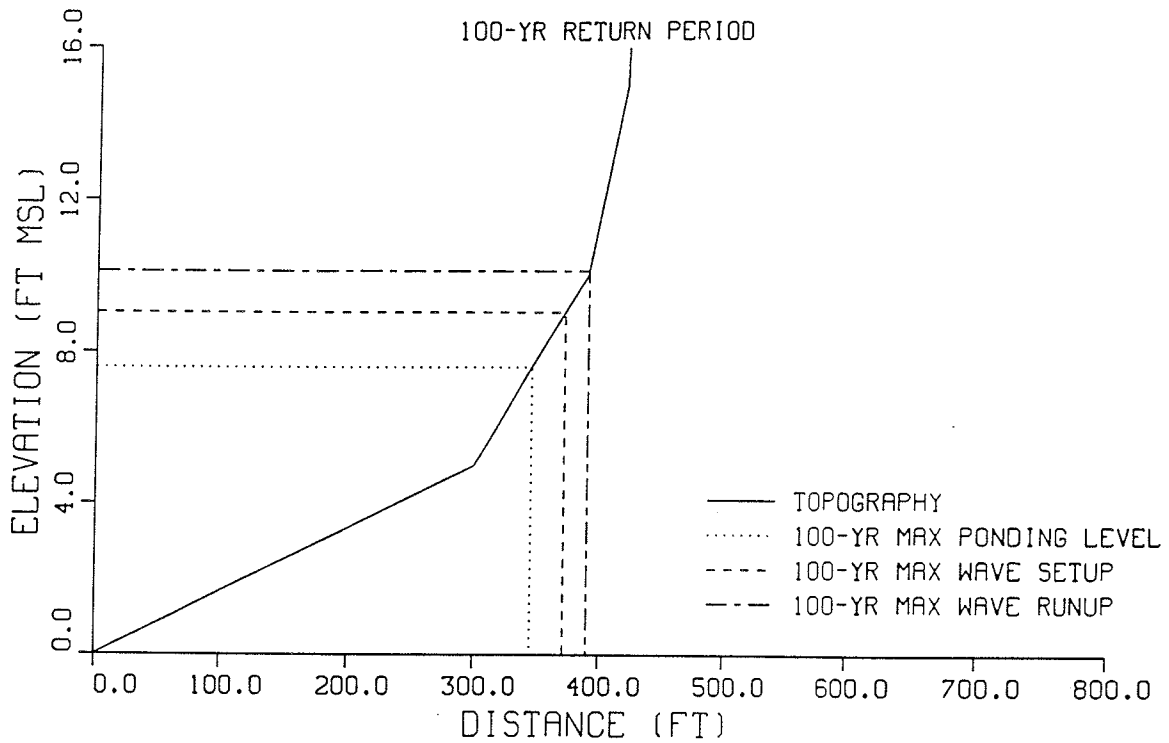




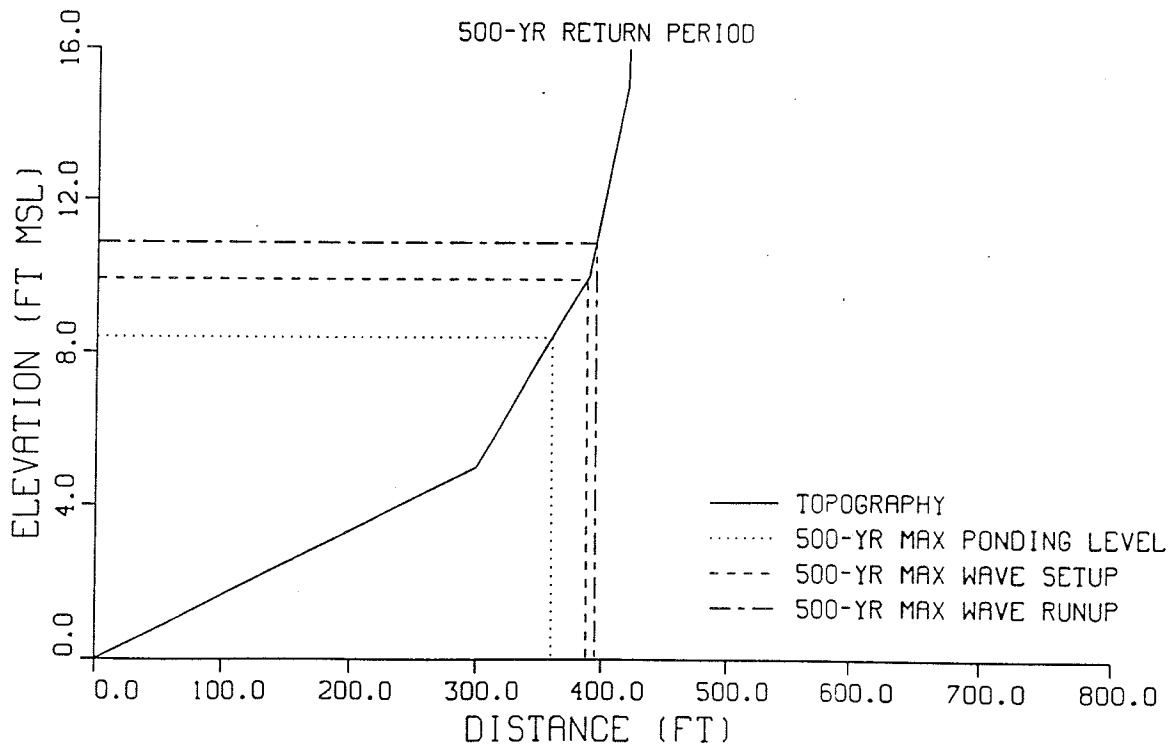
SOUTHERN GUAM TYPHOON ANALYSIS

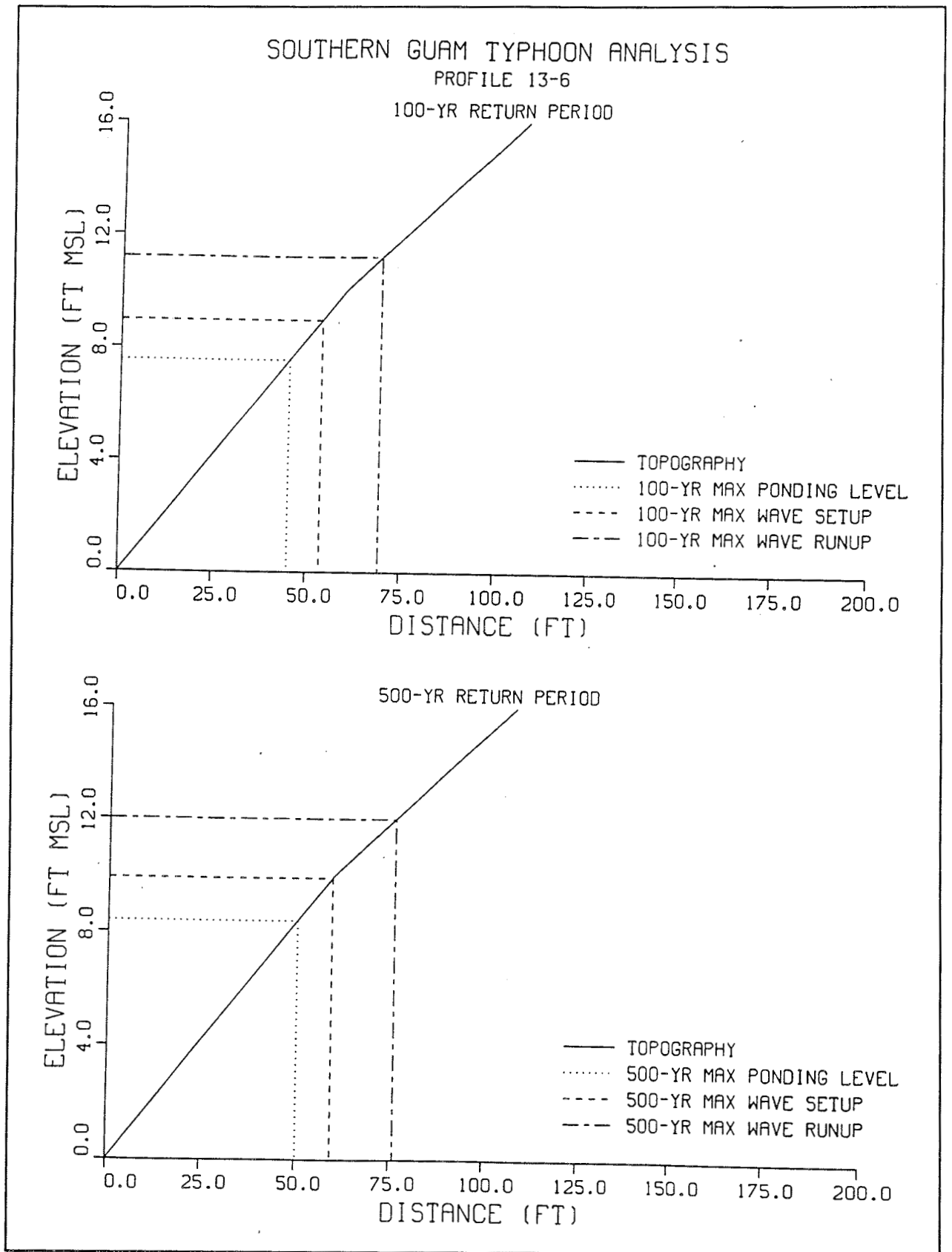
PROFILE 13-5

100-YR RETURN PERIOD



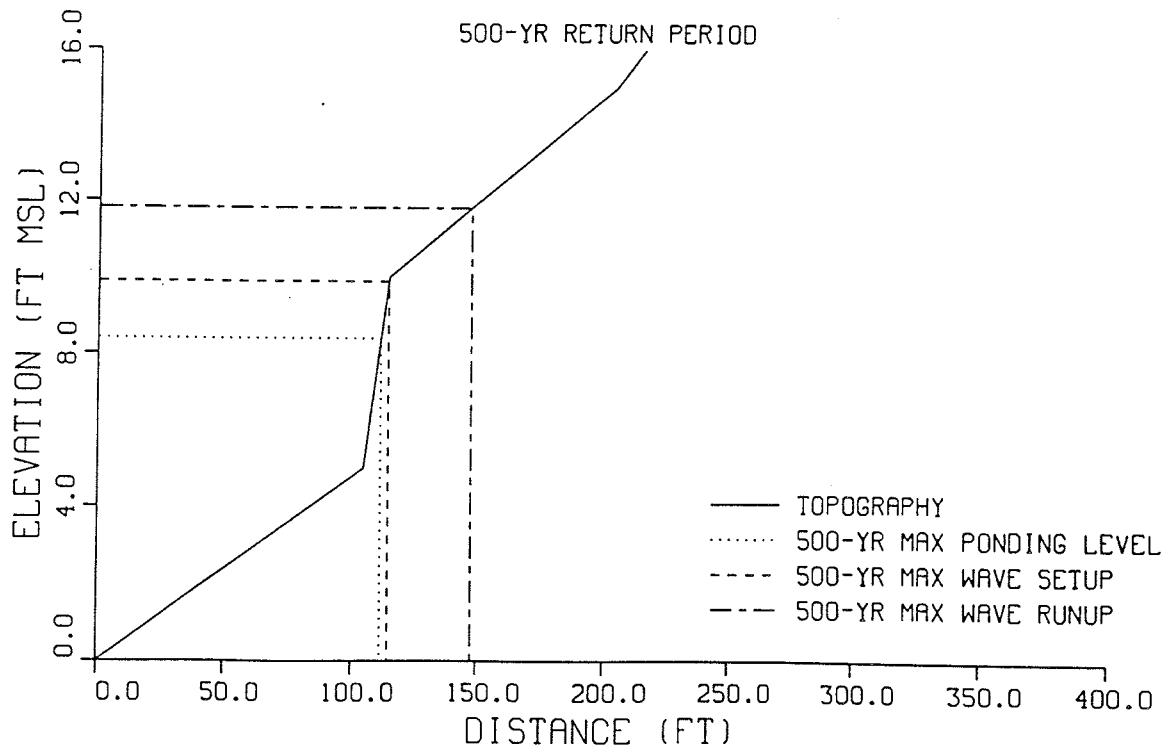
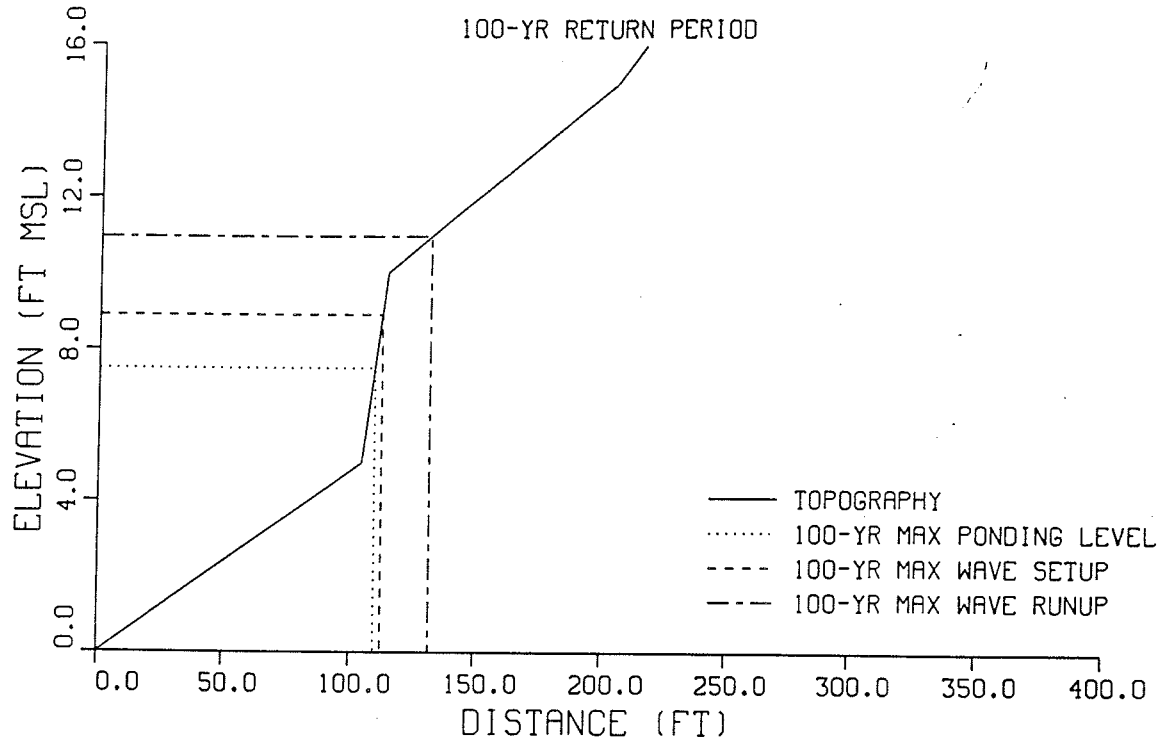
500-YR RETURN PERIOD

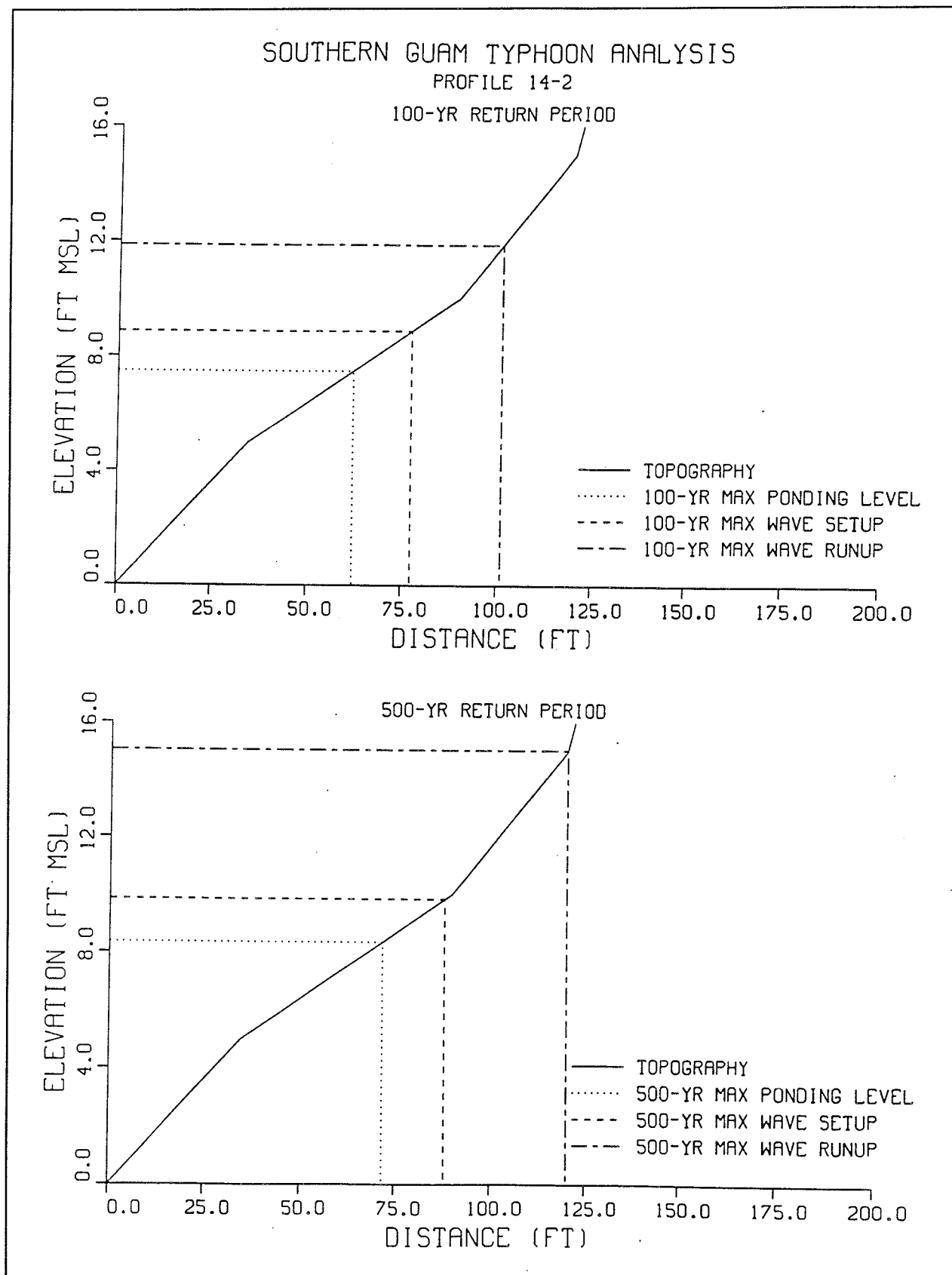




SOUTHERN GUAM TYPHOON ANALYSIS

PROFILE 14-1

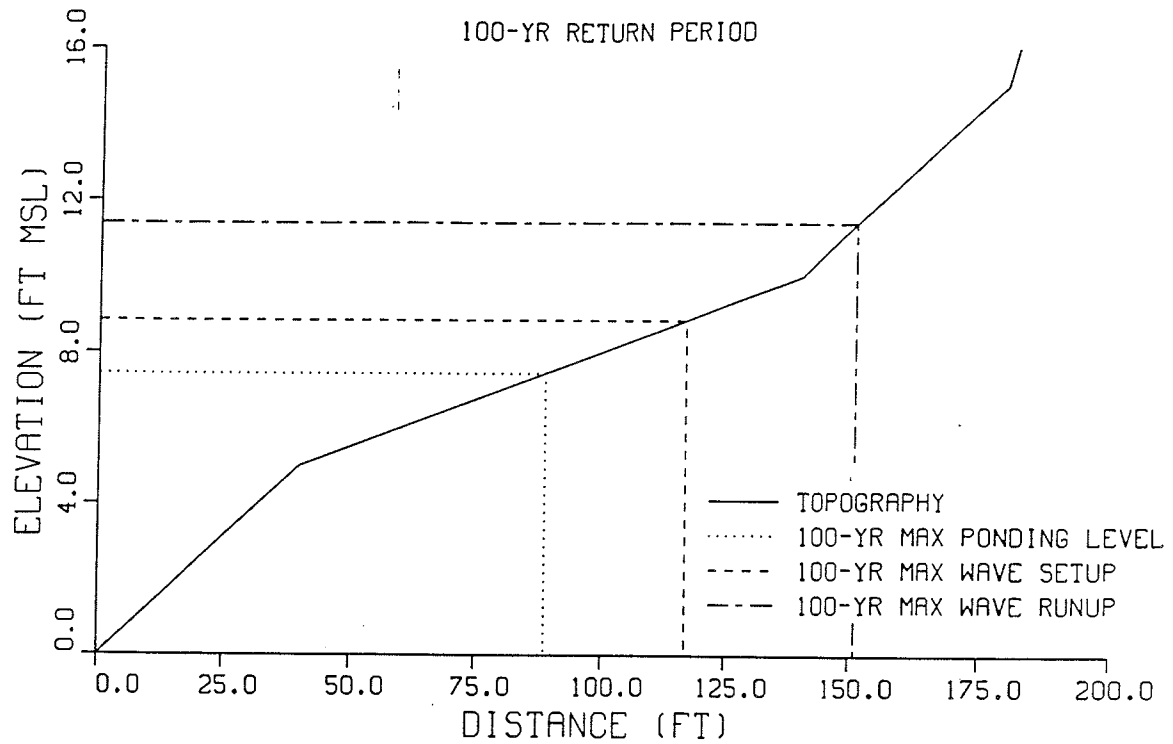




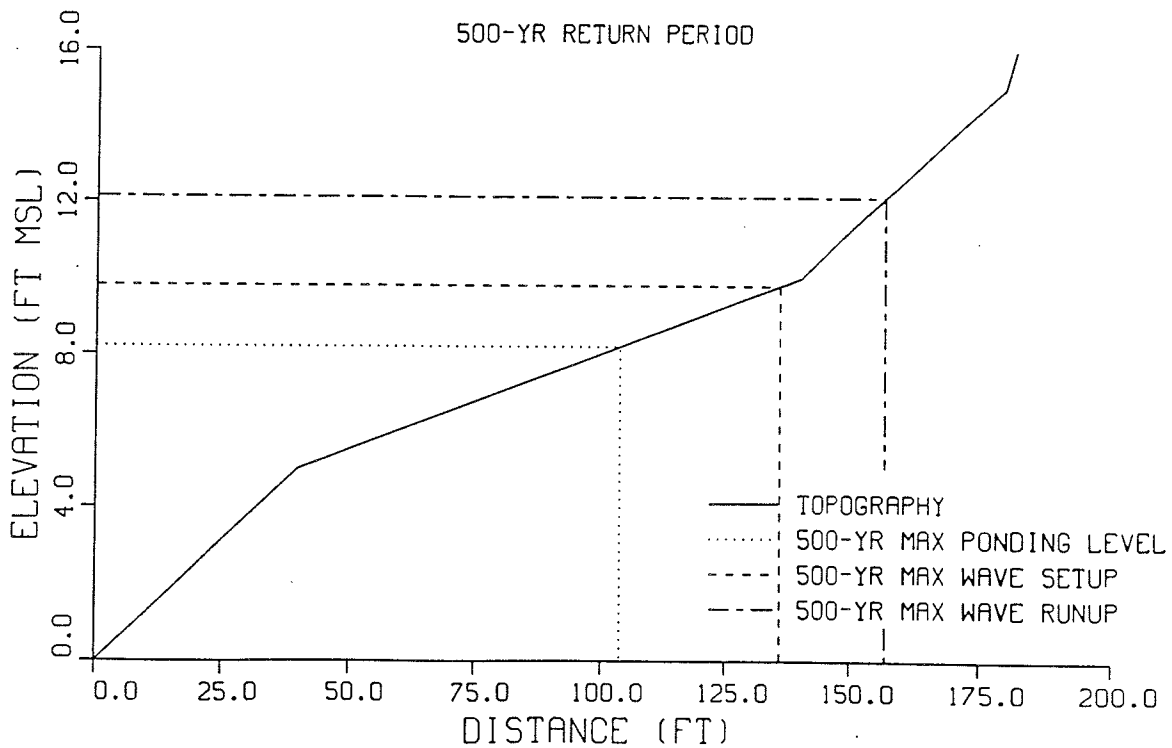
SOUTHERN GUAM TYPHOON ANALYSIS

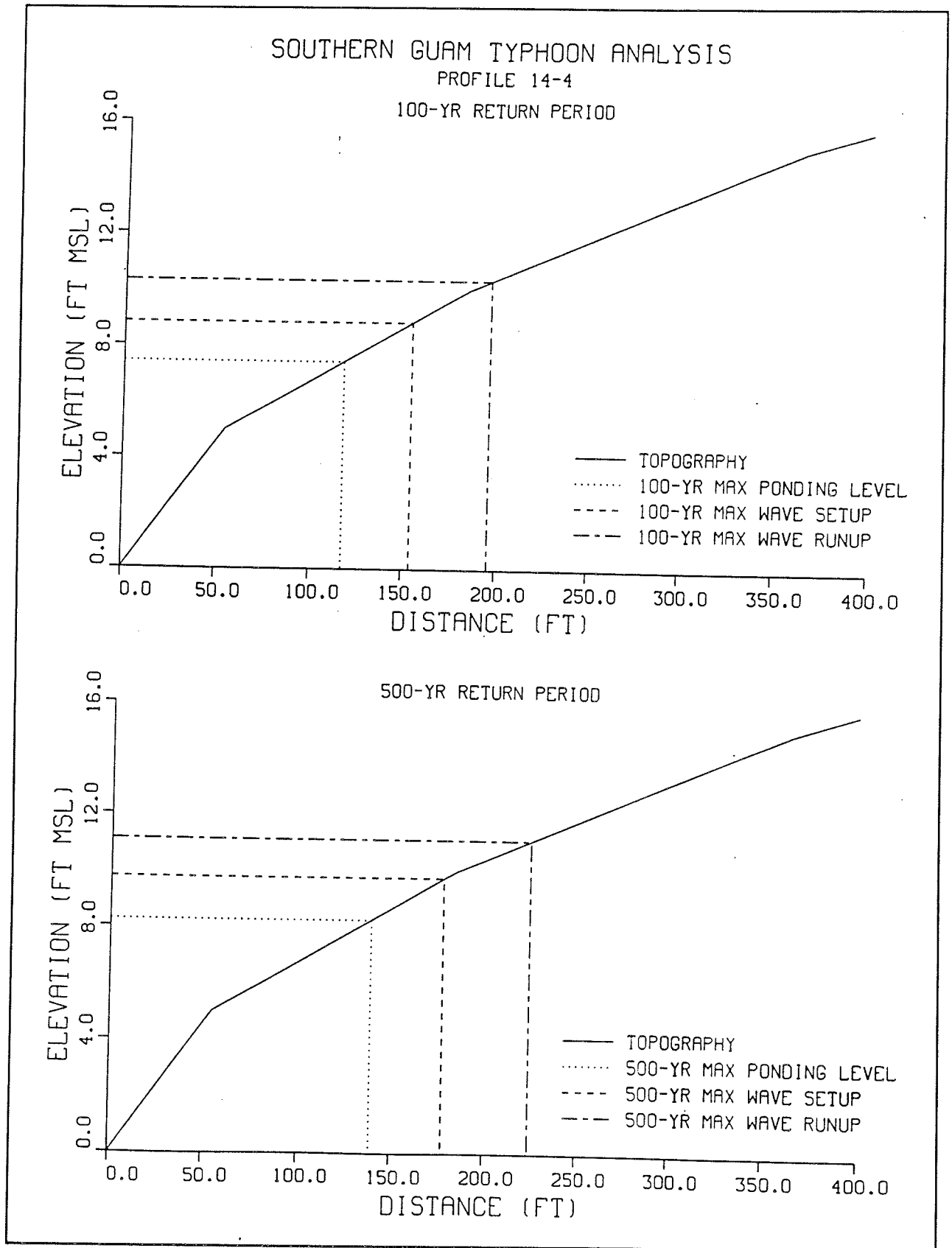
PROFILE 14-3

100-YR RETURN PERIOD



500-YR RETURN PERIOD

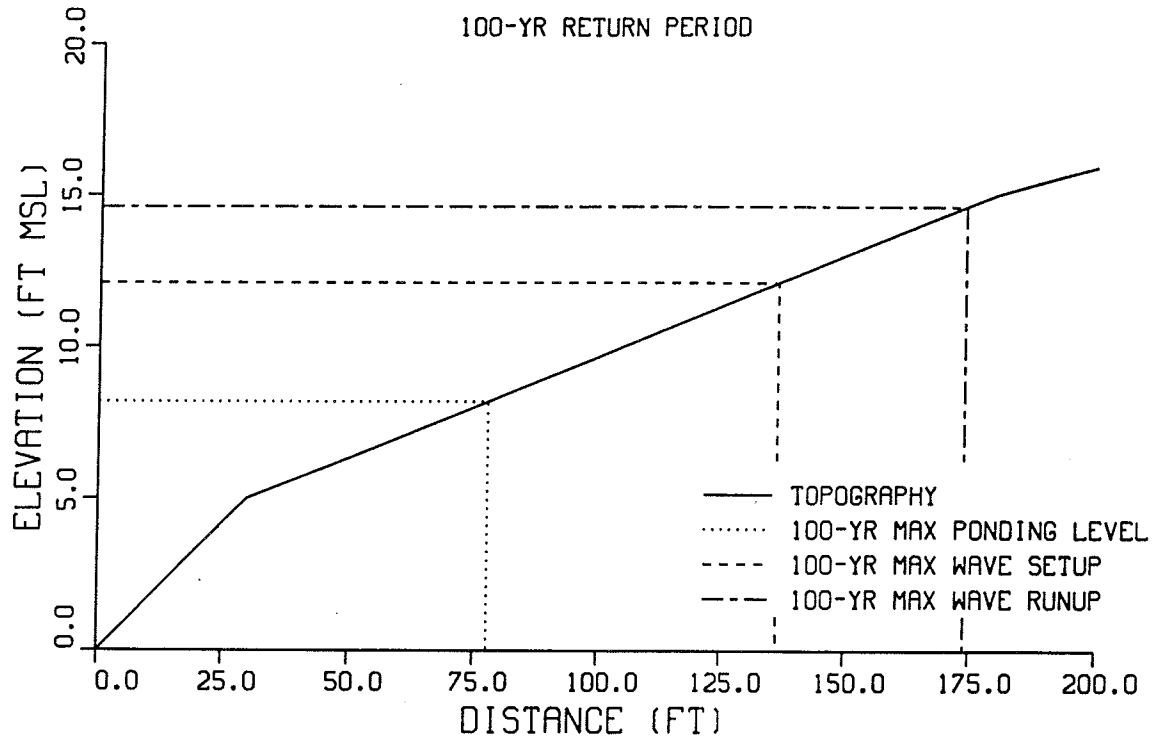




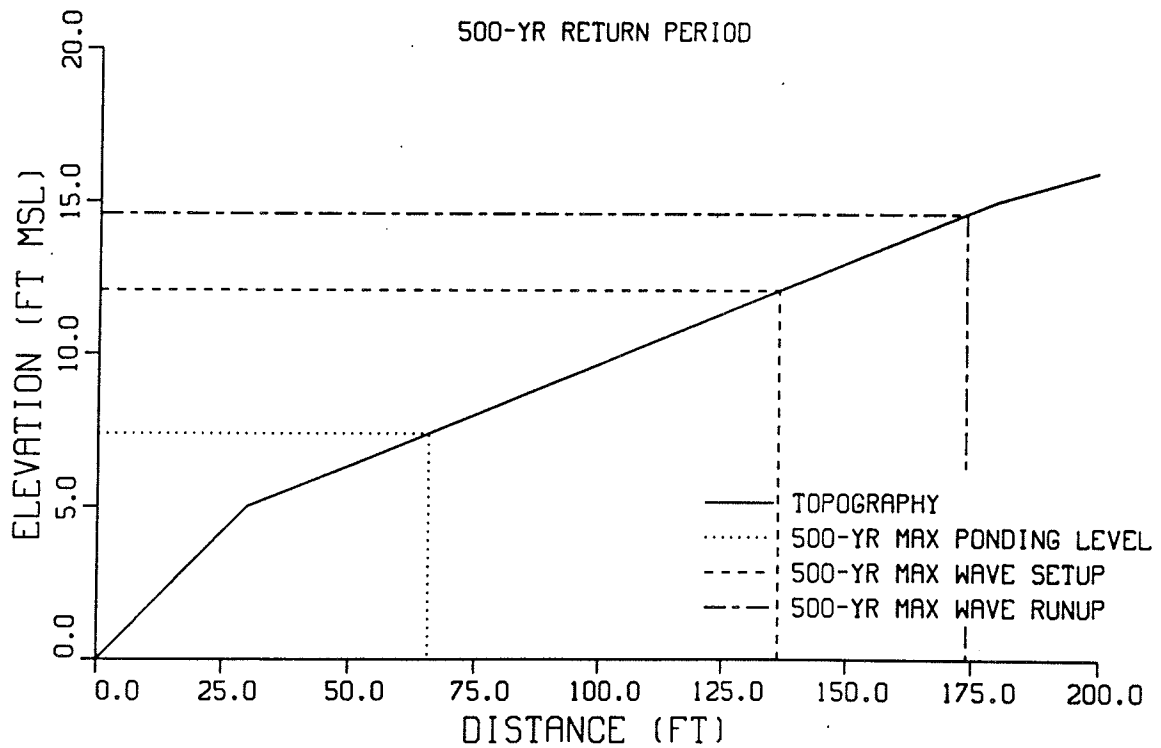
SOUTHERN GUAM TYPHOON ANALYSIS

PROFILE 15-1

100-YR RETURN PERIOD



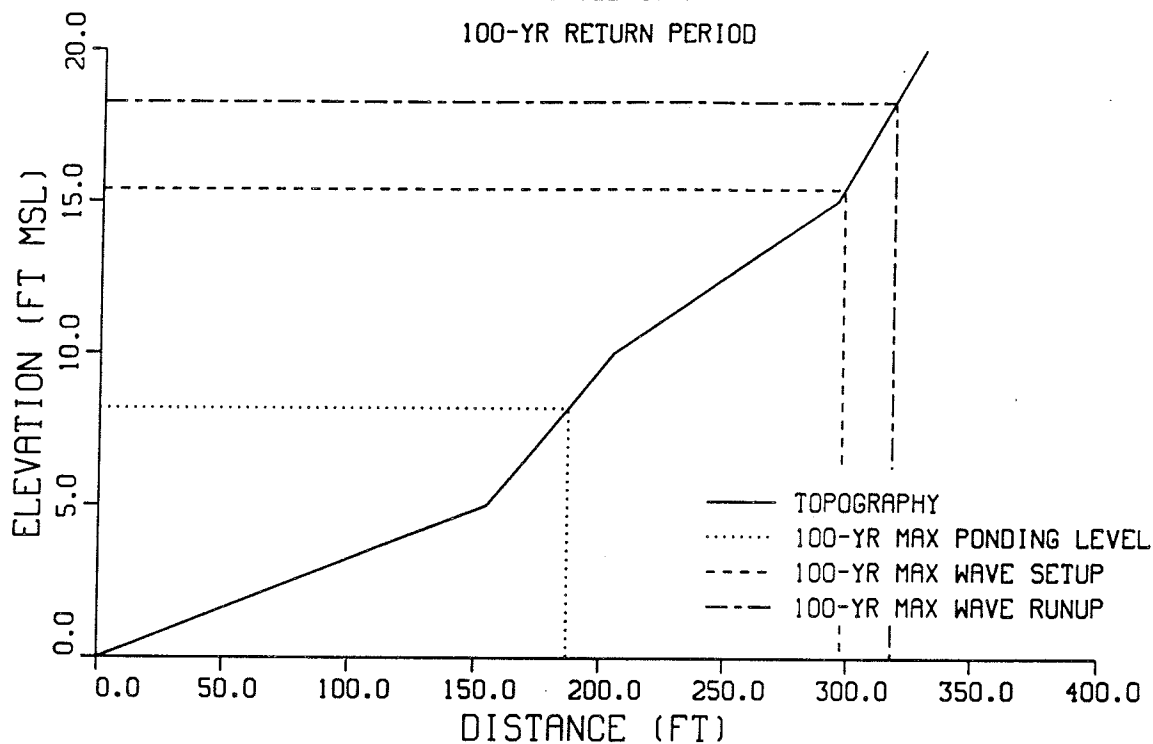
500-YR RETURN PERIOD



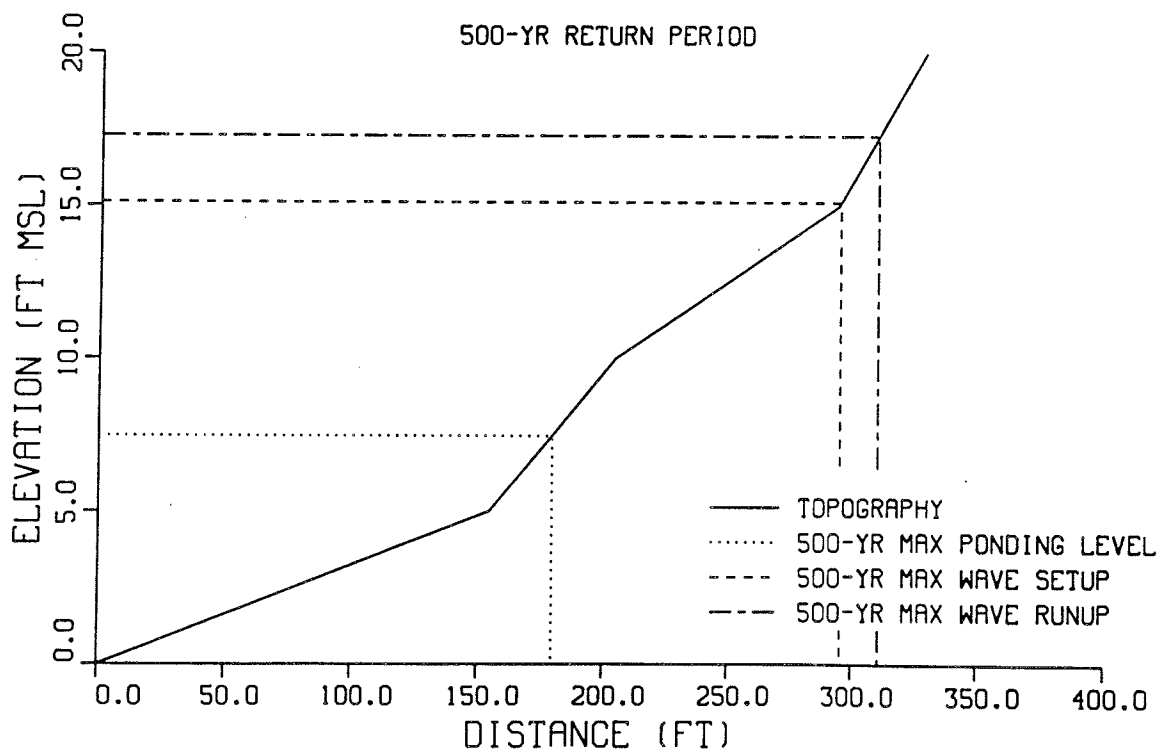
SOUTHERN GUAM TYPHOON ANALYSIS

PROFILE 15-2

100-YR RETURN PERIOD



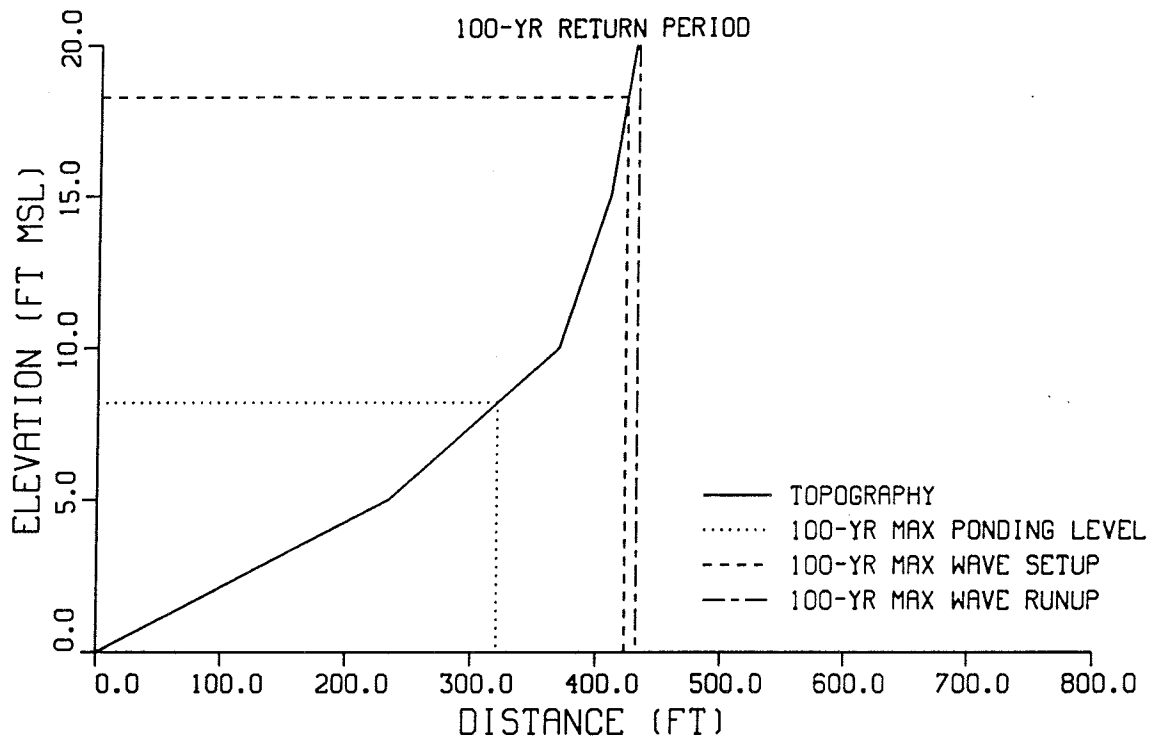
500-YR RETURN PERIOD



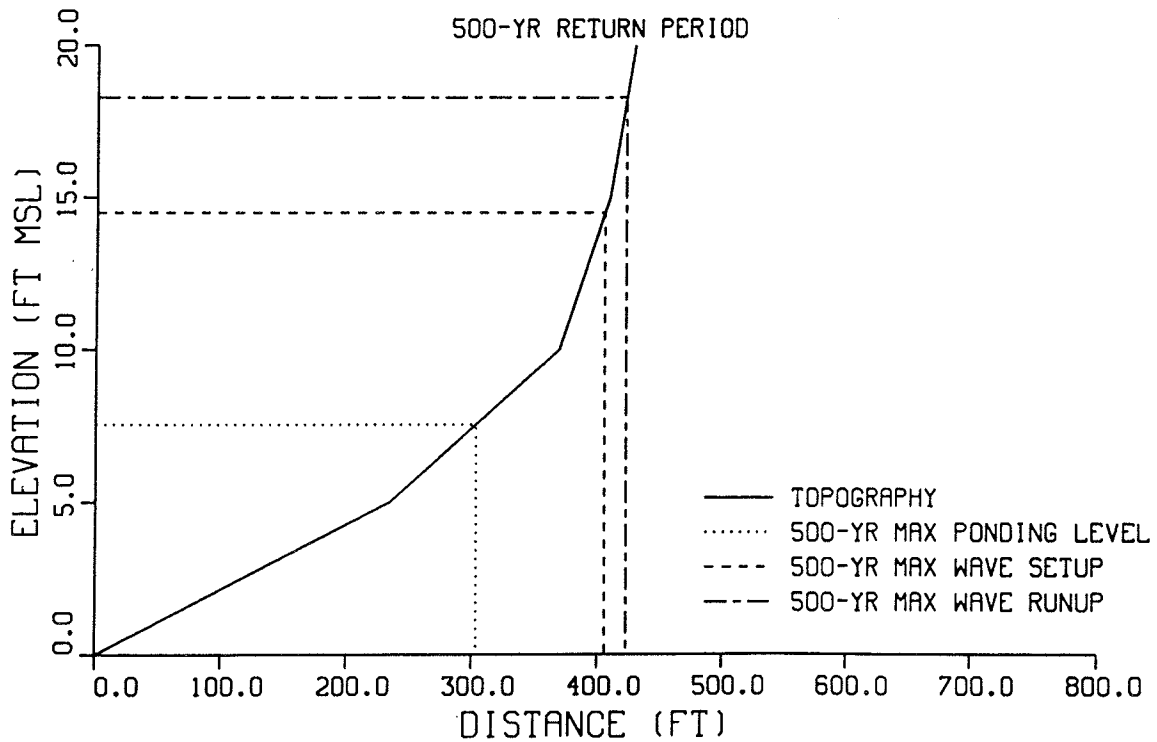
SOUTHERN GUAM TYPHOON ANALYSIS

PROFILE 15-3

100-YR RETURN PERIOD



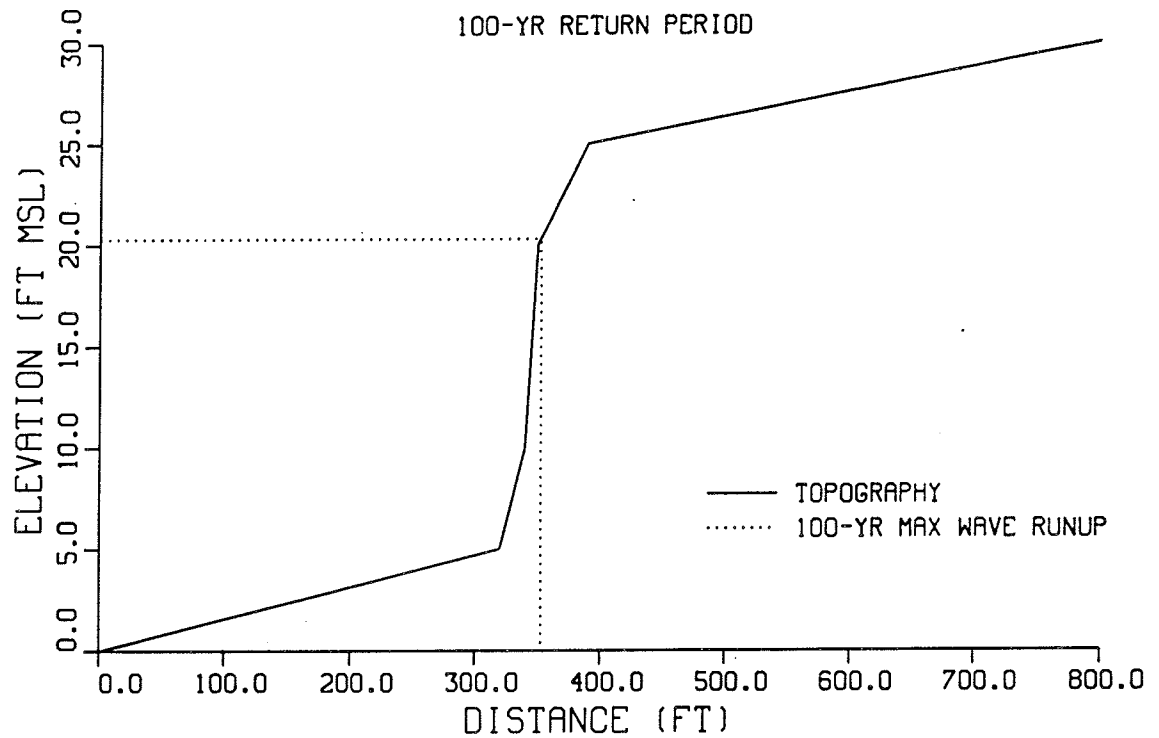
500-YR RETURN PERIOD



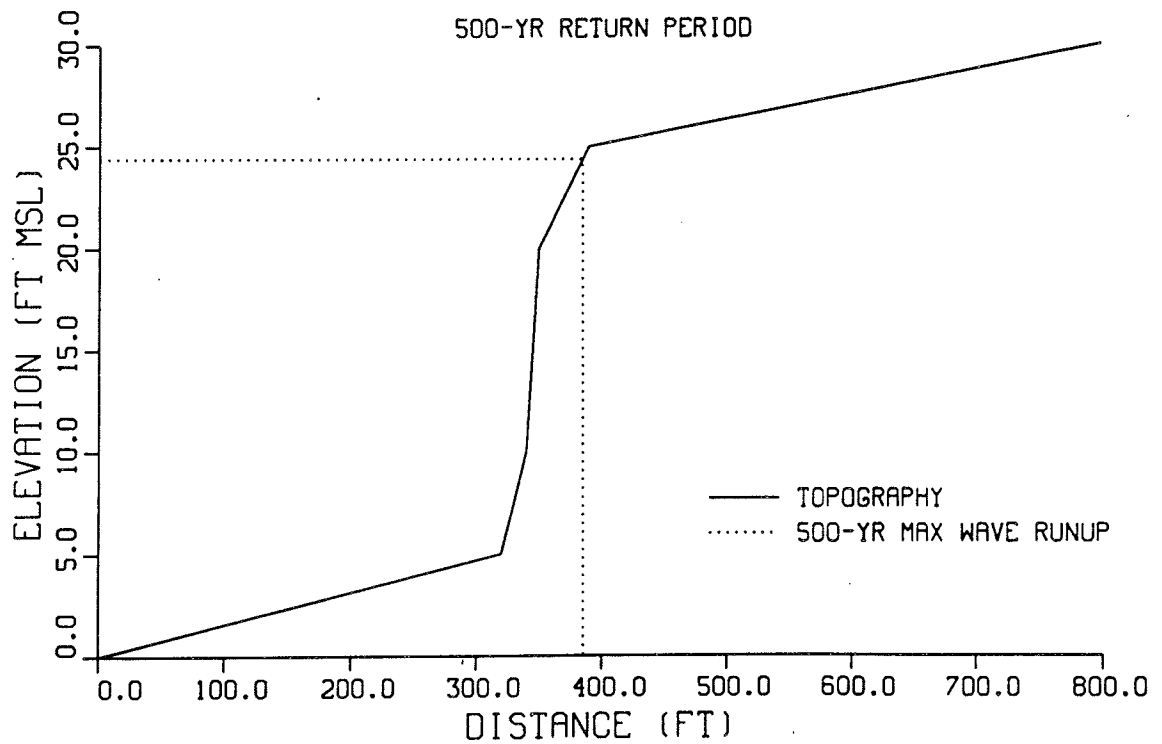
SOUTHERN GUAM TYPHOON ANALYSIS

PROFILE 15-5

100-YR RETURN PERIOD



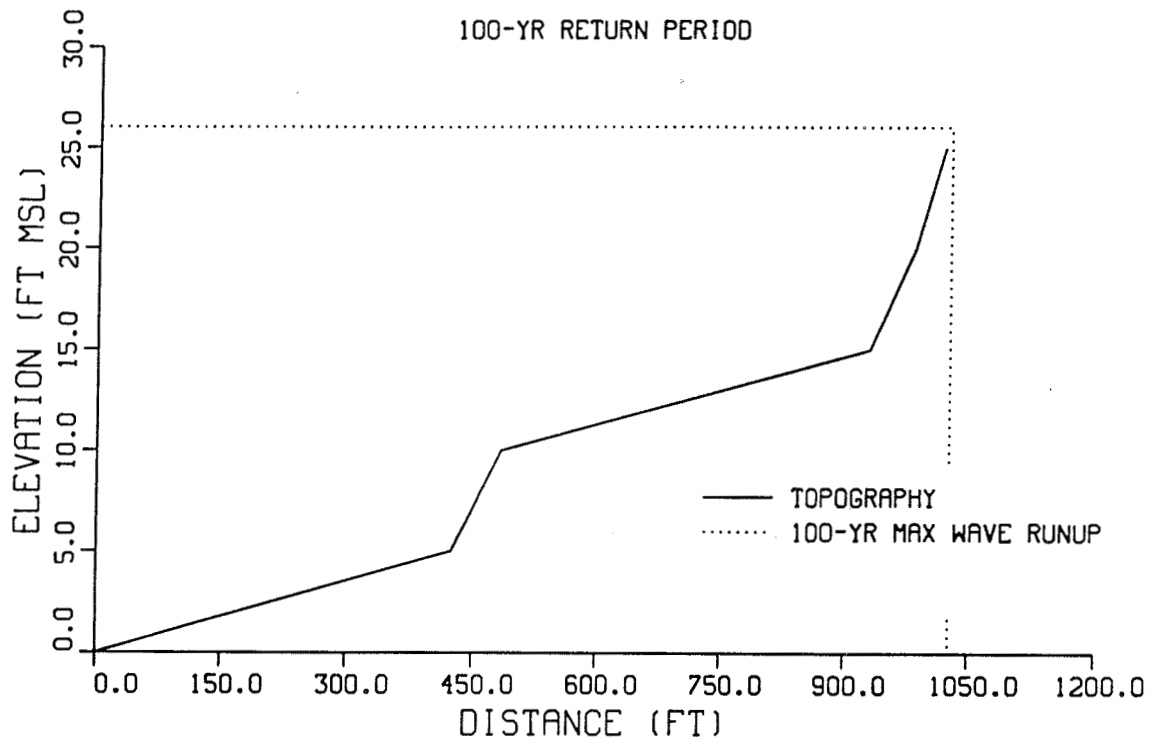
500-YR RETURN PERIOD



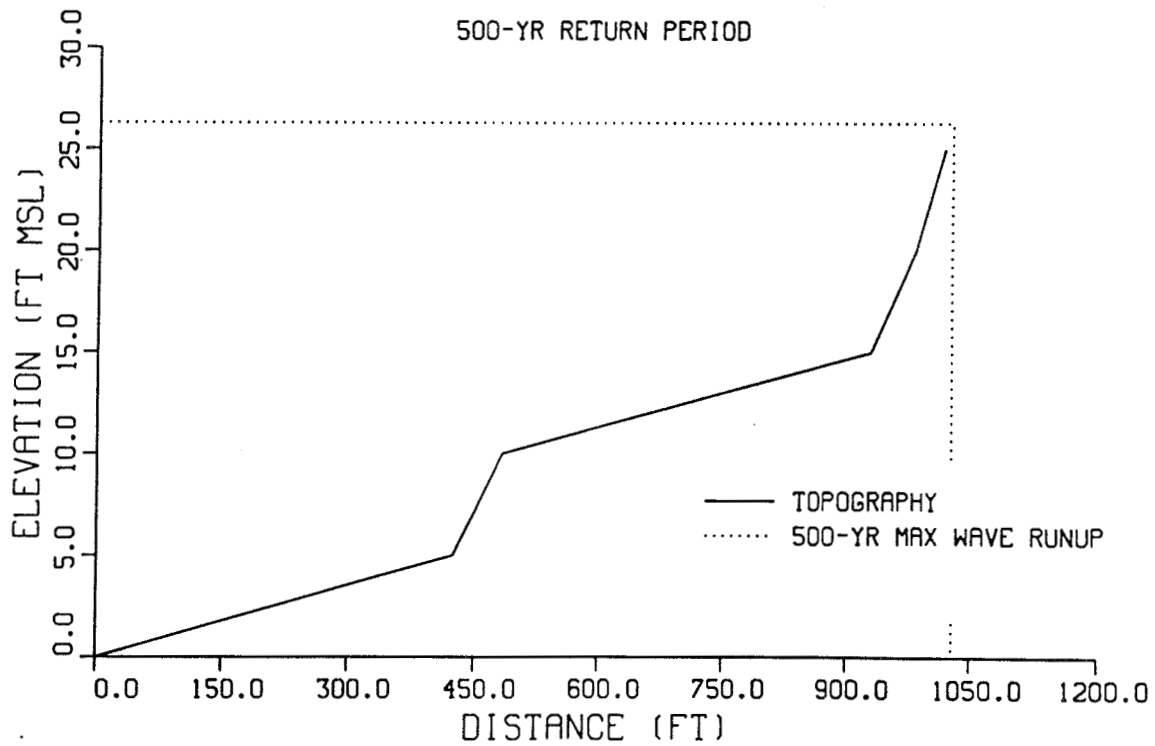
SOUTHERN GUAM TYPHOON ANALYSIS

PROFILE 16-1

100-YR RETURN PERIOD



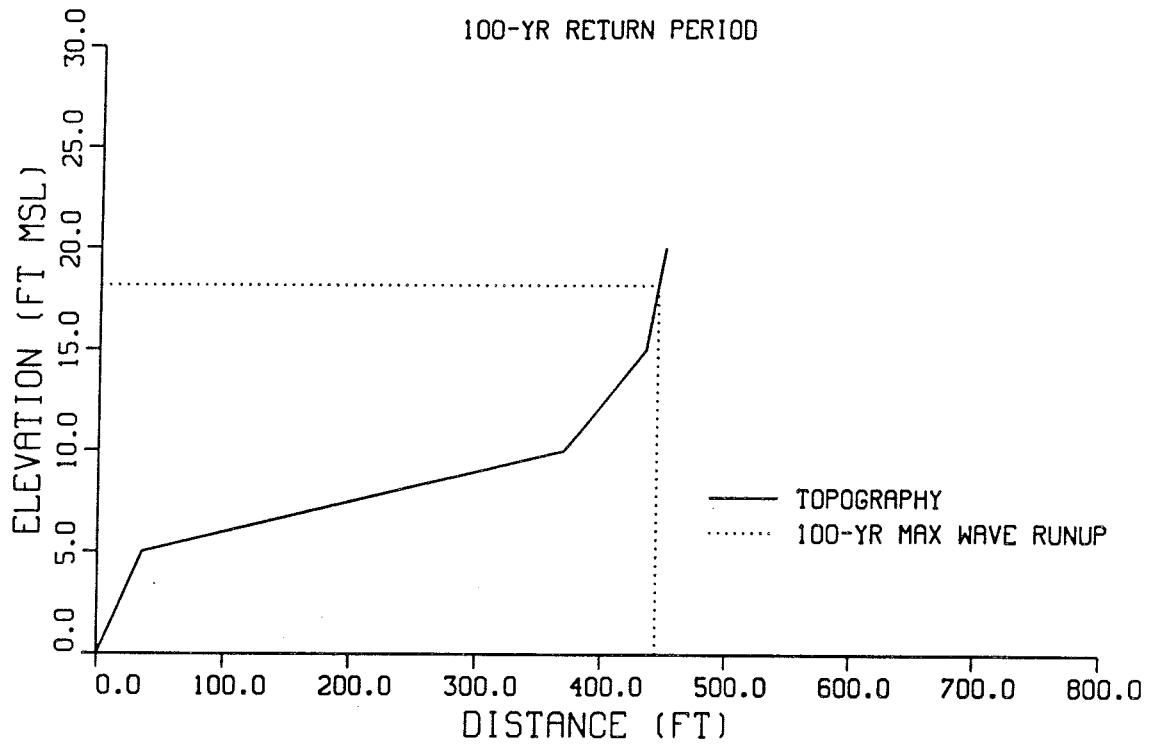
500-YR RETURN PERIOD



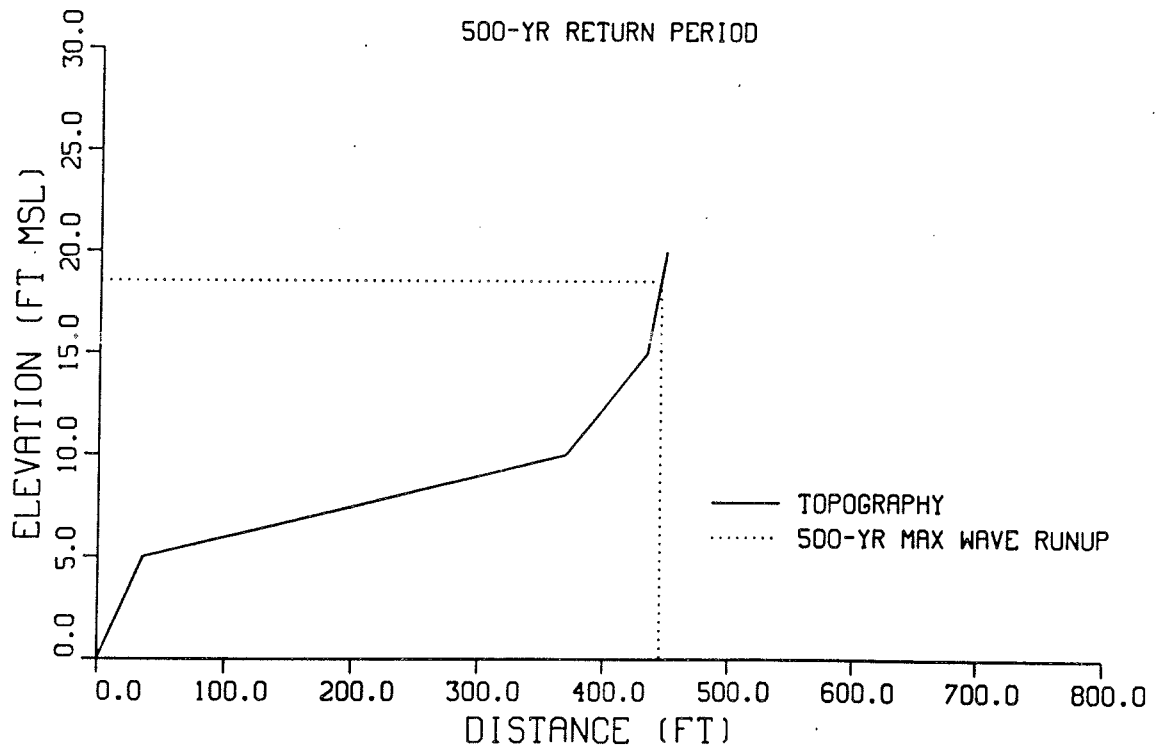
SOUTHERN GUAM TYPHOON ANALYSIS

PROFILE 16-2

100-YR RETURN PERIOD



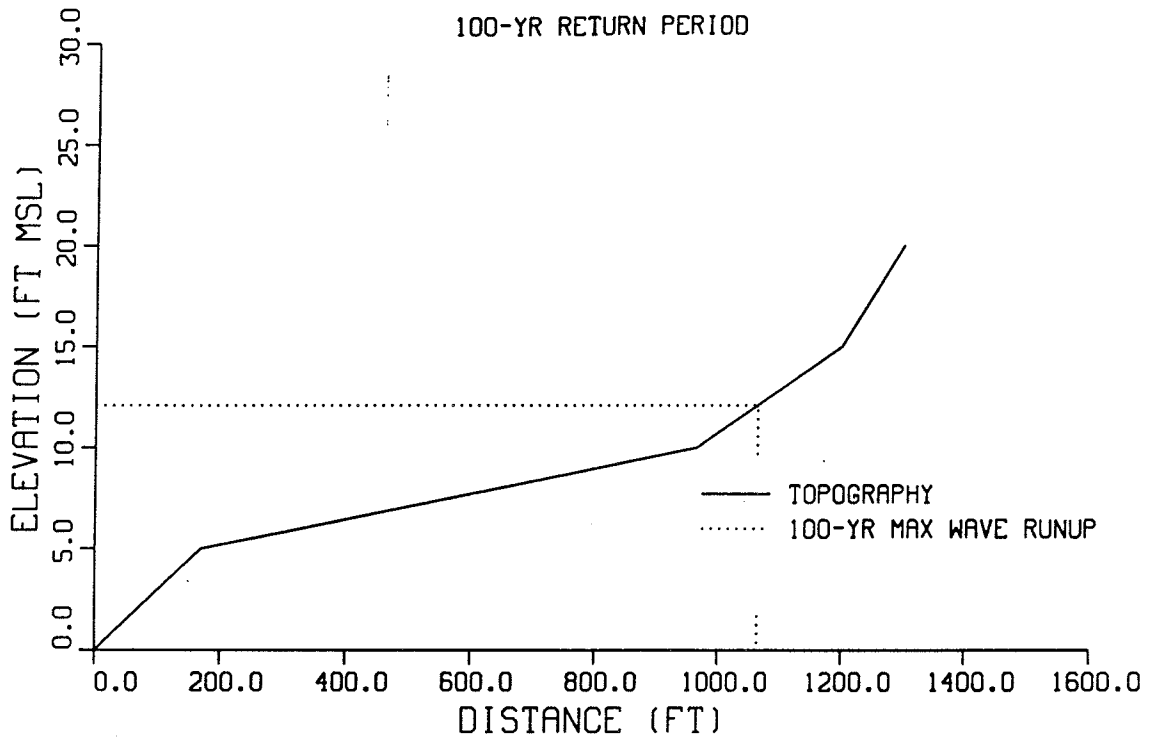
500-YR RETURN PERIOD



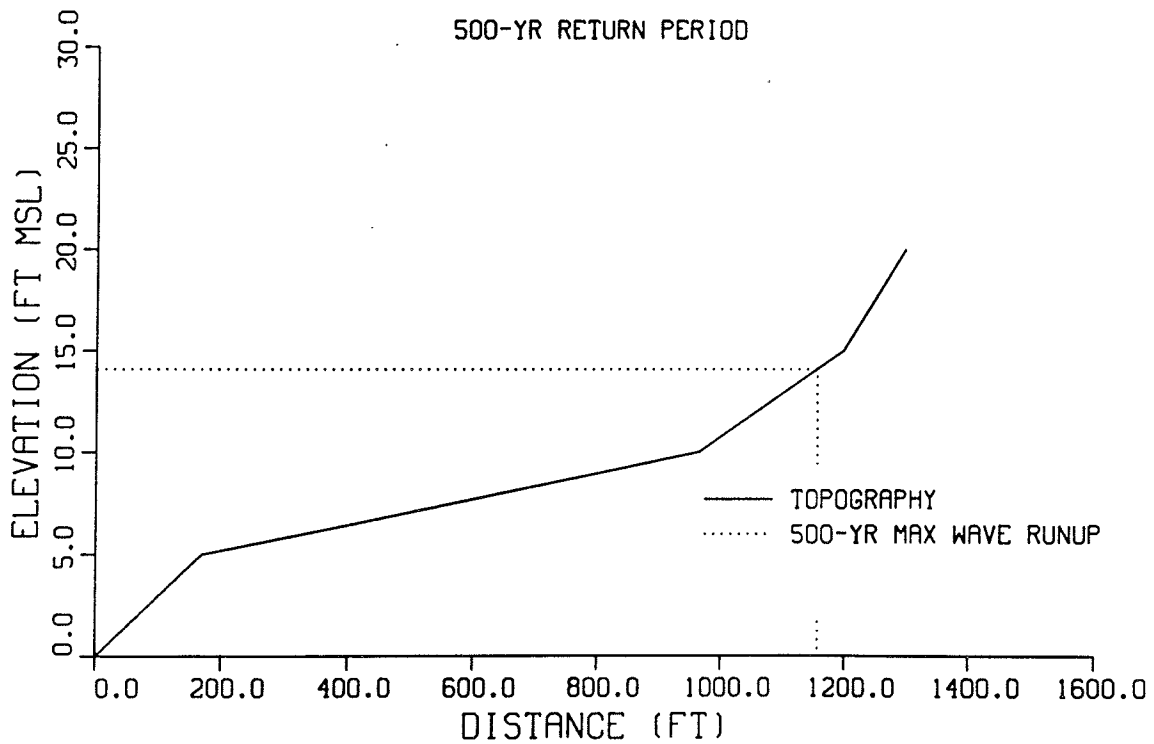
SOUTHERN GUAM TYPHOON ANALYSIS

PROFILE 16-3

100-YR RETURN PERIOD



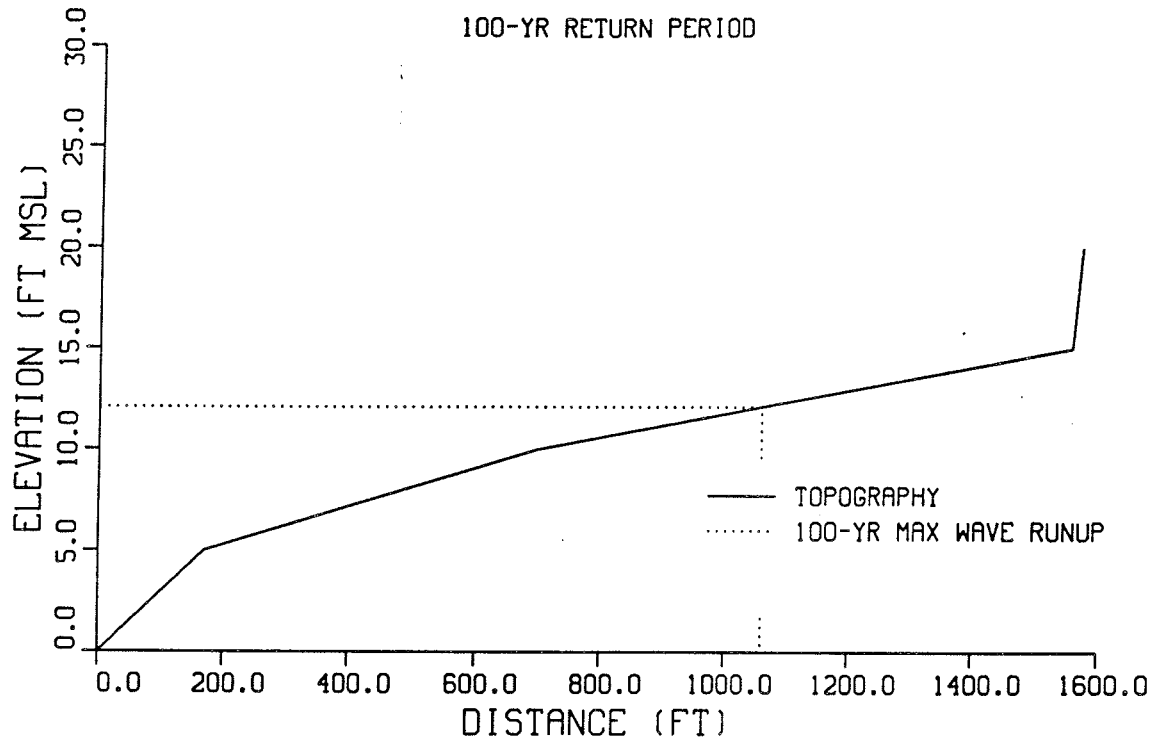
500-YR RETURN PERIOD



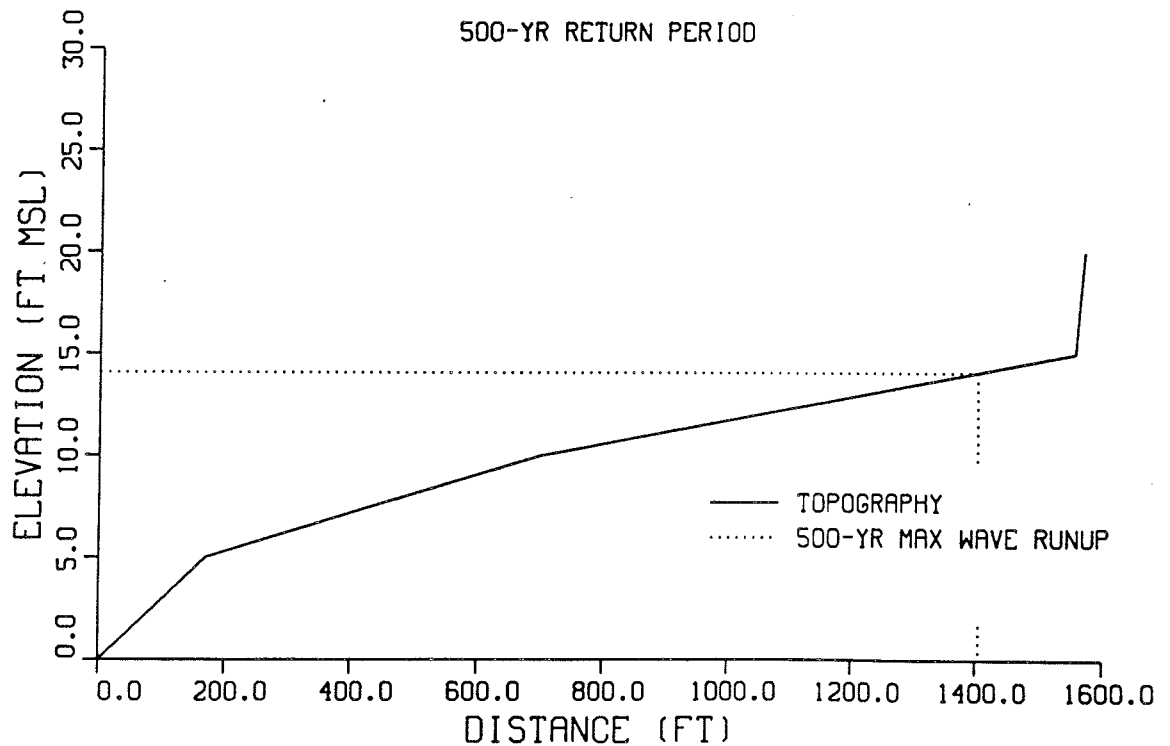
SOUTHERN GUAM TYPHOON ANALYSIS

PROFILE 16-4

100-YR RETURN PERIOD



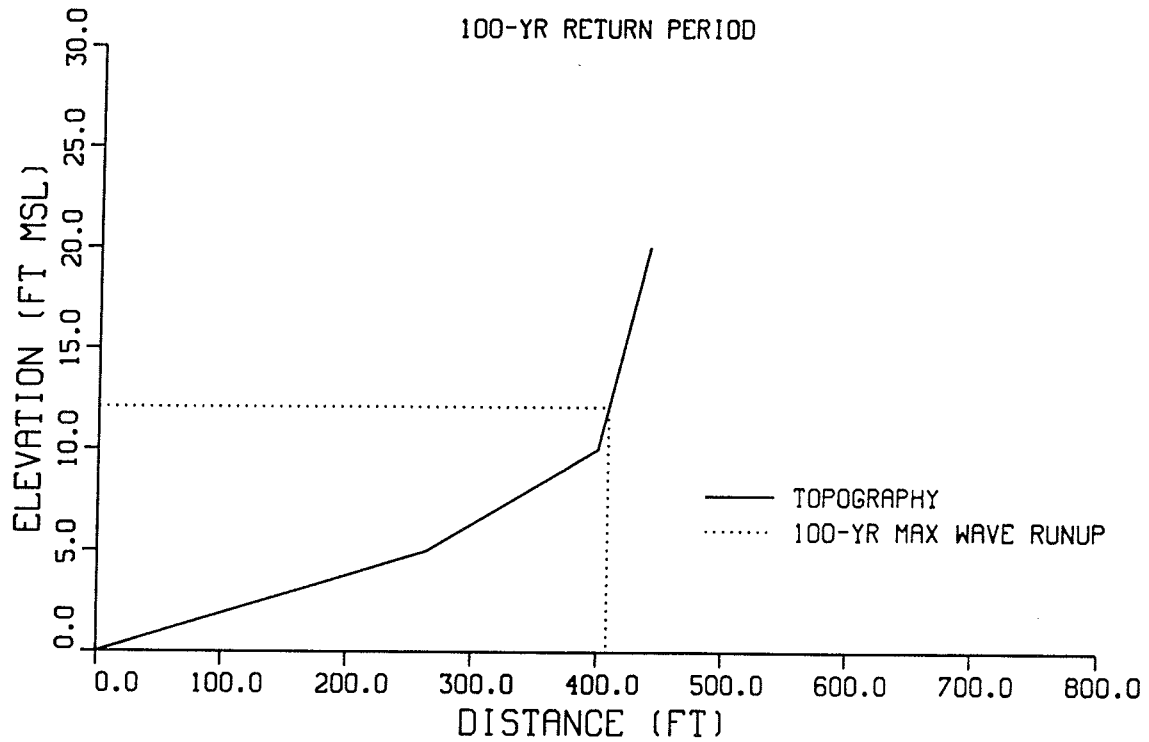
500-YR RETURN PERIOD



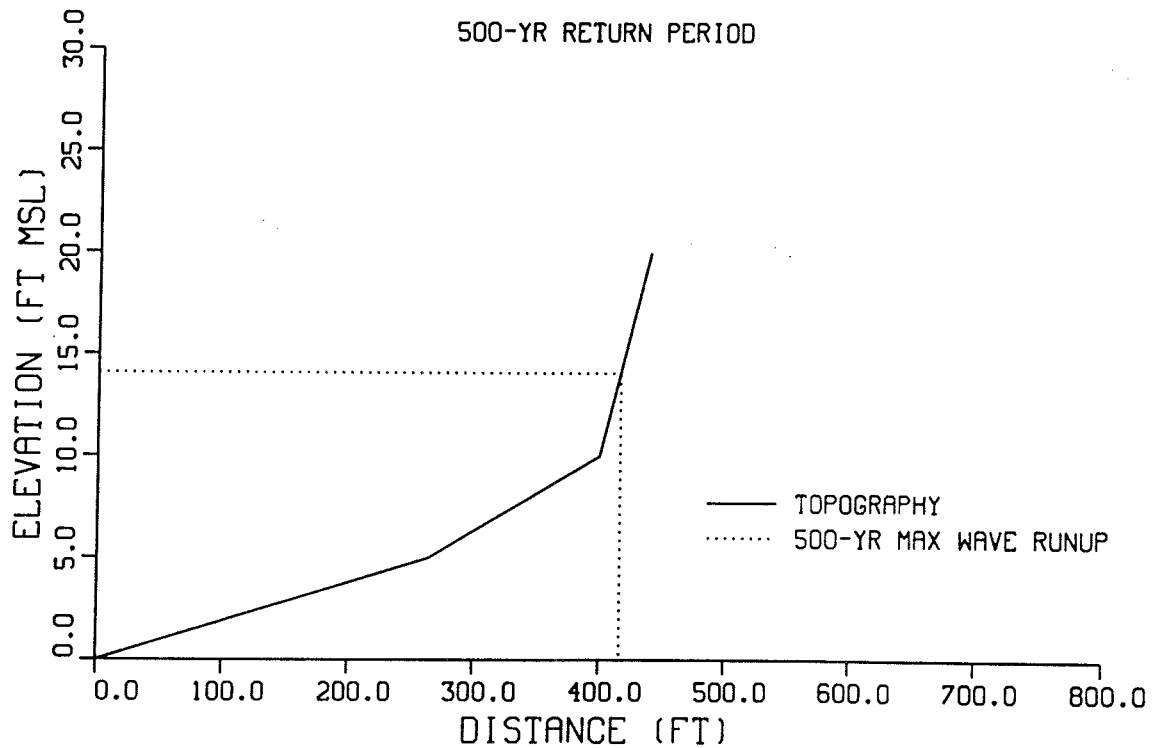
SOUTHERN GUAM TYPHOON ANALYSIS

PROFILE 16-5

100-YR RETURN PERIOD



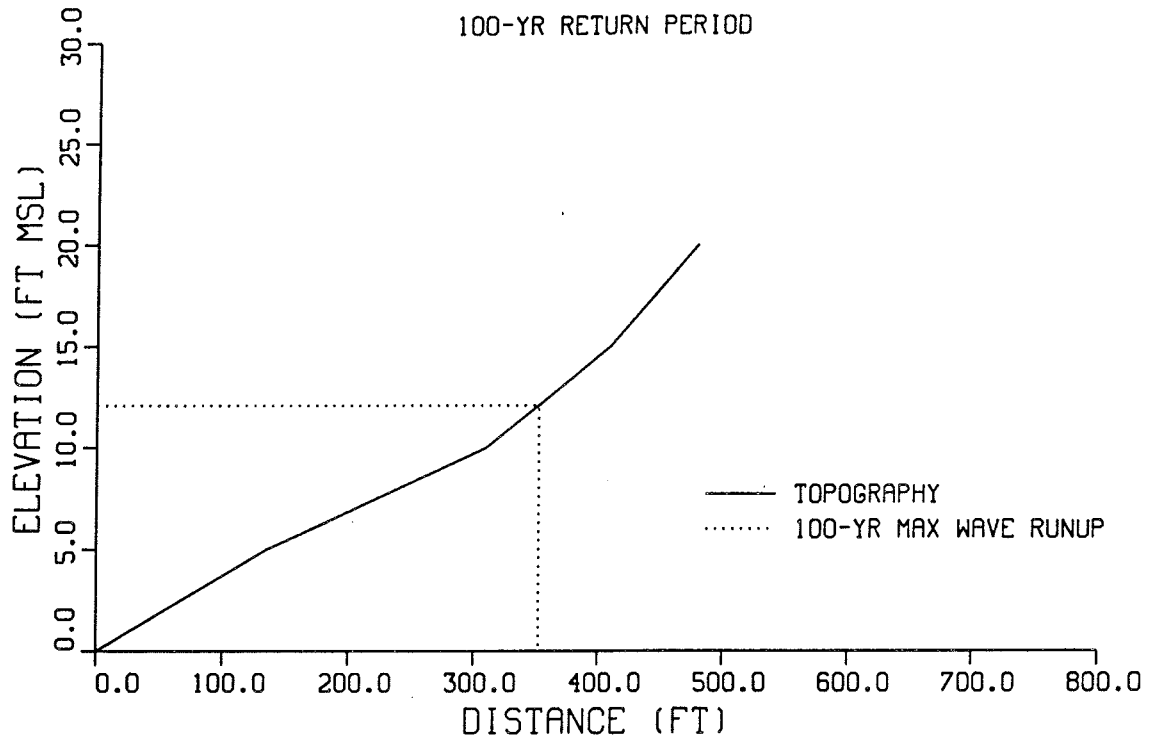
500-YR RETURN PERIOD



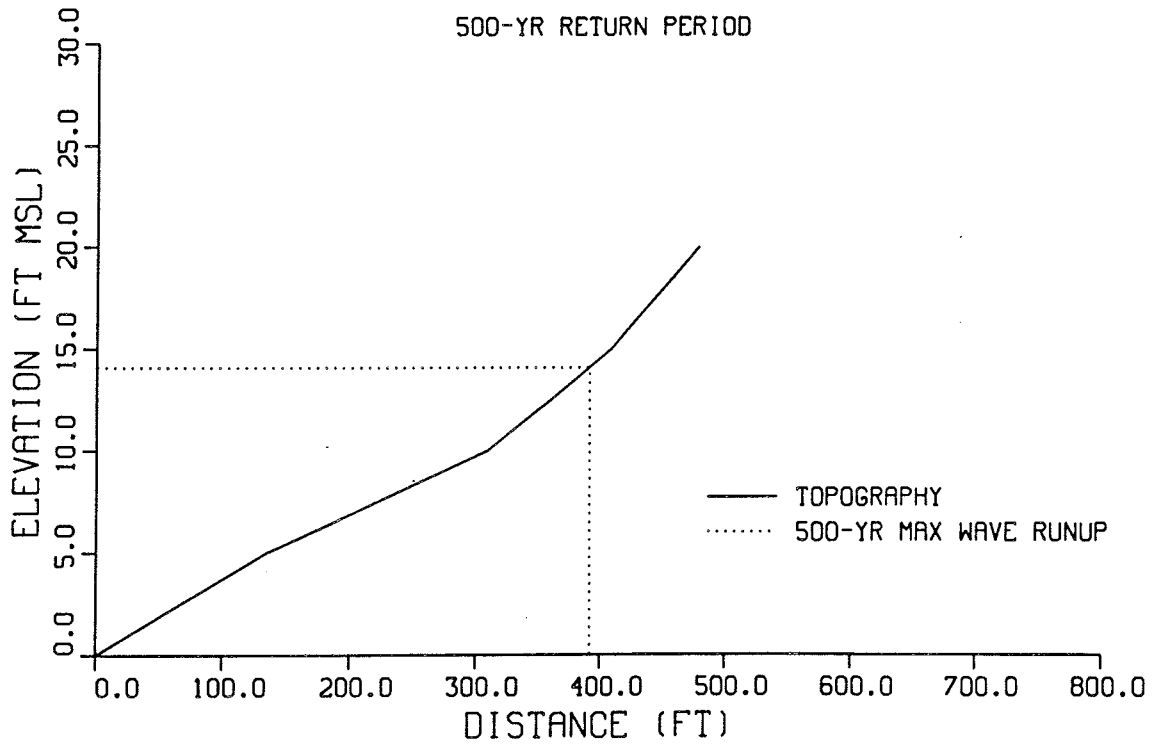
SOUTHERN GUAM TYPHOON ANALYSIS

PROFILE 16-6

100-YR RETURN PERIOD



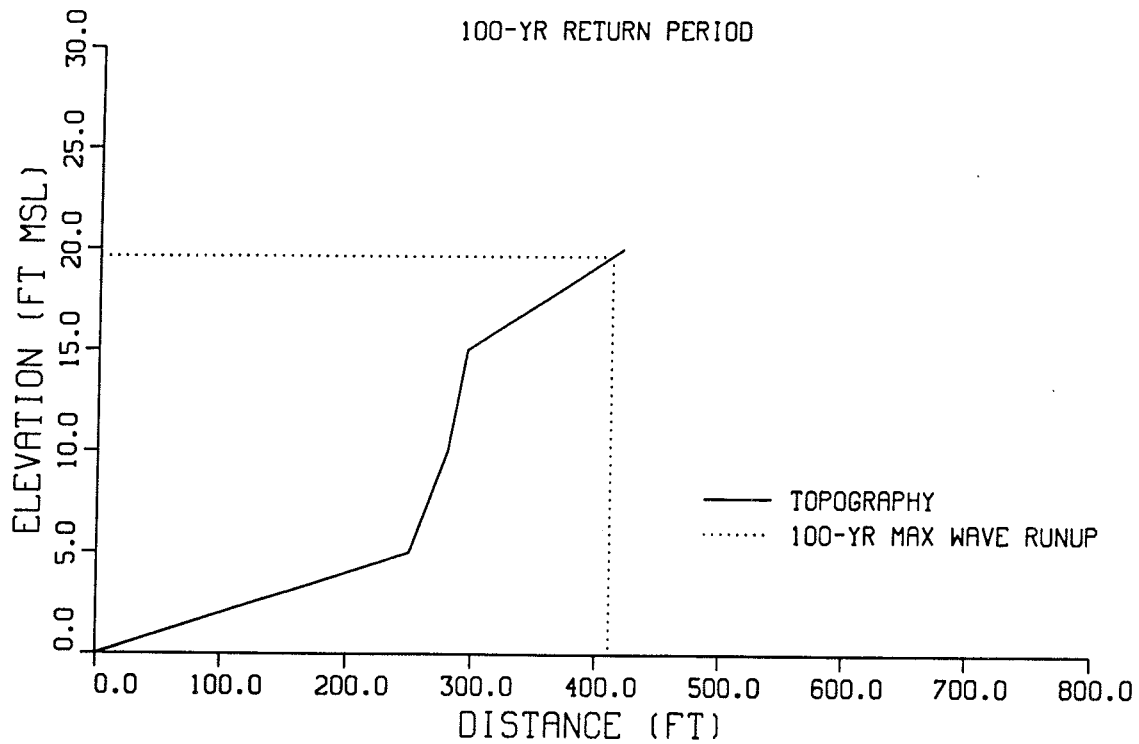
500-YR RETURN PERIOD



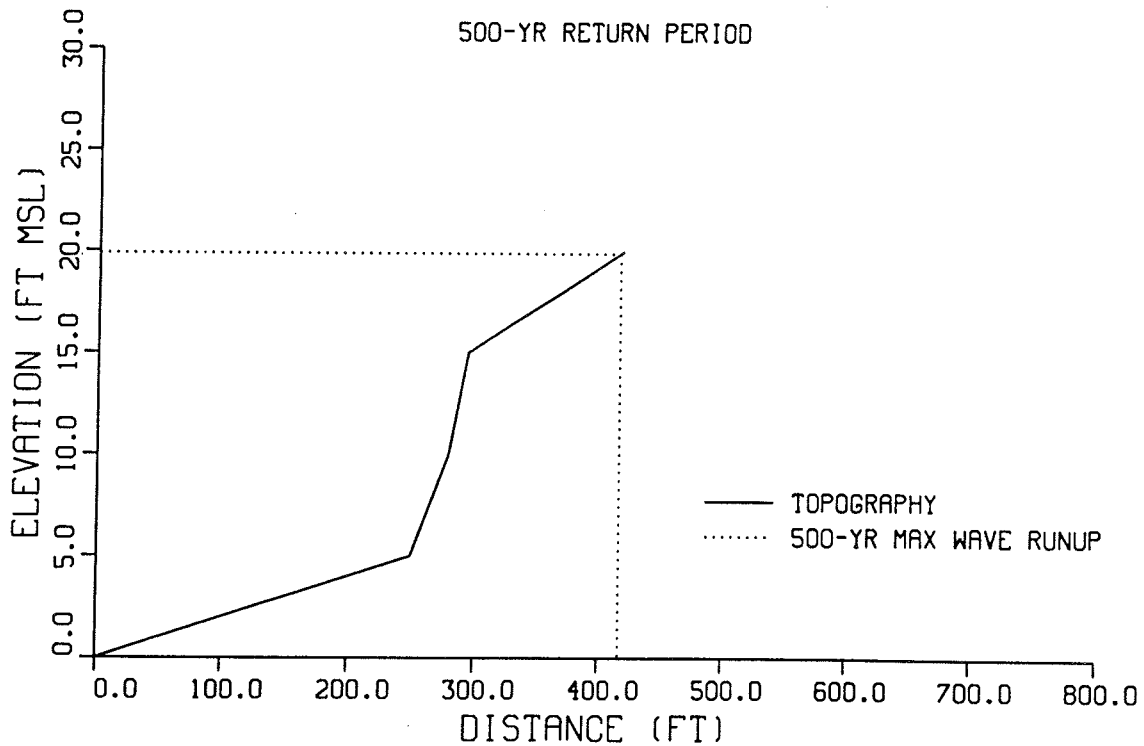
SOUTHERN GUAM TYPHOON ANALYSIS

PROFILE 16-7

100-YR RETURN PERIOD



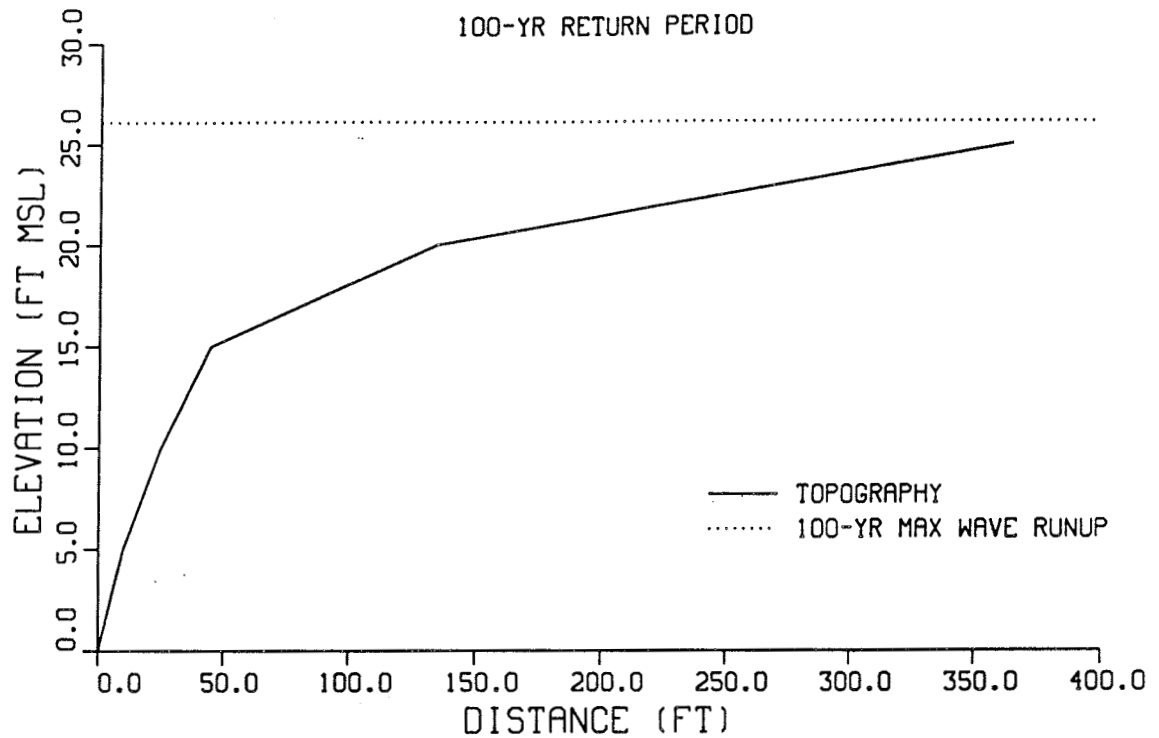
500-YR RETURN PERIOD



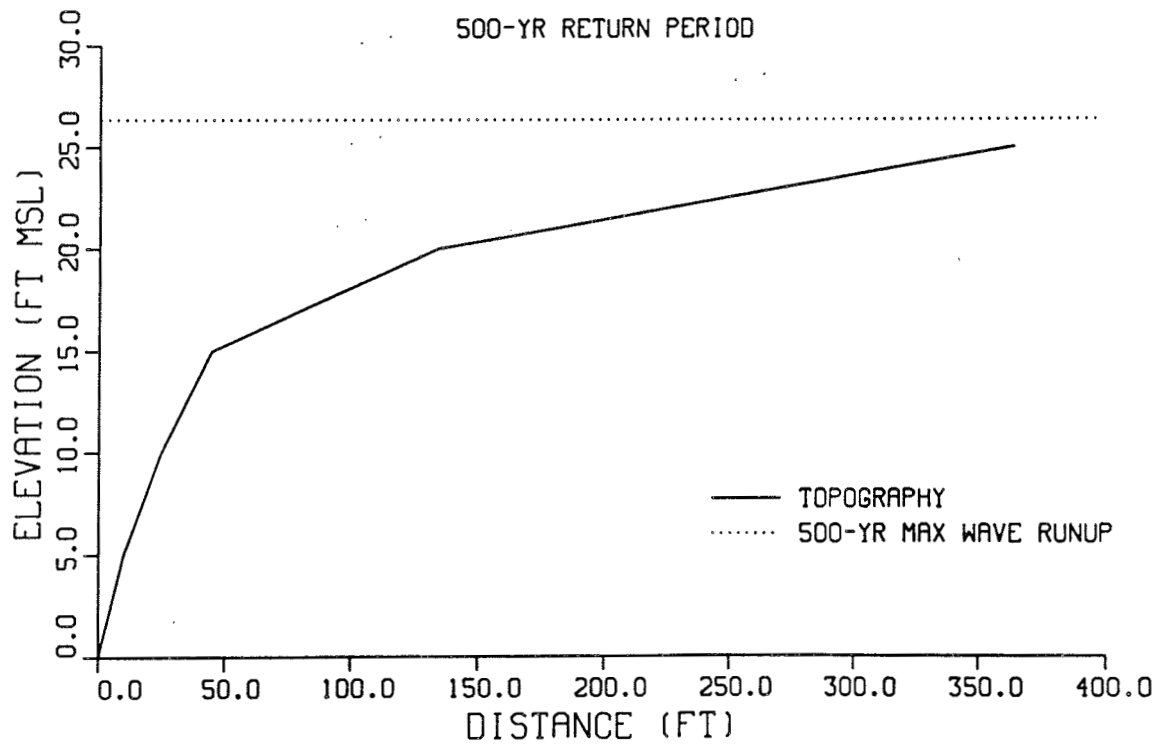
SOUTHERN GUAM TYPHOON ANALYSIS

PROFILE 16-8

100-YR RETURN PERIOD



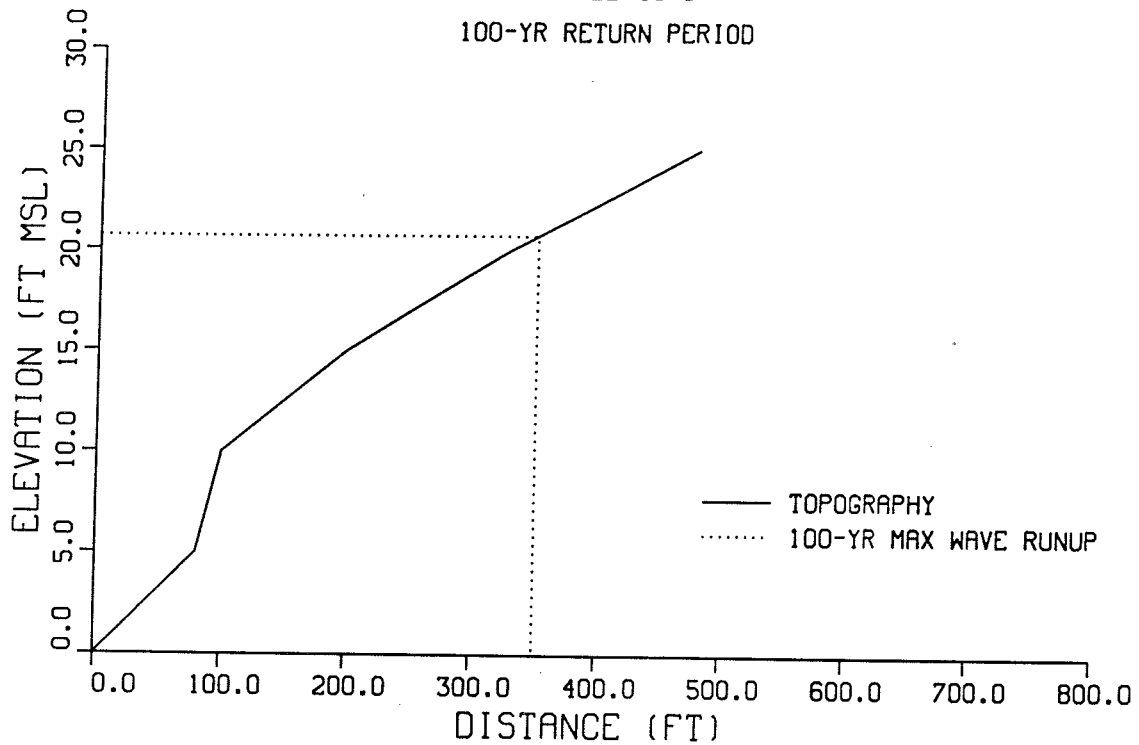
500-YR RETURN PERIOD



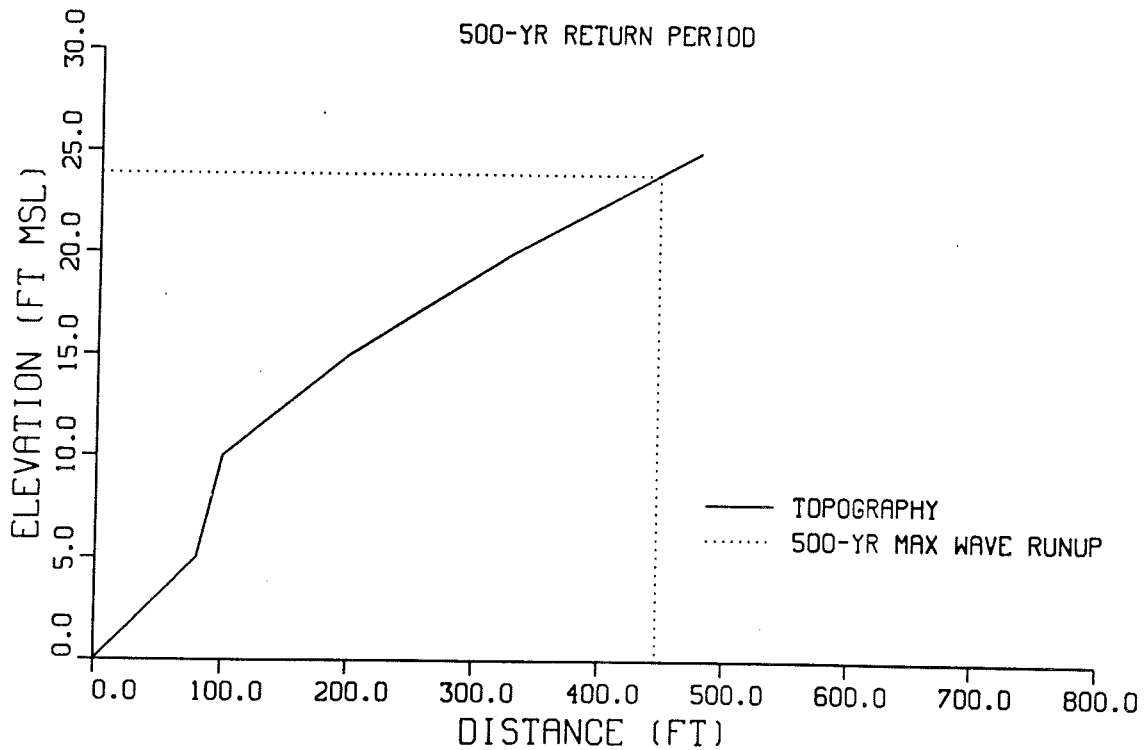
SOUTHERN GUAM TYPHOON ANALYSIS

PROFILE 16-9

100-YR RETURN PERIOD



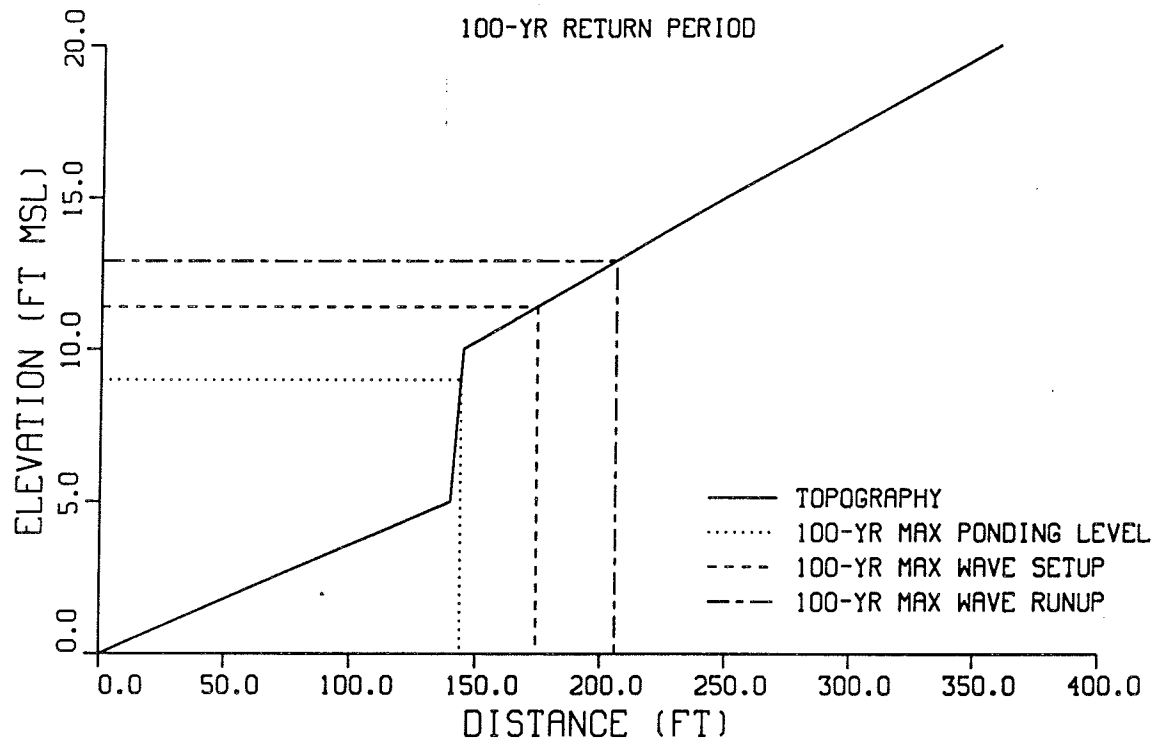
500-YR RETURN PERIOD



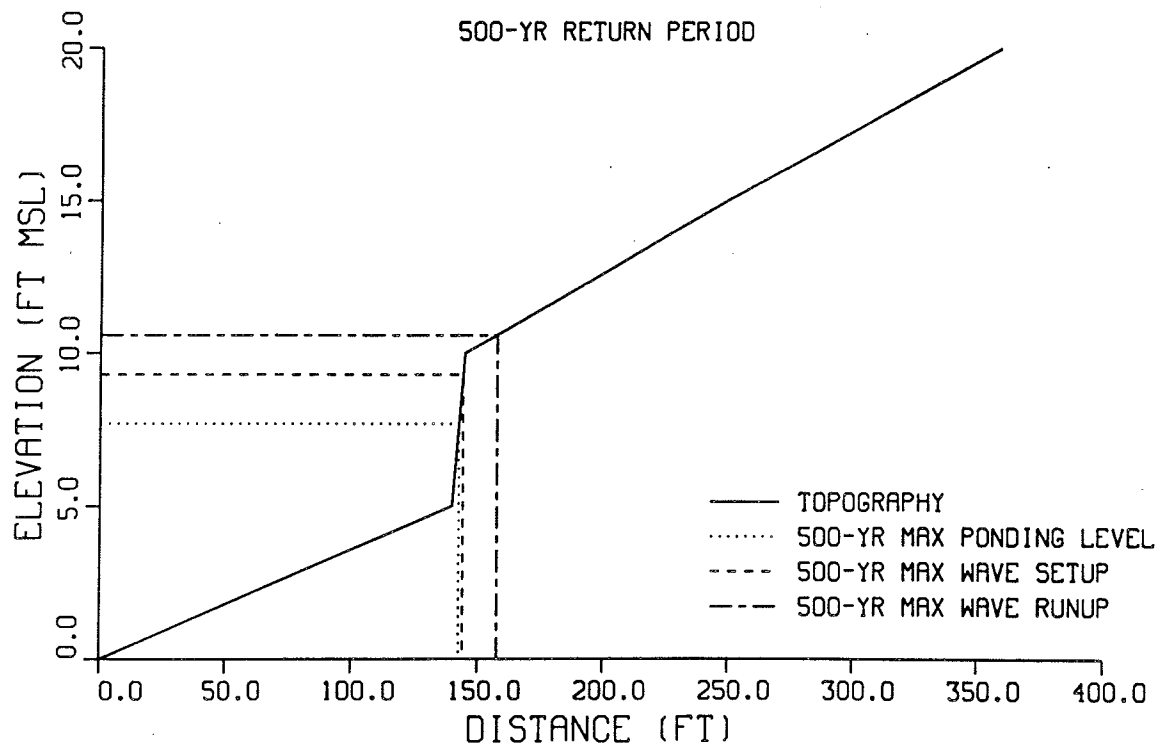
SOUTHERN GUAM TYPHOON ANALYSIS

PROFILE 6-11

100-YR RETURN PERIOD

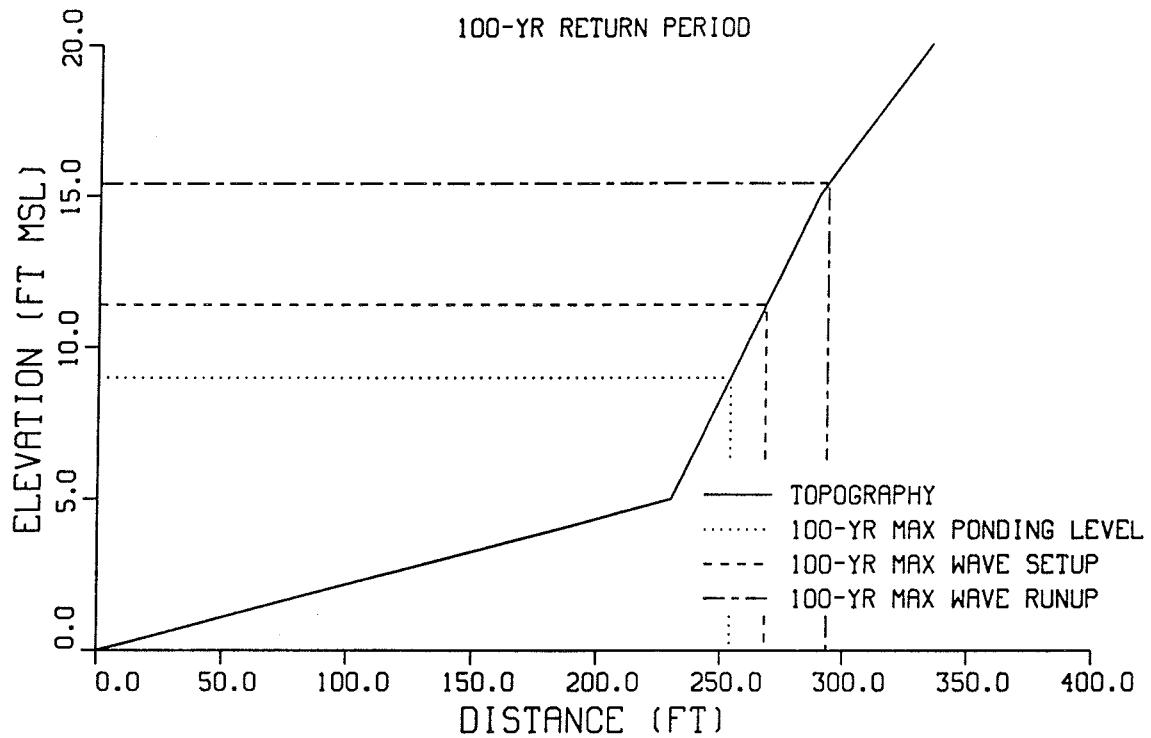


500-YR RETURN PERIOD

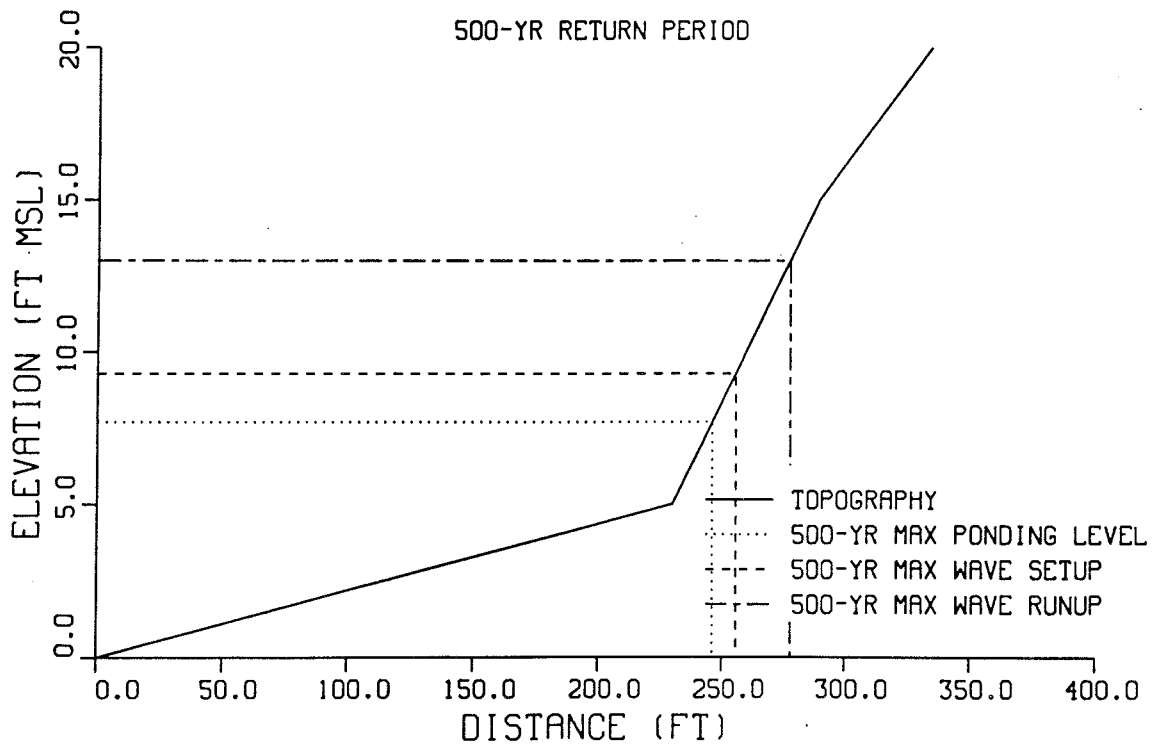


SOUTHERN GUAM TYPHOON ANALYSIS PROFILE 17-1

100-YR RETURN PERIOD



500-YR RETURN PERIOD



REPORT DOCUMENTATION PAGE			Form Approved OMB No. 0704-0188	
Public reporting burden for this collection of information is estimated to average 1 hour per response, including the time for reviewing instructions, searching existing data sources, gathering and maintaining the data needed, and completing and reviewing the collection of information. Send comments regarding this burden estimate or any other aspect of this collection of information, including suggestions for reducing this burden, to Washington Headquarters Services, Directorate for Information Operations and Reports, 1215 Jefferson Davis Highway, Suite 1204, Arlington, VA 22202-4302, and to the Office of Management and Budget, Paperwork Reduction Project (0704-0188), Washington, DC 20503.				
1. AGENCY USE ONLY (Leave blank)		2. REPORT DATE November 1996		3. REPORT TYPE AND DATES COVERED Final report
4. TITLE AND SUBTITLE Southern Guam Typhoon Stage-Frequency Analysis			5. FUNDING NUMBERS	
6. AUTHOR(S) David J. Mark				
7. PERFORMING ORGANIZATION NAME(S) AND ADDRESS(ES) U.S. Army Engineer Waterways Experiment Station 3909 Halls Ferry Road Vicksburg, MS 39180-6199			8. PERFORMING ORGANIZATION REPORT NUMBER Miscellaneous Paper CERC-96-7	
9. SPONSORING / MONITORING AGENCY NAME(S) AND ADDRESS(ES) U.S. Army Engineer Division, Pacific Ocean Ft. Shafter, HI 96858-5440			10. SPONSORING / MONITORING AGENCY REPORT NUMBER	
11. SUPPLEMENTARY NOTES Available from National Technical Information Service, 5285 Port Royal Road, Springfield, VA 22161.				
12a. DISTRIBUTION / AVAILABILITY STATEMENT Approved for public release; distribution is unlimited.			12b. DISTRIBUTION CODE	
13. ABSTRACT (Maximum 200 words) This report describes the methodology for computing storm surge surface elevation versus frequency-of-occurrence relationships for the island of Guam, the largest and most populous island in the Mariana group. Because maximum water levels represent the combination of waves, tides, and storm surge, the approach to be used in this study is based on the use of the long-wave numerical model WIFM, use of existing deepwater wave conditions for ponding and wave setup computations, and implementation of the joint probability method approach for developing frequency relationships. The report provides a detailed description of each phase of the study. Stage-frequency and computed wave setup and runup profiles are included in the report appendices.				
14. SUBJECT TERMS Finite difference modeling Frequency analysis Joint probability method			15. NUMBER OF PAGES 169	
Storm surge Typhoon modeling Wave runup			16. PRICE CODE	
17. SECURITY CLASSIFICATION OF REPORT UNCLASSIFIED			18. SECURITY CLASSIFICATION OF THIS PAGE UNCLASSIFIED	
19. SECURITY CLASSIFICATION OF ABSTRACT			20. LIMITATION OF ABSTRACT	